2
Energy Balance

http://www.staff.science.uu.nl/~delde102/AtmosphericDynamics.htm

Quotes illustrating the history of knowledge on the greenhouse effect

1827:
The question of the Earth's temperature distribution, one of the most important and most difficult of all Natural Philosophy, is made up of rather diverse elements that must be considered from a general point of view.
Jean-Baptiste Joseph Fourier, 1827: **On the temperatures of the terrestrial sphere and interplanetary space**. *Mémoires de lAcademie Royale des Sciences de l'Institute de France VII*, 570-604. A translation of this essay accompanies the article by R.T. Pierrehumbert, cited below.

1896:
The selective absorption of the atmosphere is of a wholly different kind. It is not exerted by the chief mass of air, but in a high degree by aqueous water vapour and carbonic acid… The influence of this absorption is comparatively small on the heat of the Sun, but must be of great importance in the transmission of rays from the Earth.
Svante Arrhenius, 1896: **On the influence of carbonic acid in the air upon the temperature of the ground**. *Phil. Mag.*, 41 no. 251, page 239.

1956:
Fifty years ago the carbon dioxide theory was perhaps the most widely held theory of climatic change, but in recent years it has had relatively few adherents. However, recent research suggests that the usual reasons for rejecting this theory are not valid.
(Gilbert N. Plass, 1956: **Effect of carbon dioxide variations on climate**. *American Journal of Physics*, 24, 376-387)

1975:
If man-made dust is unimportant as a major cause of climatic change, then a strong case can be made that the present cooling trend will, within a decade or so, give way to a pronounced warming induced by carbon dioxide.
Wallace S. Broecker, 1975: **Climatic change: are we on the brink of a pronounced global warming?** *Science, 189*, 460-463.

2004:
Fourier got the essence of the greenhouse effect right – the principle of energy balance and the asymmetric effect of the atmosphere on incoming Solar radiation versus outgoing radiation. The remaining physics took almost two more centuries to sort out, and the job is still not yet done. As well as the Stefan-Boltzman black body radiation law, other phenomena not understood at Fourier's time include the role of convection, … the dynamic nature of water vapour and its consequent radiative feedback, and both optical and microphysical properties of clouds. Fourier's essay set the agenda for much of this work. Inadequate understanding of vertical temperature gradient, water vapour and clouds continues to plague our theories of climate.
Raymond T. Pierrehumbert, 2004: **Warming the world**. *Nature, 432,* 677

Sections of chapter 2

Boxes of chapter 2

In this chapter we'll adhere to the following statement about "academic modelling"

"It may be that we seek enlightenment, rather than imitation. We might then look for the essence of the physical system, disregarding all processes that we think are not absolutely essential. This set of essential processes defines our model, though perhaps we should call it a toy, rather than a model. The object is to reproduce the consequences of what we think are the essentials, and the only thing that is to prevent us is our inaccurate specification of the physics. What we can hope to get right is the feedback between processes"

John Green , 1999: **Atmospheric Dynamics**, Cambridge University press (p. 160)

2.1 Introduction

What determines the temperature of the atmosphere? This is one of the central questions of meteorology. An answer to this question (but not the full answer!) can be deduced from the energy budget of the **climate system**, which **comprises the Earth's surface, the oceans and the atmosphere**. This energy budget is determined by absorption and emission of radiation by the Earth's surface and by "greenhouse gases" in the atmosphere, by transport of heat by macroscopic motions in the atmosphere and oceans, by evaporation of water at the Earth's surface, by condensation of water vapour in clouds and by freezing of cloud droplets.

This chapter is concerned with nearly all aspects of the energy budget of the climate system. It is assumed that the reader is familiar with the physics that was not yet understood in Fourier's time (see the words of Pierrehumbert above), such as the **radiation laws due to Kirchhoff, Stefan and Boltzmann, and Planck**[64]. We also assume that the reader has read sections 1.8 to 1.15, which are concerned with the **equation of state, the composition of the atmosphere, potential temperature, hydrostatic balance and static instability**.

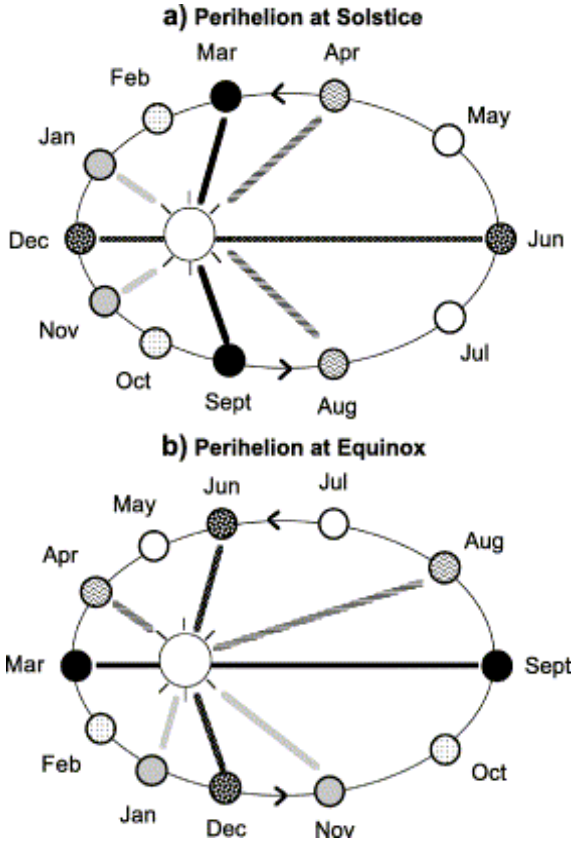

FIGURE 2.1. Schematic representation of the two extreme settings of a precessional cycle. (a) With perihelion at winter solstice and (b) with perihelion at vernal equinox. In the first case, the distance from the sun and corresponding strength of the Solar beam in the "insolation pairs" (times throughout the year that are equally far in time from solstice) are the same; in the second case, they are considerably different. Circles denoting the "mid-month" positions of the Earth on the ecliptic with the same insolation geometry of the incoming Solar beam have the same fill pattern. Progression of precession is indicated by arrows (from: Kukla, G. and J. Gavin, 2004: Milankovitch climate reinforcements, **Global and Planetary Change**, 40, 27-48).

[64] See Box 1.3 (setion 1.12) for an explanation of Planck's law and Stefan-Boltzmann's law and section 2.3 for an explanation of Kirchhof's law.

The discussion of the energy balance of the climate system starts with the topic of Solar radiation (section 2.2). Section 2.3 introduces terrestrial radiation and makes some simple calculations of the mean temperature of the Earth's surface, based on radiative balance, and discusses the role of the atmosphere in this balance. Section 2.4 looks into the process of adjustment to radiative balance. Section 2.5 discusses the observations of radiation at the "top of the atmosphere" (TOA). Section 2.6 discusses the sensitivity of climate to changes in incoming Solar radiation. In sections 2.7 to 2.9 a simplified radiation model for a homogeneous atmosphere is introduced. Equilibrium- and time-dependent solutions are discussed. Sections 2.10 to 2.15 are devoted to the role of water in the energy budget. A "parametrized" water cycle is added to the simplified radiation model. Section 2.16 deals with absorption of Solar radiation in the atmosphere, principally by ozone and water vapour. Sections 2.17-2.20 deal with the non-linear relation between greenhouse gas concentrations, cloud cover and the atmospheric infrared window, illustrated with solutions of the radiation model. Finally, sections 2.21 and 2.22 are concerned with the ice-albedo feedback and the following important question. What determines the pole-equator temperature difference?

2.2 Solar irradiance

The Sun emits a flux of energy in the form of electromagnetic waves. The average total energy associated with this flux is 3.9×10^{26} W. This is called the **Solar luminosity**. The flux density is defined as the luminosity divided by the area of the photosphere. This calculation yields a flux density of 6.4×10^{7} W m^{-2}. This energy reaches the Earth at a mean distance of 1.5×10^{11} m. The flux density at this distance is S_0=1366 W m^{-2}. S_0 is called the "**Solar constant**" or the "**Solar irradiance**".

Solar irradiance is by no means constant. It varies due to two effects. First, due to changes in the Solar luminosity and, second, due to variations in the orbit of the Earth relative to the Sun (**Figure 2.1**). The latter variations are due to gravitational forces exerted by other celestial bodies on the planet Earth. Earth's orbit around the Sun is approximately elliptical. The Earth takes one year to make one revolution around the Sun. Due to this the Earth-Sun distance varies sinusoidally throughout the year (**Figure 2.2**). The Sun is not positioned exactly in the intersection of the major axis and minor axis of the ellipse of this **elliptical orbit**, rather it lies in one of the two focal points of the ellipse. Once a year (at so-called "**perihelion**") the Earth is closest to the Sun. Nowadays, the closest approach to the Sun is on 4 January when the intensity of the Solar beam at the **top of the atmosphere (TOA)** is about 1410 W m^{-2}. Six months later the Sun-Earth distance reaches a maximum (so-called "**aphelion**"). The Solar beam intensity at TOA at aphelion is only about 1320 W m^{-2}. Thus, the intensity of the Solar beam has a pronounced seasonal cycle, which today has a range of about 90 W m^{-2} or 6.6 % of the Solar constant. The **eccentricity** of the elliptical orbit of the Earth around the Sun, i.e. the departure of this orbit from a circle has a regular cycle with a period of about 92000 years. At the beginning of the last **glacial period**, about 116000 years ago, the eccentricity was such that the amplitude of the seasonal cycle of the Solar beam intensity reaching TOA was 16.6% of the Solar constant.

The seasonal timing of perihelion and aphelion varies in a so-called **precessional cycle** with a period of about 19000-23000 years. **Figure 2.1** shows the two extreme positions of perihelion. Position (a) corresponds to the situation 705 years ago and is actually not very different from the situation now. Position (b) corresponds to the situation about 17000 years ago when large parts of Europe and Northern America were covered by thick ice sheets (**figure 2.3**).

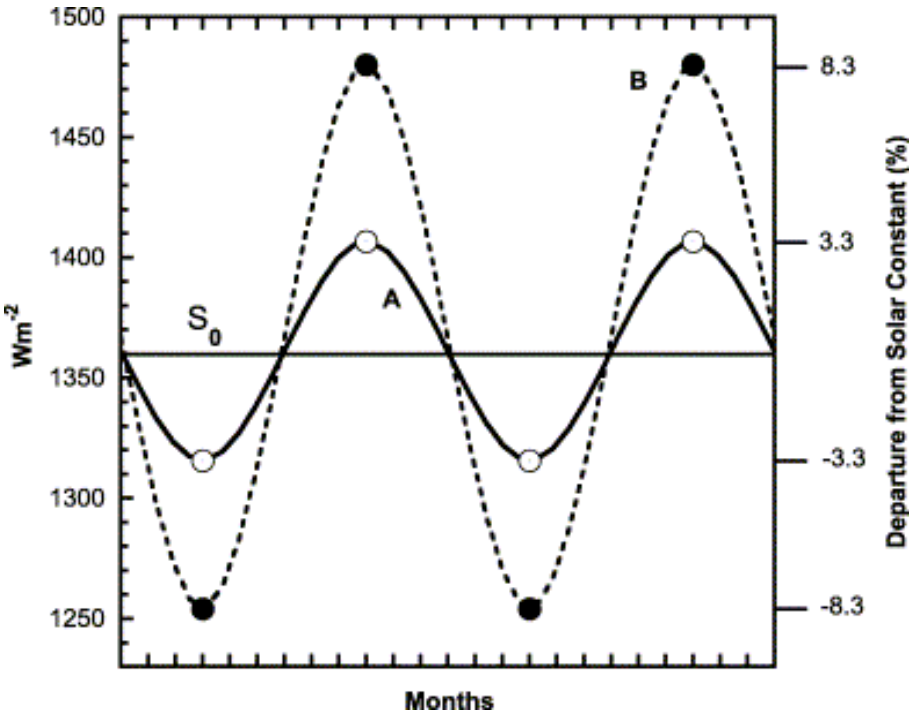

FIGURE 2.2. Biennial (over 24 months) cycle of the Solar beam intensity at the top of the atmosphere (TOA) in W m^{-2} and as percent departure from the Solar constant, for the present (A) (open circles) and 116,000 years ago (B) (full circles). S_0 is the Solar constant. (from: Kukla, G. and J. Gavin, 2004: Milankovitch climate reinforcements, **Global and Planetary Change**, 40, 27-48).

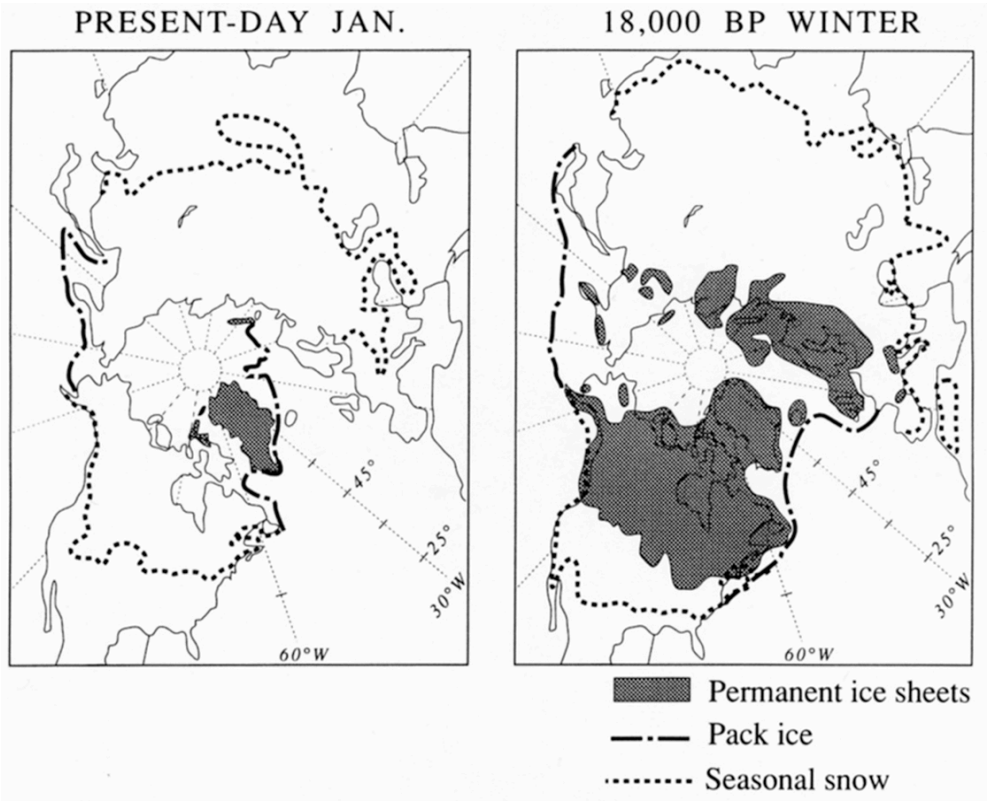

FIGURE 2.3. Extent of permanent ice-cover (shaded) seasonal snow cover (dotted line) and pack ice (perennial sea-ice, dash-dotted line) at present and estimated for the last glacial maximum (from D.L. Hartmann, 1994: **Global Physical Climatology**. Academic Press, figure 9.4).

Box 2.1 Calculating daily average Solar irradiance

The **daily average Solar irradiance**, Q (expressed in W m^{-2}), at the top of the atmosphere as a function of the Sun's declination angle (δ) and latitude (ϕ) is calculated according to

$$Q = \frac{S_0}{\pi}\left(\frac{d_m}{d}\right)^2\left(\Delta H \sin\phi \sin\delta + \cos\phi\cos\delta\sin\Delta H\right) \qquad (1)$$

In this equation S_0 is the Solar constant (=1366 W m^{-2}), d_m is the averaged distance between the Sun and the Earth in metres, which is 1 astronomical unit (AU) (1 AU equals 1.495978707×10^9 m), d represents the 'actual' Sun to Earth distance, ϕ is latitude, δ is the declination angle of the Sun (**figure 1**, this box) and ΔH is the length of daylight per day in radians ($(24\Delta H/\pi)$ hours). The derivation of eq. (1) is given in chapter 7 of Pierrehumbert (2010). The parameters, d, δ and ΔH are specified in more detail in the following. Equation (1) is used to produce the left panel of **figure 2.8** (see also **figure 1.107**).

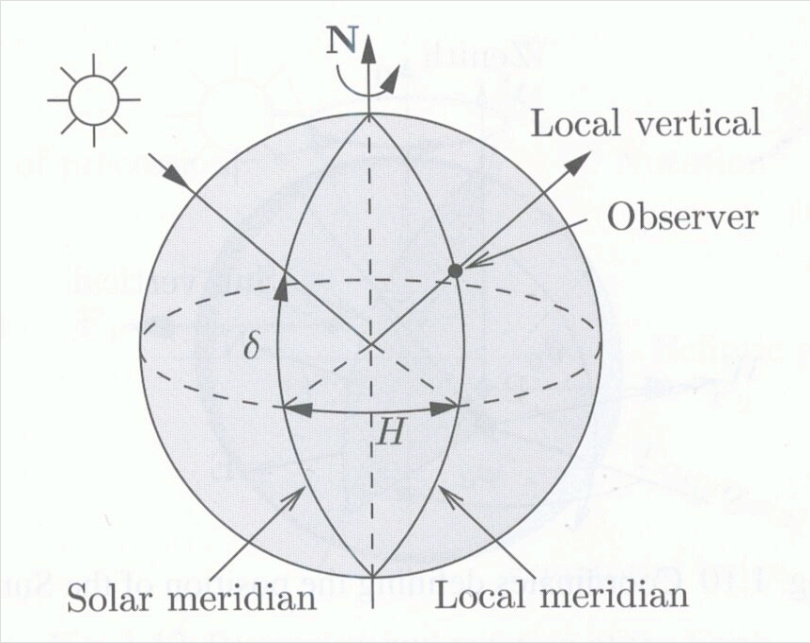

FIGURE 1 BOX 2.1. Pictorial explanation of the declinition, δ, and the "hour angle", H. Source of the figure: W. Zdunkowski, T. Trautmann and A. Bott, 2007: **Radiation in the Atmosphere**. Cambridge University Press. 482 pp.

The 'actual' distance between the Sun and the Earth, d, as a function of time, t (in days), is approximated according to:

$$d(t) = d_m\left(1 + e\sin\left\{(2\pi/365)\cdot(272 + t)\right\}\right). \qquad (2)$$

Here, e is the **eccentricity** of Earth's elliptical orbit around the Sun. Time, $t=1$ corresponds to January 1st, $t=2$ to January 2nd etc. This parametrization is based on the fact that the minimum, d_{min}, and maximum, d_{min}, of the distance, d, are at present observed on, respectively, 3 January (day 3) and 4 July (day 185). The relation between eccentricity, e, and d_{min} or d_{max} is

$$d_{\min} = d_m(1-e);\ d_{\max} = d_m(1+e)\ . \qquad (3)$$

The present value of e is 0.017. The **declination angle**, δ, is expressed in radians and expressed as a function of time, according to:

$$\delta(t) = \left(\pi\delta_{\max}/180\right)\sin\left\{(2\pi/365)\cdot(285+t)\right\} \quad . \qquad (4)$$

The parameter, $\delta_{\max}$, is the **axial tilt** or **obliquity**, which at present is 23.45°. By definition, the declination angle equals zero on March 21st (day 80).

Finally, the length of day (indicated by ΔH) needs to be specified. According to Pierrehumbert (2010) the length of day, which is a function of both latitude as well as the declination angle, is given by:

$$\Delta H = \arccos(-\tan\phi\tan\delta) \qquad (5)$$

The length of day is expressed in radians. Multiplying with $24/\pi$ yields ΔH in hours. Since at both 90ºN as well as 90ºS this formula cannot be used, conditions need to be imposed here. These are, that the length of day equals 24 hours (the polar day) or 0 hours (the polar night). At the day of transition when the Sun is supposed to be exactly over the equator, the length of day should be 12 hours at all latitudes, hence ΔH=12 hours at the poles also.

The **daily average zenith angle**, θ, in radians is calculated from (**figure 2.41**)

$$\theta = \arccos\left(\frac{24Qd^2}{S_0\Delta H d_m^2}\right) \text{ if } \Delta H>0. \qquad (6)$$

PROBLEM BOX 2.1: Yearly average insolation and obliquity

Calculate the yearly average incoming Solar radiation for the pole and for the equator if the obliquity (tilt in the figure below) is 0°, 23.5° and 54°. Assume that all other orbital parameters have values identical to present day values.

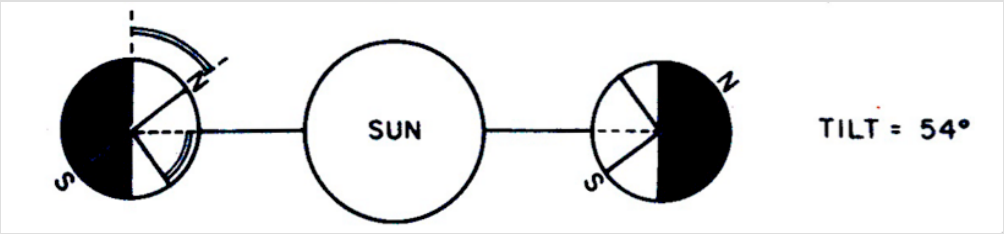

FIGURE 2 BOX 12.1. The distribution of sunlight if the tilt (or obliquity) is 54° (see also **figure 2.4**).

Reference

Pierrehumbert, R.T., 2010: **Principles of Planetary Climate**. Cambridge University Press. 652 pp.

Another very important orbital parameter is the "**obliquity**", i.e. the angle between the Earth's axis of rotation and its orbital plane, the so-called "**ecliptic**" (**figure 2.3**). This angle has varied harmonically in time with a period of 41000 years between the extreme values of

22° and 24.5°. The obliquity does not affect the total incoming radiation at TOA. It only affects the **distribution** of incoming radiation. It determines the existence and intensity of the **seasons**. The concepts of **solstice** and **equinox** are related to the obliquity. At solstice the radiation received by one (the summer-) hemisphere is at its maximum, while the other (winter-) hemisphere receives least radiation. At equinox the Sun is directly over the equator.

If its axis were not tilted (and its orbit circular), the Earth would be a far duller place. The hours of daylight and darkness would be equal everywhere, except at the poles, which would be in a situation of permanent sunrise or sunset. There would be no seasons. Plants and animals would be very specialized. Each species would occupy specific latitude bands with unchanging environments. Bird migration would not take place. Probably, a relatively narrow latitude-band in midlatitudes would have permanent spring-like temperatures (about 18°C) where life would function optimally. The lower latitudes would be too hot for most living things, except maybe in a narrow zone around the equator, where nearly permanent precipitation and thick rain forests would keep the climate bearable. The Polar regions would receive hardly any radiation at all. Large ice caps would therefore grow over the poles.

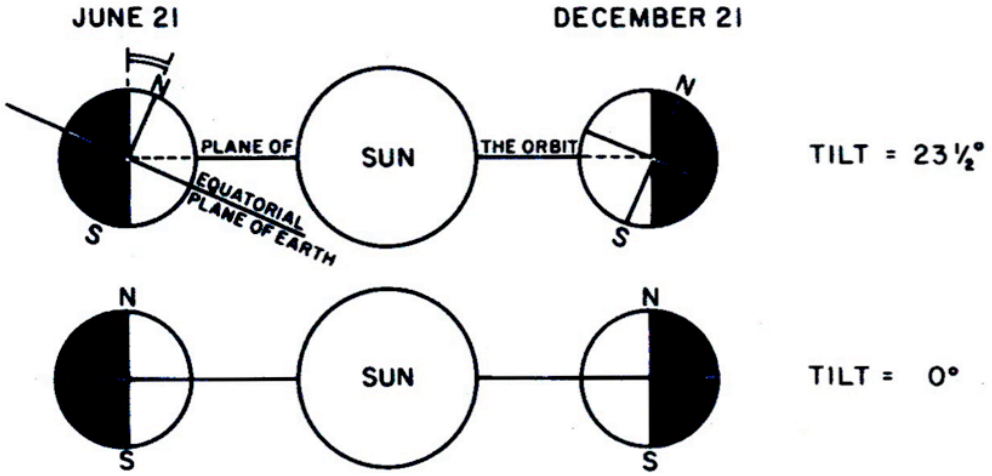

FIGURE 2.4. The effect of the tilt of the Earth's rotation axis on the distribution of sunlight. When the tilt is smaller than 23.5° (the present value), the poles receive less sunlight than they do today. When the tilt is larger than 23.5°, the poles receive more sunlight. The tilt of 0° (eternal equinox) is interesting because the poles receive no sunlight. Source: J. Imbrie and K.P. Imbrie, 1979: **Ice Ages: solving the mystery**. The MacMillan Press Ltd, London, 224 pp.)

The obliquity angle has actually never been reduced to zero, but it is thought that periods of low obliquity angle have coincided with the start of a so-called "**glacial period**", a period of many thousands of years in Earth's physical history in which layers of ice, several kilometres thick, extended from the pole well into the mid-latitudes over the continents in the northern hemisphere (**Figure 2.3**). The idea behind this hypothesis is that a low obliquity angle implies less summer insolation at the poles. This effect makes the summers so cold that snow and ice from the previous winter may survive the summer, giving the following winter a "head start". There is, however, no consensus on this hypothesis.

Of course, the distribution of Solar radiation on Earth is also influenced by the rotation of the Earth about its axis. This produces the familiar **daily cycle** in temperature, humidity, cloudiness and circulation in the lower part of the troposphere.

Solar luminosity varies in two ways. First, there is an **11-year cycle** in the number of **Sunspots**, which produces an oscillation in the Solar irradiance at TOA with an amplitude of less than 1 W m^{-2} (**figure 2.5**). Second, over a very much longer period of time, that is, 4.5

Gy, which is the approximate age of the Solar system, including the Earth, the luminosity of the Sun has increased steadily by about 30 %. We'll come back to this fact later when discussing the so-called "Faint Young Sun Paradox".

We can deduce the temperature of the Sun's photosphere by assuming that the Sun is a "**black body**". According to **Stefan-Boltzman's law** the flux density, E, of radiation emitted by the Sun is then given by (assuming that the Sun is a "black body"),

$$E = \sigma T^4 . \qquad (2.1)$$

Here σ=5.67.10^{-8} W m^{-2}K^{-4}. This gives T=5796 K.

The Solar irradiance that is intercepted by the Earth-atmosphere system is $\pi a^2 S_0$, where a is the radius of the Earth (assumed constant). A fraction α (**the "planetary albedo" or "bond abedo"**[65]) is reflected back to space. The remaining portion is absorbed. Averaging over a long time and over the total area of the globe, the absorbed Solar radiation is in balance with the radiation emitted by the Earth-atmosphere system. Therefore, we have

$$\boxed{(1-\alpha)\frac{S_0}{4} = \sigma T_E^4}. \qquad (2.2)$$

T_E is the "**emission temperature**". Assuming that α=0.3, we find from (2.2), T_E =255 K. This temperature is much lower than the observed global average surface temperature (288 K).

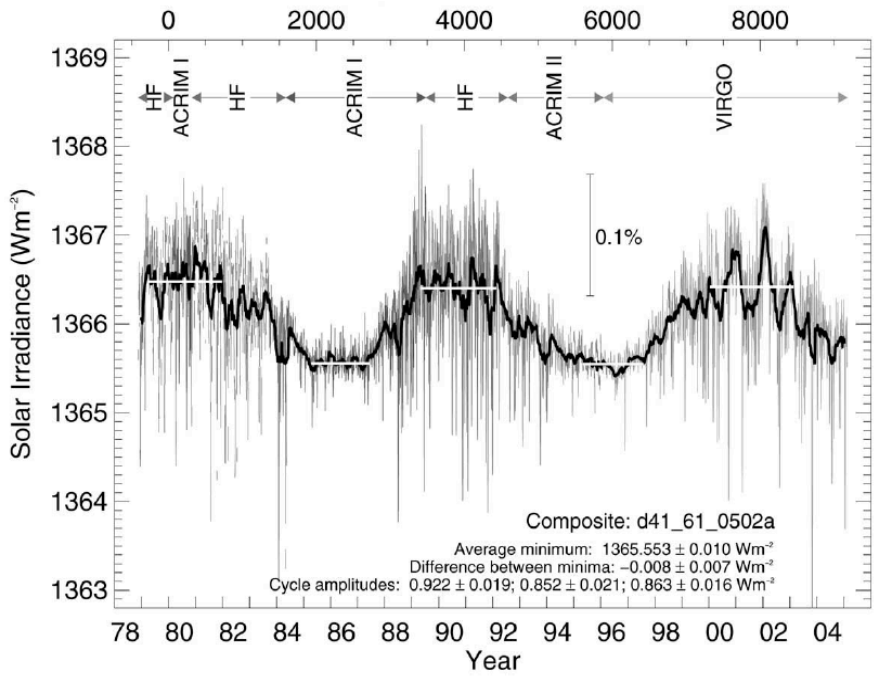

FIGURE 2.5. Composite of total Solar irradiance corrected for variations in the distance Earth-Sun (1978-2005). The indicated uncertainties are formal statistical errors (Figure 10 of Annual Report 2004 of the World Radiation Centre at Davos; see http://www.pmodwrc.ch/annual_report).

---

65 The bond albedo is the total radiation reflected from an object (Earth in this case) compared to the total incident radiation from the Sun. It has been measured to be about 0.3, and is suspected to be decreasing under influence of anthropogenically induced changes to the land surface, cloud cover and aerosol concentration in the atmosphere (Wielicki et al., 2005) (see list of references at the end of this chapter).

2.3 Greenhouse effect

Most Solar radiation is transmitted through the atmosphere to the surface of the Earth and absorbed or reflected there. Earth emits radiation almost as a black body. This radiation is partly absorbed by the atmosphere or escapes directly to space. Greenhouse gases in the atmosphere emit radiation downwards and upwards.

According to Planck's law of radiation (**Box 1.3**, chapter 1) electromagnetic waves emitted by the surface of the Earth and by the atmosphere, which have a temperature of 200-300 K (**figure 1.1**), have a much larger wavelength and lower frequency than the electromagnetic waves emitted by the Sun, which has a surface temperature of 5780 K. For this reason, the radiation emitted by the Earth and by the atmosphere is generally referred to as "**long-wave**" radiation, while Solar radiation is referred to as "**short-wave**" radiation. While short-wave radiation is transmitted through the atmosphere almost unattenuated, long-wave radiation is strongly absorbed and re-emitted by **water vapour, carbon dioxide** and other trace gases in the air. So strongly, that it is acceptable, as a very rough first order approximation, to asume that long-wave radiative **absorptance** of the atmosphere is equal to 1. This is the same as saying that the atmosphere is **opaque** to long-wave radiation.

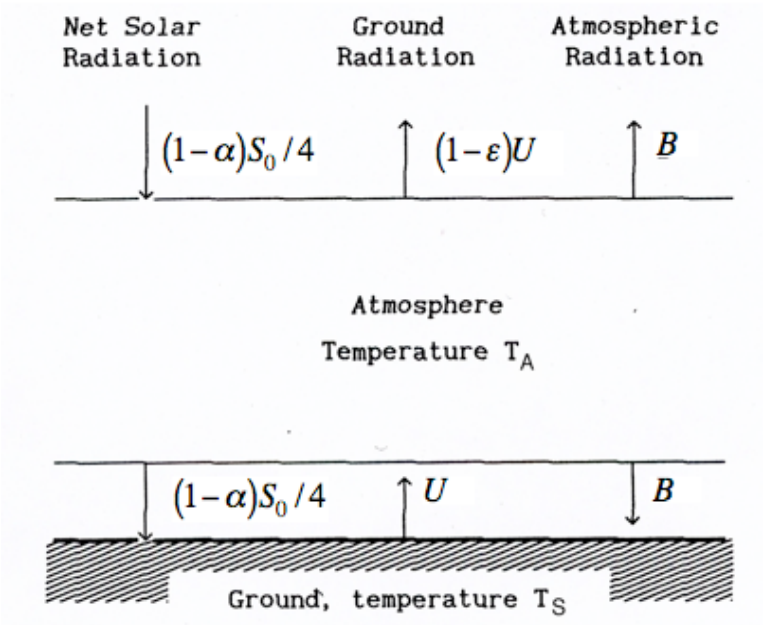

FIGURE 2.6. Single-layer model of the atmosphere. S is the Solar irradiance; α is the albedo of the ground (0.05-0.2 for water-covered ground; 0.1-0.4 for bare ground; 0.1-0.25 for vegetated ground; 0.5-0.9 for snow-covered ground); U is the terrestrial radiation, of which a fraction (1-ε) penetrates directly through the atmosphere to space; B is the radiation emitted by the atmosphere (figure adapted from James (1994), see the list of books in section ii).

Let us write down a very simple approximation of the radiation balance of the Earth-atmosphere system, based on the assumption that the atmosphere is transparent to short-wave radiation and opaque to long-wave radiation (ε=1 in **figure 2.6**). The expressions for radiative balance at the **top of the atmosphere**, of the **atmosphere** itself, and of the **Earth's surface** are, respectively (**figure 2.6**),

$$\frac{S_0}{4}(1-\alpha) = B \equiv \sigma T_E^4 = \sigma T_A^4 , \tag{2.3}$$

$$U = \sigma T_S^4 = 2B = 2\sigma T_A^4 , \tag{2.4}$$

$$\frac{S_0}{4}(1-\alpha) + \sigma T_A^4 = \sigma T_S^4 . \tag{2.5}$$

From these equations it is easily deduced that the temperature of the Earth's surface

$$T_S = \sqrt[4]{2}\,T_E . \tag{2.6}$$

Since T_E=255 K, T_S=303 K. This value is considerably higher than observed (288 K).

The discrepancy between theory and observation is explained by the fact that the atmosphere is not totally opaque to long-wave radiation, neither is it completely transparent to short wave radiation. Moreover, approximating the atmosphere by one homogeneous layer is obviously not accurate. Nevertheless, we can conclude that the presence of the atmosphere raises the temperature at the Earth's surface considerably. This effect is referred to as the "**greenhouse effect**".

We assume now that the atmosphere is "**semi-grey**", i.e. it absorbs a constant fraction ε of the long-wave radiation, but is still transparent to Solar radiation[66]. In other words, the Earth's surface emits energy at a rate U, given by

$$U = \sigma T_S^4 , \tag{2.7}$$

of which a fraction (1-ε) escapes to space. According to **Kirchhoff's law the absorptance and emittance of a body are equal at any given temperature**. Therefore, the atmosphere emits energy at a rate B given by

$$B = \varepsilon \sigma T_A^4 \tag{2.8}$$

(upwards *and* downwards). In a steady state we have

$$\frac{S_0}{4}(1-\alpha) + B = U , \tag{2.9a}$$

$$2B = \varepsilon U . \tag{2.9b}$$

This leads to

$$T_S = \left(\frac{2}{2-\varepsilon}\right)^{1/4} T_E \text{ and } T_A = \left(\frac{1}{2-\varepsilon}\right)^{1/4} T_E . \tag{2.10}$$

With ε=0.78 (i.e. 22 % of the terrestrial radiation escapes to space) and again α_p=0.3, we obtain T_S=288 K and T_A=242 K. The computed surface temperature is close to the observed

[66] In a "grey" atmosphere absorption is totally independent of wavelength

average temperature of the Earth's surface (see **Table 2.1**). The computed atmospheric temperature is representative for the observed temperature at 411 hPa. This is not a bad result for such a crude model. However, although the estimate of the average planetary albedo (α=0.3) is probably not far from reality, the estimate of the average emissivity (ε=0.78) is probably an under-estimate. It appears that actually only 10% of the terrestrial radiation (radiation emitted by the Earth's surface) escapes directly to space. Suppose that ε=0.9. We now obtain T_S=296 K and T_A=249 K. Thus, we have a better estimate of the temperature "halfway" with respect to the mass of the atmosphere (at 500 hPa), but a worse estimate of the surface temperature.

The best measure of the "**strength of greenhouse effect**" is the so-called **back-radiation**, i.e. the downward emission of radiation from the atmosphere to the Earth's surface, which, within the context of the one-layer model, is

$$F_{\downarrow} = B = \varepsilon\sigma T_A^4 = \frac{\varepsilon}{2-\varepsilon}\sigma T_E^4 \equiv \frac{\varepsilon}{2-\varepsilon} Q. \qquad (2.11)$$

As ε increases the downward radiation increases, thereby increasing the temperature of the Earth's surface. According to the above equation, the surface may absorb as much energy emitted by the atmophere as energy emitted by the Sun. In reality this theoretical limit is exceeded (**figure 2.10**).

Altitude [km]	Pressure [hPa]	Temperature [K]	Potential temperature [K]	Brunt-Väisälä frequency [s^{-1}]	water vapour density [g m^{-3}]
0	1013	288	287		5.9
1	899	282	290	0.011	4.2
2	795	275	294	0.011	2.9
3	701	269	297	0.011	1.8
4	616	262	301	0.011	1.1
5	540	256	305	0.011	0.64
6	472	249	309	0.011	0.38
7	411	243	313	0.011	0.21
8	356	236	317	0.012	0.12
9	307	230	322	0.012	0.046
10	264	223	326	0.012	0.018
15	120	217	397	0.019	0.00072
20	54.7	217	497	0.021	0.00044
30	11.7	227	808	0.021	0.00038
40	2.8	251	1349	0.022	0.000067
50	0.76	271	2107	0.021	0.000012
60	0.20	245	2789	0.016	
70	0.05	217	3670	0.017	

TABLE 2.1. The "**1976 US standard atmosphere**" is representative for the observed average temperature distribution in the Earth's atmosphere in mid-latitudes. Potential temperature is defined in section 1.9. Brunt-Väisälä frequency, N, is defined in section 1.15 (see also **figure 1.6**). The value of N displayed in the table is computed from the values of pressure and temperature that are, respectively, displayed in the second and third column. The value of N at 1 km height is representative for the layer between the altitudes of 0 and 1 km, etc. The water vapour density is taken from Kuo-Nan Liou, 1992: **Radiation and Cloud Processes in the Atmosphere**. Oxford University Press. 504 pp.

PROBLEM 2.1. **Greenhouse effect on Venus and Mars**
The distance from Mars to the Sun is 2.3×10^8 km. Mars has an average planetary albedo of 0.15. Calculate the effective temperature of Mars assuming that the Sun is the only energy source. Observations indicate an average surface temperature of Mars of 220 K. What do you conclude about the Martian atmosphere? Could you assign a value to the average emission coefficient of the atmosphere of Mars?

The distance from Venus to the Sun is 10.8×10^7 km. The average surface temperature of Venus is 750 K. There is no internal energy source on Venus. The planetary albedo of Venus is 0.77. Can you apply the one layer-model (figure 2.6) to the atmosphere of Venus?

2.4 Radiative equilibrium timescale

In this section we investigate the characteristics of the actual time dependence of adjustment to radiative equilibrium, employing the simplified radiation model that was introduced in the previous section. Again, we assume that the Earth's surface has a negligible heat capacity. We may therefore write the energy balance as follows.

$$(1-\alpha)\frac{S_0}{4} + B = U\,. \tag{2.12}$$

For an atmospheric column of unit cross-sectional area in hydrostatic balance we may write down the time dependent energy balance equation as follows.

$$\frac{c_p p_s}{g}\frac{dT_A}{dt} = \varepsilon U - 2B. \tag{2.13}$$

The mass of the atmospheric column per unit area is p_s/g. Now, assume that the temperature of the atmosphere can be expressed as

$$T_A = T_{A0} + \Delta T\ , \tag{2.14}$$

where

$$|\Delta T| << T_{A0} \tag{2.15}$$

and T_{A0} is the **radiative equilibrium temperature of the atmosphere** (derived from (2.12) and (2.13) with the left hand side of equation 2.13 equal to zero).

We now intend to derive an equation for the time evolution of the temperature perturbation, ΔT. Substituting (2.12) into (2.13), in order to eliminate U we get

$$\frac{c_p p_s}{g}\frac{d\Delta T}{dt} = \varepsilon(1-\alpha)\frac{S_0}{4} + (\varepsilon-2)B = \varepsilon(1-\alpha)\frac{S_0}{4} + (\varepsilon-2)\varepsilon\sigma(T_{A0}+\Delta T)^4\,. \tag{2.16}$$

Using Taylor's formula truncated after the second term, i.e.:

$$f(T_0+\Delta T)=f(T_0)+\Delta T\frac{df(T_0)}{dT} \tag{2.17}$$

(2.16) becomes

$$\frac{c_p p_s}{g}\frac{d\Delta T}{dt}=\varepsilon\sigma T_E^4-(2-\varepsilon)\varepsilon\sigma T_{A0}^4-4(2-\varepsilon)\varepsilon\sigma T_{A0}^3\Delta T\ . \tag{2.18}$$

The first two terms on the r.h.s. of (2.18) add up to zero. Therefore

$$\frac{d\Delta T}{dt}=-\frac{4(2-\varepsilon)\varepsilon\sigma g T_{A0}^3}{c_p p_s}\Delta T\,. \tag{2.19}$$

The solution of this equation implies exponential decay of the temperature perturbation, ΔT, on a time scale, τ_E, where

$$\boxed{\tau_E=\frac{p_s c_p}{4(2-\varepsilon)\varepsilon\sigma g T_{A0}^3}}. \tag{2.20}$$

This time scale is called the "**radiative equilibrium timescale**". It represents the time required for the atmosphere to repond *significantly* to changes in radiative forcing. It is an expression of the **thermal inertia** of the atmosphere. That is, if the Sun were to be turned off suddenly, the effects in the atmosphere of this action would be felt after a period of time in the order of τ_E. Note that the radiative timescale decreases with increasing greenhouse gas concentration (i.e. with increasing ε).

When we substitute

$$T_{A0}=300\ \text{K};\ \varepsilon=0.7;\ g=10\ \text{m s}^{-2};\ p_s=10^5\ \text{Pa};\ c_p=1000\ \text{J K}^{-1}\text{Kg}^{-1},$$

we obtain $\tau_E\approx 20$ days.

It is evidently from (2.20) that τ_E is a strong function of temperature. If we assume that T_{A0}=200 K, as is the case approximately in large regions of the atmosphere (**figure 2.7**), we get $\tau_E\approx 70$ days.

The expression for the radiative adjustment time scale we found earlier (1.79), can be written such that it resembles very strongly the expression derived here. Using (2.2) to eliminate S_0 from (1.129), we find

$$\tau_E=\frac{p_s c_p}{\sigma g T_E^3},$$

which is indeed very similar to (2.20), except that it does not contain the effect of variations in greenhouse gas content, represented by the parameter, ε. This reveals that the radiative timescale is determined basically by the heat capacity of the atmosphere and the Solar power absorbed by the planet.

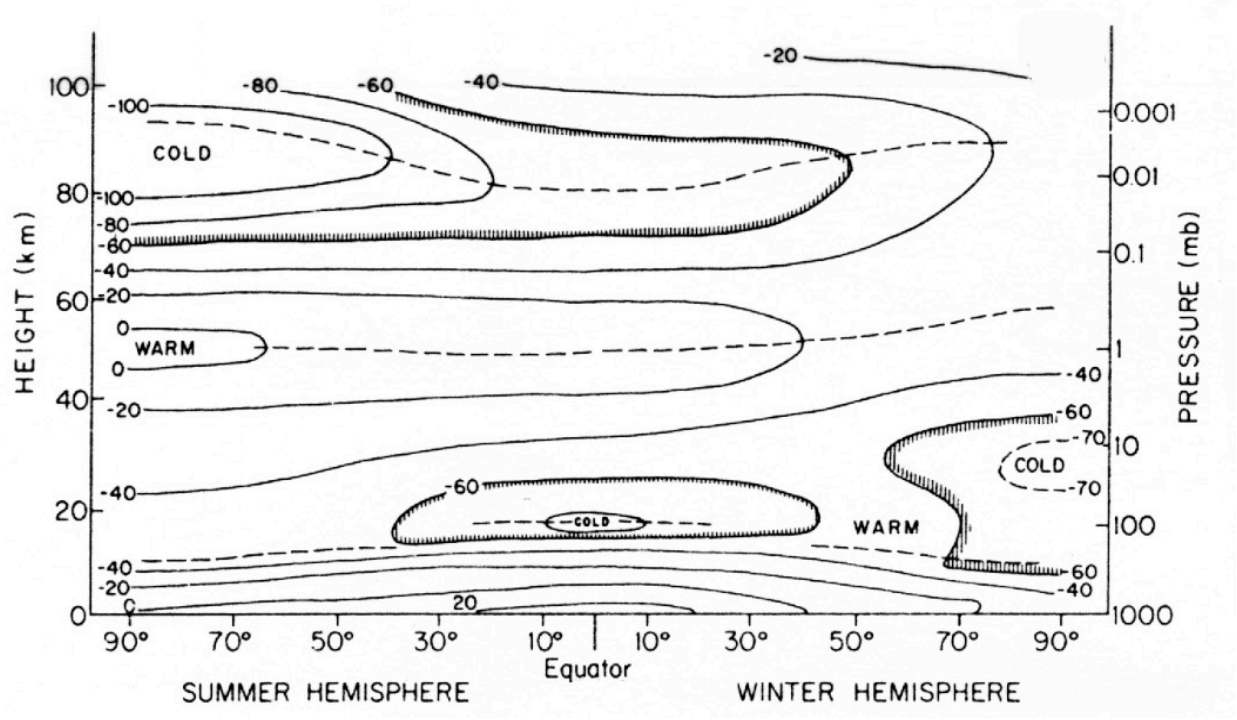

FIGURE 2.7. Meridional section showing the longitudinally averaged temperature (°C) up to 100 km at the time of the solstices. Dashed lines in (a) indicate the positions of the tropopause, stratopause and mesopause (Taken from Gill (1982), see the list of books in section ii). (see **figure 1.1**).

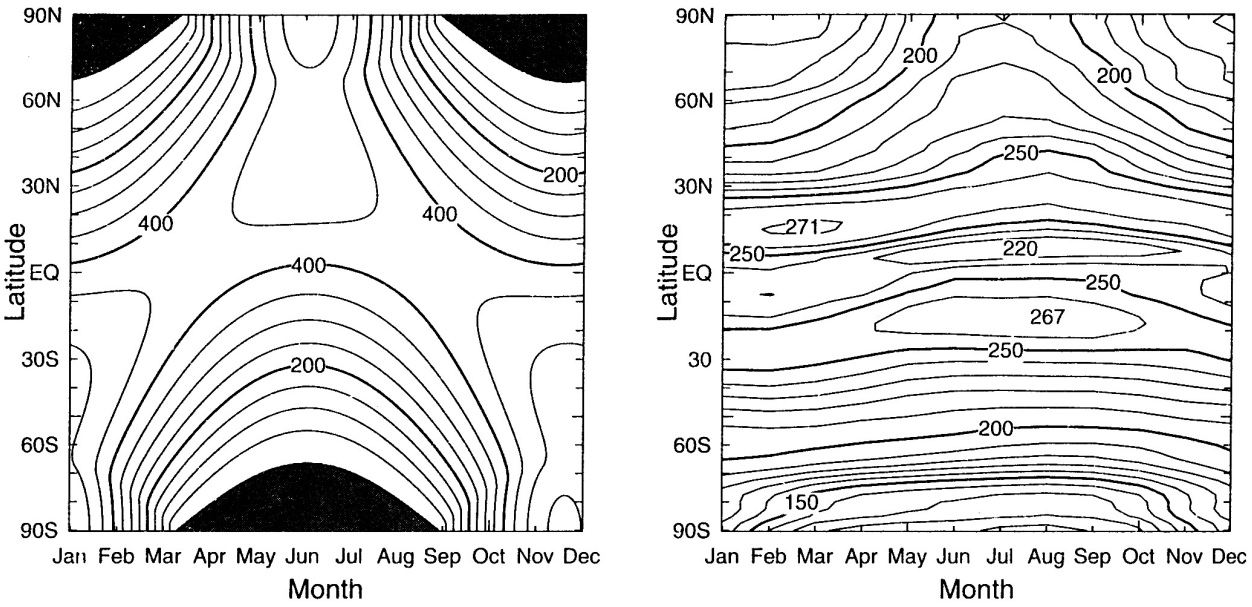

FIGURE 2.8. Daily mean incident Solar radiation (left) and outgoing long-wave radiation (right) at the top of the atmosphere as a function of latitude and time. Contour interval is 50 W m^{-2}. The left diagram is based on calculations (see **Box 2.1**), while the right diagram is based on satellite measurements between 1979 and 1994. (Source Masaki Satoh, 2004: **Atmospheric Circulation Dynamics and General Circulation Models**. Springer/Praxis Publishing, 643 pp.).

The radiative timescale, τ_E, is comparable in magnitude to the timescale associated with the seasonal cycle in incoming Solar radiation (**figure 2.8**). Therefore, we do not expect radiative equilibrium anywhere in the atmosphere. The extreme example of radiative imbalance is encountered over the winter polar cap. The black areas in the left diagram of **figure 2.8** correspond to the **polar night**. At a latitude of 75° the polar night spans a time period of approximately three months (90 days). During this period no Solar radiation is received over the polar cap poleward of ±75°, while, apparently, in the order of 100 W m^{-2} is lost to space by long-wave emission (right diagram in **figure 2.8**). Due to this, the atmosphere will obviously not be in radiative equilibrium.

The atmosphere over the winter pole will in fact cool continuously. This is seen in **figure 2.9** (and **figure 1.2**). The magnitude of the average winter cooling in the upper stratosphere lies in the order of 10 K per day! Since this is a three month (90 day) average, it would imply a physically impossible net temperature decrease of 900 K, if there were no compensating effects. There must therefore be compensating effects. In fact the temperature increase associated with **adiabatic compression** accompanying downward motion over the winter pole represents the most important compensating effect. This downward motion is part of a global scale meridional circulation called the **Brewer-Dobson circulation** (chapter 12).

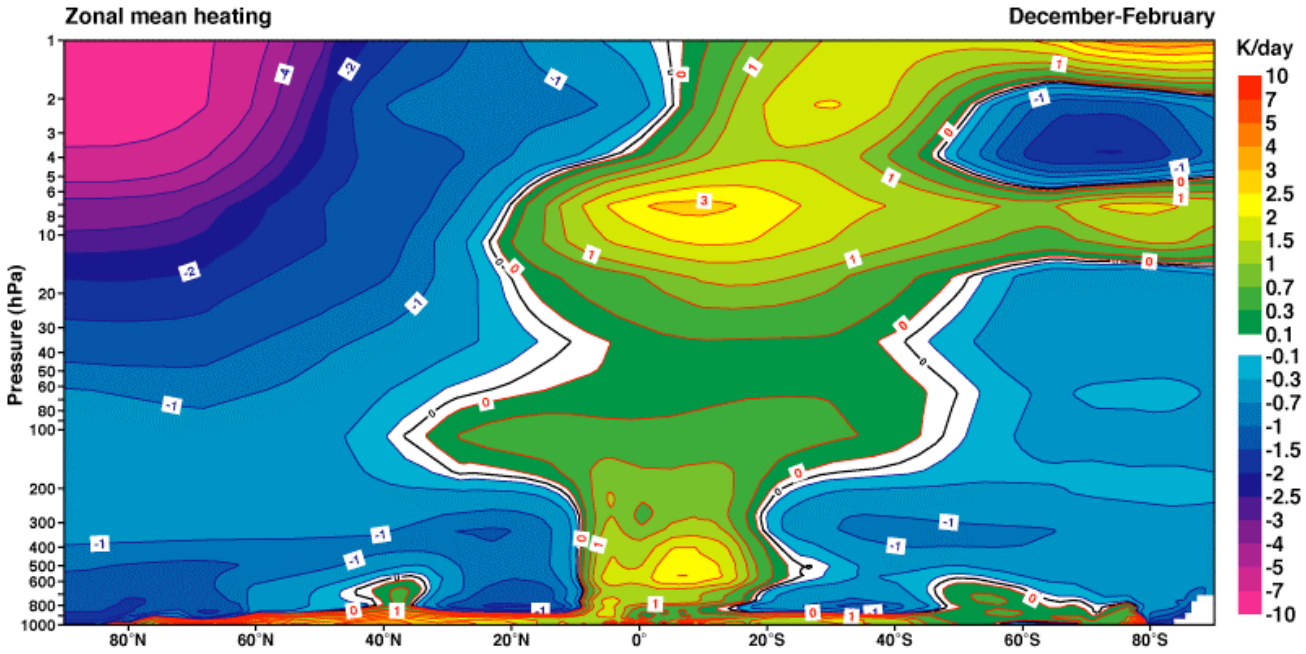

FIGURE 2.9. Time mean (for the months December, January and February and the period 1979-2001), zonal mean diabatic heating $d\theta/dt$ [K/day], also referred to as the "cross-isentropic flow". From the **ERA-40 Atlas**. ERA-40 project report series number 19 (see http://www.ecmwf.int/research/era/ERA-40_Atlas/docs/index.html). See also **figure 1.2**.

At timescales smaller than τ_E radiation will **not** be the dominant process affecting the temperature in Earth's atmosphere. Thus, since τ_E>>1 day in the major part of the atmosphere, we will hardly observe the effects of the diurnal variation of Solar irradiance. On the other hand, the yearly variation of the Solar irradiance, which is most extreme at the poles, will strongly determine the temperature in the atmosphere. This is evident in the **stratosphere, which is cold over the winter pole and warm over the summer pole** (**figure 2.7**). However, in the mesosphere (the layer between the heights of 50 km and 100

km) the reverse is the case. Surprisingly, **the summer mesosphere and also the tropopause region over the equator, are the coldest regions in the Earth's atmosphere**, even though the winter pole receives no Sunlight for 6 months, while insolation over the summer pole and over the equator is relatively high. The temperature in these regions is obviously not determined by radiation only.

PROBLEM 2.2. Radiative times scale on other planets.
Estimate the radiative equilibrium timescale for the atmospheres of, respectively, Venus, Earth, Mars and Titan using (2.20) and the data in table 2.2. If possible, compare this timescale to the planet's Solar day and its year (assume ε=1). The rotation rates of Venus, Earth, Mars and Titan in units of 10^{-5} s^{-1} are, respectively, 0.03, 7.29, 7.09 and 0.456. The orbital periods of Mars and Venus are 687 and 224 Earth days, respectively. Assume that T_s is representative for the radiative equilibrium temperature. (additional information about the properties of these planets can be found on the internet). Discuss the applicability of the theory to the situation on the planet Venus.

Planet	p_s(hPa)	c_p(J kg^{-1}K^{-1})	R(J kg^{-1}K^{-1})	g(m s^{-2})	T_s(K)
Venus	92000	850	190	8.89	731
Earth	1000	1005	287	9.81	288
Mars	7	830	190	3.74	214
Jupiter	1000	12360	3750	24.25	165
Saturn	1000	14010	3890	10.00	134
Titan	1500	1040	290	1.35	94

TABLE 2.2. Some properties of planetary atmospheres. T_S is the temperature at the surface; p_S is the pressure at the surface, R is the specific gas constant, g is the acceleration due to gravity and c_p is the specific heat capacity at constant pressure. Titan is a satellite or Moon of Saturn. The atmospheres Venus and Mars consists mainly of carbon dioxide (about 96%). The atmospheres of Jupiter and Saturn contain mainly hydrogen (about 85%) and helium (about 14 %). The atmosphere of Titan contains mainly nitrogen (65-98%). Water in the atmosphere of Earth and methane in the atmosphere of Titan frequently undergo phase changes, leading to the formation of water clouds and methane clouds, respectively. Source: Sanchez-Lavega, A., S. Perez-Hoyos and Ricardo Hueso, 2004: Clouds in planetary atmospheres: a useful application of the Clausius-Clapeyron equation. **Am.J.Phys**, **72** (6),

2.5 Observed radiation balance

An estimate of the global average energetics of atmosphere-Earth system, based among other on observations from satellites since the 1980's is displayed in **figure 2.10**. The average energy flux incident on a level surface outside the atmosphere is 342 W m^{-2}. About 31 % (the **planetary albedo**) of this energy is **scattered or reflected** back to space by molecules, tiny particles in the air (called "**aerosols**"), clouds and the Earth's surface. This leaves 235 W m^{-2} to warm the Earth's surface and the atmosphere. Averaged over long time and over the total area of the planet, the outgoing radiation must be equal to the incoming radiation. The surface latent heat flux is estimated from the observed global average annual average precipitation. The surface sensible heat flux is deduced as a residual from the condition of surface energy balance.

Some of the **outgoing radiation at the top of the atmosphere (OLR-TOA)** comes directly from the Earth's surface (i.e. $(1-\varepsilon)U$ in **figure 2.6**). The bulk of the terrestrial

radiation is intercepted by the atmosphere and re-emitted both upwards and downwards, from the clouds and by greenhouse gases such as water vapour (mainly in the troposphere), carbon dioxide (at all levels in the troposphere and the stratosphere), methane, ozone in the stratosphere and several other constituents, but not by the principal constituents of the atmosphere: nitrogen and oxygen. Clouds are strong reflectors of Solar radiation and thus act to cool the Earth's surface.

The Earth's surface loses energy by radiation, by evapotranspiration and by diffusive and turbulent transport of sensible heat. **Evapotranspiration** is the process whereby the Earth's surface and soil loses water by direct evaporation as well as transpiration by plants through stomata leaf surfaces. Water vapour entering the atmosphere from the Earth's surface is transported upwards by currents to the condensation level whereupon the latent heat is released. A large portion of the evaporation from the Earth's surface occurs over the subtropical oceans. Most of this water vapour is transported towards the ITCZ (see section 1.11 and 1.28) by the Trade winds. By far most of the latent heat is released in the tropics over the ITCZ. This is an extremely important part of Earth's energy balance.

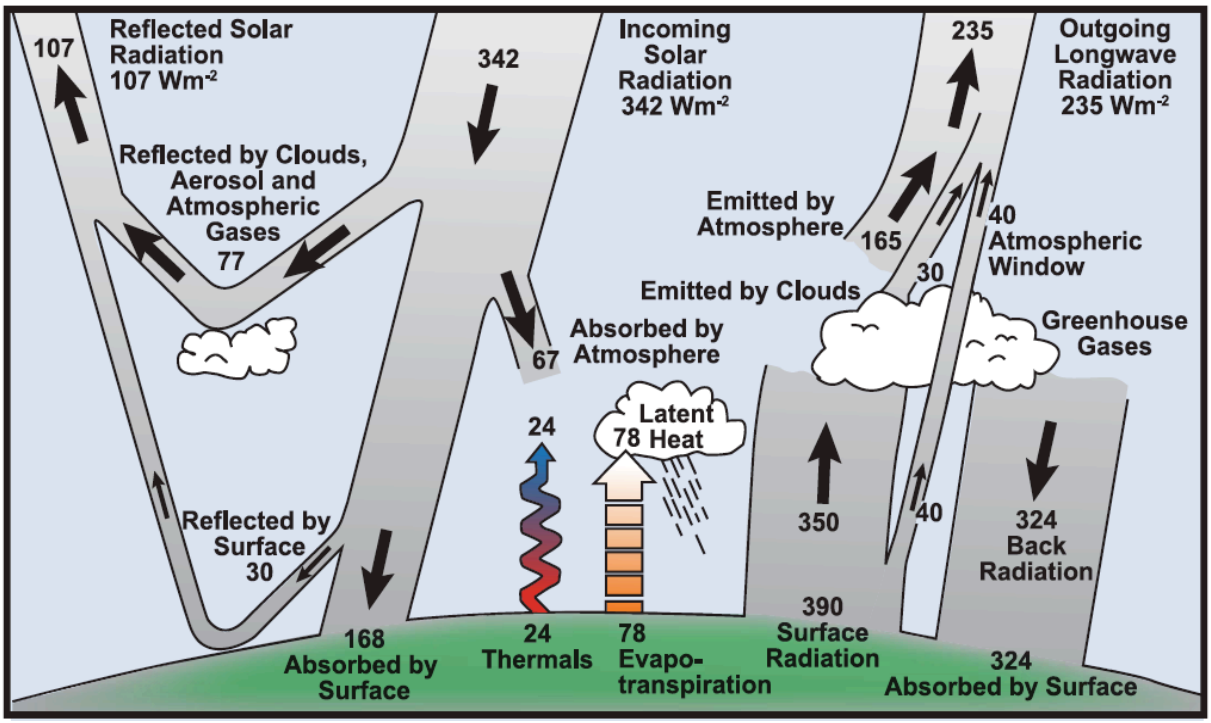

FIGURE 2.10. Earth's energy balance (J.T. Kiehl and K.E. Trenberth, K.E., 1997: Earth's annual global energy budget. **Bull.Am.Meteorol.Soc., 78,** 197-208), estimated from satellite measurements during the period 1985-1989 assimilated with a radiative-convective model, assuming that the **system is in equilibrium** (see sections 2.7 and 2.8 and **Box 2.8**). The "atmospheric window" is discussed in section 2.17. The influence of the water cycle (evaporation at the surface, latent heat release in clouds, clouds and precipitation) on the energy balance is focused on in sections 2.10-2.14 and 2.18-2.19. More versions of this iconic diagram, which appeared as figure 2 in the IPCC report of 2001 and as figure 1 in the IPCC report of 2007, have been published recently. **Figure 2.25** shows one of these updated versions of this diagram.

The top of the atmosphere net absorbed Solar radiation (ASR) is obviously a strong function of the latitude. However, as is illustrated in **figure 2.11**, there are strong departures in the ASR from what would be expected from the Sun-Earth geometry alone. These are the

result of persistent bright (reflecting) clouds in certain regions, such as over Indonesia, South East Asia, the Amazon region and Central Africa. Dark oceans reflect relatively little Solar radiation, expecially at low latitudes (the albedo of the sea surface is a function of Solar zenit angle). **Figure 2.11** does not show the ice- and snow-covered regions, poleward of 60°. Absorbed Solar radiation in these regions is relative low because of the high albedo of snow. The areal extent of these regions is an important factor in climate sensitivity.

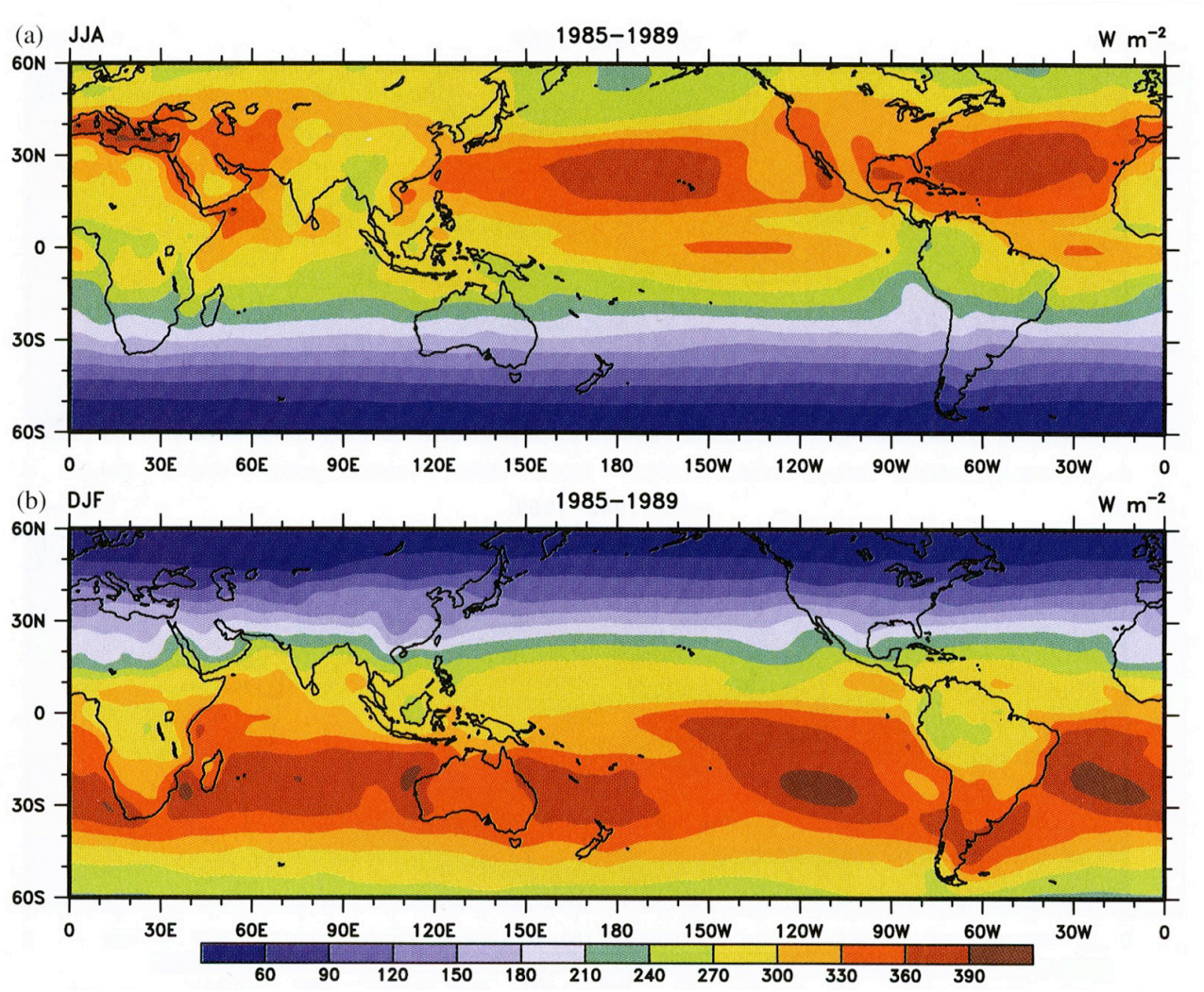

FIGURE 2.11. Top of the atmosphere absorbed Solar radiation (ASR) for the period 1985-1989 for (a) June, July and August (JJA), and (b) December, January and February (DJF). The contour interval is 30 W m^{-2} (from Trenberth, K.E., and D.P. Stepaniak, 2004: The flow of energy through the Earth's climate system. **Q.J.R.Meteorol.Soc., 130**, 2677-2701).

The distribution of the top of the atmosphere outgoing longwave radiation (OLR-TOA) (**figure 2.12**) reflects regions with persistent high cloud-tops, such as the **intertropical convergence zone (ITCZ)** (the region of upward motion separating the winter and summer **Hadley circulation**, see chapters 1 and 5), and the midlatitudes where numerous cyclones produce relatively persistent cirrus clouds. Over the dry cloud-free regions (e.g. the Sahara and Middle East in summer), most terrestrial (surface) radiation escapes to space.

The distribution of net radiation at TOA (positive downwards) (**figure 2.13**) is dominated by the latitude dependence. The high convective cloud-tops in the tropics are bright and

reflect Solar radiation, but they are also cold and hence emit relatively little long wave radiation. Therefore, the effects of these clouds, seen in **figures 2.11** and **2.12**, cancel when looking at the net effect. The main signal in the net outgoing radiation from the clouds comes from the low stratocumulus clouds that persist over cold ocean surfaces, such as off the west coasts of Peru, California and Namibia. These extensive cloud decks also reflect Solar radiation, but emit more long wave radiation because the low cloud tops (at about 2 km height above sea level) are relatively warm. Remarkably, the zero line in the average net radiation lies at 10° north of the equator (**Why?**). The other remarkable feature of **figure 2.13** is the minimum in net radiation over the Sahara desert and the Middle East in summer (JJA). This effect is similar in origin to the effect of the stratocumulus cloud decks.

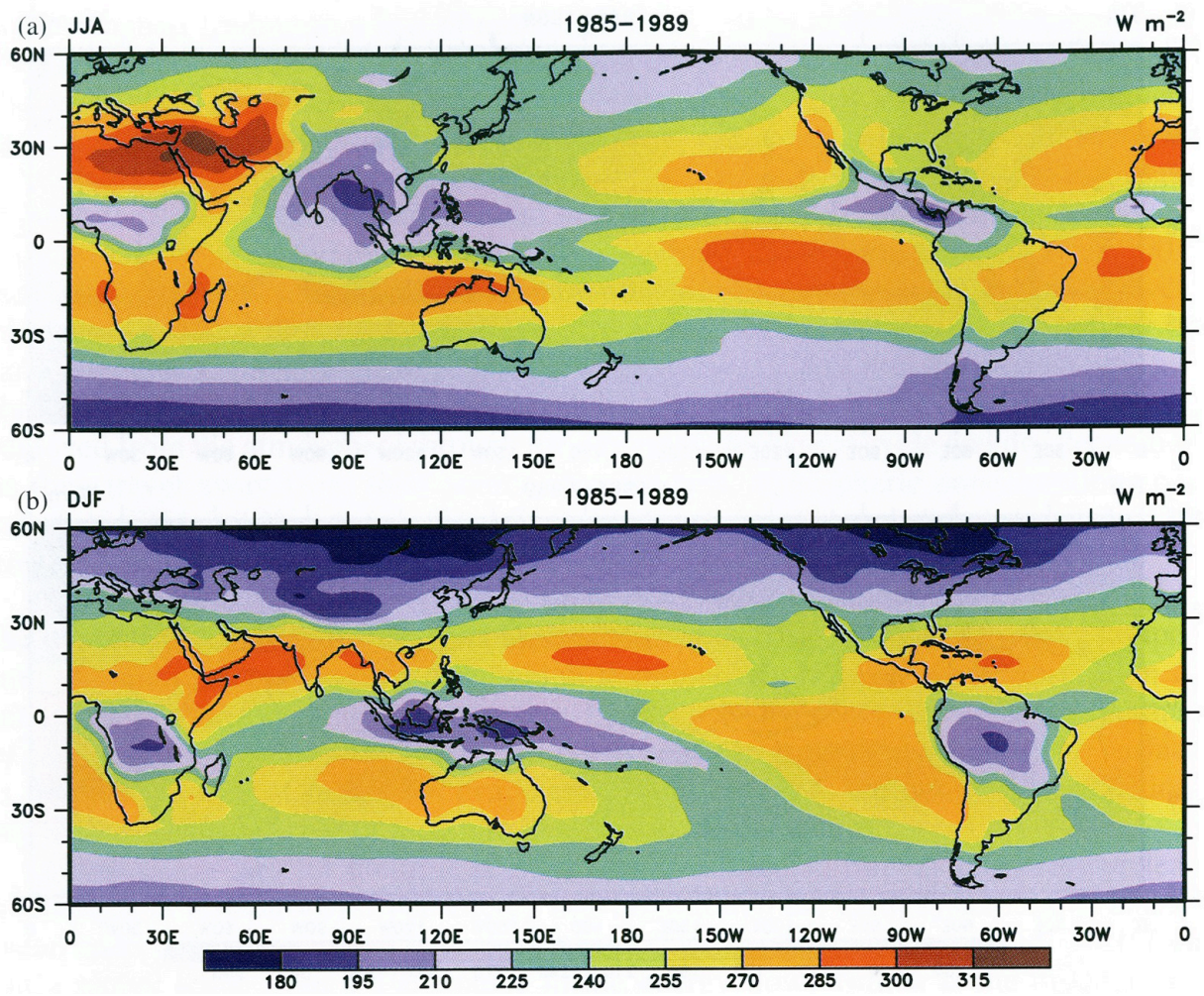

FIGURE 2.12. Top of the atmosphere outgoing long wave radiation (OLR-TOA) for the period 1985-1989 for (a) June, July and August (JJA), and (b) December, January and February (DJF). The contour interval is 15 Wm^{-2} (from Trenberth, K.E., and D.P. Stepaniak, 2004, **Q.J.R.Meteorol.Soc.**, **130**, 2677-2701).

2.6 Climate-sensitivity and the runaway greenhouse effect

Outgoing longwave radiation at TOA (OLR-TOA) in the one layer model (**figure 2.6**) is given by

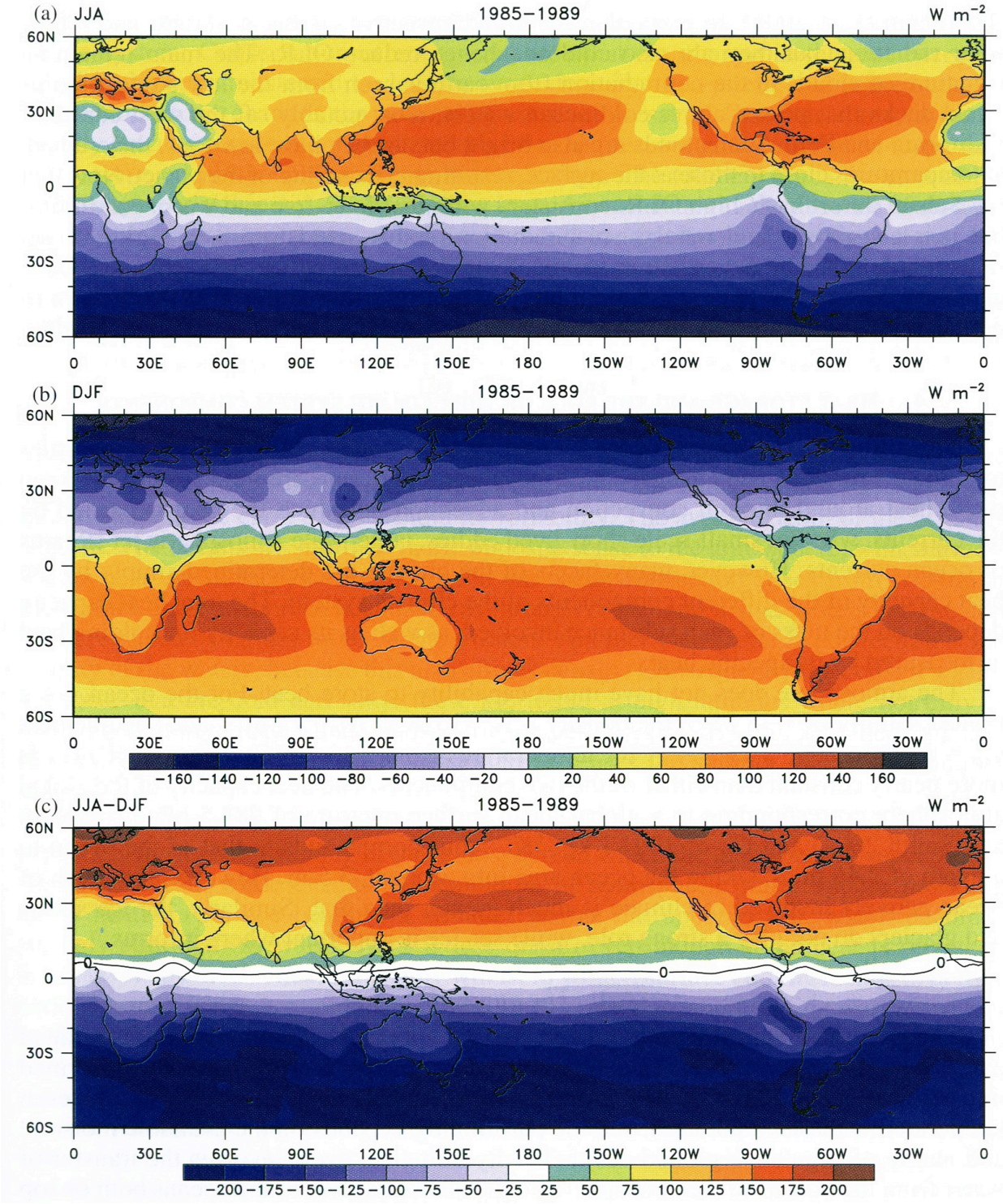

FIGURE 2.13. Top of the atmosphere net radiation (positive downwards) for the period 1985-1989 for (a) June, July and August (JJA), (b) December, January and February (DJF) and (c) the difference JJA-DJF. The contour interval is 20 W m^{-2} in (a) and (b) and 25 W m^{-2} in (c) (from Trenberth, K.E., and D.P. Stepaniak, 2004, **Q.J.R.Meteorol.Soc.**, **130**, 2677-2701).

$$OLR - TOA = (1-\varepsilon)U + B = (1-\varepsilon)\sigma T_S^4 + \varepsilon\sigma T_A^4 . \qquad (2.21)$$

With (2.10) we can eliminate T_A from this expression, yielding

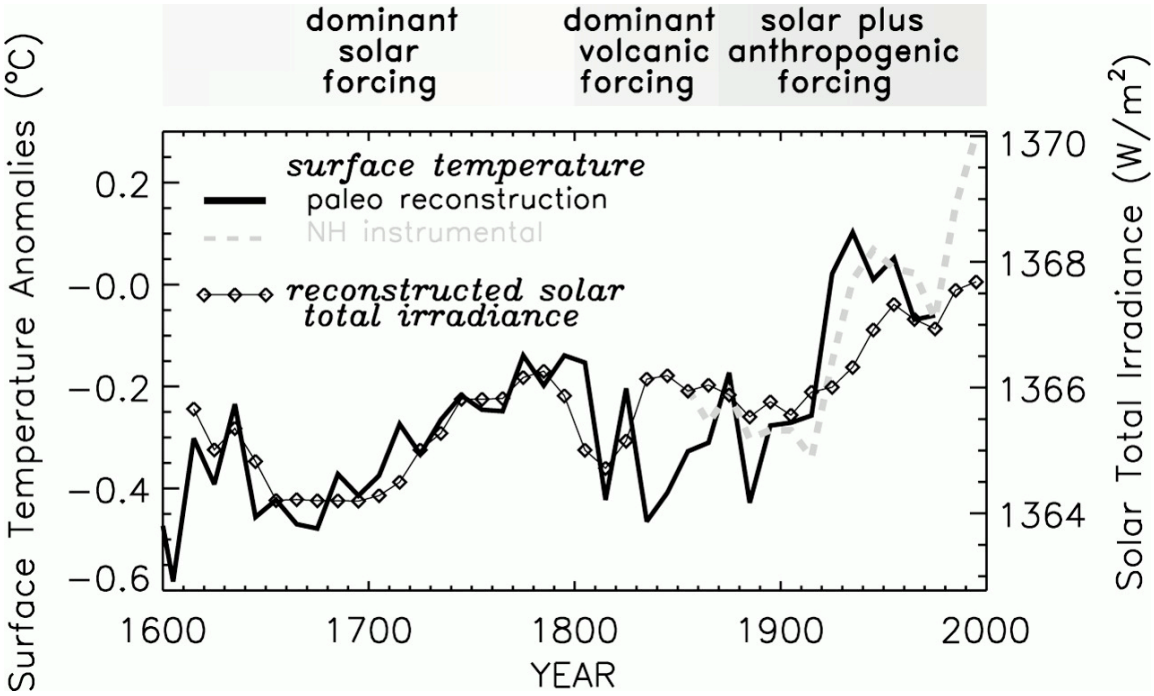

FIGURE 2.14. Decadally averaged values of Solar total irradiance and northern hemisphere summer temperature anomalies from 1610 to the present. The dark solid line is the northern hemisphere summer surface temperature reconstruction from paleoclimate data (primarily tree rings), scaled to match the northern hemisphere instrumental data (*grey dashed line*) during the overlap period. From J.Lean, 1997: The Sun's variable radiation and its relevance for Earth**. Ann.Rev.Astron.Astrophys**., 33-67. More about the relation Sun and climate can be found in D.Rind, 2002, The Sun's role in climate variations. **Science**, 296, 673-677.

$$\boxed{OLR - TOA = \left(\frac{2-\varepsilon}{2}\right)\sigma T_S^4}. \tag{2.22}$$

The equilibrium temperature of the Solar heated planet is found from the equation stating that there is balance between OLR-TOA and absorbed Solar radiation (ASR), i.e.

$$\left(\frac{2-\varepsilon}{2}\right)\sigma T_S^4 = \frac{S_0}{4}(1-\alpha). \tag{2.23}$$

The sensitivity of the surface temperature to variations in incoming Solar radiation can be investigated by deriving an expression for the surface temperature change for a 1% change in Solar irradiance, i.e. by the parameter

$$\mu \equiv \frac{S_0}{100}\frac{dT_S}{dS_0}\ .$$

.

From (2.23) we find (assuming that ε and α do not vary with T_S)

$$\mu \equiv \left(\frac{10^{-2}}{8(2-\varepsilon)}\right)\left(\frac{S_0(1-\alpha)}{\sigma T_S^3}\right). \tag{2.24}$$

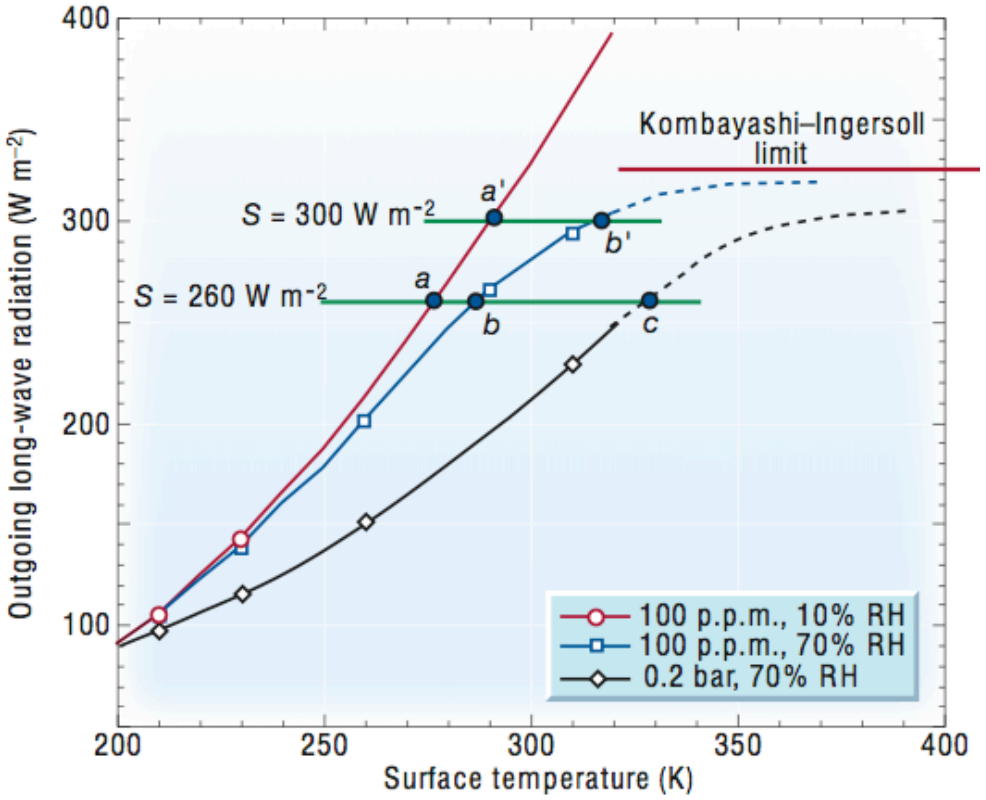

FIGURE 2.15. Equilibrium outgoing long wave radiation at the top of the atmosphere (OLR-TOA) as a function surface temperature computed with a standard radiative transfer model (section 2.7 and onward) for (a) a cloudless atmosphere with 100 ppm CO_2 and 10% relative humidity, (b) a cloudless atmosphere with 100 ppm CO_2 and 70% relative humidity, (c) a cloudless atmosphere with 0.2 bar CO_2 and 70% relative humidity. See the text for further interpretation (from R.T. Pierrhumbert, 2002: The hydrological cycle in deep-time climate problems. **Nature**, **419**, 191-198).

Apparently, **climate sensitivity to variations in Solar irradiance increases with increasing values of the atmospheric emissivity**, or greenhouse gas concentrations. On the other hand, climate sensitivity to variations in Solar irradiance decreases with increasing values of the albedo.

For α=0.3 and ε=0.7, μ=0.5 K, i.e. for a 1% change in the Solar irradiance, there is a 0.5 K change in the surface temperature. In pre-industrial decades from 1610 to 1800 surface temperature increased by 0.26 K, as irradiance increased by 2 W m^{-2} (**figure 2.14**). Extending this relationship to the present yields a Solar induced surface temperature increase of 0.25 K between 1850 and 2000, or about half the observed warming during the industrial era. The other half, presumably, comes from the increase in greenhouse gas concentrations.

Figure 2.15 shows OLR-TOA as a function of surface temperature, computed with a sophisticated radiation scheme under the following assumptions: (1) the vertical temperature profile is given by the **moist adiabat** in the troposphere (the "moist adiabat" is defined in section 1.18, **Box 1.6**)[67], superposed by 200 K isothermal stratosphere, and (2) the relative humidity is constant.

We see that addition of a greenhouse gas reduces OLR-TOA for fixed surface

[67] The average "moist adiabatic lapse rate" is about 6.5 K km^{-1} (Table 1 of Box 1.6).

temperature. The surface temperature (T_S) must increase in order to achieve a balanced radiation budget, in which absorbed Solar radiation is equal to OLR-TOA. With S=260 W m^{-2} (S is the absorbed Solar radiation), 100 ppm CO_2 and 10% relative humidity, T_S=276 K (point *a* in **figure 2.15**). If the relative humidity is increased to 70 %, T_S increases to 288 K (point *b*). If the amount of CO_2 is increased to the extremely large value of 0.2 bar (200 hPa), T_S increases to 330 K (point *c*).

The slope of the curves in **figure 2.15** is d(*OLR-TOA*)/dT_S. In the one-layer model this quantity is given by (see eq. 2.22)

$$\frac{d}{dT_S}(OLR-TOA) = 2(2-\varepsilon)\sigma T_S^3 . \qquad (2.25)$$

This slope is positive and decreases with increasing ε, i.e. with increasing greenhouse gas concentration, as is observed in **figure 2.15**, implying an increased climate-sensitivity with increasing ε. This is illustrated in **figure 2.15** by increasing the net absorbed Solar radiation from 260 Wm^{-2} to 300 Wm^{-2}. With 10% relative humidity, the warming from point *a* to *a*' is 14 K, but with 70 % relative humidity, the warming from point *b* to *b*' is 30 K. The difference between these two numbers, i.e. 16 K, is due to the **water vapour feedback** (section 2.20), which would make ε in eq. 2.23 temperature-dependent, i.e. $\varepsilon=\varepsilon(T_S)$.

Repeating the derivation of eq. 2.25 with this assumption we find

$$\frac{d}{dT_S}(OLR-TOA) = 2(2-\varepsilon)\sigma T_S^3 - \frac{\sigma T_S^4}{2}\frac{d\varepsilon}{dT_S} . \qquad (2.26)$$

If we assume that relative humidity remains constant with increasing temperature, then

$$\frac{d\varepsilon}{dT_S} > 0 . \qquad (2.27)$$

Therefore, the water vapour feedback increases climate sensitivity, because it reduces the slope of the curves in **figure 2.15**.

The extreme manifestation of high climate sensitivity due to the water vapour feedback is the **runaway greenhouse**. In **figure 2.15** this is manifest by the flattening of the curves at OLR-values higher than 320 Wm^{-2}. In the one layer model this happens when

$$\frac{d\varepsilon}{dT_S} \geq \frac{4(2-\varepsilon)}{T_S} . \qquad (2.28)$$

The probability that this occurs increases with increasing temperature, T_S, and increasing emissivity, ε. Thus, there appears to be a limit to the rate of energy loss of a planetary atmosphere by infrared radiation. This limit is referred to as the **Kombayashi-Ingersoll limit**[68]. However, this limit is reached only if dε/dT_S (the l.h.s. of the inequality 2.28) does

[68] The Kombayashi-Ingersoll limit is sometimes also referred to as the Simpson-Kombayashi-Ingersoll limit (SKI-limit), in honour of the British meteorologist, G.C. Simpson, who published a series of articles on this subject in the 1920's. This rather esoteric theoretical concept is not of real importance to Earth's atmosphere because of the existence of a so-called **infra-red window** and interesting non-linear effects of clouds on the radiation balance (sections 2.17 and 2.18).

not decrease faster than $4(2-\varepsilon)/T_S$ (the r.h.s. of the inequality 2.28) with increasing T_S. Because of the existence of an "infrared window" in the absorption spectrum of water vapour and carbon dioxide (section 2.17), ε will probably increase only very slowly with increasing temperature.

When the absorbed Solar radiation exceeds the Kombayashi-Ingersoll limit (**figure 2.15**), the surface temperature continues to increase until all the water on the planet has been evaporated into the atmosphere. This is followed by a disassociation of water into hydrogen and oxygen, after which the light hydrogen escapes to space, making the loss of water irreversible. This is believed to be the scenario through which Venus became inhabitable.

The picture of the runaway greenhouse effect that is sketched above is based on computations in which clouds are neglected. The complicated effects of clouds on the energy balance can change this picture completely, as is shown in sections 2.18 and 2.19 and **Box 2.12**.

Since the time of Arrhenius (1896) **climate sensitivity** is defined as the change of the global and annual average surface temperature following a doubling of the CO_2 concentration. A more precise definition refers to "**equilibrium climate sensitivity**", which is the **change of the global average *equilibrium surface temperature* following a doubling of the CO_2 concentration**. Equilibrium climate sensitivity was first estimated by Svante Arrhenius in 1896[69], relying on surface radiometric observations, especially those recorded by Samuel Langley in the 1880's. Assuming that the relative humidity in the atmosphere is not affected by the doubling of CO_2 concentration, he found a value of 5 K. For nearly 60 years there was no significantly better estimate of equilibrium climate sensitivity until Syukuro Manabe and Richard Wetherald (1967)[70] came up with a much lower estimate of 2 K. Of course, in contrast to Arrhenius, Manabe and Wetherald had knowledge of Planck's law (**Box 1.3**), as well as better empirical estimates of the wavelength dependence of absorption coefficients (**Box 2.3**). They also incorporated in their model an explicit feedback between surface fluxes of sensible and latent heat[71] and net radiation at the surface. Moreover, Manabe and Wetherald assumed that the temperature profile adjusts to the moist adiabatic lapse rate (**Box 1.6**). This assumption determines the vertical dependence of latent heat release. They followed Arrhenius' assumption of constant relative humidity. More specifically, they assumed that the global-, annual average relative humidity, RH, obeys the following equation (compare with the observations shown in **figure 1.13**):

$$RH = RH_g\left(\frac{\sigma - 0.02}{1 - 0.02}\right), \tag{2.29}$$

where RH_g is the relative humidity at the ground (Earth's surface) (77 %) and

$$\sigma = \frac{p}{p_s}, \tag{2.30}$$

with p_s the pressure at the Earth's surface. Because the r.h.s. is negative when $\sigma<0.02$ (in the stratosphere), the mixing ratio of water vapour is set at a fixed very low value of 3×10^{-6} if

---

69 On the influence of carbonic acid in the air upon the temperature of the ground. **Phil. Mag., 41**, 237-276 (1896).

70 Thermal equilibrium of the atmosphere with a fixed distribution of relative humidity. **J.Atmos.Sci., 24**, 241-259 (1967)

71 Latent heat is the heat that will be released if all moisture in the air is condensed to water or frozen to ice.

$\sigma \leq 0.02$. Since the publication of Manabe and Wetherald's paper the estimates of equilibrium climate sensitivity have not been narrowed down further (**Box 2.11**). The estimated value of this parameter very likely lies between 1.5 K and 5 K.

2.7 Radiative equilibrium with homogeneous distribution of greenhouse gases

The one layer radiation model (**figure 2.6**), can be made more realistic by dividing the atmosphere into more than one layer, but retaining the assumption of two separate streams of radiation, namely "Solar radiation" and "planetary radiation", that are absorbed and emitted at a rate independent of wavelength[72].

The energy balance of the Earth's surface below an atmosphere that is divided into K homogeneous layers ("shells")[73] is determined by the following components (**figure 2.16**).

(1) Radiation emitted by each atmospheric layer and reaching the Earth's surface (B).
(2) Radiation received from the Sun (S).
(3) Radiation emitted by the Earth's surface itself (U_S).
(4) Heat-transfer by conduction or convection to the atmosphere (H).
(5) Heat-transfer by conduction to soil layers below the surface (G).
(6) Heat-transfer by evaporation of water from the surface (L).

The first contribution is expressed as follows:

$$B = \sum_{m=1}^{K} \varepsilon_m (1-\varepsilon_{m+1})(1-\varepsilon_{m+2})\ldots(1-\varepsilon_K)\sigma T_m^4 \qquad (2.25)$$

Here ε_m and T_m are, respectively, the emission coefficient and the temperature of layer m. **The layer index, *m* increases from top to bottom**. This means that layer 1 is the highest layer, while layer K is the lowest layer, just above the Earth's surface.

The second contribution to the energy balance of the Earth's surface (the radiation received from the Sun) is given by

$$S = (1-\alpha) Q \tau_1 \tau_2 \ldots \tau_K . \qquad (2.26)$$

Here τ_m is the transmittance of a layer with index m and Q is the Solar irradiance at the top of the atmosphere.

The third contribution, the emission of radiation by the Earth's surface (emissivity=ε_g)[74],

$$U_S = \varepsilon_g \sigma T_S^4 . \qquad (2.27)$$

---

[72] Referred to as the "semi-grey" approximation.

[73] We assume that each layer has the same mass per unit area, i.e. the pressure difference, Δp, between each level is constant.

[74] The emissivity , ε_g, of most "natural" surfacesis greater than 0.9. For a water surface it is 0.92-0.96. For wet surfaces it is generally greater than for dry surfaces. The emissivity of aluminium foil is less than 0.05.

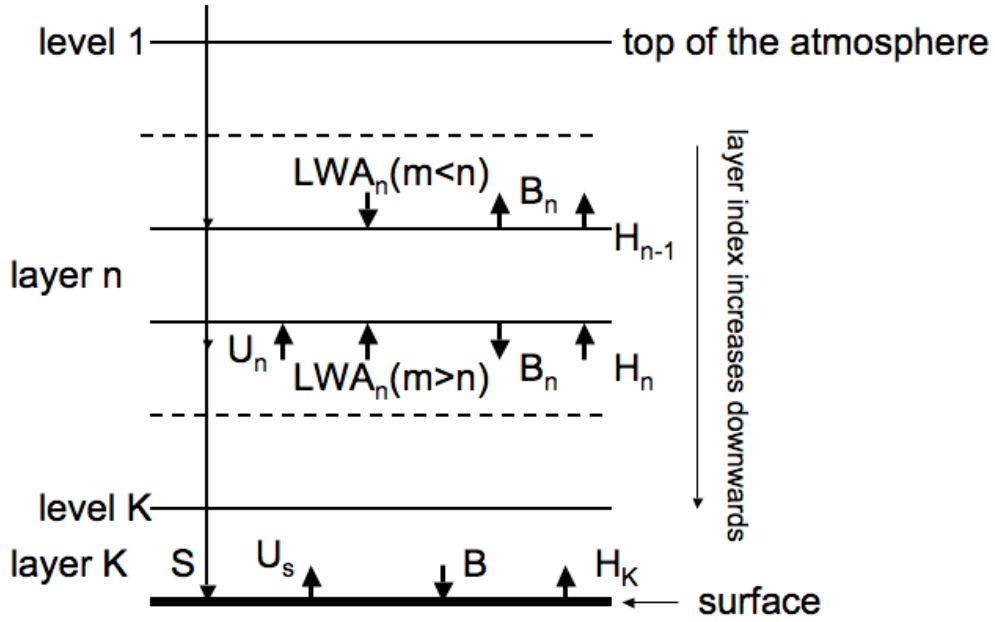

FIGURE 2.16. The K-layer radiative-convective "shell" model of the atmosphere (see the text for further explanation).

The fourth contribution is of a totally different nature. It will be neglected here. Section (2.8) is devoted to a relatively detailed discussion of this term.

The fifth and sixth contribution require consideration of the theory of heat diffusion through soil and the theory of evaporation, respectively. This is outside the scope of this chapter.

Assuming that the Earth's surface has negligible heat capacity, the energy fluxes must be in balance, i.e.

$$B + S = U_S. \tag{2.28}$$

The energy balance of an atmospheric layer (denoted by index n) is determined by the sum of the following terms (**figure 2.16**).

(1) Long wave radiation coming from other layers and absorbed by the layer in question (LWA_n).

(2) Terrestrial radiation (coming directly from the Earth's surface) (U_n).

(3) Solar radiation absorbed by the layer in question (S_n).

(4) Long wave radiation emitted downward and upward emitted by the layer in question ($2B_n$).

(5) Convergence of the convective heat flux (H_n-H_{n-1}).

Long wave radiation coming from layer m (with temperature T_m) is expressed mathematically as follows:

$$\text{if } m < n,\ LWA_n(m) = \varepsilon_m(1-\varepsilon_{m+1})(1-\varepsilon_{m+2})..(1-\varepsilon_{n-1})\sigma T_m^4 \tag{2.29a}$$

(**downwelling radiation**);

$$\text{if } m > n,\ LWA_n(m) = \varepsilon_m(1-\varepsilon_{m-1})(1-\varepsilon_{m-2})..(1-\varepsilon_{n+1})\sigma T_m^4\ . \tag{2.29b}$$

(**upwelling radiation**)

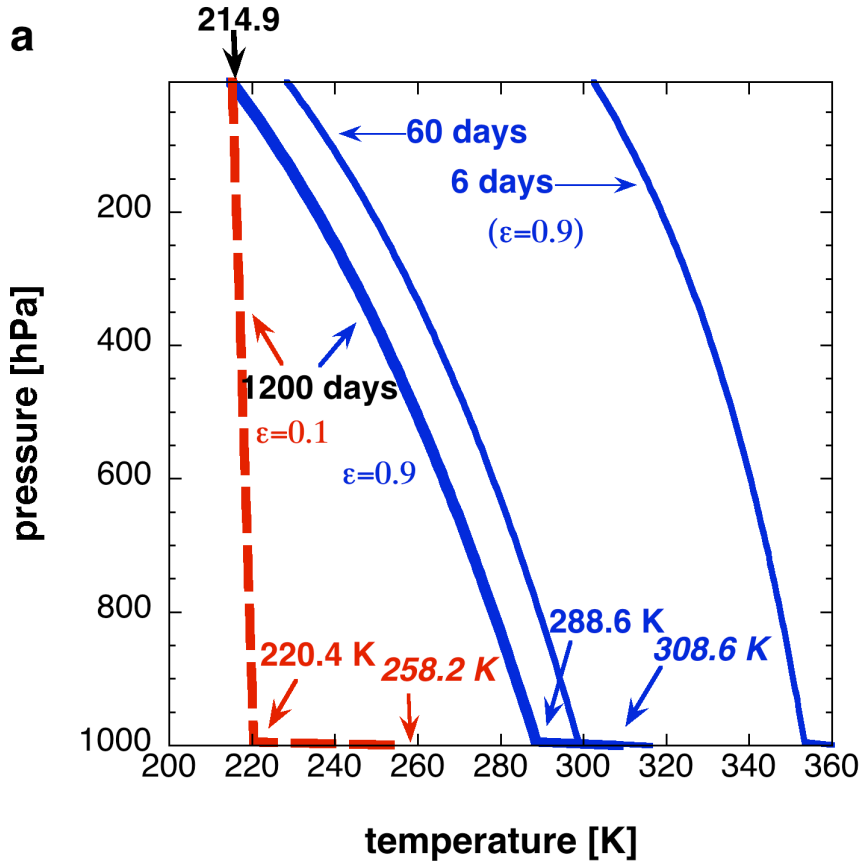

FIGURE 2.17a: for caption, see next page.

The net absorbed terrestrial radiation by layer n is

$$U_n = \varepsilon_n(1-\varepsilon_{n+1})(1-\varepsilon_{n+2})...(1-\varepsilon_K)U_S\,. \tag{2.30}$$

The net absorbed solar radiation by layer n is

$$S_n = (1-\tau_n)\tau_{n-1}\tau_{n-2}...\tau_1 Q \tag{2.31}$$

The long wave radiation emitted downward by the layer (n) is

$$B_n = \varepsilon_n \sigma T_n^4\,. \tag{2.32}$$

This radiation is also emitted upwards. Therefore the total emitted radiation is $2B_n$.

The convective heat flux is the subject of section 2.8. It is neglected here, i.e.

$$H=0 \tag{2.33}$$

If the thickness (in Pa) of the layer is Δp, and the layer is in hydrostatic balance its heat capacity is $c_p\Delta p/g$ [J K^{-1}m^{-2}]. We can now write down the energy balance of a layer (index n) as

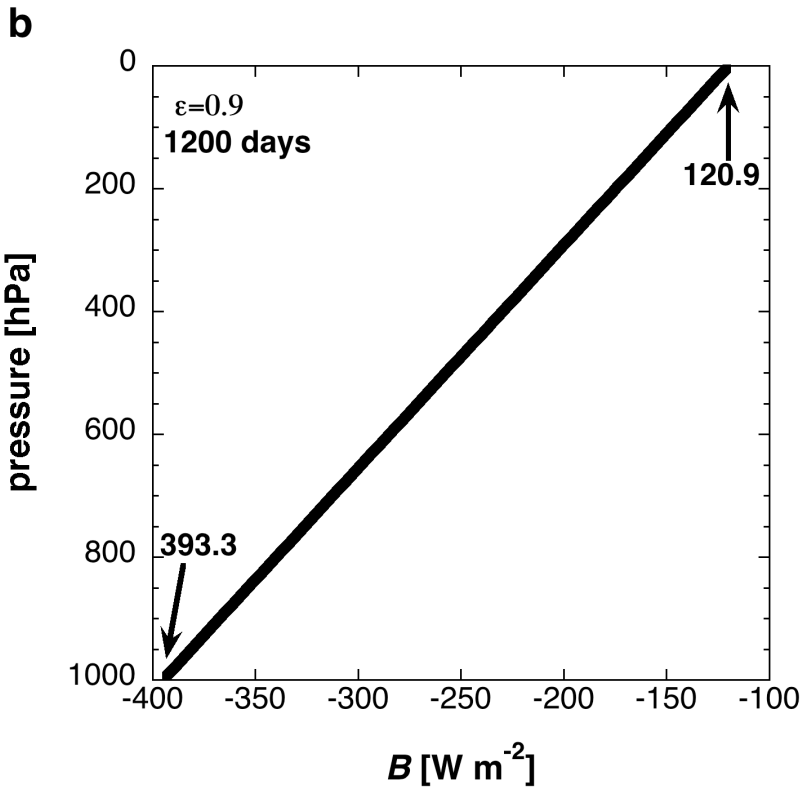

FIGURE 2.17. (a) (see previous page) Approach to a state of pure radiative equilibrium from an isothermal atmosphere at 360 K (at t=0) for a *homogeneous* atmosphere which is transparent to Solar radiation and transmits 10% of the radiation emitted by the Earth's surface to space (i.e. for the total column, ε=0.9) (solid blue curves). Solar irradiance is equal to 342 W m^{-2}, albedo is equal to 0.3 and there are *no* sensible heat fluxes. The red dashed line represents the approximate radiative equilibrium solution for ε=0.1. The skin temperature (temperature of the uppermost level), indicated at the top of the **figure**, is identical in both cases, in agreement with the analytical theory (**Box 2.4**). There is a discontinuity in temperature at the Earth's surface, which is assumed to be a black body. The temperatures of the lowermost atmospheric layer and of the Earth's surface after 1200 days are indicated in blue for the case of ε=0.9, and in red for the case of ε=0.1. These temperatures are needed in problem 2.4 to compare the numerical model with the analytical theory (**Box 2.4**). When ε is large (strong greenhouse effect) more radiation is trapped in the lower layers making temperatures higher there than at upper levels. Therefore, the static stability in the radiative equilibrium decreases with increasing strength of the greenhouse effect. When the greenhouse effect is very weak (low ε), the temperature of the atmosphere approaches the skin temperature everywhere (i.e. the atmosphere becomes nearly isothermal), except at the Earth's surface (source code of the model: http://www.staff.science.uu.nl/~delde102/RCM.htm). (b) The hypothetical black body radiation, $B_n(=\sigma T_n^4)$, of each atmospheric layer (there are 100 layers, each layer is 10 hPa "thick") as a function of pressure after 1200 days for ε=0.9. B_n is a linear function of pressure. The values of B_n in the lowermost and in the uppermost layer are indicated.

$$\frac{c_p \Delta p}{g}\frac{dT_n}{dt} = U_n + S_n - 2B_n + \sum_{m=1}^{n-1} LWA_n(m) + \sum_{m=n+1}^{K} LWA_n(m). \qquad (2.34)$$

Equations (2.28) and (2.34) together constitute a simplified K-layer radiation model.Equation (2.34) can be solved numerically by dividing the time-axis into discrete steps and approximating the time derivative in (2.34) numerically using the **Runge-Kutta**

scheme[75], which is considered to be a relatively accurate **numerical approximation** for the time derivative. We can integrate (2.34) until a steady state is reached in which the net outgoing long wave radiation at the top of the atmosphere (OLR-TOA) is equal to the net absorbed Solar radiation (ASR).

Figure 2.17a shows the **approach to pure radiative equilibrium** according to the model described in this section[76], assuming 100 layers, global average, yearly average Solar irradiance ($Q=S_0/4$, with S_0=1366 W m^{-2}), *no* turbulent or convective vertical sensible heat transfer, an albedo equal to 0.3, an atmospheric short-wave net transmission coefficient equal to 1 and an atmospheric long-wave net transmission coefficient (τ_{LW}) equal to 0.1 (the blue curves). **Assuming a homogeneous distribution of longwave absorbing gases**, the latter assumption implies that the emissivity of each atmospheric model layer (of constant mass per unit area) is given by

$$\varepsilon_n = 1 - \left(\tau_{LW}\right)^{(1/K)}. \qquad (2.35)$$

In a semi-grey[77] atmosphere, that is transparent to Solar radiation (as is the case here), in radiative equilibrium, T^4 is a linear function of pressure (**figure 2.17b**), **except at the Earth's surface**, where there is a **discontinuity**. This is demonstrated in **Box 2.4**. At the top of this atmosphere (p=0) the global average temperature is about 215 K. This is referred to as the **planetary skin temperature** (**Box 2.4**).

The radiative timescale estimated from this experiment appears to be approximately 1 month, which is of the same order of magnitude as estimated from linear theory (section 2.4). However, note that even after 60 days the temperature deviates by nearly 10 K from the radiative equilibrium state. After 1200 days the net absorbed Solar radiation (ASR) (239.05 W m^{-2}) is equal to the outgoing longwave radiation at the top of the atmosphere (OLR-TOA), implying that the radiative equilibrium has been reached. In our calculation Solar radiation is absorbed completely by the Earth's surface. In reality this is only 168 W m^{-2}, while 67 W m^{-2} is absorbed by the atmosphere (**figure 2.10**).

Box 2.2. Attenuation of radiation: Bouguer-Lambert-Beer law

Suppose that a narrow beam of monochromatic radiation passes through a homogeneous medium (with constant composition). The beam is directed along the z-axis and its radiant energy per unit area, per unit time (irradiance) at $z=z_0$ is I_0. Upon transmission from $z=z_0$ to $z=z_0+\Delta z$ the irradiance changes by $\Delta I=I_1-I_0$, where I_1 represents the irradiance at $z=z_0+\Delta z$. Pierre Bougeur was the first (in 1729) to hypothesize that, if Δz *is* "sufficiently small", attenuation is proportional to Δz and to I_0, i.e.

$$\Delta I = -\kappa I_0 \Delta z\,. \qquad (1)$$

---

[75] Suppose we have an ordinary differential equation of the type, $dX/dt=F(X)$. We then find $X(t+\Delta t)$ by following the following recipe.

$X_0 = X(t),\ X_1 = X_0 + F(X_0)\Delta t/2,\ X_2 = X_0 + F(X_1)\Delta t/2,\ X_3 = X_0 + F(X_2)\Delta t,\ X_4 = X_0 - F(X_3)\Delta t/2,$

$X(t+\Delta t) = (X_1 + 2X_2 + X_3 - X_4)/3$

[76] The model source code can be found at http://www.staff.science.uu.nl/~delde102/RCM.p .

[77] Semi-grey: transparent to Solar radiation, grey to terrestrial radiation

The proportionality constant, κ, is called the **absorption coefficient**. At a distance Δz the irradiance is

$$I_1 = I_0(1-\kappa\Delta z). \tag{2}$$

At a distance $2\Delta z$ the irradiance is

$$I_2 = I_1(1-\kappa\Delta z) = I_0(1-\kappa\Delta z)^2. \tag{3}$$

Therefore, after transmission over a distance $z=N\Delta z$, the irradiance is

$$I_N = I_0\left(1-\frac{\kappa z}{N}\right)^N. \tag{4}$$

Making the individual layers very thin and keeping z constant gives the best approximation to the irradiance-change over a distance z. Therefore, the irradiance, I, at a distance z is given by

$$I = I_0 \lim_{N\to\infty}\left(1-\frac{\kappa z}{N}\right)^N \approx I_0\exp(-\kappa z). \tag{5}$$

Next to Pierre Bougeur, Johan Heinrich Beer and August Lambert also got credit for this "law".

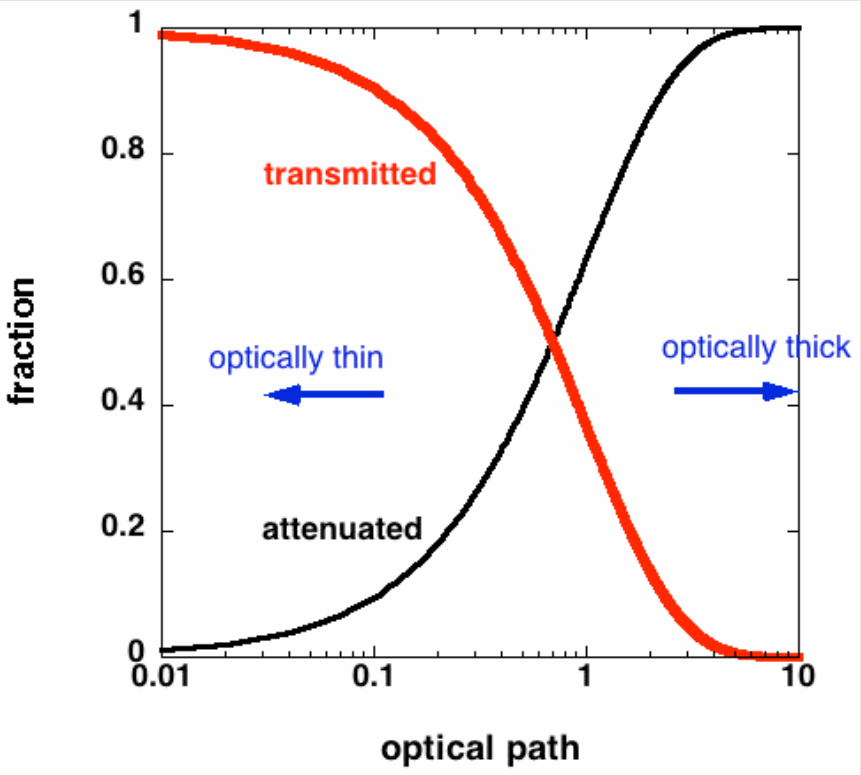

FIGURE Box 2.2. Fraction of the irradiance that is transmitted (red) or absorbed (black) as a function of optical path. An atmosphere with a net optical path much greater than 1 is called **optically thick**. An atmosphere with a net optical path much smaller than 1 is called **optically thin**.

The absorption coefficient, κ, has the dimension of inverse length. In fact, $1/\kappa$ is the distance over which a narrow beam of radiation is attenuated by a factor $1/e$. Craig Bohren and Eugene Clothiaux (2006) in their very clear exposition of the fundamentals of atmospheric radiation refer to the parameter, $1/\kappa$, as the **absorption length**. The quantity κz is referred to as the **optical path**. **Optical path is a dimensionless quantity!** Radiation passing through a medium with an optical path of 1 is attenuated by a factor $1-(1/e)=0.63$. A medium with an optical path greater than 3 absorbs more than 95% of the incoming radiation (**figure this box**). Such a medium is called "**optically thick**". If the optical path is less than 0.1 the medium is called "**optically thin**" (more than 95 % of the irradiance is tranmitted).

The absorption length of a material depends on wavelength of the transmitted radiation. The absorption length of liquid water and solid water (ice) as a function of wavelength, for example, varies by many orders of magnitude. Visible (Sun) light, having wavelengths in the range 0.38 to 0.75 μm, is attenuated much less than infrared radiation. The intensity of visible light is reduced by a factor of $1/e$ over a distance in the order of 10 m. Light with wavelengths between 0.4 and 0.5 μm, which is recognized by humans as "blue", penetrates furthest into water (about 50 m). In the infrared (around 10 μm) the absorption length of water is in the order of 10^{-4}-10^{-5} m! Therefore, infrared or long-wave radiation is absorbed very strongly by water and ice. This may be very important for the climate of Earth's atmosphere, because clouds consist of water and ice particles (section 2.13). We must, however, be careful in extrapolating the measurements of the absorption length of water and ice to a mixture of air, water droplets and ice particles (clouds).

Box 2.3. Absorption coefficient, absorption cross-section and the principal CO_2 absorption band

The absorption length of a gas depends on the concentration of its molecules, i.e. on the number of molecules per unit volume. Suppose that a layer of an absorbing gas, containing n_a molecules per unit volume, is illuminated by narrow beam of radiation. The decrease of the transmitted irradiance over a distance Δz is

$$\Delta I = \sigma_a n_a I_0 \Delta z, \qquad (1)$$

where σ_a is the **absorption cross-section (in m^2 per molecule)** and $\kappa=\sigma_a n_a$ is the **absorption coefficient**. The absorption coefficient, therefore, depends on the molecular concentration. This equation is valid best when the positions of the absorbing molecules are uncorrelated. The absorption coefficient can also be expressed as $\kappa=\sigma_a \rho_a$, where σ_a is the **absorption cross-section (in m^2 per kg)** and ρ_a is the density of the absorber.

Air is mixture of different types of molecules: Nitrogen (N_2), Oxygen (O_2), water vapour (H_2O), carbon dioxide (CO_2), methane (CH_4), ozone (O_3) and several others. Not every type of molecule absorbs radiation. In the atmosphere water vapour and carbon dioxide are the principal absorbers of long-wave radiation (largest absorption coefficient), while water vapour and ozone are the principal absorbers of short-wave radiation. In that case, eq. 1 should become

$$\Delta I = \left(\sigma_a[CO_2]n[CO_2] + \sigma_a[H_2O]n[H_2O]\right) I_0 \Delta z. \qquad (2)$$

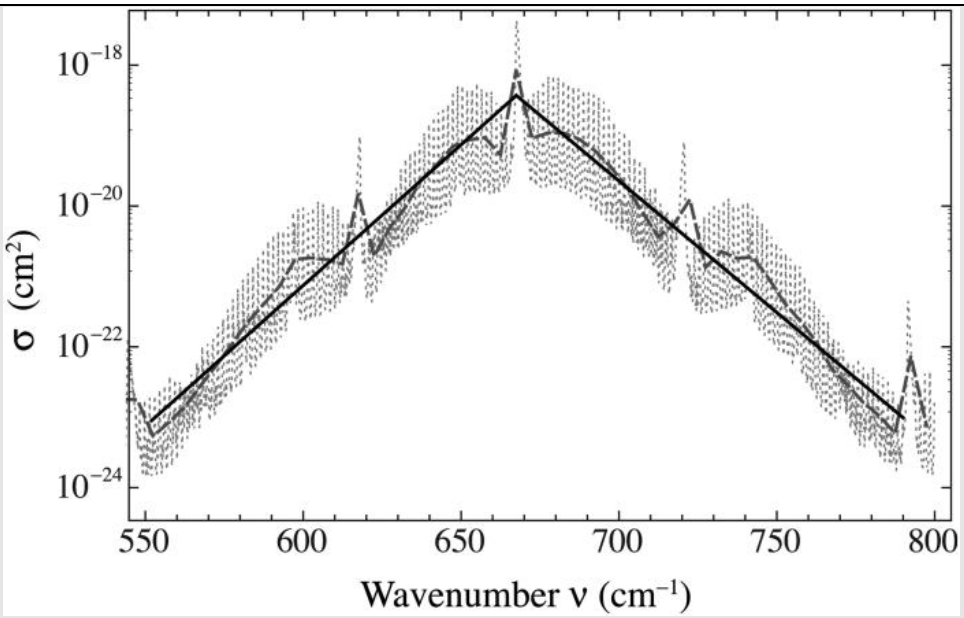

FIGURE 1 Box 2.3. Absorption cross-section per molecule of CO_2 as a function of wavenumber, ν, between 550 cm^{-1} (18 micrometre) and 800 cm^{-1} (12.5 micrometre) (light gray dotted curve). The relation between wavenumber, ν, and wavelength, λ, is $\lambda=1/\nu$. Therefore, 800 cm^{-1} corresponds to 12.5 micrometre and 550 cm^{-1} corresponds to 18 micrometre. This represents the so-called "**CO_2-absorption band**". The peak is found at 667.5 cm^{-1} (15 micrometre). Also shown are a "coarse grained" spectrum (medium gray dashed line) obtained by averaging over intervals of width 5 cm^{-1}, and a drastically simplified version (black, solid line) that is used for order-of-magnitude estimates. The analytical expression pertaining to the latter version is given in **Box 2.6**. The reasons for the fact that CO_2 absorbs radiation preferably in this wavelength band are not discussed here, but, for example, in the book by Bohren and Clothiaux (2006 (see the list at the end of this chapter). Source: Wilson, D.J. and Gea-Banacloche, J., 2012. **Am.J.Phys., 80** (4), p. 306-315.

Here, $\sigma_a[CO_2]$ and $\sigma_a[H_2O]$ are the absorption cross-sections of, respectively, carbon dioxide and water vapour and $n[CO_2]$ and $n[H_2O]$ are the molecular concentrations of these constituents in air.

A considerable complication in computing the absorption of radiation in a gas is related to the fact that the absorption cross-section depends extremely erratically on the wavelength (or wavenumber or frequency) of the incident radiation. This is illustrated in **figure 1 (this box)**, which shows the absorption coefficient of CO_2 within the wavelength interval between 12.5 and 18 micrometre. The absorption cross-section within this principal **absorption band of CO_2** varies by at least 1 or 2 orders of magnitude over extremely short wavelength intervals.

Do we have to take account of these variations when computing the transmission of radiation through the atmosphere? This would require an extreme amount of computer time. A solution to this problem is perhaps to split the spectrum into relative large wavelength intervals, $d\lambda$, whereby the absorption coefficient, $\kappa(\lambda)$, is averaged over this interval according to

$$\langle \kappa \rangle = \frac{\int \kappa(\lambda) F(\lambda) d\lambda}{\int F(\lambda) d\lambda}. \qquad (3)$$

Here, $F(\lambda)$ is the spectral irradiance per unit wavelength interval. This function is usually not constant either over any finite wavelength interval. An example of such averaging, in this

case over wavenumber intervals of 5 cm^{-1}, is indicated by the long-dashed line in the **figure (this box)**. A more drastic approximation would be a triangular function in a logarithmic plot as is shown by the solid line in the same **figure**.

In how far are we allowed to apply the Bouguer-Lambert-Beer law to finite portions of the spectrum of radiation if the absorption cross-section varies wildly over many orders of magnitude within each portion? The value of the absorption coefficient depends also on pressure and, to a lesser degree, on temperature in the gas. In the atmosphere, pressure varies by many orders of magnitude. Therefore, these effects should be taken into account also. These problems are addressed in **boxes 2.5** and **2.6**.

PROBLEM 2.3. **An atmosphere containing two greenhouse gases**

Suppose that the atmosphere can be represented in a *model* by one homogeneous layer of air that consists of a mixture of gases, of which two are greenhouse gases, which are both "well-mixed"[78]). The "bulk" long-wave emission coefficient of this atmosphere is (**Box 2.2**),

$$\varepsilon = 1 - \exp\left(-\delta_1 - \delta_2\right)$$

where δ_1 and δ_2 are the optical paths of, respectively, first and the second greenhouse gas. Let us define the following quantities:

$$\varepsilon_1 \equiv 1 - \exp\left(-\delta_1\right) \text{ and } \varepsilon_2 \equiv 1 - \exp\left(-\delta_2\right).$$

(a) Demonstrate that

$$\varepsilon = \varepsilon_1 + \varepsilon_2 - \varepsilon_1\varepsilon_2.$$

Note that, because $\varepsilon_1 \le 1$ $\varepsilon_2 \le 1$, $\varepsilon \le 1$. Now, suppose the concentration of the first greenhouse gas is increased, while the concentration of the second greenhouse gas remains constant. The bulk emission coefficient will change by

$$d\varepsilon = \left(1 - \varepsilon_2\right) d\varepsilon_1$$

The change in ε_1 can be expressed as

$$d\varepsilon_1 = d\left(1 - \exp\left(-\delta_1\right)\right) = d\delta_1 \left(\exp\left(-\delta_1\right)\right) = \left(1 - \varepsilon_1\right) d\delta_1 \ .$$

The optical path, δ_1, can be expressed as (**Box 2.3**)

$$d\delta_1 = \sigma_1 \rho_1 \Delta z \,,$$

where ρ_1 is the density of the first greenhouse gas, σ_1=0.3 $m^2 kg^{-1}$ is its constant "absorption cross-section" (**Box 2.3**) and Δz is the thickness of the atmospheric layer under consideration.

(b) If this atmospheric layer represents the full mass of the atmosphere,

[78] This implies that the mixing ratio's of both greenhaouse gases are constant in space.

$$\Delta z = \frac{p_s}{\rho g} ,$$

where p_s is the pressure at the Earth's surface and ρ is the density of the air. Why?

(c) Show that

$$\delta_2 = \sigma_2 W ,$$

where W is the vertically integrated amount of the second greenhouse gas per square metre (section 1.10) and σ_2 is its constant absorption cross-section. Approximately at what value of W does the model atmosphere become optically thick if σ_2=0.1 $m^2 kg^{-1}$?

The change in δ_1 is proportional to the change in the vertically integrated mass of the first greenhouse gas per square metre according to

$$d\delta_1 = \frac{\sigma_1 p_s}{g} \frac{d\rho_1}{\rho} .$$

So, now we can write,

$$d\varepsilon_1 = (1-\varepsilon_1)\frac{\sigma_1 p_s}{g}\frac{d\rho_1}{\rho} = (1-\varepsilon_1)\frac{\sigma_1 p_s}{g} dq_1 \approx (1-\varepsilon_1)\frac{\sigma_1 p_s}{g} dr_1 ,$$

where q_1 is the specific concentration by mass and r_1 is the mixing ratio by mass of the first greenhouse gas (section 1.8). Therefore, the bulk emission coefficient of the atmosphere after the increase of the concentration first greenhouse gas is

$$\varepsilon = (\varepsilon_1)_0 + d\varepsilon = (\varepsilon_1)_0 + (1-\varepsilon_2)(1-\varepsilon_1)\frac{\sigma_1 p_s}{g} dr_1 ,$$

where $(\varepsilon_1)_0$ is the value of ε before the increase of the concentration of the first greenhouse gas.

(d) Compute the bulk emission coefficient of this model atmosphere and the temperature, T_s, of the surface below for W=25 kg m^{-2} and q_1=390 ppmv.

(e) Compute the change in surface temperature when q_1 changes from 200 ppmv to 280 ppmv. Do this for W=25 kg m^{-2}, for W=10 kg m^{-2} and for W=1 kg m^{-2}. The specific gas constant of the first greenhouse gas is 189 J K^{-1} kg^{-1}.

PROBLEM 2.4 Comparing the model with analytical theory

Show that the model results, displayed in figure 2.17, agree with the theory of **Box 2.4**. Check the surface temperature, the temperature difference between the surface and the atmosphere just above, the skin temperature and the linear dependence of B on δ. Take account of the fact that the model assumes that the atmosphere consists of 100 layers of equal mass.

PROBLEM 2.5 Optical path and surface temperature on Mars and Venus

Suppose that the atmosphere of a planet, similar to the atmosphere of Mars, is homogeneous and that it consists mostly of one greenhouse gas (96 % by mass), which aborbs long wave radiation with an absorption cross-section (**Box 2.3**) of 0.3 m^2 kg^{-1}. The average surface pressure on this planet is 636 Pa. The Solar constant on this planet is 590 W m^{-2}, the acceleration due to gravity, g=3.75 m s^{-2} and its planetary albedo is 0.15. Compute the average optical path of the atmosphere and the average radiative equilibrium temperature of the surface of this planet, applying the theory of **Box 2.4**. Repeat this exercise for a planet with a much more massive atmosphere with the same composition, similar to the atmosphere of Venus. The average surface pressure on this planet is about 9×10^6 Pa, its albedo is 0.75, the acceleration due to gravity is 8.8 m s^{-2} and the Solar constant is 2600 W m^{-2}. Compare your computed temperatures with the observed average surface temperatures on Mars and Venus and discuss the reasons for the differences (hint: see figures 2.30, 2.31 and 2.52).

Box 2.4. Radiative equilibrium temperature profile in a homogeneous atmosphere from the solution of Schwarzschild's equation

Let us investigate the **radiative equilibrium** of a *continuously stratified* atmosphere containing one well-mixed greenhouse gas, assuming that it is transparent to Solar radiation. The long-wave radiative fluxes passing in and out of an *optically thin* layer in this atmosphere are shown in **figure 1**. Upwelling radiation is indicated by a subscript "+"; downwelling radiation is indicated by a subscript "-". Radiative balance yields

$$\Delta I_- = \Delta I_+ . \qquad (1)$$

Bougeur's law (eq. 1 of **Box 2.2**) states that the absorbed irradiance is proportional to the incident irradiance. **Kirchhof's law states that emissivity equals absorptivity**. This leads to **Schwarzschild's equation** for the reduction of the intensity of the **upwelling** beam applicable to an *optically thin* layer (see Box 2.2) for an explanation of optical depth):

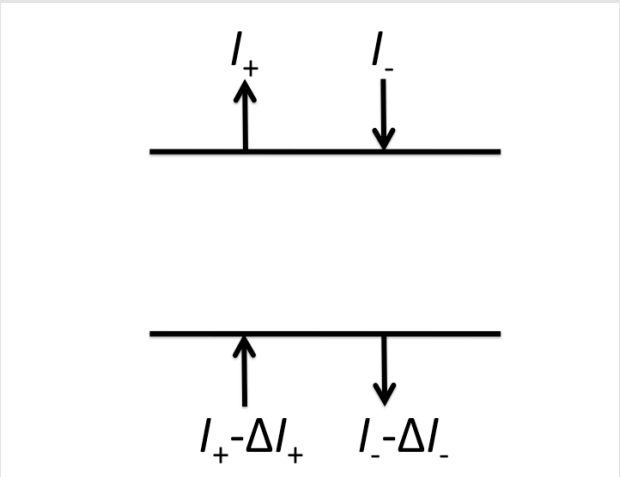

FIGURE 1 (Box 2.4)

$$-\Delta I_+ = \kappa\Delta z\left(I_+ - \Delta I_+\right) - \kappa\Delta z B \approx \kappa I_+\Delta z - \kappa B\Delta z\,. \qquad (2)$$

where $B=\sigma T^4$ is the *upward* black body emission. For the **downwelling** beam ($\Delta z<0$) Schwarzschild's equation reads

$$\Delta I_- = \kappa I_-\Delta z - \kappa B\Delta z\ . \qquad (3)$$

Eqs. 2 and 3 represent the **two-stream approximation**. Because of (1), we can equate the r.h.s. of (2) and the r.h.s. of (3), yielding

$$-\kappa I_+\Delta z + \kappa B\Delta z = \kappa I_-\Delta z - \kappa B\Delta z\,,$$

which leads to

$$I_+ + I_- - 2B = 0\ . \qquad (4)$$

Addition of eqs. (2) and (3) yields

$$\Delta I_+ + \Delta I_- = -\kappa\left(I_+ - I_-\right)\Delta z\ . \qquad (5)$$

With the following definitions:

$$\bar{I} \equiv I_+ + I_- \text{ and } I \equiv I_+ - I_-\ , \qquad (6)$$

eqs. (1), (4) and (5) can be written, respectively, as

$$\Delta I = 0;\ \bar{I} \equiv 2B;\ \Delta\bar{I} \equiv -\kappa I\Delta z\,,$$

or, with $-\kappa dz = \left(\sigma_a q_a / g\right)dp = d\left(\sigma_a q_a p/g\right) \equiv d\delta$, where δ is the **optical path** and σ_a is the *constant* absorption cross-section for the absorber with a *constant* specific concentration, $q_a \equiv \rho_a/\rho$ (**Boxes 2.1** and **2.2**):

$$\frac{dI}{d\delta} = 0;\ \bar{I} \equiv 2B;\ \frac{d\bar{I}}{d\delta} \equiv I\,. \qquad (7)$$

Integration of the latter (third) equation, applying the second equation to find the constant of integration, yields

$$B \equiv \frac{1}{2}\left(I\delta + 2B_0\right), \qquad (8)$$

where B_0 is the value of B at TOA (top of the atmosphere) (δ=0). At TOA we also know that, assuming radiative equilibrium,

$$I_+ = \frac{1}{4} S_0 (1-\alpha) \equiv Q.$$

Furthermore, there is no downwelling long-wave radiation at TOA. Therefore, at TOA

$$I = I_+ = Q. \qquad (9)$$

In view of the first equation in (7), this equation in fact holds for all optical paths! Therefore (8) can be rewritten as

$$B \equiv \frac{1}{2}(Q\delta + 2B_0), \qquad (10)$$

implying that B is a linear function of the optical path.

The second equation in (7) can also be written as

$$\bar{I} = I + 2I_- \equiv 2B, \qquad (11)$$

which, at TOA, reduces to

$$I = 2B \text{ or } Q = 2B_0. \qquad (12)$$

Now (10) becomes

$$B \equiv \sigma T^4 = \frac{1}{2} Q(\delta + 1) \qquad (13)$$

or

$$\boxed{T = \left(\frac{Q(\delta+1)}{2\sigma} \right)^{1/4}}. \qquad (14)$$

This is the final expression for the radiative equilibrium temperature in the atmosphere as a function of optical path, δ. At TOA (δ=0) (and also approximately for for δ<<1) the temperature is

$$\boxed{T \equiv T_{skin} = \left(\frac{Q}{2\sigma} \right)^{1/4} = \frac{1}{\sqrt[4]{2}} T_E} \qquad (15)$$

T_{skin} is the so-called "**skin temperature**". If the atmosphere contains no greenhouse gases, this is its temperature (about 215 K if T_E=255 K).

Eq. (14) does *not* hold for the Earth's surface because Solar radiation is absorbed here. Radiative equilibrium at the Earth's surface yields:

$$Q + I_- - I_+ = 0,$$

The second equation in (7) can be rewritten as,

$$I_- = 2B - I_+.$$

Assuming that the Earth's surface emits long-wave radiation as a black body, this becomes

$$2\sigma T_S^4 = Q + 2B,$$

or, with (13) (i.e. $B = \frac{1}{2}Q(\delta_S + 1)$, where δ_S is the optical path at z=0):

$$T_S = \left(\frac{Q(\delta_S + 2)}{2\sigma}\right)^{1/4}. \qquad (16)$$

The temperature of the Earth's surface is higher than the temperature of the atmosphere just above the Earth's surface, which is, according to (14),

$$T_{Sa} = \left(\frac{Q(\delta_S + 1)}{2\sigma}\right)^{1/4}. \qquad (17)$$

Note that T_{Sa} approaches the skin temperature if the atmosphere is optically thin, i.e. if $\delta_S << 1$ (**Box 2.2**). T_{Sa} increases continuously with optical depth, or with total greenhouse gas content. **The stratosphere is defined here as the "optically shallow" upper layer of the atmosphere, where δ<1, with a temperature close to the skin temperature.**

Reference

Andrews, D.G., 2010: **An Introduction to Atmospheric Physics**. Cambridge University Press. Orlando. 237 pp. (section 3.7.2 of the second edition).

In **figure 2.18 the** radiative equilibrium **potential temperature** for a homogeneous atmosphere, with ε=0.7, is compared with the US-Standard Atmosphere. The correspondence between the US-Standard Atmosphere and the model atmosphere above 400 hPa is surprisingly good. Below this level the model temperature is 15 to 25 K lower than the Standard Atmosphere.

The Brunt-Väisälä frequency, N, defined as (section 1.15)

$$N = \sqrt{\frac{g}{\theta}\frac{\partial\theta}{\partial z}},$$

is a measure of the static stability of the atmosphere. N is positive at all levels, except at surface (section 2.8). In the Standard Atmosphere the value of N changes quite abruptly around 250 hPa. Below this level (in the troposphere) $N \approx 0.01$ s^{-1}. Above this level (in the stratosphere) $N \approx 0.02$ s^{-1}. (show this, assuming the the stratosphere has a constant temperature equal to the skin temperature). The level of this abrupt change is called the **tropopause**. The homogeneous atmosphere in radiative equilibrium does not exhibit this abrupt change, rather the value of N increases gradually from 0.012 s^{-1} at low levels to about 0.02 s^{-1} at upper levels where the optical path (measured from the top of the atmosphere), $\delta << 1$.

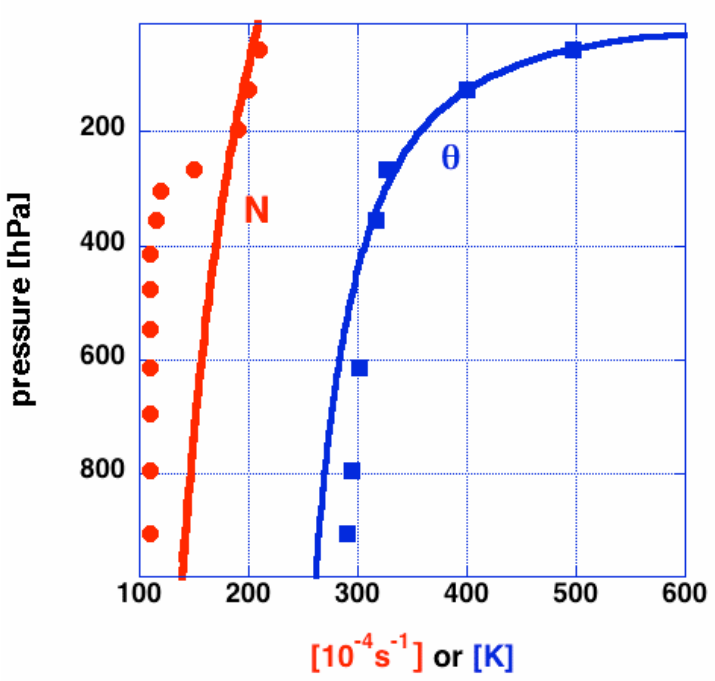

FIGURE 2.18. **The state of pure radiative equilibrium** for a homogeneous atmosphere in terms of potential temperature (solid blue line on the right) and Brunt-Väisälä frequency (solid red line on the left), computed by integrating the one-dimensional radiation model described in this section assuming 100 layers, yearly average Solar irradiance (342 W m^{-2}), an albedo equal to 0.3, a homogeneous atmosphere which is transparent to Solar radiation and a net atmospheric long-wave transmission coefficient (τ_{LW}) equal to 0.3 (ε=0.7), until ASR=OLR-TOA. The blue squares (red dots) indicate the potential temperature (Brunt-Väisälä frequency) according to the US-standard atmosphere (**table 2.1**). The potential temperature of the Earth's surface is not shown in the graph.

PROBLEM 2.6 Accuracy of statements about the greenhouse effect made by a non-specialist

Assess the accuracy of the following statements about the greenhouse effect.

(1)"An increase in the greenhouse effect will warm the lower atmosphere (troposphere) and cool the upper atmosphere (stratosphere) – where less outbound infrared radiation will reach after more atmospheric trapping."

(2) "One hundred years of theory and the simulations of modern computers are the primary grounds for greenhouse science. Empirical support is weaker, to some extent inevitably so for reasons of long lags and natural variability."

William R. Cline, 1991**:** Scientific basis for the greenhouse effect. **The Economic Journal, 101**, 904-919 (pages 909 and 910).

2.8 Radiative-convective equilibrium

Earth's atmosphere is actually never in perfect radiative equilibrium for two reasons. **First,** because the Earth's surface is usually much warmer than the atmosphere, molecular heat conduction between the Earth's surface and the atmosphere will immediately render the state of radiative equilibrium **hydrostatically unstable** (section 1.15). This will lead to convection currents and concomitant relatively rapid upward transport of heat. This will bring the blue line in **figure 2.18** closer to the blue squares. **Second**, the incoming Solar radiation at any individual point on Earth varies with the **seasons**. Since, the time scale of these variations is of the same order of magnitude as the radiative adjustment time scale (section 2.4), exact equilibrium will never be reached at any point in time in the atmosphere, except maybe near the equator, where seasonal variations in insolation are small (**figure 2.8**). In this section we further discuss the first effect. The second effect is discussed in section 2.9.

The motions that are the result of hydrostatic instability will tend to mix the air such that a state of neutral stability is established with potential temperature constant with height. In a model that is not able to represent explicitly the currents that accomplish this mixing, the sensible heat transfer from the Earth's surface to the atmosphere due to these currents is **parametrized** by assuming that this heat transfer is proportional to the potential temperature difference between the surface and the lowest model layer. Following this recipe (or **parametrization**), the fourth contribution to the heat balance of the Earth's surface is

$$\boxed{\begin{aligned} &H_K = k_H(\theta_S - \theta_K) \text{ if } \theta_S > \theta_K, \\ &H_K = 0 \text{ if } \theta_S \le \theta_K. \end{aligned}} \qquad (2.36)$$

[79] (section 2.7). The subscript, K, indicates that the heat transfer is to layer K (**figure 2.16**), the lowest atmospheric layer; θ_S is the potential temperature of the Earth's surface; the parameter k_H is a "**heat-transfer coefficient**". The idea behind (2.36) is that heat is transferred upward almost exclusively by convection currents, which exist only when there is hydrostatic instability, i.e when potential temperature decreases with increasing height (section 1.15).

The value of the transfer coefficient, k_H, can be estimated by considering the timescale of the relaxation to the state of neutrality, which follows from the equation for the time-rate of change of the temperature of the lowest model layer. Neglecting the effects of radiation, this equation is

$$\frac{dT_K}{dt} = -\frac{k_H g}{c_p \Delta p}(\theta_K - \theta_S).$$

From this equation it follows that the time-scale τ_{CA} of **convective adjustment** is given by

$$\tau_{CA} = \frac{c_p \Delta p}{k_H g} = \frac{c_p p_s}{K k_H g} \approx \frac{10^7}{K k_H} \text{ [s]}.$$

[79] The potential temperature representative of a particular isothermal layer is taken to be the potential temperature "halfway" (in terms of pressure) the layer.

Therefore,

$$k_H \approx \frac{10^7}{K\tau_{CA}} \quad . \tag{2.37}$$

From this we see that the transfer coefficient, k_H, is inversely proportional to the resolution (or number of model layers), K. The eddies that take care of the convective adjustment have time scales (τ_{CA}) in order of 10 minutes to 1 hour. Therefore, let us assume that $\tau_{CA} \approx 1000$ [s]. With K=50 layers, we then obtain the following estimate for k_H.

$$k_H = 200 \text{ W m}^{-2}\text{K}^{-1} \tag{2.38}$$

In the previous section we assumed that the **heat capacity of the Earth's surface** was zero, implying energy balance at all times. We now relax this assumption by introducing a layer below the surface of the Earth with a heat capacity, C, so that the energy balance equation becomes

$$C\frac{dT_S}{dt} = S + B - U_S - H_K, \tag{2.39}$$

instead of (2.28). The radiation fluxes, S, B and U_S are specified by (2.26) (2.25) and 2.27), respectively.

The parametrization (2.36) of the vertical sensible heat flux between the Earth's surface and the atmosphere can also be applied to the rest of the model atmosphere. Thus, the sensible heat flux from model layer n+1 to model layer n is written as follows.

$$\begin{aligned} H_n &= k_H(\theta_{n+1} - \theta_n) \text{ if } \theta_{n+1} > \theta_n, \\ H_n &= 0 \text{ if } \theta_{n+1} < \theta_n. \end{aligned} \tag{2.40}$$

For simplicity we assume that the eddy transfer coefficient, k_H, is constant, although it should be noted that there is a large body of literature concerned with the dependence on height of k_H.

We can now write down the energy balance equation for a layer (with index n) as follows.

$$\boxed{\frac{c_p \Delta p}{g}\frac{dT_n}{dt} = LWA_n + U_n + S_n + 2B_n + H_n - H_{n-1}}. \tag{2.41}$$

The effects of convection are therefore included implicitly by assuming that convection drives the temperature gradient towards a state of neutral static stability (section 1.15). This process is referred to as **convective adjustment**. For an atmosphere in which condensation processes are unimportant, the state of neutral static stability is the adiabatic temperature lapse rate (eq. 1.66), i.e. constant potential temperature with height.

Figure 2.19a shows the equilibrium solution (OLR-TOA=ASR) for two values of ε, obtained by integrating numerically equations (2.39) and (2.41), with convective sensible heat transfer parametrized as in (2.36) and (2.40). Also shown (for the case where ε=0.7) is the corresponding solution without convective heat transfer. The convective heat transfer

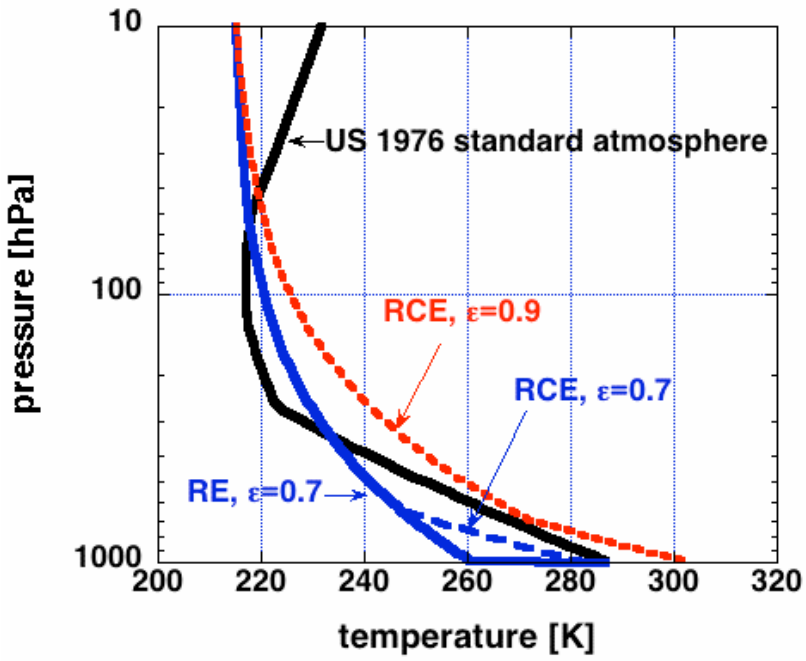

FIGURE 2.19a. **Radiative equilibrium (RE) temperature (blue solid line) and radiative-convective equilibrium (RCE) temperature (dashed lines)** in a **homogeneous atmosphere**, computed by integrating the one-dimensional radiation model until ASR=OLR-TOA, assuming 50 layers. In the case of radiative-convective equilibrium k_H=200 $Wm^{-2}K^{-1}$. The Solar irradiance is 342 W m^{-2}, the albedo is 0.3, the net short-wave transmission coefficient is 1 and the net atmospheric long-wave emission coefficient (ε) is 0.7 or 0.9. The US-1976 standard atmosphere temperature is also shown (black solid line).

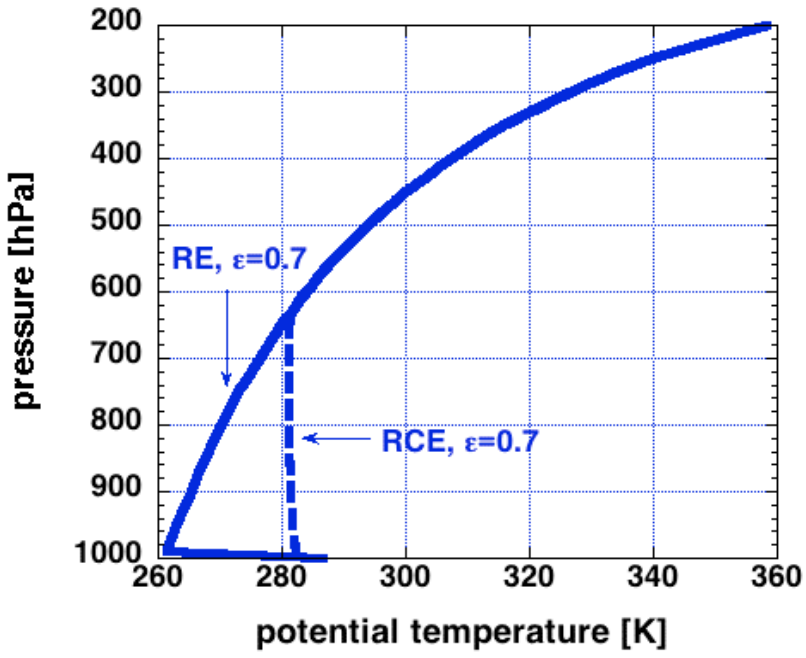

FIGURE 2.19b. **Radiative equilibrium (RE) (solid line) and radiative-convective equilibrium (RCE) (dashed line)** in a **homogeneous atmosphere** in terms of the potential temperature for ε=0.7, computed by integrating the one-dimensional radiation model until ASR=OLR-TOA, assuming 50 layers. In the case of radiative convective equilibrium k_H=200 $Wm^{-2}K^{-1}$. See the caption of **figure 2.19a** for the values of other parameters.

apparently cools the Earth's surface at the cost of heating the lowest layers of the atmosphere in such a way that near neutrality is maintained (**figure 2.19b**). Radiation is continuously driving the lower atmosphere away from neutrality. Therefore, *exact* neutrality (constant potential temperature) in the convective layer is never reached.

The model temperature profile differs appreciably from the "observed" temperature profile (the US-1976 standard atmosphere). This, of course, is mainly due to the fact that in the real atmosphere greenhouse gases are not distributed homogeneously. Water vapour is the most important greenhouse gas. Two thirds of the water vapour is found in the lowest 2 km of the atmosphere (section 1.10). Furthermore, the atmosphere (e.g. ozone and water vapour) absorbs Solar radiation and, moreover, evaporation "cools" the Earth's surface, while condensation "heats" the middle to upper troposphere. Clouds reflect Solar radiation, but also absorb long wave radiation. All these complicating effects will be considered in the following sections.

PROBLEM 2.7 The equlibrium Energy balance produced by the model with and without convective adjustment

Compare the equilibrium energy balance at the Earth's surface according to the model with and without convective adjustment with the numbers displayed in figure 2.10. Discuss the differences. (The data-set can be found at http://www.staff.science.uu.nl/~delde102/climatedynamics.htm).

2.9 Radiatively determined state

This section discusses the second reason for radiative disequilibrium in the atmosphere, mentioned at the beginning of the previous section. Until now we have been concerned only with calculating the energy balance averaged over the globe and over a time period of at least 1 year, in which case we could assume constant insolation. Of course (**figure 2.8**), at any specific point on Earth the insolation varies sinusoidally with a period of 1 year (polewards of the Tropic of Cancer at 23°N and polewards of the Tropic of Capricorn at 23.5°S) or (weakly) with a period of 6 months (between the Tropics of Cancer and Capricorn). Polewards of the Arctic Circle at 66.5°N or polewards of the Antarctic Circle at 66.5°S, the insolation is absent during at least 1 day in winter. In fact, at the poles the Sun is not visible for half a year. This period is referred to as the **polar night**. Over regions where the polar night lasts more than approximately 20 days (calculate the minimum latitude where this is the case), i.e. of the same order of magnitude as the radiative equilibrium time scale, the atmosphere can cool down significantly. Some interesting quantitative consequences of this fact will be discussed in this section. More details will be given in chapters 12.

Figure 2.20 shows the result of two integrations of the one dimensional radiation model with insolation representative of 45°N. The model is allowed to spin up for two years. The evolution of ASR (absorbed Solar radiation), ground temperature, OLR- TOA (outgoing long-wave radiation at the top of the atmosphere) and surface sensible heat flux are shown for two values of the heat capacity of the Earth's surface. In the case denoted by the letter [c] the value of C in (2.39) (10^6 J m^{-2}K^{-1}) is representative for a dry continent. In the case denoted by the letter [m] the value of C (10^8 J m^{-2}K^{-1}) is representative for the ocean. This is equivalent to assuming that Solar radiation penetrates and is absorbed by a layer of water that is approximately 25 m deep.

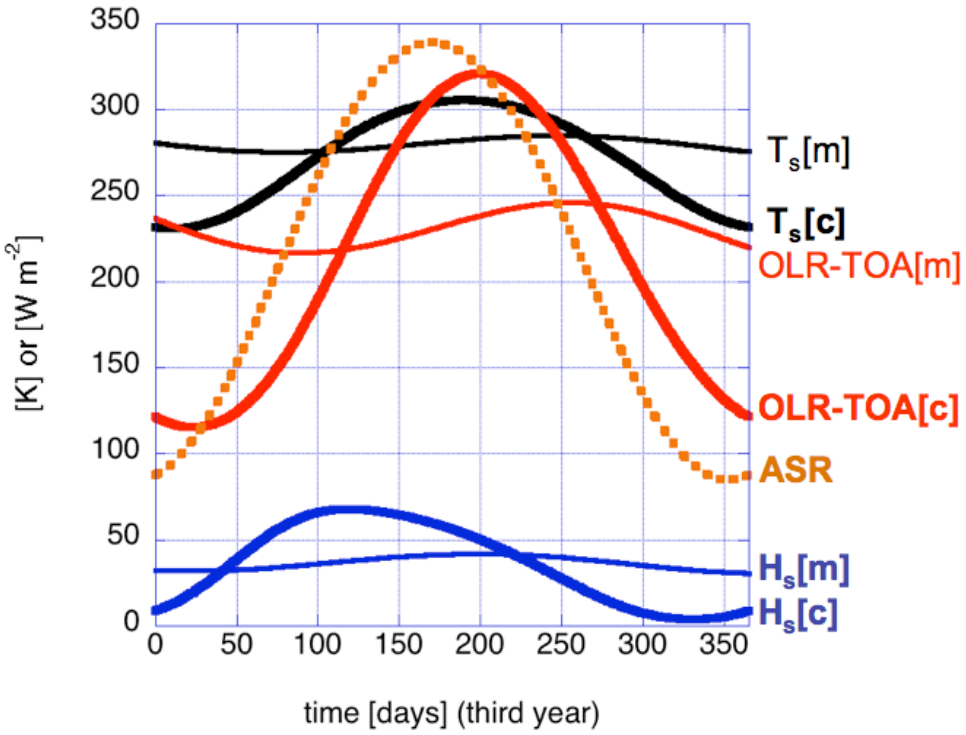

FIGURE 2.20. **The radiative-convective determined state at a latitude of 45° as a function Julian day**, in terms of the surface temperature and outgoing long-wave radiation at the top of the atmosphere (OLR-TOA) in two cases: (case 1) denoted by 'c' for which $C=10^6$ J K^{-1}m^{-2}, and (case 2) denoted by 'm' for which $C=10^8$ J K^{-1}m^{-2}, computed by integrating the one-dimensional radiation model over three model years with insolation representative 45°N on Earth, showing only the result for the last (third) year. Further assumptions are the following: k_H=100 Wm^{-2}K^{-1}, K=100 layers, albedo=0.3, the atmosphere is homogeneous with a net short-wave transmission coefficient equal to 1 and a net atmospheric long-wave transmission coefficient (τ_{LW}) equal to 0.3. The daily cycle of the insolation is neglected. ASR is the absorbed Solar radiation (obviously the same in both cases).

We see (**figure 2.20**) that ASR is in balance with OLR-TOA only at two points in time each year. For the continental case [c] this is day 29 (29 January) and day 203 (22 July). In general OLR-TOA lags behind ASR by about 29 days, which, again corresponds approximately to the radiative adjustment time scale found in section 2.4. In contrast, in case [m] the time scale of thermal adjustment is dominated not by radiation in the atmosphere, but by the large heat capacity of the Earth's surface, which makes the system react very slowly, and with a much smaller amplitude, to changes in insolation. The surface temperature in this case is representative of the surface temperature over the ocean, while surface temperature in case [c] is representative of Siberian conditions (very cold winters and relative warm summers).

The strong sensitivity of the model-"climate" to the value of C (the specific heat capacity of the Earth's surface) indicates that a more sophisticated climate model should include more details of the actual absorption of radiation by the Earth's surface and the diffusion or mixing of heat into the soil or water. For example, a layer of water of about 25 m is heated by Solar radiation.

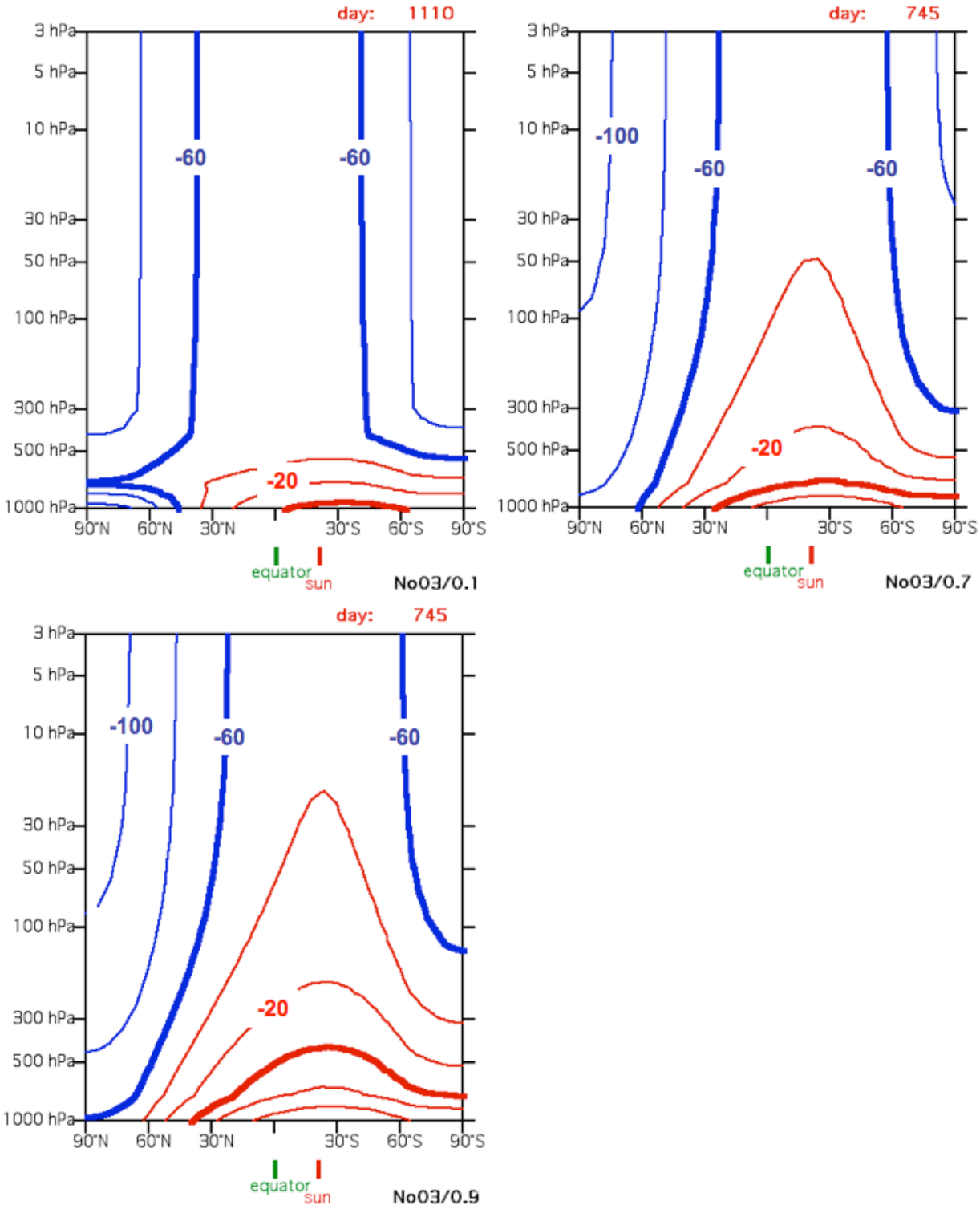

FIGURE 2.21. The radiative-convective determined temperature (isopleths labeled in °C; interval is 20°C) for a **homogeneous atmosphere** (atmosphere is transparent for Solar radiation and albedo is 0.3 everywhere) on **January 16** (0 hours) as a function of latitude and pressure, (logarithmic scale) according to the radiative-convective model (using 200 layers) with $C=10^7$ J $K^{-1}m^{-2}$, for $\varepsilon=0.1$ (upper left panel), for $\varepsilon=0.7$ (upper right panel) and for $\varepsilon=0.9$ (lower panel) (other parameter values are given in the caption of **figure 2.20**). Note the symmetric temperature distribution in the stratosphere with respect to the equator in the case of a weak greenhouse effect ($\varepsilon=0.1$). In the lower troposphere the asymmetric temperature distribution with respect to the equator is principally induced by the response to the Earth's surface, which is assumed to be a black body in all three cases.

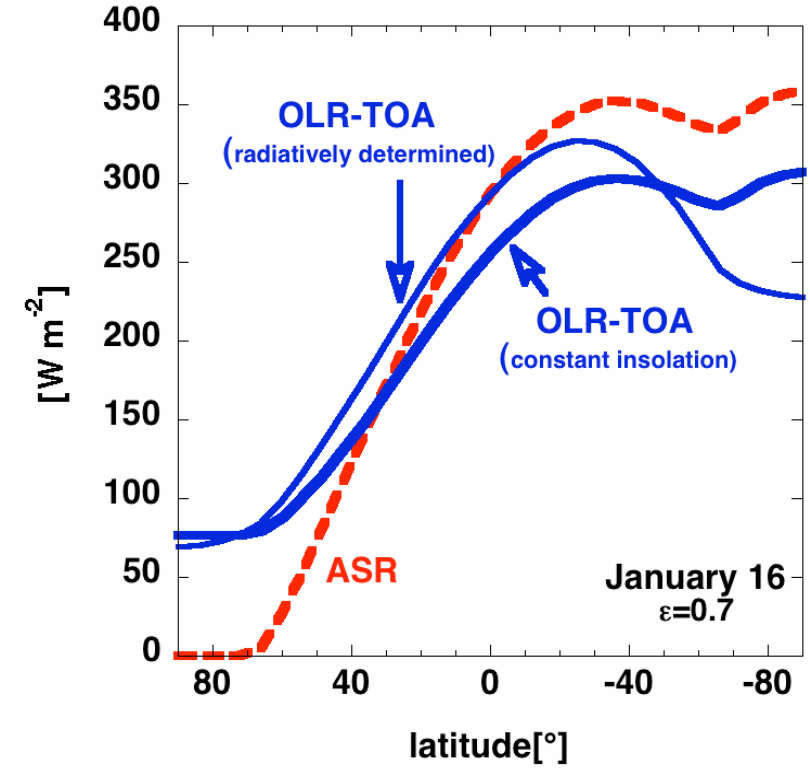

FIGURE 2.22. Total absorbed Solar radiation (ASR) on January 16 (dashed line), the radiatively determined outgoing long-wave radiation at the top of the atmosphere (OLR-TOA) (i.e. determined by imposing the seasonal cycle of insolation) on January 16 (thick solid line), and OLR-TOA after integrating the model over **90 days under constant insolation** corresponding to January 16 (thin solid line) as a function of latitude. In the latter case the the atmosphere is assumed to be isothermal (250 K) initially. All other parameter values are identical to those corresponding to the upper-right panel of **figure 2.21** (e.g. ε=0.7) (albedo=0.3 everywhere). The summer pole is realtively close to radiative-convective equilibrium, i.e. OLR-TOA aproaches ASR as progresses. The winter hemisphere, poleward of 50° is far from radiative-convective equilibrium, i.e. ASR<<OLR-TOA.

Figure 2.21 shows the radiative-convective determined thermal state on January 16 for a homogeneous atmosphere in three cases: ε=0.1 (weak greenhouse effect), ε=0.7 and ε=0.9 (strong greenhouse effect), computed by integrating the one-dimensional radiative-convective model, from an isothermal state on January 1 (0 hrs) (250 K) over a period of 745 days (2 years and 15 days) or 1110 days (3 years and 15 days). The integration is performed for 31 latitudes (in steps of 6°) with insolation representative of present day conditions on Earth (left panel of **figure 2.8**).

From a comparison of the right upper panel of **figure 2.21** (which is perhaps the most representative of contemporary conditions in Earth's atmosphere) with the lower part of **figure 2.7** (representing the observations), we find that the radiative-convective pole-to-equator temperature contrast near the surface of the Earth is much greater than in reality, especially in winter. Also, the radiative-convective model is not able to reproduce the temperature minimum over the tropics at about 15 km above sea level (100 hPa). We shall see (chapter 12) that this feature can only be explained when account is taken of both latent heat release in the ITCZ and of the adiabatic effect of the forced upward motion in the ITCZ on temperature. Furthermore, according to the radiative-convective model, the winter polar stratosphere is colder than in reality. We will see in chapter 12 that this discrepancy Is

largely remedied when the thermal effect of compression due to the forced downward motion is taken into account. Furthemore, the summer polar stratosphere in the radiative-convective determined state is also colder than in reality. This is due to the neglect of absorption of Solar radiation by oxygen and ozone (section 2.16).

The radiatively determined temperature increases with increasing value of ε everywhere, except over the winter pole. The polar winter stratosphere (above about 200 hPa and poleward of 60° latitude) is 10-20 K colder in the case that ε=0.9 compared to the case that ε=0.1. In fact, when the greenhouse effect is weak (ε=0.1), the stratospheric temperatures over the winter pole hardly differ from the stratospheric temperatures over the summer pole! The explanation for this fact can found in the **extremely long radiative response time in the stratosphere** when ε=0.1 (in the order of 1 year!) (eq. 2.20). Therefore, the stratosphere is hardly able to respond to the seasonal variation in insolation in the practical absence of greenhouse gases. The dynamical consequence of the cooling of the winter polar stratosphere, due to increasing greenhouse gas content, is now (in 2011) a subject of intense study. These studies must of course also take acount of the effect of absorption of Solar radiation by ozone in the stratosphere. This effect will be discussed in section 2.16.

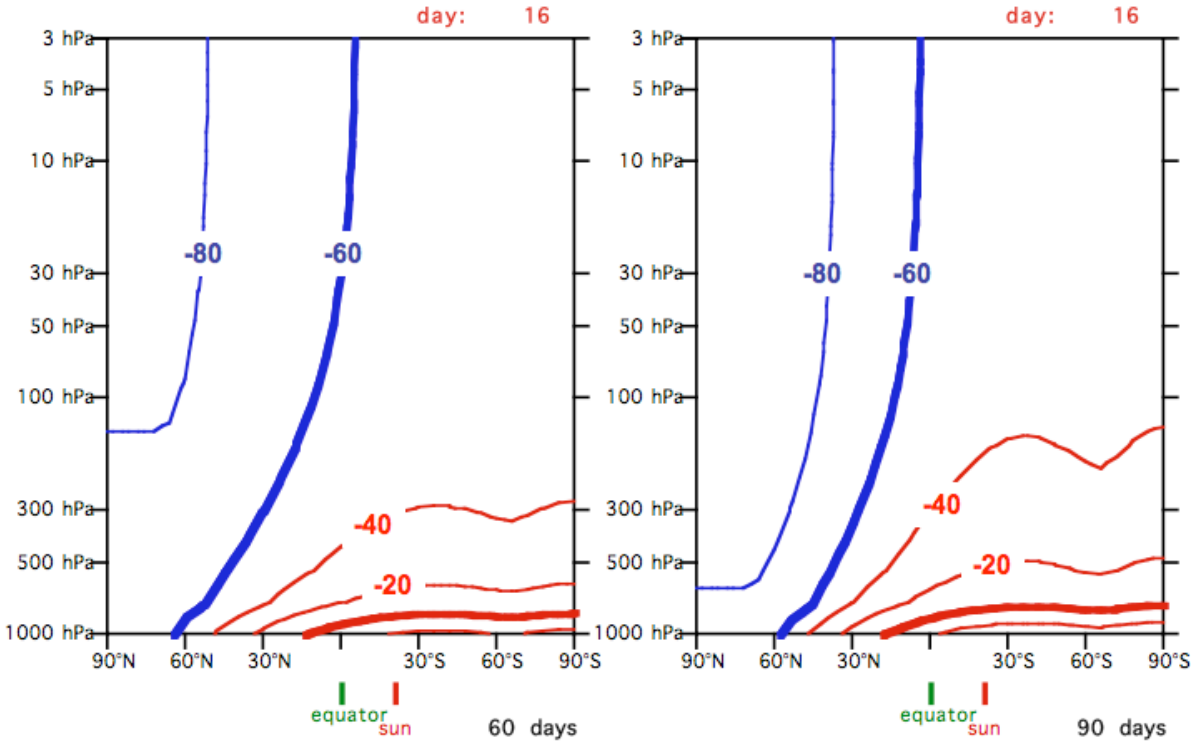

FIGURE 2.23. The temperature distribution (labeled in °C) for a *homogeneous* atmosphere as a function of latitude and pressure (logarithmic scale) according to the radiative-convective model obtained after a 60-day (left panel) and a 90-day (right panel) integration under **constant insolation** corresponding to January 16. Initially the atmosphere is isothermal (250 K). All other parameter values are identical to those corresponding to the upper-right panel of **figure 2.21** (ε=0.7) (albedo=0.3 everywhere). The summer hemisphere the temperature distribution reflects the absorbed solar radiation (ASR in **figure 2.22**). Therefore, there is practically no temperature difference between the summer pole and the equator. In the radiatively determined case (upper right panel of **figure 2.21** there is a significant equator pole temperature in the summer hemisphere, reflecting the history of the insolation.

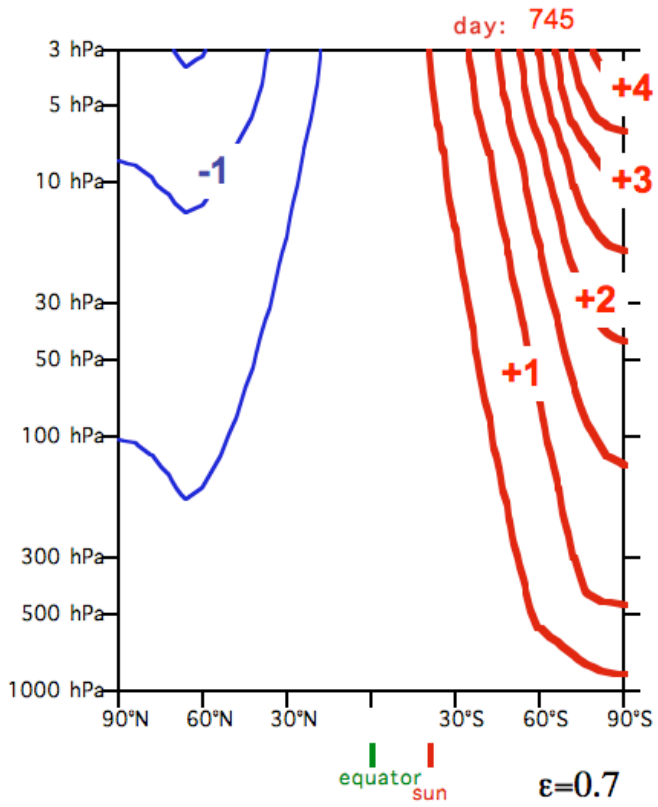

FIGURE 2.24. The radiative-convective determined "cross-isentropic flow" (=dθ/dt) (labeled in K/day) for a *homogeneous* atmosphere on January 16 (0 hrs) (day 745 of the integration) (*northern hemisphere winter*) as a function of latitude and pressure, (logarithmic scale) according to the radiative-convective model (using 200 layers) with C=10^7 J $K^{-1}m^{-2}$, for ε=0.7 (other parameter values are given in the caption of **figure 2.20 and 2.21**). The atmosphere is transparent for Solar radiation.

Evidently (**figure 2.21**), the equator to pole temperature contrast and therefore also the thermal wind (chapter 1) over the winter hemisphere increases with increasing greenhouse gas content. This subject will be discussed further in chapter 12.

The troposphere responds to the seasonally changing temperature of the Earth's surface. Since the Earth's surface is assumed to have an emissivity equal to 1 (i.e. it is a black body), the response of the troposphere to the seasonal variation in insolation is qualitatively similar in both cases (ε=0.1 and ε=0.7).

The **actual radiative-convective equilibrium temperature distribution** for January 16 can be determined easily by integrating the model with "permanent January 16 insolation". Over the winter pole this integration would require infinite time, because of the absence of insolation. The polar night atmosphere cools down permanently, but ever more slowly, and in theory would approach absolute zero in infinite time. Elsewhere the atmosphere comes close to the radiative-convective equilibrium within 60 days (**figure 2.22**). We also see in **figure 2.22** that the radiatively determined state is far from radiative equilibrium *also at the summer pole*.

In **figure 2.23** we observe clearly that the pole-equator temperature gradient over the summer hemisphere is practically absent if the atmosphere is in radiative equilibrium and that, associated with this, the temperature over the summer pole is significantly higher than in the **radiative-convective determined state** (lower panel of **figure 2.21**). We may

conclude from these numerical experiments that the temperature distribution in the atmosphere depends strongly on the length of the seasons compared to the radiative adjustment time scale. In other words, **the thermal inertia of the atmosphere plays a crucial role in determining the actual temperature distribution in the atmosphere**.

An impression of the degree of radiative equilibrium is obtained by computing the "**cross-isentropic flow**". The cross-isentropic flow for layer n is determined from the following equation (see eq. 2.41) (assuming $dp_n/dt=0$).

$$\frac{d\theta_n}{dt} = \left(\frac{p_{ref}}{p_n}\right)^{\kappa} \frac{dT_n}{dt} = \left(\frac{p_{ref}}{p_n}\right)^{\kappa} \frac{g}{c_p \Delta p}\left(LWA_n + U_n + S_n - 2B_n + H_n - H_{n-1}\right) \qquad (2.42)$$

Figure 2.24 shows the "**cross-isentropic flow**" ($=d\theta/dt$) in the radiative- convective determined state on January 16 for $\varepsilon=0.7$ (corresponding to the temperature distribution shown in the lower panel of of **figure 2.21**).

As expected, we find that the summer hemisphere (the right half of **figure 2.24**) is heating, while the winter hemisphere (the left half of **figure 2.24**) is cooling. The tropics are approximately in radiative convective equilibrium. This is obviously due to the very weak seasonal variation in insolation in the tropics (**figure 2.8**, left panel). However, this simple pattern of radiative-convective determined heating and cooling does *not* correspond to reality, even not qualitatively. Reanalysis of observations (**figure 2.9**) shows diabatic cooling over the summer pole up to 10 hPa (30 km a.s.l.) and diabatic heating in the tropics at all heights. This is an effect of "mechanically forced" downward motion over the mid-latitudes and poles in the **Brewer-Dobson circulation** (sections 1.12 and chapters 11 and 12), leading to compression of air over the poles and, thus, higher temperatures than would be expected on the basis of only the radiation budget, enhancing the emission of radiation, both in the summer hemisphere and in the winter hemisphere. At the **intertropical convergence zone** (ITCZ) (**figures 1.44 and 1.45**), where the trade winds from both hemispheres converge, air is forced to rise, leading to the formation of clouds attended by **latent heat release due to condensation of water vapour and freezing of liquid cloud droplets**. The important topic of the interaction between dynamics and radiation is, however, outside the scope of this chapter. It is discussed in detail in chapter 12.

Figure 2.9 shows heating below 800 hPa in both the winter- and summer hemispheres polewards of 20° latitude, except over the polar cap (polewards of 80°). The heating of the lowest atmospheric layers is strongest in the winter hemisphere, mainly because of the strong heating ocurring over the relatively warm ocean waters, especially in the Gulf-stream area in the Atlantic sector.

PROBLEM 2.8 Maritime and continental climates

Search observational data (on the internet; see, for instance, http://climexp.knmi.nl/ or http://www.ecad.eu/) of the temperature at the Earth's surface representative of maritime and continental climates at approximately 45°N. Compare the data with the model data shown in figure 2.20.

2.10. Energy fluxes associated with the water cycle

The water cycle has a large influence on the energy budget of the atmosphere. Let us look at a recent version of the well-known picture of the annual mean and global mean energy balance, which is shown in **figure 2.25** (an older version is shown in **figure 2.10**). According to this synthesis of observations carried out between the years 2000 and 2004 Solar radiation that is absorbed by the Earth's surface amounts to 161 W m^{-2}. Part of this energy is used both to heat the surface as well as to evaporate water from the surface, if available. The surface heating together with conduction of this heat to the atmosphere makes the atmosphere hydrostatically unstable. This leads to convection, which takes care of the transport of sensible and latent heat upward into the atmosphere.

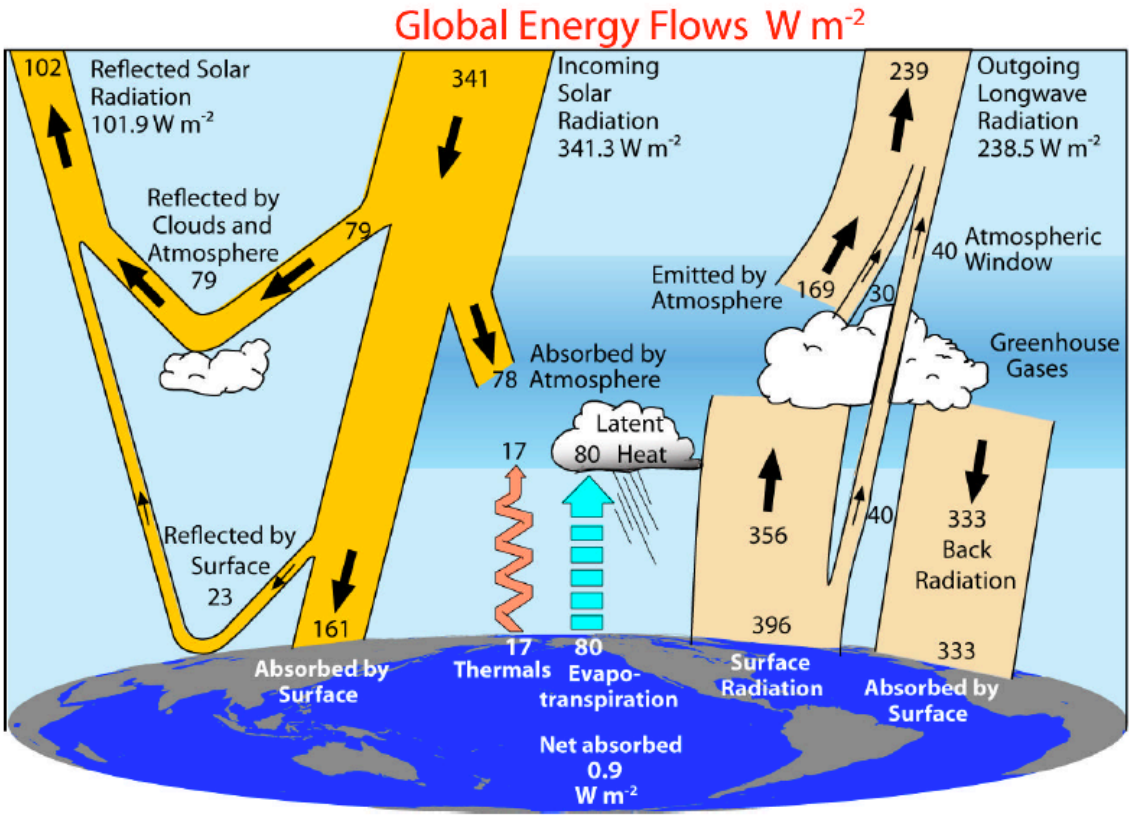

FIGURE 2.25. Global annual mean Earth's energy budget for the period running from March 2000 to May 2004 in W m^{-2}. Note that the sytem is **not in equilibrium**: the net absorbed flux is 0.9 W m^{-2}. The width of the arrows indicates the flow of energy in proportion to its importance. Source: Trenberth, K.E., et al., 2009: Earth's Global Energy Budget. **Bull.Amer.Meteorol.Soc., 90**, 311-324.

Evaporation is a quantity that is very difficult to measure. It is sometimes assumed that latent heat transport from the Earth's surface to the atmosphere (i.e. evaporation at the surface) is coupled to the surface sensible heat transport through a "**Bowen ratio**"[80] (**Box 2.9**), which is the ratio of the sensible heat transport to the latent heat transport. According to the numbers displayed in **figure 2.25**, the annual and global average Bowen ratio, *B*, is 17/80=0.21. However, the Bowen ratio is by no means constant. It depends strongly on both

[80] Lewis, J.M., 1995: The story behind the Bowen ratio. **Bull.Amer.Meteorol.Soc., 76**, 2433-2443.

the availability of water at the surface as well as on the net radiation that is received at the Earth's surface. Over the oceans, B is in the order of 0.1, while over the land areas that receive a substantial flux of energy in the form of short wave Solar radiation, B is larger, depending on the availability of (soil) water ($B>1$ if the surface is very dry).

The water cycle is driven by **net radiation** at the surface, which is the sum of absorbed Solar radiation and absorbed back radiation (long wave) minus emitted surface radiation (long wave).

PROBLEM 2.9 Trends in the energy budget

Figures 2.10 and 2.25 show the global annual mean energy for the periods of, respectively, 1985-1989 and 2000-2004.

(a) In how far is the climate system in radiative equilibrium?

(b) Is the Earth's surface in radiative equilibrium?

(c) Calculate the planetary albedo in both cases.

(d) Calculate the cloud albedo, assuming that the cloud cover fraction is 0.5.

(e) Calculate the Bowen ratio in both cases and discuss the reasons for the change in the Bowen ratio.

(f) What can you say, based on a comparison of these figures, about the human-induced greenhouse effect.

(g) The net absorbed energy for the period 2000-2004 is estimated to be 0.9 W m^{-2}. Where, do you think, does this energy go?

(h) The most recent estimate of Earth's energy balance was published in **Nature Geoscience** of 23 September 2012 (see the figure in **Box 2.8**). Discuss the differences between the figure in Box 2.8 and figure 2.25.

(i) Compare the net radiation at the surface in the three figures (2.10. 2.25 and **Box 2.8**). Discuss the implications for the future of the water cycle.

The sensible heat flux over land in winter is directed into the Earth over most of the land areas. This implies that the Bowen ratio is negative here. Greenland, especially, is a sink of sensible heat in winter (**figure 2.26a**). This is the result of the advection of relatively warm air from the oceans to the cold, mostly snow- and ice-covered continents, where this air looses heat by downward sensible heat transport.

On the other hand, over the western ocean boundary currents (the Gulf stream in the western Atlantic ocean and the Kuroshio current in the western Pacific ocean), where in the winter the low level air is much colder than the sea surface, the sensible heat flux from the ocean to the atmosphere is very large (up to 300 W m^{-2}).

The effect of the hydrological cycle on the energy budget is reflected in the evaporation of water from the Earth's surface and in the **release of latent heat in clouds**. The latter effect represents an **internal heat source**, which drives the **Hadley circulation** (illustrated in **figure 1.45**). In the ITCZ latent heat release represents an enormous contribution to the energy budget. For instance, the yearly precipitation of 2370 kg m^{-2} at Singapore represents a vertically integrated *continuous* heat source of 188 W m^{-2}! Over the western Pacific, just south of the equator the average column integrated heating in the months of December January and February exceeds 1000 W m^{-2} (**figure 2.27**)!

Figure 2.27 shows the global distribution of the average column integrated heating of the atmosphere by latent heat release, sensible heating and the net effect of absorption and emission of radiation. We observe net heating in the ITCZ, obviously associated with the huge condensation rates taking place there. The special aspect of condensation heating in the

tropics is that it occurs at comparatively great height in the atmosphere (**figure 2.28**). Diabatic heating in the mid-latitudes in connection with precipitation systems in depressions, apparently, does not take place at such great heights. Tropical diabatic heating, associated with condensation, is thus of great influence on the deep circulation in the atmosphere.

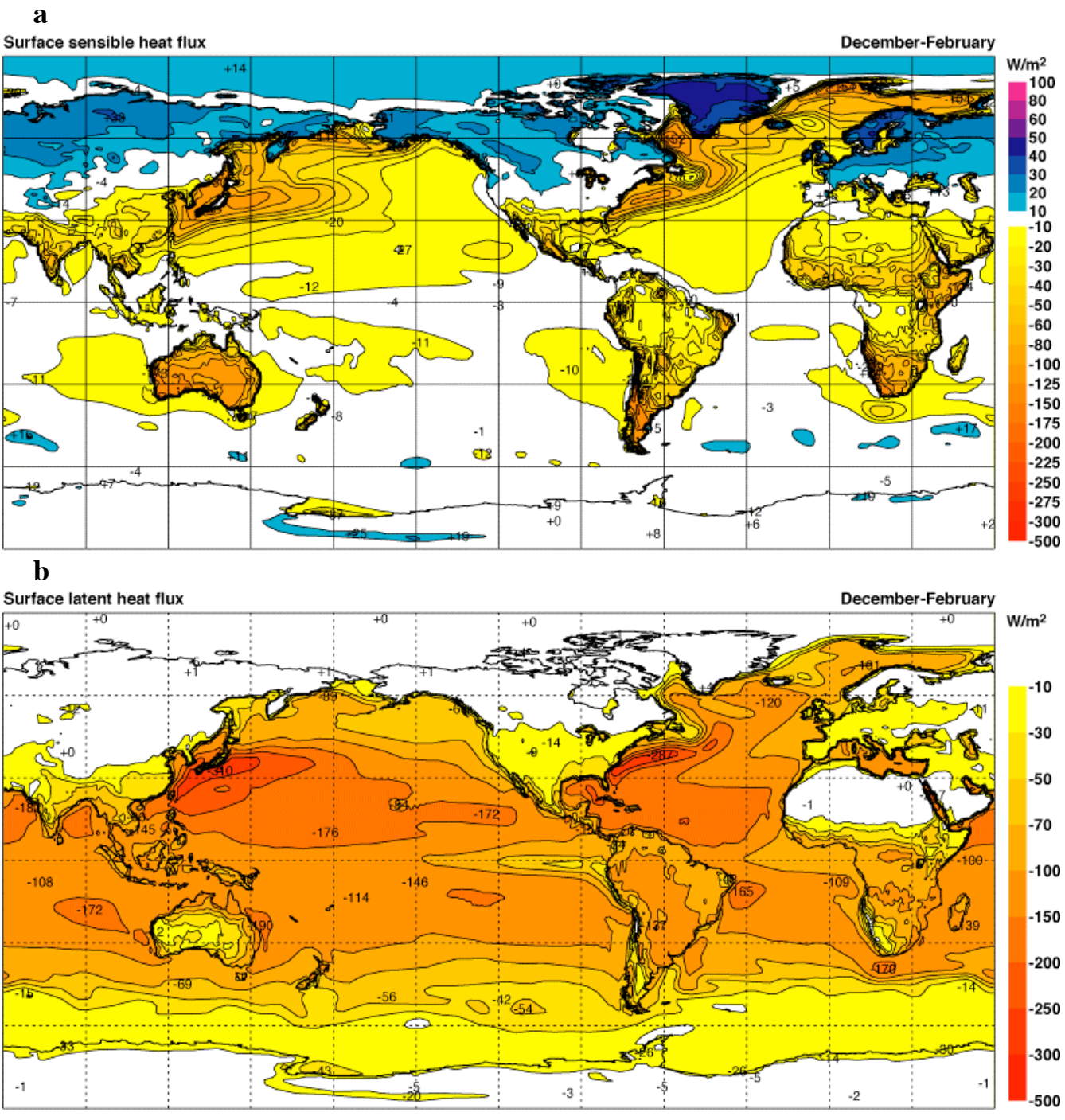

FIGURE 2.26. Global distribution of the average (in December January and February) sensible (a) and latent (b) energy fluxes in W m^{-2} at the surface of the Earth (negative values correspond to fluxes directed into the atmosphere). The average is for the period 1979-2001. Source: http://www.ecmwf.int/research/era/ERA-40_Atlas. Note that the sensible heat flux is negative over lnad surfaces in the winter hemisphere pole ward of about 50°.

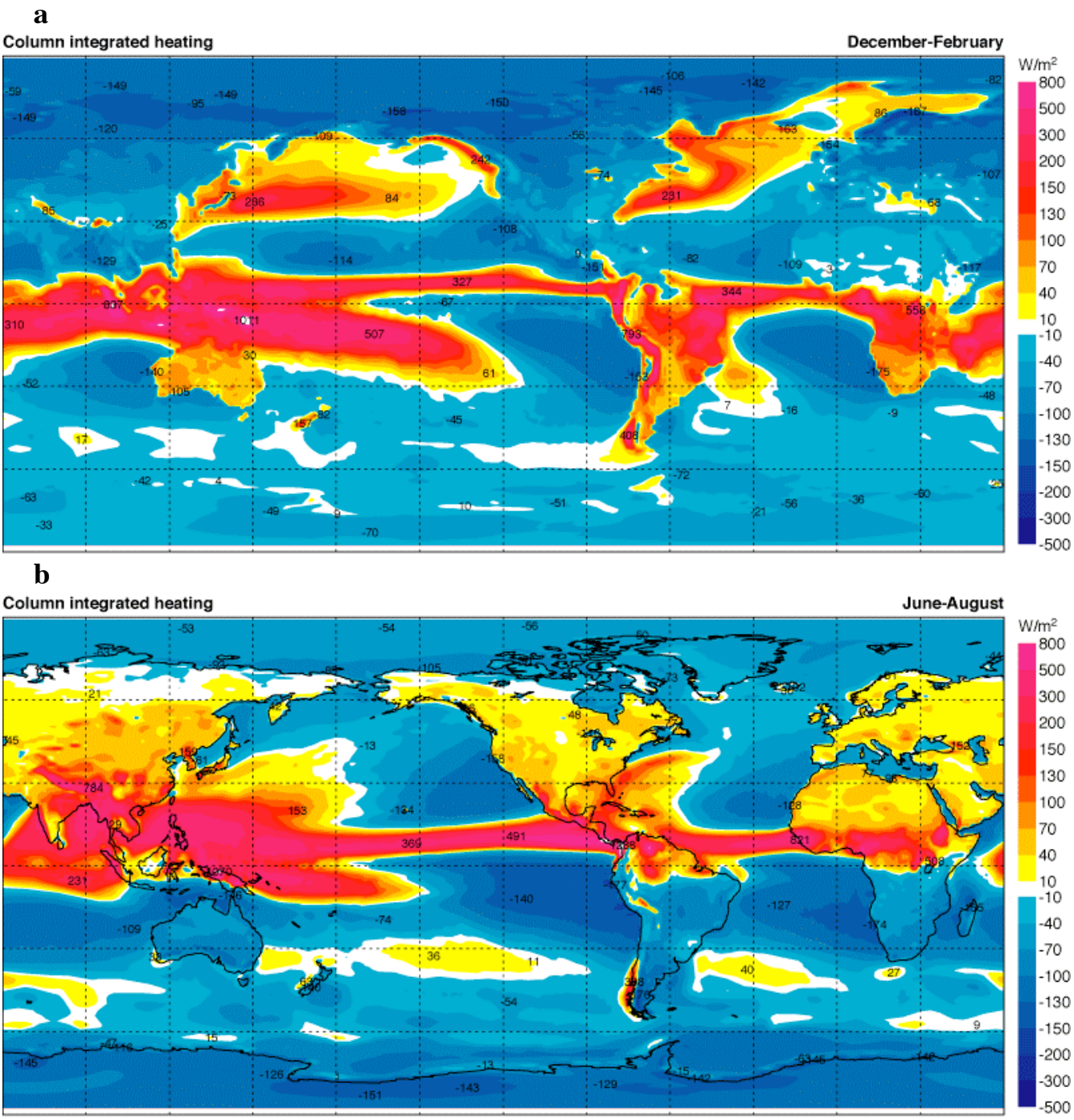

FIGURE 2.27. Global distribution of the average column integrated heating of the atmosphere in W m^{-2} in, repectively, (a) December January and February (DJF) and in (b) June, July and August (JJA) In the northern hemisphere winter (DJF) there is significant heating over the mid-latitude Pacific- and Atlantic oceans due to the high degree of hydrostatic instability in these areas, due to cold air advection from the cold continents over the relatively warm sea surface. The heating in these areas is in the form of latent heat release and sensible heating (heat transfer from the ocean to the atmosphere). In the tropics the heating is principally due to latent heat release. The cooling in the regions that are coloured blue is due to emission of radiation. The average is for the period 1979-2001. Source: http://www.ecmwf.int/research/era/ERA-40_Atlas.

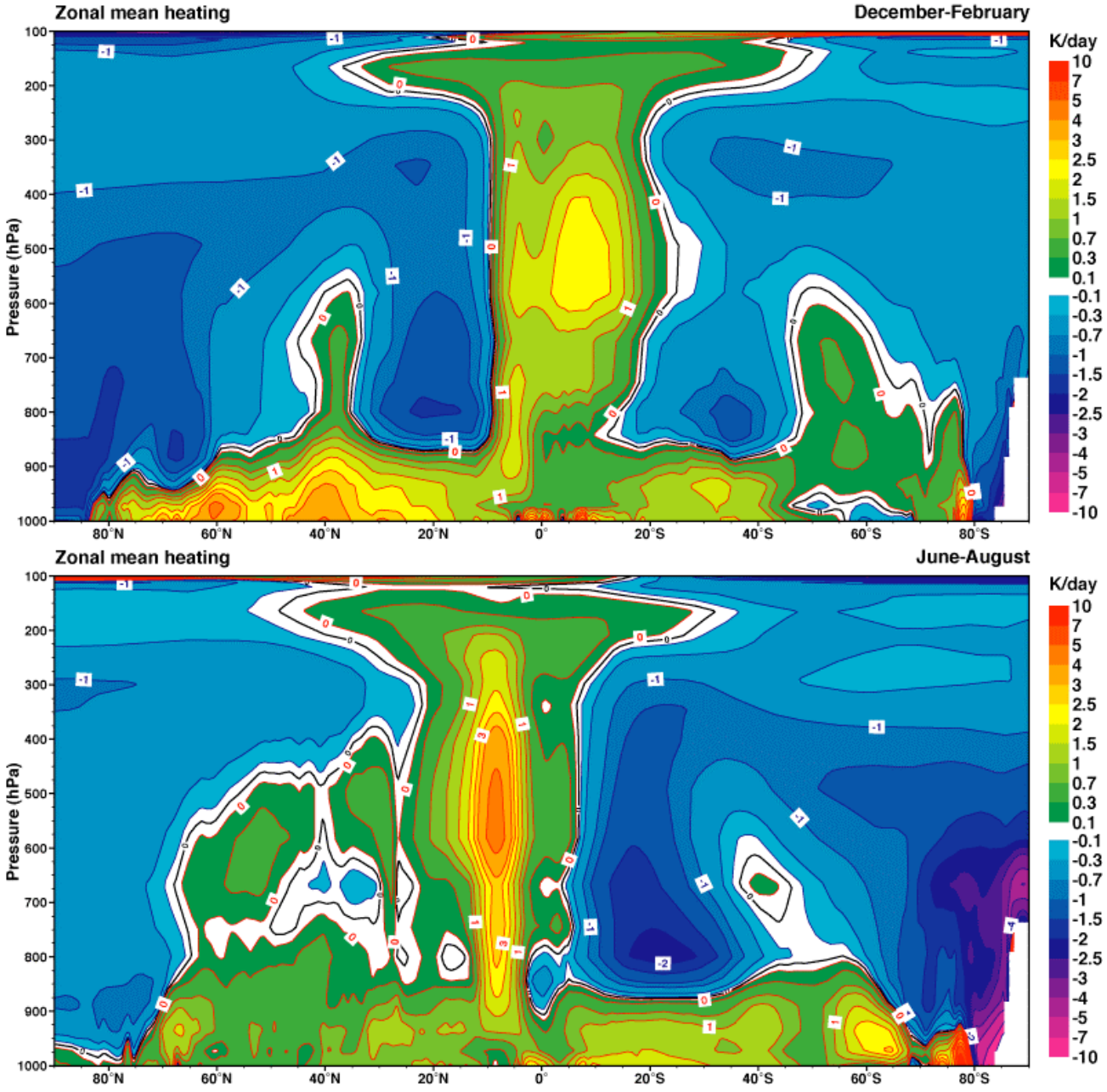

FIGURE 2.28. Zonal average diabatic heating rate in, respectively, December, January and February and in June, July and August. The average is for the period 1979-2001. Source: http://www.ecmwf.int/research/era/ERA-40_Atlas.

PROBLEM 2.10 Internal atmospheric diabatic heating

(a) What is the reason for the strong diabatic cooling (about 2 K per day) in the sub-tropics of the winter hemisphere (around 20°S) at about 800 hPa (figure 2.28). Hint: take note of the existence of the Hadley circulation (figure 1.45).

(b) What mechanism is the cause of the diabatic heating below 900 hPa at this latitude (around 20°S)?

2.11 Absorption and emission of radiation by greenhouse gases

Assuming that radiation passes vertically through the atmosphere the attenuation of radiation intensity, I, due to absorption by a greenhouse gas, for an incremental distance dz, can be expressed, according to the **Bouguer-Lambert-Beer law** as (**Box 2.2** and **Box 2.3**)

$$dI = -\sigma_a \rho_a I dz \equiv -I d\delta \qquad (2.43)$$

Here ρ_a is the density of the absorber and σ_a is the **absorption cross-section** of this absorber [m^2kg^{-1}] and δ is the associated **optical path**. Unit optical path implies that radiation is attenuated by a factor e^{-1}. Note that the absorption cross-section is now expressed in units of m^2kg^{-1} instead of in units of m^2 per molecule.

With the hydrostatic relation,

$$dp = -\rho g dz,$$

the optical path becomes

$$d\delta = \sigma_a \rho_a dz = -\frac{\sigma_a \rho_a}{g\rho} dp = -\frac{\sigma_a q_a}{g} dp \ . \qquad (2.44)$$

The specific concentration, q_a, is defined as

$$q_a = \frac{\rho_a}{\rho} \ .$$

(see also eq. 1.9).

If the layer is well-mixed, the specific concentration of any constituent is constant within the layer. The total optical path, δ, of such a layer resulting from absorption of long wave radiation by an absorber is the integral of (2.44) from the bottom (at pressure p_b) to the top (at pressure p_t) of the layer:

$$\delta = -\frac{1}{g} \int_{p_b}^{p_t} \sigma_a q_a dp \, .$$

If we may assume that σ_a is constant the expression for δ becomes

$$\delta = \sigma_a \int_{p_t}^{p_b} \rho_a dz = \sigma_a W_a \, . \qquad (2.45)$$

Here, W_a represents the vertically integrated absorber amount in kg m^{-2}. If the absorber is water vapour, W_a represents the precipitable water, PW (section 1.10). Eq. 2.45 predicts that the optical path is linearly proportional to the absorber amount. The constant of proportionality is the absorption cross-section, σ_a.

Figure 2.29 shows a plot of the optical path as a function of precipitable water. This is a very rough estimate, which is based on laboratory measurements of the attenuation by water vapour of radiation in the wavelength interval between 5 and 30 μm.

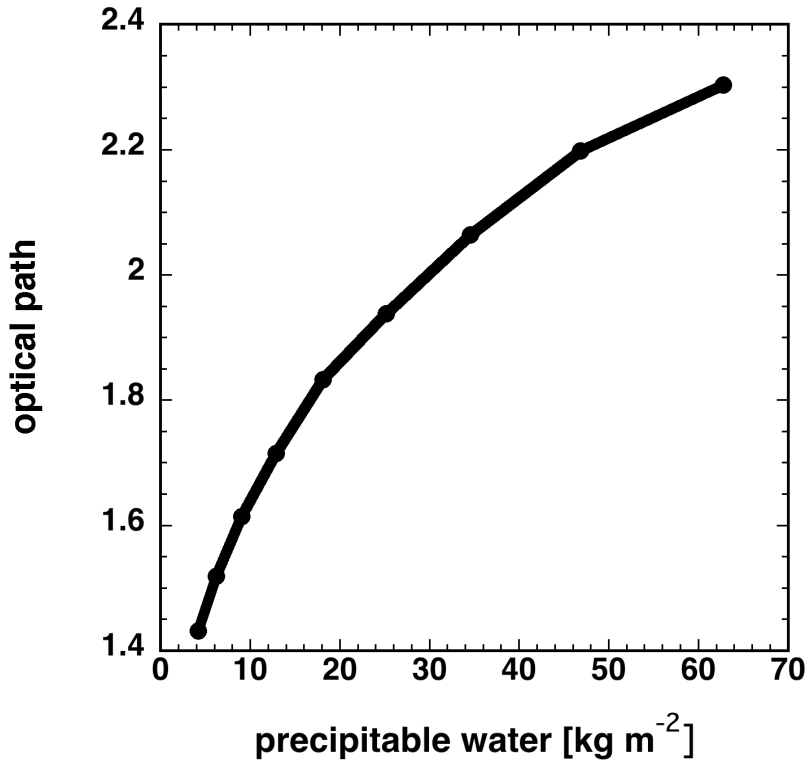

FIGURE 2.29. Atmospheric optical path as function of precipitable water, estimated from laboratory measurements. Data taken from a paper by R.W. Bliss Jr., 1961, **Solar Energy, 5,** p. 103-120.

In deriving eq. 2.45 we have assumed that absorption and emission of long-wave radiation is characterized by one constant absorption cross-section for all wavelengths of radiation. **Figure 2.29** demonstrates that this is not true for water vapour if PW>10 kg m^{-2}, i.e. the optical path is in fact *not* linearly proportional to the absorber amount. Nevertheless, if we would really want to assign one wavelength-independent value to the absorption cross-section of water vapour within a realistic average range of precipitable water contents around the global average value of 25 kg $^{-2}$, we would, based on the data of **figure 2.29**, end up with

$$\overline{\sigma}_v \approx 0.04 - 0.3 \text{ m}^2\text{kg}^{-1}.$$

When we adopt the simplifying assumption, in the following, that water vapour absorbs long-wave radiation equally at all wavelengths, we use a value $\overline{\sigma}_v$=0.125 m^2 kg^{-1}.

In reality water vapour and carbon dioxide absorb radiation in specific and different wavelength- or frequency intervals. Water vapour absorbs radiation *principally* in the wavelength-intervals 5-7 μm and >19 μm (**figure 2.30**). Carbon dioxide absorbs radiation principally in two wavelength intervals *within the range of terrestrial emission*, i.e. in the intervals 4-5 μm and 13-17 μm (**figure 2.30**). The first interval can in fact be neglected, as far as the atmosphere of Earth is concerned, because little energy is radiated in this interval (**figure 2.31**). Within the second interval the dependence on wavelength of the absorption cross-section of CO_2 is extremely complex, as is illustrated in **figure 1** of **Box 2.3**.

The CO_2 absorption band at 13-17 μm is found to the right of the peak of the terrestrial spectrum (**figure 2.31**). This band represents 19% of the total long wave radiation energy

emitted by the Earth's surface, assuming that 210 K<T_g<288 K. The two water vapour absorption "intervals" are found farther away from the peak in the terrestrial radiation spectrum. There is relatively little absorption of radiation near the peak of the terrestrial radiation energy spectrum, in the wavelength interval between 8 and 13 μm (**figure 2.30**). This wavelength interval is, therefore, referred to as the "**atmospheric infrared window**". The relatively weak sensitivity of Earth's temperature on CO_2-concentration is principally due to the existence of the infra-red window (section 2.17).

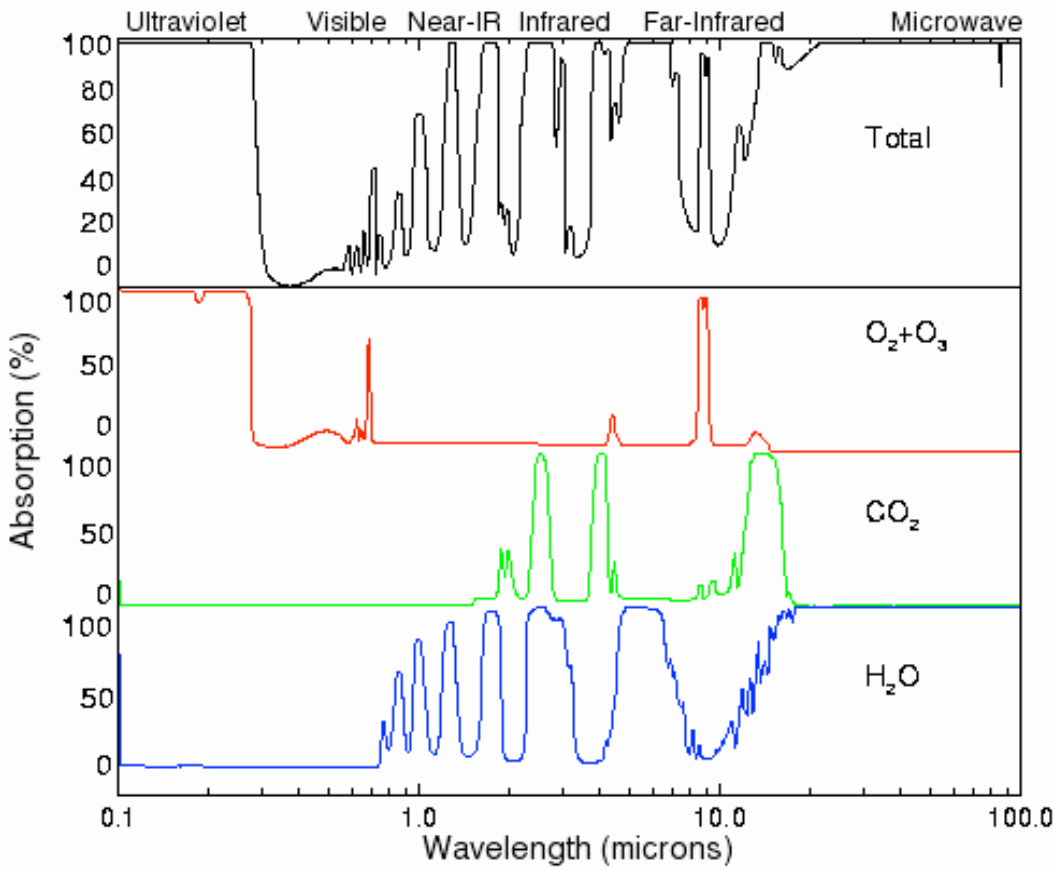

FIGURE 2.30. Attenuation of radiation by various gases in the atmosphere as a function of wavelength of the incident radiation. Most of the ultraviolet light (below 0.3 microns) is absorbed by ozone (O_3) and oxygen (O_2). Carbon dioxide has four significant absorption bands in the infrared region between 2 and 17 microns. Only the absorption band between 13 and 17 microns falls in the range of wavelengths of the terrestrial emission (wavelengths greater than 4 microns). Water vapour has several absorption bands in the infrared, and even has some absorption well into the microwave region. Source: http://brneurosci.org/co2.html.

Assuming that the mean temperature of the Earth's surface is 288 K, we find that the about 31% of the total long wave irradiance emitted by the Earth's surface falls into this infra-red window. This is about 120 W m^{-2}. In other words, with a perfectly transparent window and no clouds, about 31% of the radiative energy flux that is emitted by the Earth's surface escapes to space. According to the data in **figures 2.10 and 2.25**, only about 10% of the radiation that is emitted by the Earth's surface escapes to space *through the atmospheric window*. The infrared window is therefore not perfectly transparent, principally because clouds intercept radiation that is emitted in this wavelength interval below cloud base. Oxygen, ozone and water vapour also absorb radiation within the infrared window.

However, as a first order approximation, the effect of these contributions to the absorption of long-wave radiation can be neglected compared to the effect of clouds.

The absorption cross-section of liquid water is at least one or two orders of magnitude larger than the absorption cross-section of water vapour or carbon dioxide. Therefore, clouds, which consist mostly of liquid water droplets, are potentially strong amplifiers of the greenhouse effect. This, of course, depends upon the degree of cloud cover. The global average cloud cover fraction is about 0.65 (0.54 over land and 0.69 over oceans). This means that clouds block about 65% of the long wave irradiance that is emitted below cloud base. But they also block the short wave irradiance. **Cloud cover fraction is therefore a crucial parameter in climate studies**.

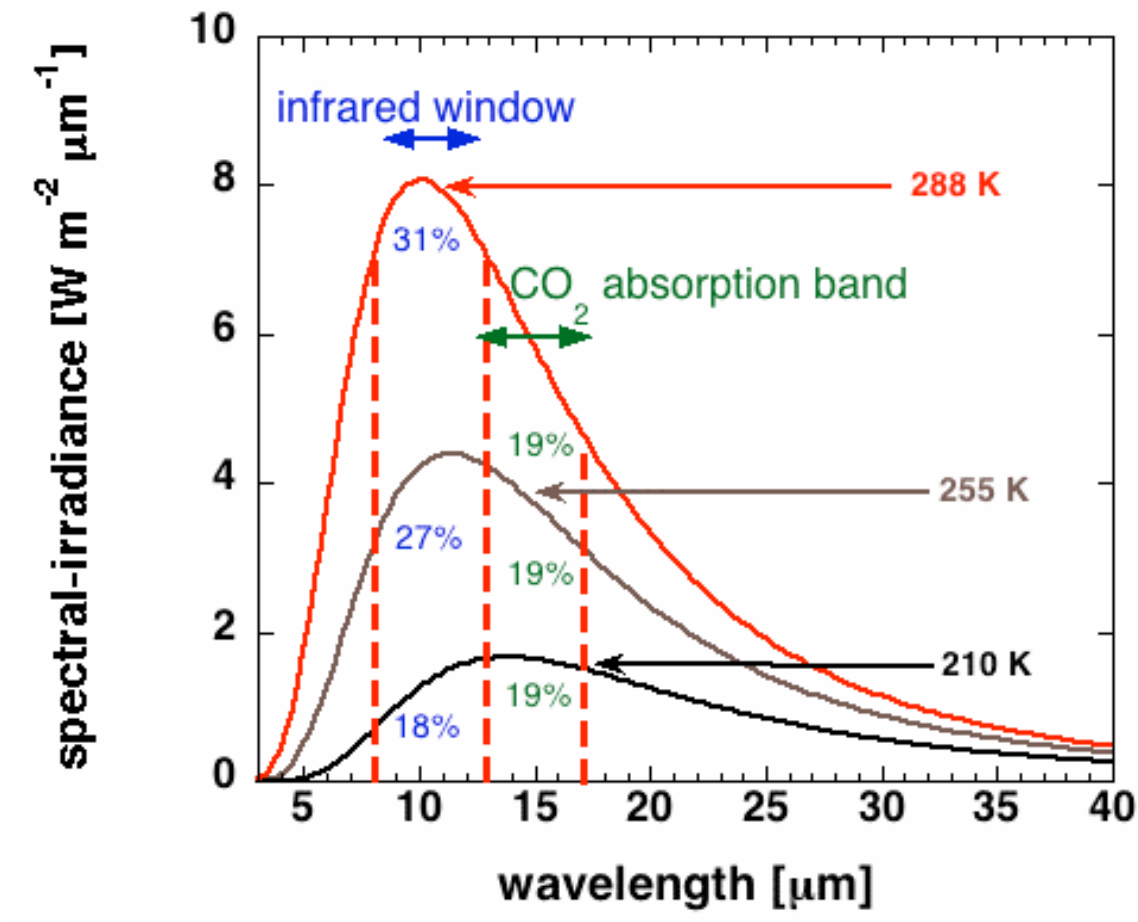

FIGURE 2.31. Spectral irradiance as a function of wavelength (**"Planck's curve"**) for a black body with a temperature of 288 K, of 255 K and of 210 K. The wavelength intervals of the infrared window and of the carbon dioxide absorption band (13-17 micrometre) are indicated by straight vertical dashed lines. The percentages refer to the spectral irradiance within the specified interval as a fraction of the total spectral irradiance at the specified temperature. At lower temperatures relatively less and less energy is emitted in the "window"-interval because the curve shifts to higher wavelengths.

The following 8 sections are devoted to the complex effect of the water cycle on the energy balance of the atmosphere and the Earth's surface. In section 2.12 some useful statistics of cloud cover fraction in relation to the water vapour distribution are presented. Section 2.13 is devoted to the discussion of the albedo- and greenhouse effects of clouds.

Section 2.14 explains how the energetic effects of water (phase changes and interaction with radiation) are incorporated into a radiative-convective model. Solutions of this model are discussed in sections 2.15-2.19.

As a first order approximation we can define three wave length intervals in the long wave (terrestrial) spectrum, one representing the atmospheric window and the others representing, respectively, the carbon dioxide absorption band and the aggregate of intervals where absorption by water vapour dominates. But before discussing this, it is necessary to discuss a very complex matter, namely the interaction of clouds with radiation. As stated before, the impact of this interaction on atmospheric temperature depends crucially on the degree of cloud cover and cloud liquid water path. The follow section discusses the first and most important of these two parameters, i.e. cloud cover. "Liquid water path" is introduced in section 2.13.

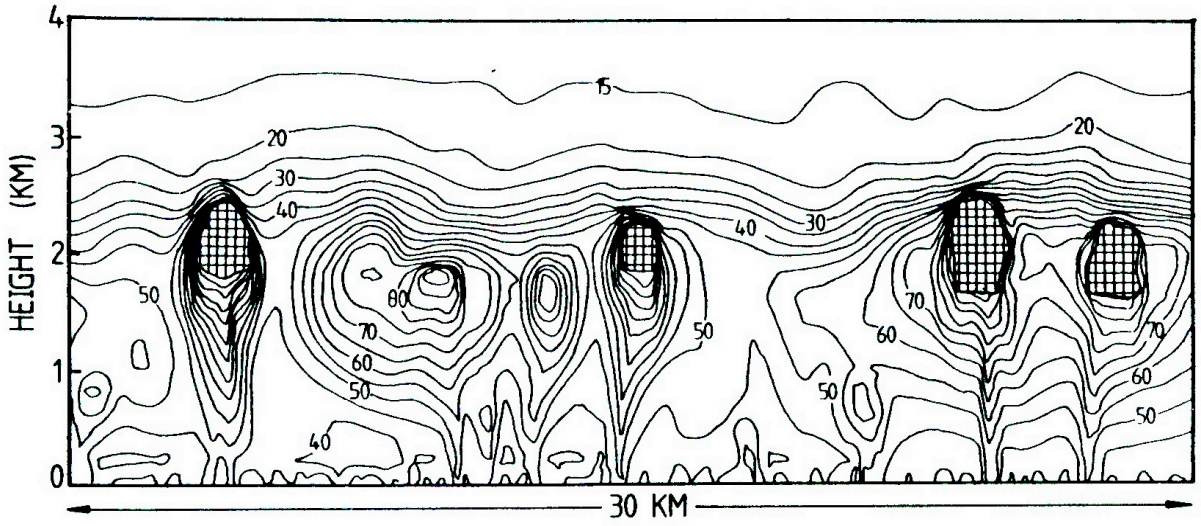

FIGURE 2.32. Model simulation of the relative humidity in the atmospheric boundary layer at midday in June in The Netherlands. The hatched regions correspond to clouds (regions where the relative humidity is 100%). The degree of cloud cover in this case is about 20%. Source: A. van Delden and J. Oerlemans, 1982: Grouping of clouds in a numerical cumulus convection model. **Contr.Atmosph.Phys**., 55, 239-252.

2.12 Cloud cover

The instantaneous horizontal distribution of relative humidity, and therefore also of clouds, is nearly always very inhomogeneous. This is illustrated in **figure 2.32**, which shows the result of a model simulation of the convective boundary layer. The numerical model is initialized with a horizontally homogeneous temperature distribution derived from a radiosonde, which was launched on a sunny summer day in June 1981, a few hours after sunrise when no clouds were present yet. The temperature at the surface is perturbed slightly and randomly in order to initiate convection due to the hydrostatic instability of the surface layer. Water vapour enters the atmosphere at the ground by evaporation and is transported to the top of the unstable boundary layer in the convective updraughts. The relatively moist air in the updraughts becomes saturated above a **"lifting condensation level"**. This leads to the formation of characteristic **puffy clouds**, called **cumulus clouds** (indicated in **figure 2.32** by the hatched regions; see also **figures 2.33 and 2.34**). At the same time relatively dry air moves downwards. In the upper part of the boundary layer saturated cloudy air resides

closely alongside relatively very dry air. Near the Earth's surface the relative humidity is distributed more uniformly. The average surface relative humidity is about 40-45%. Despite this low relative humidity at the surface, the degree of cloud cover in the upper part of the boundary layer in the simulation is still about 20 %.

Of course, not all clouds are formed in the same way as cumulus clouds in the summer season, i.e. from hydrostatic instability at the Earth's surface. Especially in winter in mid-latitude- and in polar regions, clouds are dominantly the result of slow slanted and weak ascent of relatively warm air over very large regions in connection with adjustment to thermal wind balance, especially within mid-latitude depressions and fronts (**Box 1.7**). This process produces the **layered clouds**, such as **cirrus and (alto) stratus** (**figures 2.35**).

Cloud cover has been observed by eye and documented systematically at many measuring sites over the world, especially after the Second World War. **Figure 2.36** shows the distribution of the annual average cloud cover fraction for measuring sites over, respectively, land and ocean. The average cloud cover fraction over the oceans, according to this analysis, is 0.69. Over land this fraction is much lower: 0.54. The estimates of total cloud cover fraction based on satellite observations are different: for the years 1983 to 1997 this yields annual average cloud cover fractions of 0.58 for land areas and 0.72 for ocean areas[81]. Direct observations, therefore, yield a global average cloud cover fraction of 0.65-0.68. However, the NCEP-2 reanalysis global average cloud cover for the period 1979-2008 is much lower: 0.55.

FIGURE 2.33. Artists (by Lee Boyd) impression of cumulus clouds seen from below, illustrating that clouds intercept Solar radiation. Source: http://cloudappreciationsociety.org/.

[81] Rossow, W.B., and R.A. Schiffer, 1999: Advances in understanding clouds from ISCCP. **Bull.Amer.Meteorol.Soc**., 80, 2261-2287.

FIGURE 2.33. Large cumulus clouds.

FIGURE 2.35. Layered clouds: cirrus in the foreground and alto-stratus in the background. The feathery cirrus clouds are more transparent to Solar radiation than the altostratus.

Figure 2.37 shows the average cloud cover over the globe in, repectively January and July, according to the Japanese reanalysis. The basic features of the climate of the Earth that were described earlier are revealed in the cloud cover once again: the ITCZ and also the mid-latitude "storm tracks" are characterized by a high cloud cover of more than 70%, while the subtropical land areas enjoy very frequent clear skies. Interesting additional features of the cloud cover climate are the very cloudy areas over certain subtropical ocean regions.

Examples are the coastal waters near Peru, and near California and also near Namibia. All these regions are characterized by a low sea surface temperature because of upwelling of cold water in the ocean. A relatively stable and very humid boundary layer forms in these areas. This boundary layer is almost always capped by a layer of low strato-cumulus or stratus clouds and a temperature inversion (similar to the tropopause) at about 2 km above sea level (see the vertical profile of the July-average relative humidity at St Helena that is plotted in **figure 1.13**).

Cloud-type	**Cloud-top [km]**	**Frequency [%]**	**albedo**
High	10	23	0.20
Middle	4.1	9	0.48
Low	2.7	31	0.69

TABLE 2.3. Cloud classification adopted by Manabe and Wetherald (1967) (S.Manabe and R.T.Wetherald, 1967: Thermal equilibrium of the atmosphere with a fixed distribution of relative humidity. **J.Atmos.Sci., 24**, 241-259).

Traditionally, meteorologists classify clouds into three categories: **high clouds** (cirrus and deep convective cumulo-nimbus clouds), **middle clouds** (altocumulus and altostratus) and **low clouds** (cumulus, stratus and stratocumulus). Most common clouds are low-level, liquid clouds. According Manabe and Wetherald (1967) (**table 2.3**) about 31 % of the globe is covered exclusively by low clouds, while about 23% of the globe is covered by high clouds with tops around 10 km above sea level. These "high clouds" come in different forms, i.e. the "feathery" thin type of cloud called "cirrus" (**figure 2.35**) and the "thunderstorm" type of cloud called "cumulonimbus" (**figure 2.33**). The cumulonimbus cloud is observed most frequently in the tropics and over the continents in summer, while cirrus is observed at all latitudes.

More recent estimates of cloud cover, based on satellite measurements[82], indicate that low-level cloud-amounts are about 40% larger than high-level cloud-amounts. Furthermore, by far most clouds contain relatively little condensed water. This is expressed in terms of the **"liquid" water path**, *LWP*, which is defined in the same way as precipitable water (*PW*) (eq. 2.45), i.e. as

$$LWP \equiv \int_{z=0}^{\infty} q_L \, dz \quad . \tag{2.46}$$

In equation (2.46) $q_L = \rho_L / \rho$ is the specific concentration of condensed (liquid) water in the atmosphere ($=\rho_L$ is atmospheric condensed water content in kg m^{-3}). About 85% of all clouds have water paths less than 150 g m^{-2}, whereas less than 10% of clouds have water paths large enough to produce precipitation, i.e. greater than 250 g m^{-2}.

The optical properties of cirrus and cumulonimbus are very different. Less Solar radiation penetrates through the thick cumulonimbus clouds, which have their base at about 1 km above sea level, than through the thin cirrus clouds. Cumulonimbus clouds have a high albedo as well as a high emissivity, while cirrus clouds have a low albedo and a low emissivity (section 2.13, **figure 2.40**).

---

[82] Rossow, W.B., and R.A. Schiffer, 1999: Advances in understanding clouds from ISCCP. **Bull.Amer.Meteorol.Soc., 80**, 2261-2287.

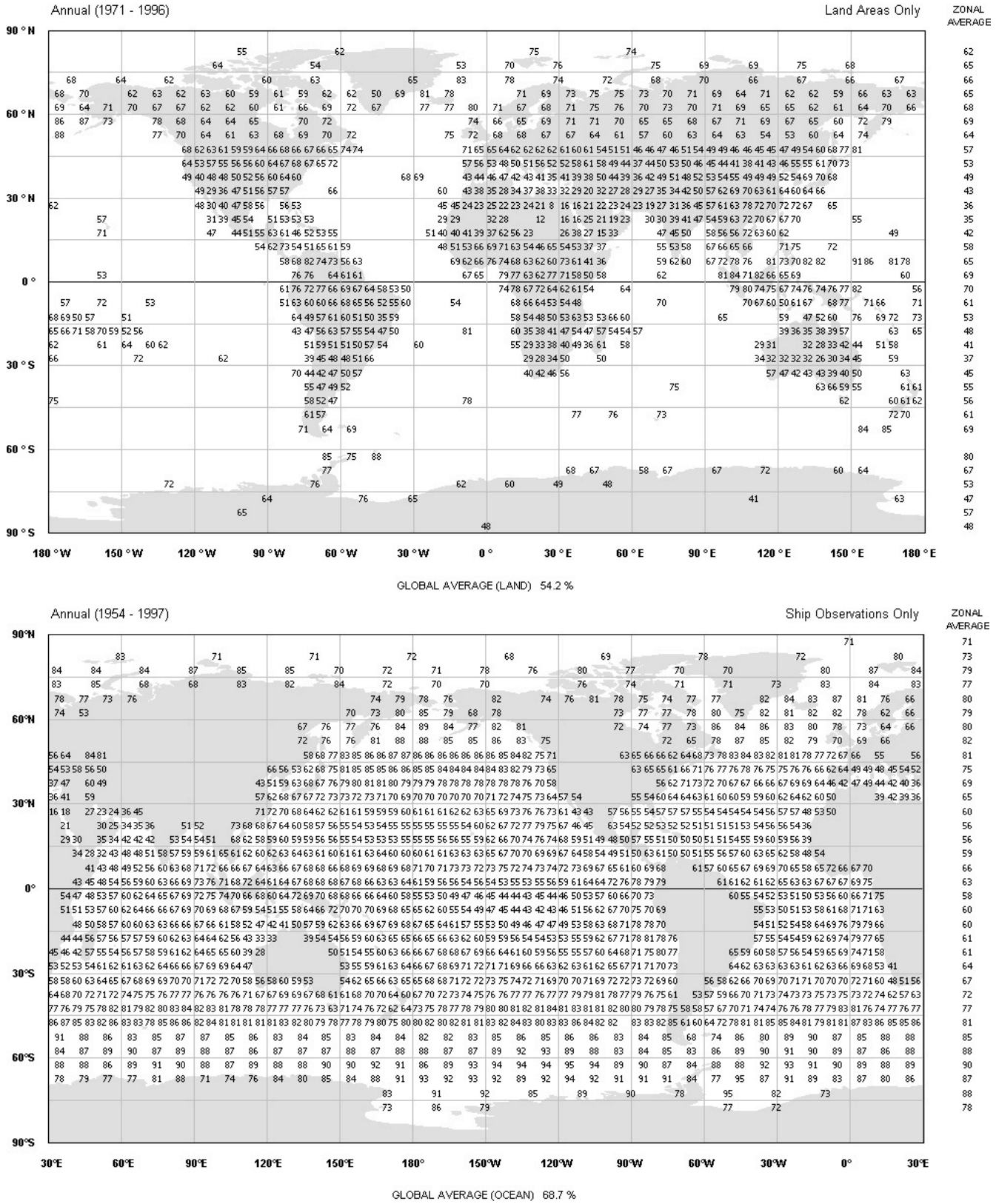

FIGURE 2.36. Annual average cloud cover in % over land (upper panel) and over sea (lower panel) according to an analysis of cloud observations. Average is for the periods 1971-1996 (land) and 1954-1997 (sea). Source: http://www.atmos.washington.edu/~ignatius/CloudMap/index.html.

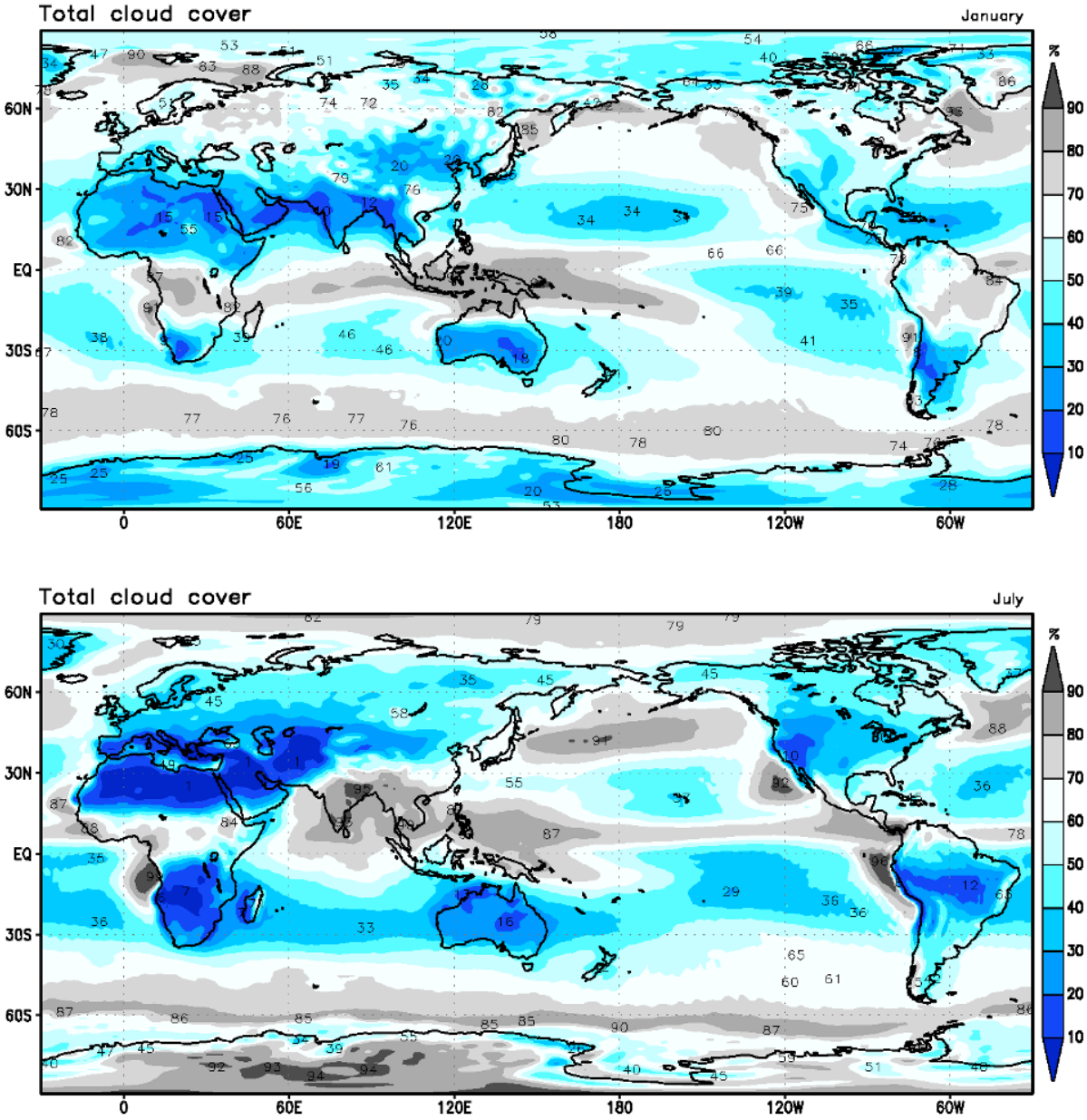

FIGURE 2.37. Average cloud cover in January (upper panel) and July (lower panel) according to the reanalysis of the Japan Meteorological Agency. Labels in %. Average is for the period 1979-2004. Source: http://jra.kishou.go.jp/JRA-25/index_en.html.

Obviously, the right description of the distribution of cloud types is of great importance in radiation calculations. Unfortunately, we are still far from achieving this goal. For example, the fraction of the area covered by marine stratocumulus clouds is systematically underestimated by the ERA-40[83] reanalysis and it still remains to be seen whether the new reanalyses are much better in this respect. Significant progress in the performance of models in getting a correct the cloud-distribution will be made only with the future introduction of

[83] Allan, R.P., et al., 2004: Simulation of Earth's radiation budget by the European Centre for Medium Range Weather Forecasts 40-year reanalysis. J.Geoph.Res., 109, D18107.

high-resolution non-hydrostatic models with an explicit representation of clouds. This depends fully on an increase in the speed of the central processor units of computers by several orders of magnitude. Assuming that the computation speed increases by roughly a factor 10 every 10 years, we may expect global non-hydrostatic climate models with a realistic explicit representation of clouds within 20 to 30 years from now (2012).

In view of the strong coupling between the humidity at the Earth's surface and humidity at greater heights in the atmosphere (section 1.10), one may wonder whether a similar coupling exists between the relative humidity at the Earth's surface and the degree of cloudiness. The statistical relation between cloud cover and humidity at the Earth's surface can be determined from daily-average values of cloud cover fraction and relative humidity at 1.5 m height. Cloud cover fraction is expessed by meteorologists in octa's, while relative humidity is expressed as a percentage of the saturation value at the observed temperature (eq. 1.29). **Figure 2.38** shows the probability density function of daily-average relative humidity near the Earth's surface for two sites with a very different climate, i.e. Badajoz (south-west Spain) and Helgoland (North Sea). The climate of Badajoz is "bimodal", i.e. in the winter-half of the year it is representative of the midlatitudes (precipitation is relatively abundant), while in the summer-half of the year it is representative of the subtropical deserts, i.e. the climate is determined by the drying effect of the downward branch of the Hadley circulation (**figure 1.12**). Helgoland is a very small island (1.7 km^2) in the German Bight (North Sea) about 70 km from the coast with a purely maritime climate all year round.

The probability density function of daily average relative humidity is determined by dividing the full range of possible values of relative humidity (0-100%) into 50 bins of 2%, then counting the number of days that fall into each bin, and subsequently dividing the number of days in each bin by the total number days.

The bimodal climate of Badajoz is manifested by the two maxima in the probability density function (**figure 2.38**). The first maximum, at a relatively high relative humidity of 81%, is associated with the wet winter season, while the second maximum, at a low relative humidity of 55%, is associated with the dry climate of the summer season. The probability density function of relative humidity corresponding to Helgoland has only one maximum at a high relative humidity of 83%.

Figure 2.39 demonstrates that, despite these large differences in moisture-climate, the average degree of cloud cover that is observed at a specified value of the relative humidity near the Earth's surface is not much different at the two sites.

The interesting question now, is the following. Is the relative humidity at the Earth's surface determined by cloud cover fraction or is cloud cover fraction determined by the relative humidity at the Earth's surface? At first sight the latter statement seems most likely, since the Earth's surface is the only source of tropospheric water vapour and since there is a strong coupling between the density of water vapour at the Earth's surface and the density of water vapour aloft (eq. 1.26). Moreover, the lifting condensation level for air parcels that start their ascent at the Earth's surface (section 1.16) increases with decreasing relative humidity of the air parcel at the Earth's surface. Obviously, the probability that a cloud will form decreases with increasing the lifting condensation level. However, cloud cover fraction is also strongly correlated with the net radiation flux at the Earth's surface, i.e net radiation increases with decreasing cloud cover. Net radiation determines both the temperature at the Earth's surface and the evaporation at the Earth's surface. It is reasonable to assume that both these quantities increase approximately linearly with net radiation. However, because the saturation vapour pressure increases exponentially with temperature (**figure 1.8**), the relative humidity at the Earth's surface will decrease with increasing net radiation. So, this would imply that the relative humidity of the atmosphere near the Earth's surface is positively correlated with the cloud cover fraction, in accord with **figure 2.39**.

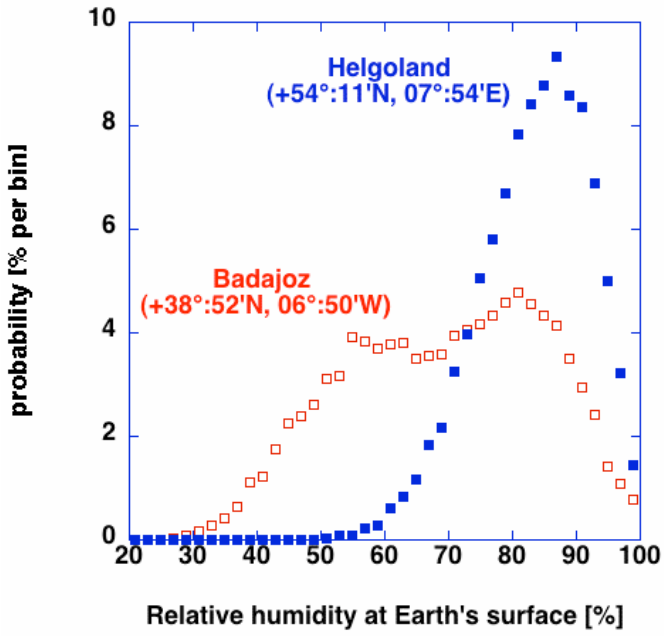

FIGURE 2.38. Frequency distributions of daily-average relative humidity at 1.5 m above the ground (divided into bins of 2%) for Badajoz-Talavera (1961-2008) (red open squares) and for Helgoland (1952-2008) (blue solid squares). The daily-average value is calculated from observations made at 06, 12 and 18 UTC. Data from (http://eca.knmi.nl/).

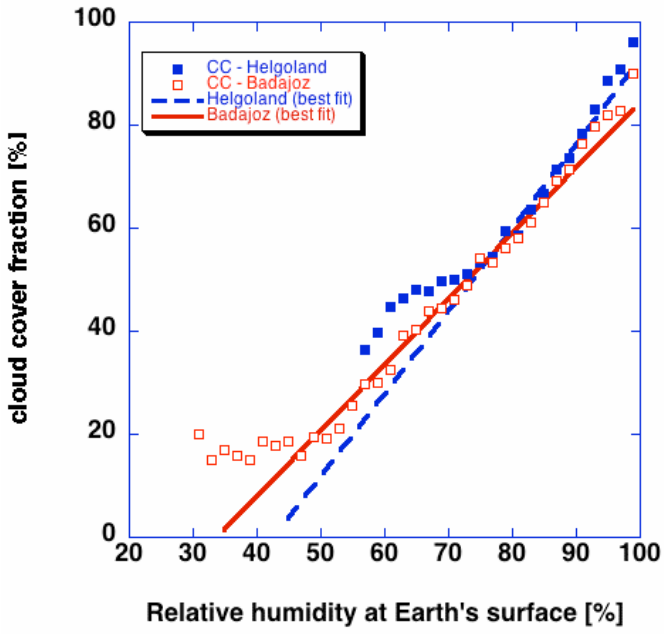

FIGURE 2.39. Weighted daily average cloud cover (in %) plotted against daily average relative humidity at 1.5 m above the ground in Badajoz (1961-2008) (open red squares) and Helgoland (1952-2008) (closed blue squares). For each bin of 2% in relative humidity the sum of all values of cloud cover is computed and this number is divided by the total number of events in the particular bin. The daily-average value of A_c, that is derived in this way, is based on observations made at 00, 06, 12 and 18 UTC. If the probability density function for relative humidity falls below 0.1%, the weighted daily-average cloud cover is not plotted. The solid red line (for Badajoz) and the dashed blue line (Helgoland) represent the best (weighted least square) linear fit to these averages. Data from (http://eca.knmi.nl/).

Figure 2.39 suggests that the following **relation between relative humidity, RH_g, at the ground and cloud cover fraction, A_c**, exists.

$$A_c = C\left(RH_g - RH_0\right) \text{ for } RH_g > RH_0 \ , \tag{2.47a}$$

$$A_c = 0 \text{ for } RH_g \le RH_0 \ . \tag{2.47b}$$

Here, C is a constant number and RH_0 is the surface relative humidity below which the sky is cloudless. The values of C and RH_0 are obtained by applying a weighted least square fit to the data points shown in **figure 2.39** (weighted with the probability shown in **figure 2.38**). This procedure yields a value of RH_0 of 34% for Badajoz and of 43% for Helgoland. The latter value, however, is meaningless, because a daily-average relative humidity of 43% or lower is hardly ever observed at Helgoland. The value of C that best fits the data points in **figure 2.39** corresponding to Badajoz is C=1.28. In section 2.19 we'll invoke (2.47) as a **parametrization of cloud cover** in the radiative convective model[84]. This parametrization seems to be most robust for $0.7<RH_g<0.85$, which, with C=1.28 and RH_0=34%, would correspond to $0.46< A_c <0.65$. The global- and time-average relative humidity at 1000 hPa, which is a pressure level close to the ground, for the period 1979-2008, according to the NCEP-2 reanalysis, is 0.77. For this value of RH_g the parametrization (2.47) yields A_c=0.55, which corresponds exactly to the NCEP-2 reanalysis estimate of the global- and time-average value of A_c for this period, but is significantly lower than estimates based on satellite observations and direct observations, which indicate that the global average value of A_c is about 0.65. This discrepancy is rooted in the difficulty of an unambiguous determination of cloud cover fraction.

2.13 The influence of clouds on radiation

Clouds reflect Solar radiation, behaving like a snow-covered surface, but they also absorb and emit long wave radiation practically as a black body, thus, behaving like a perfect greenhouse gas. Therefore, cloud cover is an important parameter in climate modelling because clouds have an enormous influence on the radiation balance.

Figure 2.40 demonstrates that both the long wave emissivity of clouds and the short wave albedo depend on the liquid water path, *LWP* (defined by eq. 2.46). Cloud albedo increases more gradually with *LWP* than cloud emissivity. Most clouds, except cirrus, have liquid water paths in excess of 100 g m^{-2}, and therefore are effectively black bodies. Precipitating clouds have liquid water paths in excess of 250 g m^{-2}.

The net radiative effect of clouds on the temperature at the Earth's surface depends on a small difference between the large effects of, respectively, cloud albedo and cloud emissivity. Getting this net effect right in climate models obviously represents a daunting task. Cloud cover fraction, cloud thickness and cloud top temperature are important parameters in this respect. Clouds with cold high tops emit very little radiation to space while clouds with low relatively warm cloud top heights emit more radiation to space and thus tend to cool the atmosphere.

---

[84] For an overview of similar cloud parametrization schemes, see p. 349-353 in D.J. Stensrud, 2007: **Parameterization Schemes**. Cambridge University Press. 459 pp.

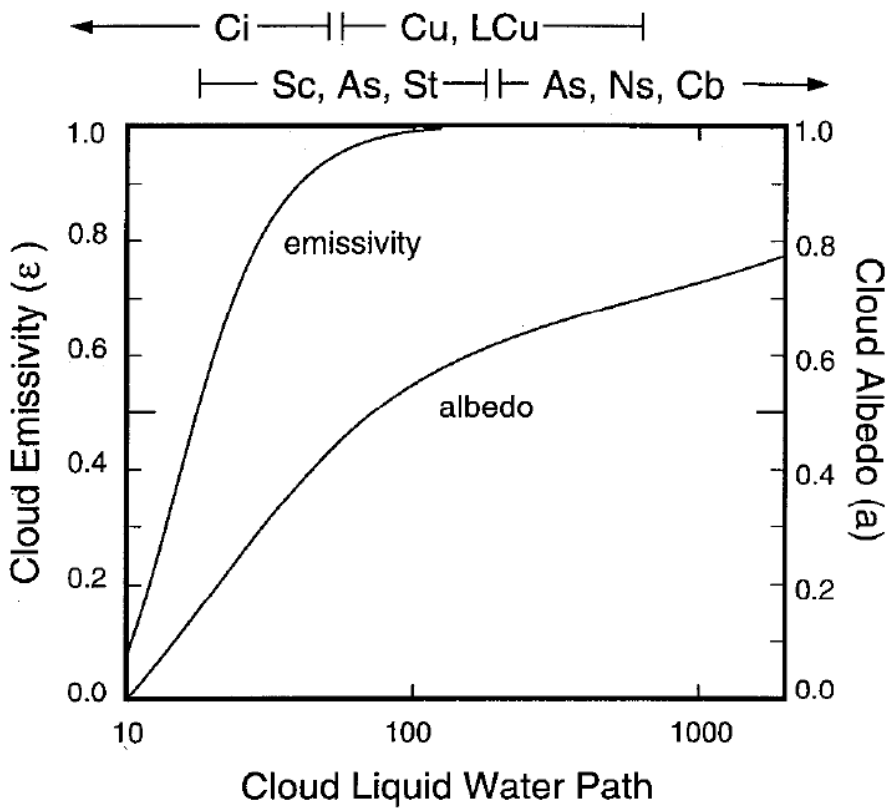

FIGURE 2.40. Cloud albedo and cloud emissivity as a function of liquid water path (in units of g m^{-2}) of a cloud. Cloud types associated with the values of liquid water path are displayed on the upper abscissa. Ci stands for cirrus, Cu for cumulus, Sc for stratocululus, St for stratus, As for altostratus, Ns for nimbostratus, Cb for cumulonimbus. Whereas albedo increases relatively slowly with liquid water path, the emissivity increases rapidly. Thus, a cloud appears to be optically black even for relatively thin clouds. Source: Webster, P.J., 1994: The role of hydrological processes in Ocean-atmosphere interactions. **Rev.Geophysics, 32**, 427-476.

A global climate model cannot resolve every cloud. At the time of writing (2012) the horizontal resolution of General Circulation climate Models (GCM's) is in the order of 100 km. For comparison, the model, which was used for the cumulus cloud simulation, a result of which is illustrated in **figure 2.32**, has a horizontal resolution of only 200 m. For the assessment of the radiative effects of clouds in a model one needs information about the degree of cloud cover within each grid cell. If the horizontal resolution is 100 km or more, the cloud cover must be "parametrized", i.e. expressed in terms of explicitly calculated variables. For this purpose we can, for example, make use of the statistical relation between cloud cover and relative humidity near the Earth's surface that was found in the previous section (eq. 2.47).

The average albedo, α, for the area corresponding to particular model grid cell is usually related to the cloud cover, A_c, by the following simple equation.

$$\boxed{\alpha = (1 - A_c)\alpha_g + A_c\alpha_c}\,. \qquad (2.48)$$

Here, α_g is the area average albedo of the Earth's surface within the grid cell and α_c is the average albedo of the cloud-top. Cloud cover fraction, A_C, is expressed as fraction, i.e. as a number between 0 and 1.

A few words on the albedo of the Earth's surface are in order. Albedo strongly depends on the type surface. Fresh snow, for example, reflects about 90% of the incident Solar radiation. However, since about 70% of the Earth's surface is covered by water, the global average albedo is actually strongly determined by the albedo of water. A water surface reflects less than 10% of the incident Solar radiation if the Solar zenith angles (**figure 2.41**), lies between 0° and 60°. On the other hand, a calm water surface may reflect about 50 % of the Solar radiation at zenit angles greater than 80°, such as at the times of sunset or sunrise, or in the winter at high latitudes. Between 60°S and 60°N the annual average surface albedo is in the order of 0.1 (**figure 2.42**). Outside this band of latitudes, the presence of ice and snow as well as higher zenit angles, strongly enhances annual average surface albedo. The estimates of the global average (area weighted) surface albedo, based on **figures 2.10 and 2.25**, are 0.18 and 0.14, respectively. In the radiative-convective model we adopt the following values for, respectively, the ground albedo and the cloud albedo.

$$\alpha_g = 0.1 \text{ and } \alpha_c = 0.45 \ . \qquad (2.49)$$

Assuming a global average cloud cover fraction of 0.6, we get (from eq. 2.48) an approximate value of the planetary albedo of 0.31, which is close to the generally accepted value of this quantity (0.3)[85].

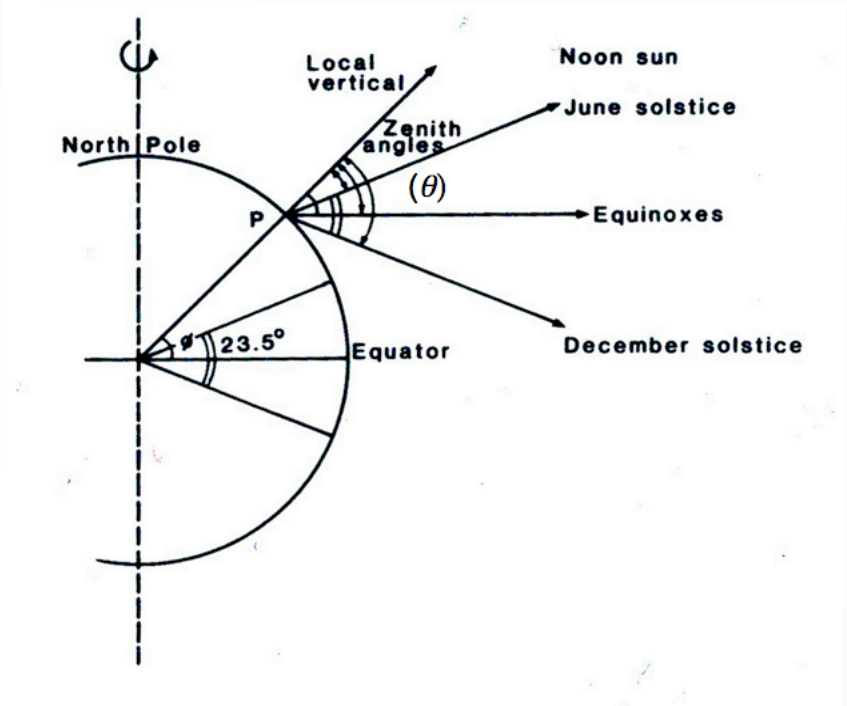

FIGURE 2.41. Angles subtended by the sun at noon at P at equinoxes and solstices, using the Earth's equatorial plane (so that the Sun seems to rise and fall by 23.5° seasonally). The symbol, θ, is used to designate the zenith angle (see eq. 6, **Box 2.1**). Source: McIlveen, R., 1986: **Basic Meteorology: A physical outline**. Van Nostrand Reinhold (UK). 457 pp.

[85] The global average, annual average planetary albedo according to different climate models ranges from 0.29 to 0.31 (see e.g. R.J. Charlson et al., 2005, **Science, 308**, p. 806).

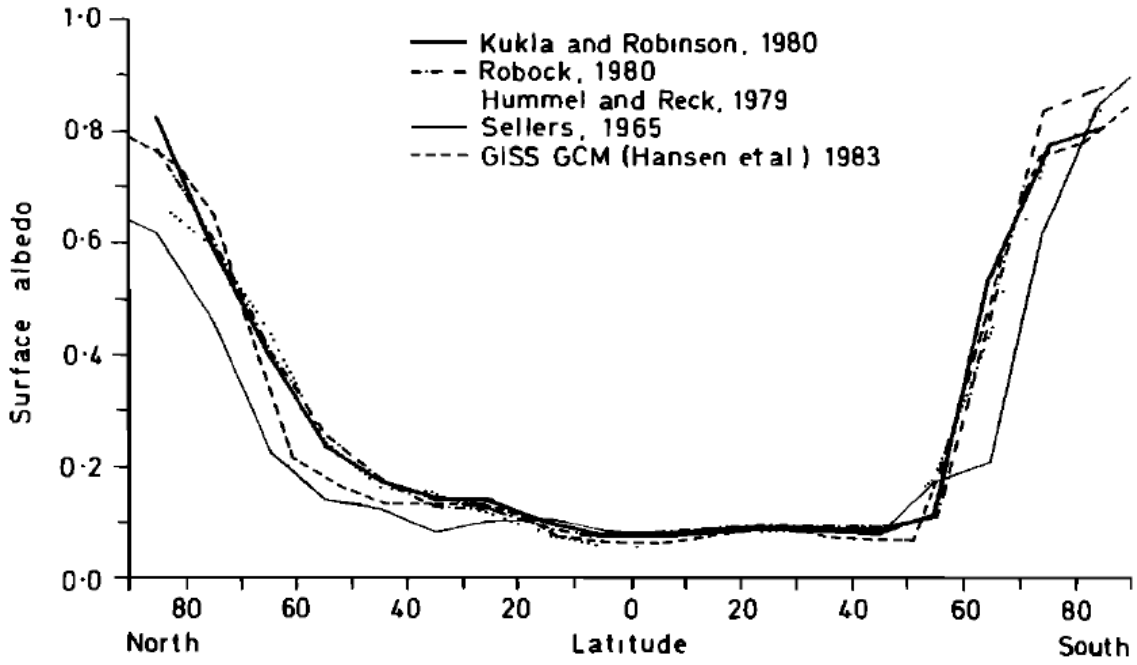

FIGURE 2.42. Zonal average and annual average estimates of the surface albedo. Source: A. Henderson-Sellers and M.F. Wilson, 1983: Surface albedo data for climate modeling. **Rev.Geophys.Space.Phys**., 21, 1743-1778.

2.14 The water cycle in the radiative-convective model

This section describes a method to incorporate the energetics of the water cycle in the radiative-convective model. This method begins by assuming two types of greenhouse gases. The first type is the well-mixed greenhouse gas. Its concentration is constant with height. Carbon dioxide is by far the most important well-mixed greenhouse gas. The second type of greenhouse gas is distributed inhomogeneously. Water vapour is the prime example of this type of greenhouse gas. Beside this, liquid water is assumed to be present in the atmosphere if the relative humidity exceeds a specified critical value, which is defined later in this section. Long wave radiation interacts with this atmospheric liquid water, i.e. with the model-clouds. The attenuation of long wave radiation by the well-mixed greenhouse gas, by water vapour, and by clouds in a particular layer of the atmosphere is calculated using Bougeur-Lambert-Beer law (**Box 2.2** and **Box 2.3**). The long wave radiation intensity is split into two parts, a part, I_1, which passes through clear part of the sky and a part, I_2, which passes through the cloudy part of the sky. Cloud cover fraction is the same at all levels where $q_L>0$. Applying the Bougeur-Lambert-Beer law to the two beams separately gives the following expressions for the attenuation of long wave radiation.

$$\frac{dI_1}{I_1} = \left(\rho_m \sigma_m + \rho_v \sigma_v\right) dz \ . \tag{2.50a}$$

and

$$\frac{dI_2}{I_2} = \left(\rho_m \sigma_m + \rho_v \sigma_v + \rho_L \sigma_L\right) dz \ . \tag{2.50b}$$

Here ρ_m, ρ_v and ρ_L are the mass densities of, respectively, the well-mixed greenhouse gas, water vapour and liquid water, and σ_m, σ_v and σ_L are the absorption cross-sections of, respectively, the well-mixed greenhouse gas, water vapour and liquid water [in m^2kg^{-1}]. The total intensity, I, of the long wave radiation is related to the partial intensity and the cloud cover by

$$I_1 = (1 - A_c)I \text{ and } I_2 = A_c I \qquad (I = I_1 + I_2) \,. \tag{2.51}$$

Since the radiative convective model is formulated in terms of layers of constant mass per unit area, eq. (2.50) is written as (using the hydrostatic relation, $\partial p/\partial z = -\rho g$)

$$\frac{dI_1}{I_1} = \frac{dI_2}{I_2} = -\frac{1}{g}(q_m\sigma_m + q_v\sigma_v)dp \text{ if } q_L = 0 \tag{2.52a}$$

or

$$\frac{dI_1}{I_1} = -\frac{1}{g}(q_m\sigma_m + RH_c q_s\sigma_v)dp \equiv d\delta_1 \text{ if } q_L > 0 \tag{2.52b}$$

and

$$\frac{dI_2}{I_2} = -\frac{1}{g}\left(q_m\sigma_m + RH_c q_s\sigma_v + \left(\frac{q_L}{A_c}\right)\sigma_L\right)dp \equiv d\delta_2 \text{ if } q_L > 0 \,. \tag{2.52c}$$

Here q_m, q_v and q_L are the specific concentrations of, respectively, the well-mixed greenhouse gas, water vapour and liquid water, dp represents the change in pressure across a model layer from the bottom to the top of this layer and $d\delta_1$ and $d\delta_2$ are the optical paths of, respectively, the beam that goes through the clear sky and the beam that goes through the clouds. **The two beams are independent!** This implies that the beam that goes through the clear sky will never encounter clouds along its path. The beam that goes through the clouds will, of course, encounter cloud-free conditions above and below cloud base. In these regions the expressions for $d\delta_1$ and $d\delta_2$ are identical. Within the cloud a part of the precipitable water exists in the form of liquid (condensed or cloud) water. In (2.52c) q_L is divided by the cloud cover fraction because q_L itself is an average of the specific concentration of liquid water over both the cloudy area and the clear area. The parameter, RH_c represents a critical layer averaged relative humidity above which condensation takes place and clouds form in this layer. The parameter, q_s, is the saturation specific humidity (determined by the Clausius Clapeyron equation given in section 1.9). The parametrization of cloud formation and precipitation will be discussed later in this section.

On the basis of the discussion given in section 2.11, we specify the values of the absorption coefficient of water vapour and the well-mixed greenhouse gas in the infrared as follows.

$$\sigma_v = 0.125 \text{ m}^2 \text{ kg}^{-1} \tag{2.53a}$$

The value of the absorption coefficient of liquid water (clouds) in the atmosphere is fixed at

$$\sigma_L = 5 \text{ m}^2 \text{ kg}^{-1}. \tag{2.53b}$$

The value of σ_m is the result of the tuning of the model to get the approximately the right temperature at the Earth's surface, giving

$$\sigma_m = 0.3 \text{ m}^2 \text{ kg}^{-1} \tag{2.53c}$$

Remember: we are still assuming that these coefficients are independent of the wavelength of the (long-wave) radiation, which is an assumption that we we'll be forced to reject later in this chapter.

Liquid water is present at a specific level in the atmosphere if the relative humidity at that level exceeds a critical value, RH_c, given by the following formula.

$$RH_c = RH_{c,0} + \Delta RH_c \left\{ \left(\frac{p}{p_g} \right)^2 - 1 \right\}. \tag{2.54}$$

Here, p_g is the pressure at the Earth's surface. The values of the parameters $RH_{c,0}$ and ΔRH_c are fixed as follow.

$$RH_{c,0} = 98\%; \Delta RH_c = 10\% \tag{2.55}$$

This implies that condensation of water vapour occurs at the Earth's surface if the global average relative humidity at the Earth's surface is greater than 98%, while condensation of water vapour takes place at 500 hPa (with p_g=1000 hPa) if the global average relative humidity at that level is greater than 90.5%.

The time rate of change of the specific water concentration ($q_w = q_v + q_L$; q_L is the specific liquid water content) due to condensation (exiting the atmosphere immediately as precipitation) is represented as a "relaxation process" by the following formula.

$$\frac{\partial q_w}{\partial t} = \frac{q_w - RH_c q_s}{\tau_c} \text{ if } q_w > RH_c q_s; \frac{\partial q_w}{\partial t} = 0 \text{ if } q_w \le RH_c q_s. \tag{2.56}$$

Here τ_c is a timescale that is representative for the rate at which liquid water is removed as precipitation. The value of τ_c is not known, but it can be used to tune the model to a realistic liquid water path, LWP, which lies in the order of 200 g m^{-2}. The value of τ_c, adopted by different authors, varies from 2 hours in the radiative-convective model of Wang et al.[86] to 4 hours in a simplified GCM (called "Speedy")[87]. Here we adopt τ_c =1.5 hours. The saturation specific humidity, q_s, is defined as (sections 1.8 and 1.9),

---

[86] Wang, W-C., W.B. Rossow, M-S Yao, M. Wolfson, 1981: Climate sensitivity of a one-dimensional radiative convective model with cloud feedback. **J.Atmos.Sci., 38**, 1167-1178.

[87] Molteni, F., 2003: Atmospheric simulations using a GCM with simplified physical parametrizations. I: model climatology and variability in multi-decadal experiments. **Climate Dynamics**, 20, 175-191)

$$q_s \equiv \frac{\rho_{v,s}}{\rho} = \frac{e_s}{R_v}\left(\frac{p}{R_d} + \frac{e_s}{R_v}\right)^{-1} \approx \frac{R_d e_s}{R_v p} \tag{2.57}$$

The atmospheric specific liquid water content, q_L, is not a model variable. However, we need the value of q_L in order to solve (2.52c). We prescribe its value as follows.

$$q_L = \left(q_v - RH_c q_s\right) \text{ if } q_v > RH_c q_s;\ q_L = 0 \text{ if } q_v \le RH_c q_s. \tag{2.58}$$

Water vapour enters the atmosphere by evaporation from the surface of the Earth. The rate of evaporation at the Earth's surface can be specified *a priori*, or it can be coupled to the convective sensible heat flux through a specified Bowen ratio (section 2.10)[88], i.e.

$$\boxed{E_s = \frac{H_s}{BL_v}\ [\text{kg m}^{-2}\text{s}^{-1}]}, \tag{2.59}$$

where B is the Bowen ratio, L_v is the latent heat of evaporation ($2.5\text{x}10^6$ J kg^{-1}), E_s is the evaporation rate at the Earth's surface and H_s is the sensible heat flux at the Earth's surface. The sensible heat flux is determined by the vertical potential temperature gradient just above the Earth's surface (eq. 2.36). Note that we use the subscript ‘s’ to indicate the "surface" as well as "saturation".

Finally, the latent heat released within a specified layer of the atmosphere when water vapour condenses in the atmosphere is computed from

$$J = L_c \frac{\partial q_v}{\partial t}\frac{dp}{g}\ \left[\text{J s}^{-1}\text{m}^{-2}\right]. \tag{2.60}$$

Here dp is the layer-thickness in terms of the pressure difference across the layer in question. L_c is the latent heat of condensation (identical to the latent heat of evaporation).

Finally, we are left with an important question: **how is the water vapour is mixed in the atmosphere?** The radiative convective model does not explicitly account for the motions that take care of this mixing. In order to solve this problem, we employ the empirical evidence showing that water vapour is distributed to a high degree of accuracy according to eq. 1.26, which is written here as follows.

$$\boxed{\rho_{water} = \rho_{v,g} \exp\left\{-\frac{z}{H_v}\right\}}. \tag{2.61}$$

The parameter ρ_{water} represents the density of water vapour as a function of height, but we **assume that part of this water vapour is actually in condensed form if the relative humidity exceeds the critical value** (defined in 2.54). This distribution leads to a very simple equation for total precipitable water, PW (eq. 1.27):

$$\boxed{PW = \rho_{v,g} H_v}. \tag{2.62}$$

---

[88] In reality about 0.5 % of the Solar radiation that reaches the Earth’s surface is used for photosynthesis. We will neglect this effect.

The time rate of change of PW is determined in the radiative convective model by

$$\boxed{\frac{dPW}{dt} = E - P}\,. \tag{2.63}$$

Therefore, solving eq. 2.63, then using eq. 2.62 to obtain $\rho_{v,g}$, with a prescribed value of the scale height, H_v, and assuming that eq. 2.61 determines the vertical distribution of water in the atmosphere, completes the formulation of the radiative convective model including the water cycle. Our model is still "grey" and cannot yet distinguish between high and low clouds, but it does allow for a first informative evaluation of the effect of the water cycle on the average vertical temperature profile.

2.15 Radiative equilibrium in the "grey" moist radiative convective model

Now we describe and discuss some interesting aspects of the equilibrium solutions of the moist radiative convective model, assuming, as in previous sections, that the absorbing gases in the atmosphere are "grey", i.e. *long wave* absorption coefficients are independent of the wavelength of the incident radiation. The Solar irradiance, reaching the top of the atmosphere, is 1366 W m^{-2} [89]. Here we assume that Solar radiation passes through the clear atmosphere below 20 hPa unattenuated, and we keep the cloud fraction, A_c, fixed during the integration.

Solar radiation is reflected by clouds and by the Earth's surface. The reflected radiation is also reflected at cloud base. The cloud albedo both of the cloud top and of the cloud base, α_c is 0.45. The albedo of the surface of the Earth, α_g is 0.1 (eq. 2.49). The values of the absorption cross-sections are given in eq. 2.53. The value of A_c is held constant at 0.60[90]. The scale height, H_v, governing the water vapour distribution is 2000 m, which is the generally accepted globally averaged value of this parameter (section 1.10). The concentration of the well-mixed greenhouse gas is 400 ppmv, which is the value reached in the year 2014. Kiehl and Trenberth (1997) adopted a much lower value (353 ppmv) (Box 2.7), which is representative for the 1980's.

---

[89] This is the value that is assumed by Kiehl and Trenberth (1997) in an attempt to reproduce the observed annual mean global mean energy balance with a radiative convective model with prescribed distribution of clouds (figure 2.10)

[90] The global average value of A_c is actually quite uncertain. According to the second NCEP reanalysis (http://www.esrl.noaa.gov/psd/data/gridded/data.ncep.reanalysis2.html) which is an ongoing project aimed at obtaining the best possible analysis of the state of the atmosphere from 1979 onwards (the year 1979 marks the beginning of the use of satellite observations in numerical weather prediction), the globally average value of A_c for the period 1979-2008 is 0.55. The value of A_c that is assumed by Kielhl and Trenberth (1997) is 0.62, The estimate of the global average value of A_c that is derived from satellite data is 0.68 (Rossow, W.B., and R.A. Schiffer, 1999: Advances in understanding clouds from ISCCP. **Bull.Amer.Meteorol.Soc**., 80, 2261-2287).

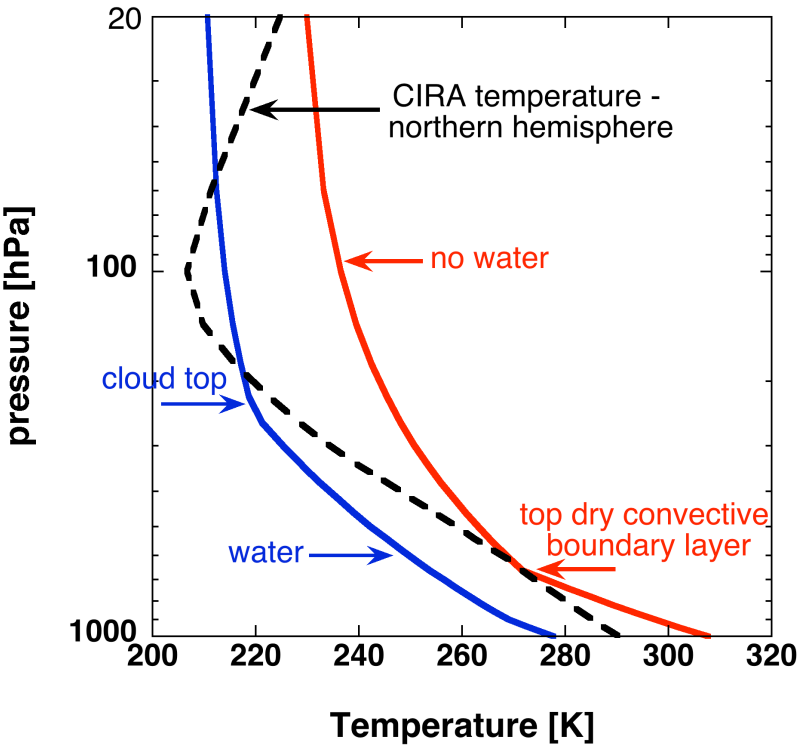

FIGURE 2.43. Radiative-convective equilibrium temperature as a function of pressure according to the "grey" moist radiative convective model (with 25 layers and k_H=400 $Wm^{-2}K^{-1}$) for two cases, compared to the **"observed" COSPAR international reference atmosphere (CIRA)** annual average temperature of the northern hemisphere (black dashed curve). The **curve labeled "no water" (red curve) is for the case with no water vapour or clouds in the atmosphere**. In the second case (blue curve labeled "water"), **surface evaporation is 80 W m^{-2}, cloud fraction is 0.6 and H_v=2000 m**. In both cases the concentration of the *well-mixed* greenhouse gas is 400 ppmv. The "clear sky" atmosphere is transparent to Solar radiation in both cases. The Earth's surface behaves as a black body, i.e. its emission coefficient is equal to 1. The top of the convective layer in the dry case (red curve) is located at about 700 hPa. The sensible heat flux is non-zero below this level and zero above this level. In the presence of water (blue curve) the top of the cloud layer is located at nearly 200 hPa. The equilibrium precipitable water is 10.7 kg m^{-2}. There is a hint of a "tropopause" at 200 hPa in the moist state. The CIRA-northern hemispheric average tropopause, which is heavily biassed towards the tropics, is at 100 hPa. The temperature increases with increasing height above the tropopause. This feature is not reproduced by the model, because absorption of Solar radiation by ozone is neglected here. Moisture in the atmosphere cools earth's climate, principally due to reflection of Solar radiation by clouds.

Finally, the surface evaporation flux is prescribed and held constant at 80 W m^{-2}, which is the global average value (**figure 2.25**), derived from the estimated global average precipitation (2.76 kg m^{-2} day^{-1}). This value is also not very certain. The second NCEP reanalysis for the period 1979-2008, for example, gives close to 3 kg m^{-2} day^{-1}, while the GPCP-2 analysis for the period 1979-2001 gives 2.61 kg m^{-2} day^{-1} [91].

Figure 2.43 shows the equilibrium temperature profiles, calculated with the moist radiative convective model, for two cases, neglecting absorption of short wave Solar radiation in the atmosphere, together with the observed profile (annual average for the

[91] Adler, R.F. et al., 2003: The Version-2 precipitation climatology project (GPCP) monthly precipitation analysis (1979-present). **Journal of Hydrometeorology**, 4, 1147-1167.

northern hemisphere between the equator and 85°N) according to the COSPAR International Reference Atmosphere (CIRA). In the first case the atmosphere contains water vapour and clouds (the blue solid curve, labeled "water"). Considering the strong simplifications in the radiation code, the qualitative agreement of the modelled temperature profile with the observed profile is quite reasonable. For instance: a tropopause seems to show up at about 200 hPa, coinciding with the top of the clouds in the model. The tropopause, i.e. the relatively sharp transition in the modeled temperature gradient at p=200 hPa is caused mainly by latent heat release in the troposphere (**figure 2.44**). The observed average tropopause height, according to CIRA, is about 100 hPa. This is a reflection of the tropical cold point tropopause, which is the result of a rather complicated interaction between dynamics and diabatic effects (chapter 12).

The equilibrium value of PW (10.9 kg m^{-2}) is much lower than the generally accepted value (24 kg m^{-2}), while the sensible heat flux (28 W m^{-2}) is significantly larger than the value that is deduced from recent observations (17 W m^{-2}) (**figure 2.25**), although it should emphasized that this value is not directly "observed", as is explained in **Box 2.8**.

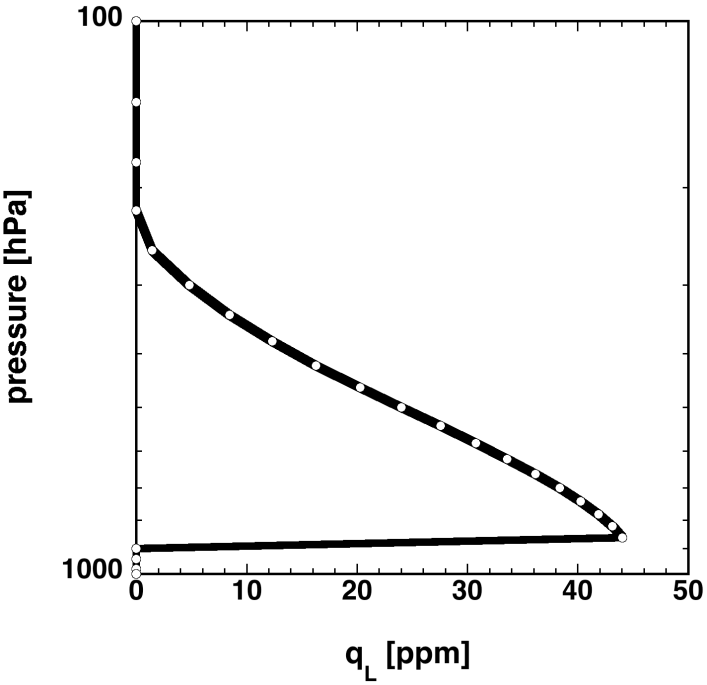

FIGURE 2.44. Liquid water content as a function of pressure, in terms of the specific concentration, q_L, according to the equilibrium solution of the moist radiative convective model assuming grey long wave radiative transfer. The total latent heat released in the cloud layer is 80 W m^{-2} (prescribed). According to **figure 2.40**, the total liquid water path of real clouds lies somewhere between 10 and 1000 g m^{-2}. The equilibrium liquid water path of the simulated clouds is in the order of 173 g m^{-2}.

The presence of water, apparently, has the effect of cooling the Earth's surface and the atmosphere above at all levels. In the model and in reality this is principally due to reflection of sunlight by clouds. Ice and snow may also increase the planetary albedo, an effect that is not included in the calculations that are described here. The albedo effect of the presence of water in the climate system is easy to understand. However, because the interaction between the water cycle and radiation is highly non-linear, other thermal effects of the water cycle are much more difficult to track. For example, evaporation of liquid water at the Earth's surface cools the surface. The evaporated water vapour condenses and freezes at levels between 900 hPa and 200 hPa, where it heats the atmosphere due to latent heat release. The

greenhouse effect of the overlying atmosphere is much weaker at cloud levels than near the surface, mainly because about 70% of all water vapour resides in the lowest 2 km of the atmosphere. So, this effect actually enhances the escape of long wave radiation to space and thus cools the climate system. However, more evaporation may also leed to thicker clouds and more water vapour in the atmosphere, which would enhance the greenhouse effect of clouds and water vapour, leading to an increase in temperature. But thicker clouds would also lead to a higher albedo, which would in turn, reduce temperatures.

If the water cycle is neglected (i.e. PW=0), and we allow for only one type of greenhouse gas (the type that is distributed homogeneously, like CO_2), the radiative equilibrium temperature profile (red line in **figure 2.43**) is remarkably different from observed temperature profile. It exhibits a "dry" convective layer, with nearly constant potential temperature from the ground to about 700 hPa, topped by a layer with a temperature that decreases smoothly with height approaching the skin temperature for α=0.1 (the assumed albedo of bare ground) of about 230 K (**Box 2.4**, eq. 15). Note that the temperature of the stratosphere in the other case (with water) is about 211 K, which is nearly precisely the skin temperature at α=0.34, the planetary albedo in this case.

The principal conclusions of this section are the following. The basic division of the atmosphere into a troposphere and a stratosphere, and the sharp boundary between these two layers (the tropopause), is to a certain extent reproduced by the radiative convective model only if the water cycle (evaporation, release of latent heat in clouds and strong absorption and emission of long wave radiation by clouds) is included, despite the neglect of absorption of Solar radiation by ozone and water vapour as well as the neglect of the wavelength dependence of gaseous absorption of long wave radiation. We find a tropopause at about 200 hPa. Without the water cycle, we find that the “semi-grey” atmosphere consists of a neutrally stratified layer (potential temperature is constant), extending to about 700 hPa, superposed by a statically stable layer where the upper levels tend to become isothermal.

2.16 Absorption of Solar radiation

According to **figures 2.10 and 2.25**, about **19-23% of the Solar radiation reaching the top of the atmosphere is absorbed in the atmosphere**, and therefore does not reach the Earth’s surface. **Solar radiation is absorbed principally by ozone and by water vapour (about 11-12 %)**. It is also absorbed, reflected and scattered by air molecules, clouds and by small particles, called **aerosols**, released into the atmosphere by humans or by volcanoes. For example, during the eruptions of Mount Chichon in Mexico in 1982 and of Mount Pinatubo in the Philipines in 1991 large amounts of dust, soot and other particles were injected into the stratosphere (**figure 2.45**).

The effect of Solar radiation absorption can be investigated theoretically using the one-layer model of section 2.3 (**figure 2.6**). Assuming that a fraction γ of the incoming Solar radiation (Q=S_0/4) is absorbed by the atmosphere and repeating the analysis of section 2.3 we obtain the following expressions for the radiative equilibrium temperature of respectively the atmosphere and the Earth’s surface.

$$T_A = \left\{ \frac{2(1-\alpha)(1-\gamma) + \gamma\left(1+\alpha(1-\gamma)\right) - (2-\varepsilon)(1-\alpha)(1-\gamma)}{\varepsilon(2-\varepsilon)\sigma} Q \right\}^{1/4}, \qquad (2.64a)$$

FIGURE 2.45. Injection of soot, ashes and dust into the stratosphere during the eruption of Mount Pinatubo (Philipines). Photograph taken from the east side of Clark Air Base on June 12, 1991, 08:51 hours, by Dave Harlow (U.S. Geological Survey).

$$T_S = \left\{ \frac{2(1-\alpha)(1-\gamma) + \gamma\left(1+\alpha(1-\gamma)\right)}{(2-\varepsilon)\sigma} Q \right\}^{1/4} . \qquad (2.64b)$$

From these expressions we deduce that, if ε=0.78 and γ=0.2, the temperature of the model atmosphere increases by 14.1 K, while the temperature of the Earth's surface decreases by 1.7 K, with respect to the case where ε=0.78 and γ=0 (section 2.3).

Let us mimic the effect of the big volcanic eruptions of 1982 and 1991 on Solar radiation (**figure 2.46**). At Moana Loa (Hawaii) these eruptions reduced the Solar radiation intensity by 3 to 4 %. Therefore, we choose γ=0.23 instead of 0.2. According to the above equation this yields a relatively modest additional temperature decrease at the Earth's surface of 0.36 K.

Releasing particles into the stratosphere that absorb Solar radiation would therefore cool the Earth's surface. Inspired by this simple theoretical conclusion chemistry Nobel-prize winner Paul Crutzen[92] has seriously proposed to inject soot into the stratosphere as a solution to human-induced global warming. This would constitute a spectacular example of what is referred to as "**geo-engineering**". The increase of atmospheric carbon dioxide concentration, which has been observed very accurately over the past 50 years, constitutes an example of unintentional geo- engineering. With the proposed *intentional* geo-engineering we would definitely enter a new geological era. Paul Crutzen has suggested the term, "**anthropocene**", to designate this era[93].

---

[92] **Climate Change**, **77** (2006): 211-219.

[93] Jan Zalasiewicz et al., 2008: Are we now living in the anthopocene? **GSA Today**, 18 (2), 4-8.

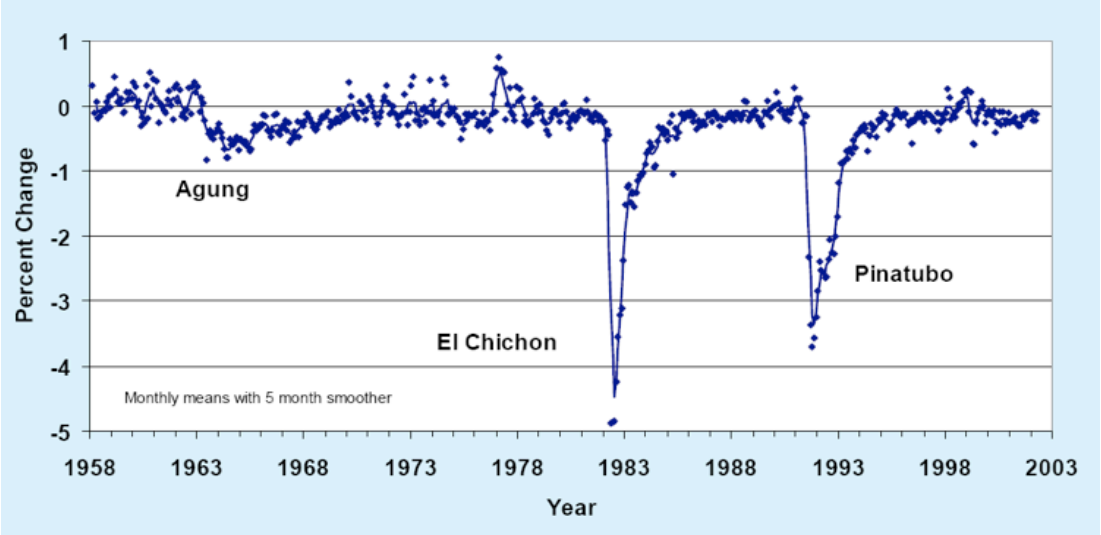

FIGURE 2.46. Net Solar radiation at Mauna Loa Observatory, relative to 1958, showing the effects of major volcanic eruptions. Annual variations are due to transport of Asian dust and air pollution to Hawaii. Source: http://www.esrl.noaa.gov/gmd/. [94]

The spectral distribution of the radiation coming from the Sun and reaching the top of the atmosphere (**figure 1.20**) corresponds approximately to that coming theoretically from a black body with a tmprature of 5525°C. As the Solar radiation passes through the atmosphere, radiation within specific wavelength intervals is absorbed, especially by ozone and water vapour and also reflected by clouds or scattered back to space. Ozone and oxygen absorb almost all radiation with wavelengths for which λ<350 nm. Although this is no more than about 5-6% of the total Solar flux reaching TOA, it nevertheless strongly determines the temperature in the upper stratosphere, where most ozone is formed (section 1.12).

Applying Bouguer-Lambert-Beer law (eq. 5 of **Box 2.2**) to Solar radiation that propagates downward through a layer of air of thickness $|\Delta z| = |\Delta p/(\rho g)|$, not necessarily perpendicular to the Earth's surface yields,

$$I_{k+1} = I_k \exp\left(-\frac{\kappa_a \Delta p}{\rho g \cos\theta}\right) . \qquad (2.65)$$

The index, k, indicates the level (**figure 2.16**) and θ is the Solar zenith angle (**figure 2.41**) (eq. 6, **Box 2.1**). The absorption coefficient, κ_a, is frequently written in terms of an absorption cross-section, σ_a, which has units of m^2 per molecule (**Box 2.3**), as

$$\kappa_a \equiv n_a \sigma_a \ . \qquad (2.66)$$

The parameter n_a is the number density of the absorber in molecules per cubic meter. Using the hydrostatic relation and the equation of state in both forms given in section 1.8, we deduce that the density of air can be expressed in terms of the number density of all air molecules, n, as

[94] More about the relation between Volcanic eruptions and climate can be found in the following paper. Robock, A., 2000: Volcanic eruptions and climate. **Rev.Geoph.**, **38**, 191-219,

$$\rho = \frac{nk_B}{R}, \tag{2.67}$$

where k_B is Boltzman's constant and R is the specific gas constant of air. With this, eq. 2.65 becomes

$$I_{k+1} = I_k \exp\left(-\frac{n_a}{n}\frac{R}{gk_B}\frac{\sigma_a}{\cos\theta}\Delta p\right) \equiv I_k \exp\left(-\Delta\delta_k\right) . \tag{2.68}$$

Here $\Delta\delta_k$ is **optical path of layer *k*** (bounded by an upper level k and a lower level (k+1)). In order to use this relation to calculate absorption of Solar radiation by ozone (for a given Solar zenith angle), we need to know the ozone molecule number concentration, n_a, and the corresponding absorption cross-section, σ_a.

The ozone molecule number concentration in the atmosphere has been measured by satellites and by radiosondes over many years. The time average ozone concentration as a function of pressure is shown in **figure 1.22**. The absolute concentration reaches a maximum value of 3.7×10^{18} molecules per cubic meter at approximately 30 hPa (about 23 km), while the mixing ratio reaches a maximum value of about 7.6 ppmv[95] at approximately 7 hPa (33 km). Using these data, we can easily compute an approximate value of the optical path of ultra-violet Solar radiation that is absorbed by ozone. Assuming that for that part of the Solar spectrum $\sigma_a=2\times10^{-22}$ m^2, we find (using 2.68) that the upper 10 hPa (1000 Pa) of the atmosphere (i.e. the layer between 0 hPa and 10 hPa) represents an optical path of approximately about $3/\cos(\theta)$. With an average Solar zenit angle, θ=60°, this implies that Solar ultraviolet radiation flux is weakened by a factor e^{-6} between TOA and 10 hPa.

This order of magnitude calculation is approximately in accord with measurements (**figure 2.47**). The optical path for incoming ultra-violet Solar radiation with wavelengths between 200 and 300 nm reaches a value of 1 at a height above sea-level lying between 40 and 50 km (50 km corresponds to 1 hPa). Radiation with wavelengths smaller than 200 nm is largely absorbed at heights above 100 km.

The fact that the absorption cross-section is strongly dependent on the wavelength of the radiation is illustrated in **figure 2.48**). It is well known that radiation with wavelengths smaller than 350 nm is involved in ozone photochemistry (section 1.12), but Ozone also absorbs radiation in the visible part of the Solar spectrum (**figure 2.48**). This absorption band is called the "**Chappuis band**". It principally affects radiation with wavelengths of 500-700 nm (1 nm=10^{-9}m) (right panel of **figure 2.49**). Solar irradiance within this wavelength interval represents 27% of the total irradiance entering the atmosphere[96]. So, despite the fact that the absorption cross-section per molecule in the Chappuis band is about a factor 1000 smaller than the absorption crosssection per molecule in the ultraviolet absorption band (right panel of **figure 2.49**), absorption in the Chappuis band is very significant, in particular in the lower stratosphere (below 20 hPa).

We'll retrict our attention to levels below 20 hPa. Therefore we divide the atmosphere

---

[95] **ppmv=parts per million by volume**. Mixing ratio in ppmv is the fraction of the volume that is occupied by the gas. From the ideal gas law (section 1.8) it follows that the volume occupied by different gases at the same temperature and pressure are proportional to the number of molecules of the gases. Therefore, the mixing ratio by volume is expressed as the ratio of the number of molecules.

[96] R.S.Lindzen and D.I.Will, 1973: An analytic formula for heating due to ozone absorption. **J.Atmos.Sci.,** 30, 513-515.

into 25 layers of 40 hPa, so that the highest model level is at 20 hPa. We assume that the irradiance in the Hartley, Huggins and Herzberg bands (wavelength<350 nm), which represents nearly 6% of the total irradiance, is depleted above 20 hPa (**figure 2.47**). Below this level Solar radiation is absorbed only in the Chappuis band (27% of the total irradiance). The optical path of each model layer in the Chappuis band is calculated from equation 2.68, assuming that the average zenith angle is 60° and using the time average, global average ozone molecule number mixing ratio (n_3/n) (**figure 1.22**). According to Strobel (1978) [97] the Solar irradiance-weighted average absorption cross-section in the Chappuis band is $\sigma_a=2.85\times10^{-25}$ m^2 per molecule (**figure 2.49**). Here we adopt this value.

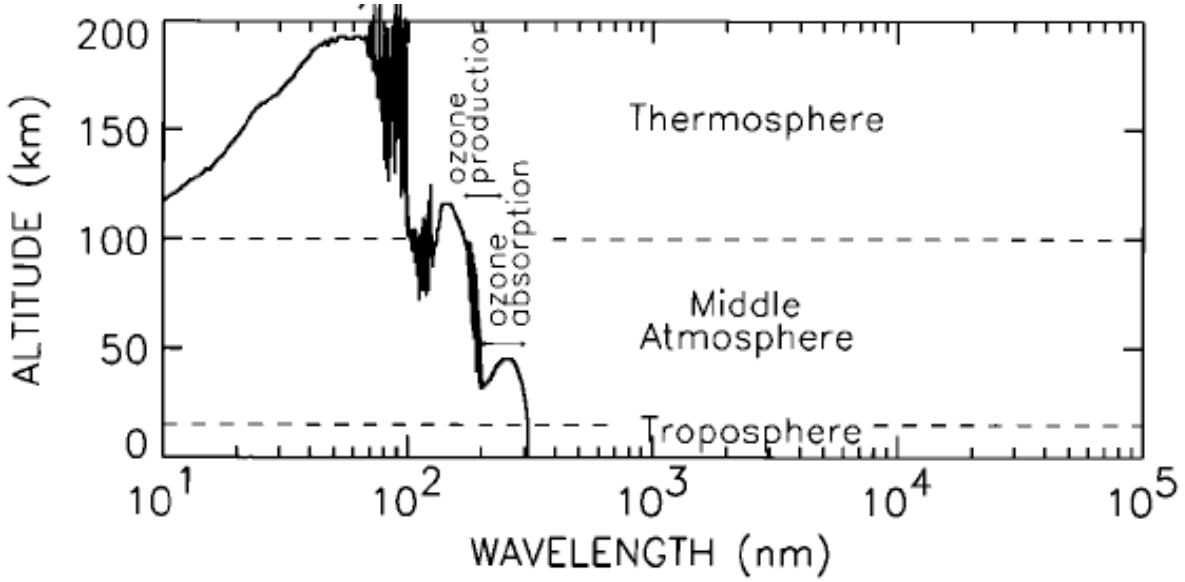

FIGURE 2.47. Altitude at which the incident energy from an overhead Sun is attenuated by a factor of 1/*e* (unit optical path) plotted as a function of wavelength of the incident radiation. Also indicated are the wavelength intervals that dominate ozone production and absorption (section 1.12). Source: Lean, J. and D. Rind, 1998: Climate forcing by changing Solar radiation. **J. Climate, 11**, 3069-3094.

Solar radiation that reaches the Earth's surface, is partly reflected (Earth's albedo is assumed to be independent of the wavelength of the incident radiation) and again passes through the atmosphere and takes part in the absorption process.

The radiative equilibrium temperature profile, calculated with these assumptions, is shown in **figure 2.50**. In case (a) absorption Solar radiation by ozone in the Chappuis band is neglected, while in case (b) this effect is taken into account. The net effect of absorption of Solar radiation by ozone is the heating of the stratosphere at 20 hPa by about 19 K and at 60 hPa by about 2 K.

PROBLEM 2.11. **Increased CO_2-concentrations will lead to stratospheric cooling.**
Demonstrate that the stratosphere in radiative equilibrium cools due to an increase of the CO_2-concentration *only* if Solar radiation is absorbed in the stratosphere (e.g. by O_3). Approximate the stratosphere as one optically thin layer.

---

97 D.F. Strobel, 1978: Parameterization of the atmospheric heating rate from 15 to 120 km due to O_2 and O_3 absorption of Solar radiation. **J.Geophys.Res., 83**, no. C12, 6225-6230.

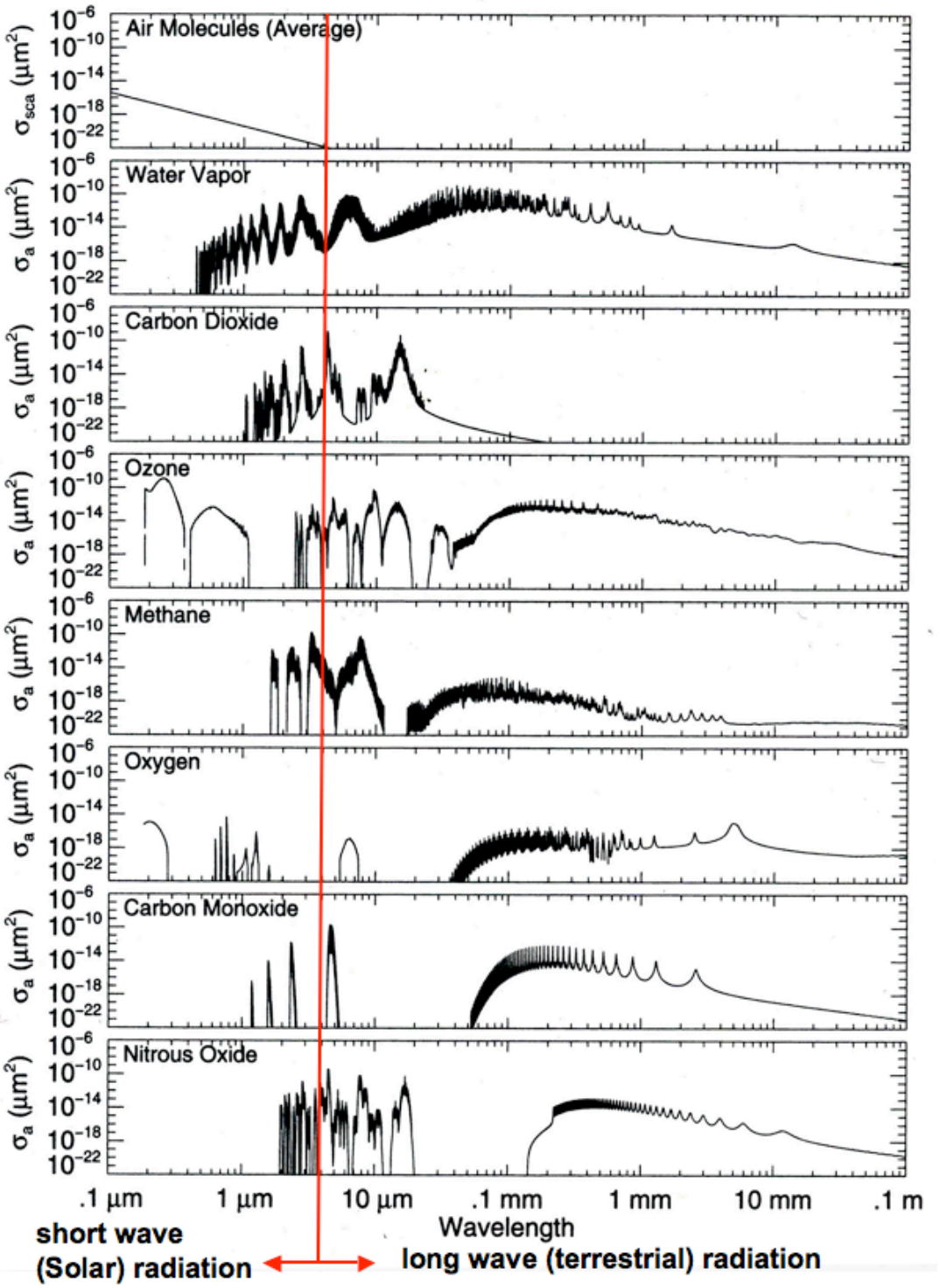

FIGURE 2.48. Absorption crosssections of the strongest absorbing atmospheric constituents (at 1013 hPa and 294 K) and average scattering cross-section for air molecules (top panel). The vertical solid line indicates the approximate boundary between Solar and terrestrial radiation. Water vapour and ozone are the strongest absorbers of Solar radiation, although the effect of absorption of Solar radiation by carbon dioxide in the stratosphere cannot be neglected. Water vapour, carbon dioxide, ozone, methane and nitrous oxide are the strongest absorbers of terrestrial radiation. The strong **scattering of Solar radiation (upper panel) at short wavelengths** is what makes the **sky look blue**. Scattering affects about 10 % of the Solar irradiance, which is not completely negligible. On the other hand, scattering of long wave radiation in Earth's atmosphere is negligible. Source: Bohren, C.F. and E.E. Clothiaux, 2006: **Fundamentals of Atmospheric Radiation**. Wiley-VCH, 472 pp.).

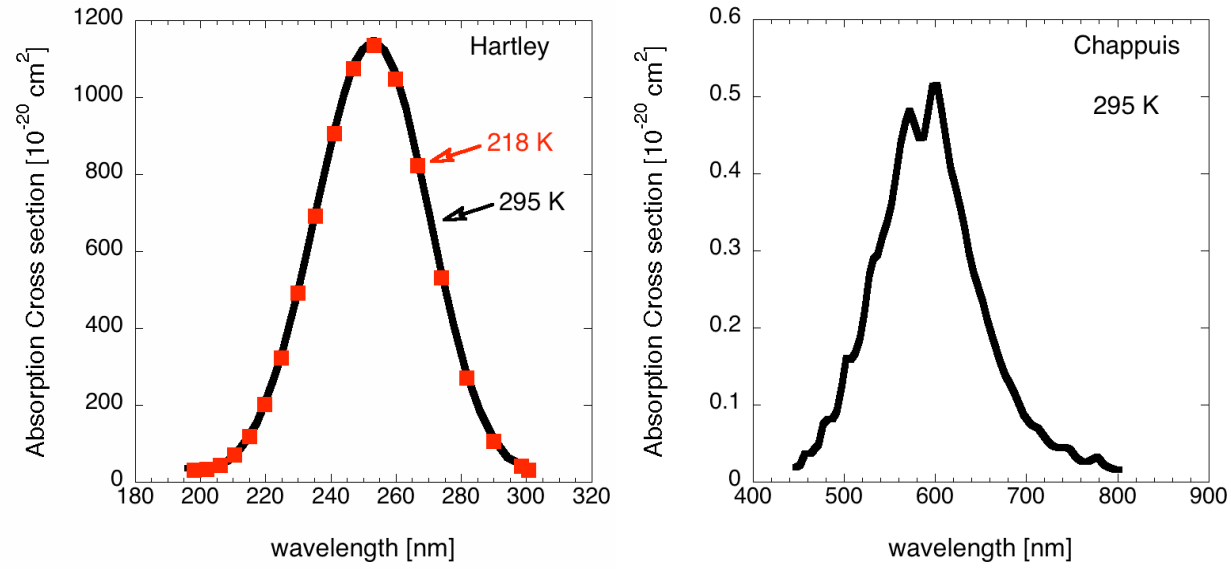

FIGURE 2.49. Ozone absorption crosssections as a function of wavelength in the Hartley band (left panel) and the Chappuis band (right panel). The absorption cross-sections in the Hartley band are only very slightly dependent on temperature. Based on experimental data that can be found online at http://jpldataeval.jpl.nasa.gov/.

Ozone, however, does have a slight "greenhouse gas effect"[98], which we have neglected here. In the stratosphere this effect leads to cooling because infra-red radiation emitted by ozone molecules can escape to space. Carbon dioxide and water vapour in the stratosphere have the same effect. It is thought that the cooling of the stratosphere over the past decades has been caused by the increase in the concentrations of these two constituents in the stratosphere[99] (see problem 2.11).

The effect of absorption of Solar radiation by water vapour is incorporated in the radiative convective model simply by assuming an absorption cross-section for absorption of short wave radiation by water vapour (σ_{vSW}) so that eq. 2.68 becomes

$$\Delta\delta_n = -\frac{\Delta p}{g\cos\theta}\left(\frac{Rn_{O3}\sigma_{O3SW}}{nk} + q_v\sigma_{vSW}\right). \qquad (2.69)$$

Here we have replaced σ_a in (2.68) by σ_{O3SW} (given here in m^2 per molecule). Actually, most of the absorption of Solar radiation by water vapour occurs at wavelengths larger than 700 nm. However, at the time of writing this text (2012) there still exists great uncertainty about the nature and intensity of Solar radiation absorption by water vapour, in particular that associated with so-called "**water vapour dimers**", which are bound pairs of water vapour molecules.

98 i.e., ozone also absorbs and emits infrared radiation.

99 V. Ramaswamy, et al., 2000: Stratospheric temperature trends: observations and model simulations. **Reviews of Geophysics**, 39, 71-122.

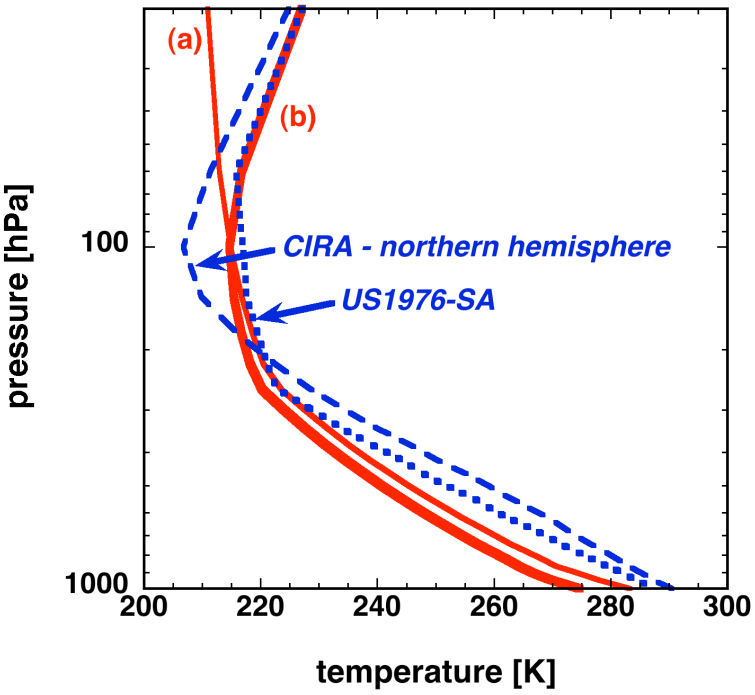

FIGURE 2.50. Radiative-convective equilibrium temperature as a function of pressure in an atmosphere that is "grey" to long wave radiative transfer for two cases, compared to the "observed" **COSPAR international reference atmosphere (CIRA)** annual average temperature of the northern hemisphere (0°N-85°N) (blue long-dashed curve) and the **US-1976 Standard Atmosphere (SA) (blue short-dashed curve).** In case **(a)** (also shown in **figure 2.43**) the "clear sky" atmosphere is **transparent to Solar radiation.** In case **(b) ozone absorbs Solar radiation in the Chappuis band (5.6 W m^{-2})**, while ozone does not absorb or emit long wave radiation. The values of the absorption cross-sections of the well mixed greenhouse gas (353 ppm), of water vapour and of clouds are given in eq. 2.53a,b,c. In case (b) it is assumed that 6% of the Solar radiation is absorbed above the highest model level (20 hPa). In other words, the average Solar irradiance at 20 hPa is 94% of 341.75 W m^{-2}. Absorption of Solar radiation by other constituents, such as water vapour, is neglected (K=25 layers, k_H=400 Wm^{-2}K^{-1} H_v=2000 m, A_c=0.6, ε_g=1.0 (ε_g is the emission coefficient of the Earth's surface) and surface evaporative energy flux is 80 W m^{-2}).

In order to incorporate the wavelength dependence of absorption of Solar radiation due to both ozone and water vapour into the radiative convective model, the Solar spectrum (**figure 1.20**) is divided into four wavelength intervals, or "channels". Channel 1 represents the Hartley, Huggins and Herzberg bands (wavelength<350 nm). Channel 2 represents radiation in the wavelength interval between Hartley, Huggins and Herzberg bands and the Chappuis band. Channel 3 represents the Chappuis band. The remaining part of the incoming Solar radiation falls into channel 4 (53% of the total Solar irradiance). This range of wavelengths is termed "**near-infrared**". The atmosphere is assumed to be transparent to Solar radiation in channel 2. In channel 3 there is absorption by ozone, while in channel 4, absorption is only due to water vapour. We, therefore, neglect the fact that carbon dioxide, methane and nitrous oxide also have absorption bands in the Solar spectrum (**figure 2.48**) and that Solar radiation is **scattered by air molecules and aerosols**.

Here, the absorption cross-section, associated with absorption of radiation in channel 4, by water vapour, is assumed to be 0.001 m^{2}kg^{-1}. With this value, which is based on the value

that was suggested by Arking (0.0012 m^2kg^{-1})[100] in 1999, and the assumptions explained above, we find that about 12 W m^{-2} of the total Solar irradiance (341 W m^{-2}) is absorbed by water vapour, which is probably an under-estimate. We also find that the Solar flux that is absorbed by the Earth's surface is about 200 W m^{-2}, which is significantly larger than the estimates that are displayed in **figures 2.10 and 2.25** (168 and 161 W m^{-2}, respectively), but not far outside the range of values that were calculated with the climate models of the 1990's[101]. The discrepancy is probably explained by the neglect of *scattering* and absorption of Solar radiation by aerosols, carbon dioxide, ammonia and methane.

Box 2.5. Average absorption coefficient

Because the absorption coefficient depends on wavelength, eq. 5 of **Box 2.2** holds only for monochromatic radiation (radiation with a fixed wavelength). Therefore, each spectral component of a beam of radiation is attenuated exponentially according to this equation. The total transmitted irradiance of a beam consisting of a continuous spectrum of wavelengths is

$$I = \int F_0(\lambda)\exp\left[-\kappa(\lambda)z\right]d\lambda, \qquad (1)$$

where $F_0(\lambda)$ is the spectral irradiance **per unit wavelength** at z=0. When $\kappa(\lambda)z<<1$ we can approximate the exponential function in (1) by the first two terms in its Taylor series expansion to obtain

$$I = \int F_0(\lambda)\left(1-\kappa(\lambda)z\right)d\lambda = \left(\int F_0(\lambda)d\lambda\right) - \left(\int F_0(\lambda)\kappa(\lambda)d\lambda\right)z. \qquad (2)$$

Since the integrated irradiance at z=0 is

$$I_0 \equiv \int F_0(\lambda)d\lambda, \qquad (3)$$

eq. 2 becomes

$$I = I_0 - I_0\langle\kappa\rangle z = I_0\left(1-\langle\kappa\rangle z\right), \qquad (4)$$

where

$$\langle\kappa\rangle = \frac{\int\kappa(\lambda)F_0(\lambda)d\lambda}{\int F_0(\lambda)d\lambda} \qquad (5)$$

is the weighted average absorption coefficient in the wavelength interval of interest. For $\langle\kappa\rangle z << 1$, eq. (4) can be approximated by

$$I = I_0\exp\left(-\langle\kappa\rangle z\right). \qquad (6)$$

---

[100] A. Arking, 1999: Bringing climate models into agreement with observations of atmospheric absorption. **J.Climate, 12**, 1589-1600.

[101] Zhanqing L, L. Moreau and A. Arking, 1997: On Solar energy disposition: a perspective from observation and modeling. **Bull.Amer.Meteorol.Soc., 78**, 53-69.

So, for weak absorption (small absorption coefficient and/or a thin layer), the integrated irradiance is also attenuated exponentially, whereby the assumed absorption coefficient is a weighted average of the actual spectral absorption coefficient according to (5).

Most radiation budget calculations in climate models assume that the spectrum can be divided into a finite number of wavelength intervals (spectral bands) and thus use weighted average absorption coefficients for each wavelength interval for each constituent. Applying (6) in these calculations implies that the model atmosphere should be divided into layers with a thickness, Δz, complying with (using the hydrostatic equation)

$$\Delta z = \frac{\Delta p}{\rho g} << \frac{1}{\langle \kappa \rangle}, \qquad (7)$$

or

$$\Delta p << \frac{\rho g}{\rho_a \langle \sigma_a \rangle} = \frac{g}{q_a \langle \sigma_a \rangle}, \qquad (8)$$

where q_a is the specific concentration of the absorber and $\langle \sigma_a \rangle$ is the weighted average (in the spectral interval of interest) of its absorption cross-section per kg ($m^2\ kg^{-1}$).

As an example, we take the Chappuis absorption band of ozone between 500 nm and 700 nm) (**figure 2.49, right panel**). The weighted average absorption cross-section of ozone in this interval is $\langle \sigma_a \rangle = 2.85 \times 10^{-25}$ m^2 per molecule. The ozone molecule number concentration is less than 4×10^{18} molecules m^{-3} (**figure 1.22**). Therefore, in this case, criterion (8) becomes

$$\Delta p << 10^5 \text{ hPa},$$

which poses absolutely no problem. However, criterion (8) is not always easily satisfied in the case of the infrared absorption band of carbon dioxide.

Box 2.6. Computing the transmissivity of a layer

In this box a method is presented that computes the average transmissivity, or average emissivity, of an atmospheric layer containing a homogeneously distributed absorber, i.e. with a constant specific concentration throughout the layer, taking account of wavelength dependent absorption cross sections. The radiation that is transmitted through this layer, integrated over the wavelength interval λ_1 and λ_2 is (eq.1 of **Box 2.5**)

$$I = \overline{F} \Delta\lambda = \int_{\lambda_1}^{\lambda_2} F_0(\lambda) \exp\left[-\kappa(\lambda) z\right] d\lambda = \int_{\lambda_1}^{\lambda_2} F_0(\lambda) \exp\left[-\sigma(\lambda) W\right] d\lambda, \qquad (1)$$

where $\overline{F}$ is the average irradiance per unit wavelength over the wavelength interval $\Delta\lambda = \lambda_2 - \lambda_1$, σ is the absorption cross-section of the absorber, W is the amount of absorber integrated over the path (i.e integrated over the thickness of the layer) in kg m^{-2} and $F_0(\lambda)$ is the irradiance per unit wavelength at the top of the layer. **Assuming that $F_0(\lambda)$ is constant over the wavelength interval** λ_1 to λ_2, we may define

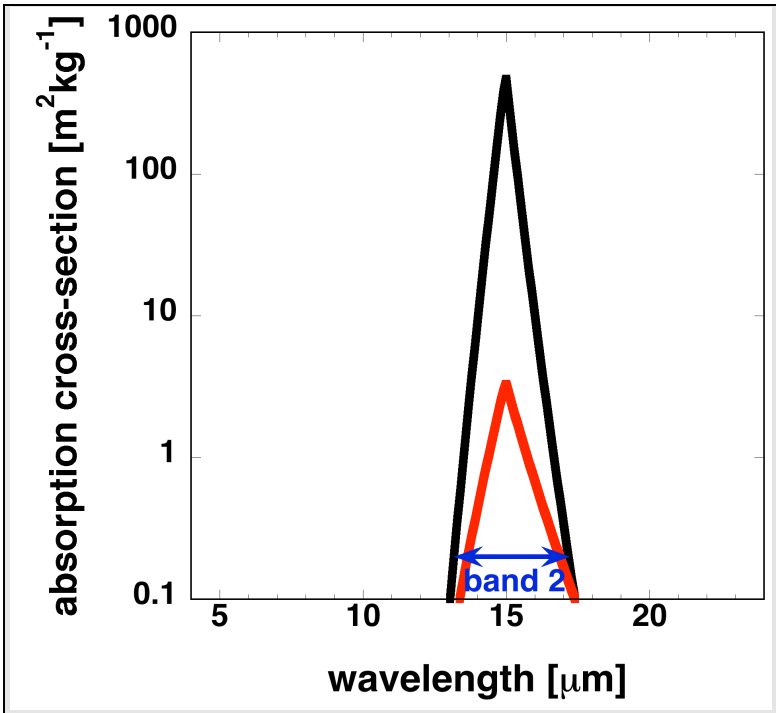

FIGURE 1, Box 2.6. The absorption cross-section of carbon dioxide for long-wave radiation as a function of wavelength, according to eq. 6a,b of this Box with ν_0=667.5 cm^{-1}, σ_0=3.71×10^{-23} m^2, $r_- = 0.092$ cm and $r_+ = 0.086$ cm (upper **black** curve) and with ν_0=667.5 cm^{-1}, σ_0=0.025×10^{-23} m^2, $r_- = 0.044$ cm and $r_+ = 0.038$ cm (lower **red** curve). This "curve" is an extremely simplified and smoothed of the real curve (**figure 1** of Box 2.3; **figure 2.52**). The **blue double arrow** indicates the range of wavelengths that correspond to band 2 (the carbon dioxide absorption band) in the radiative convective model.

$$\overline{F}_0 = \frac{1}{\Delta\lambda}\int_{\lambda_1}^{\lambda_2} F_0(\lambda)d\lambda \ , \qquad (2)$$

so that

$$\overline{F}\Delta\lambda = \overline{F}_0 \int_{\lambda_1}^{\lambda_2} \exp\left[-\sigma(\lambda)W\right]d\lambda , \qquad (3)$$

which leads to the following equation for the **transmissivity**, τ, of the layer:

$$\boxed{\tau \equiv \frac{\overline{F}}{\overline{F}_0} = \frac{1}{\Delta\lambda}\int_{\lambda_1}^{\lambda_2} \exp\left[-\sigma(\lambda)W\right]d\lambda}. \qquad (4)$$

The corresponding optical path is

$$\boxed{\delta = -\ln\tau}. \qquad (5)$$

Let us compute the transmisivity for the absorption band of CO_2. The triangular function, shown as a solid line in **figure in box 2.3**, is the result of a least squares fit to the coarse-grained data in the interval 550 cm^{-1}<ν< 790 cm^{-1}, or with λ=1/ν, 12.66 μm<λ< 18.18 μm. The function is given by

$$\sigma(\nu) = \sigma_0 \exp\left[-r_+|\nu - \nu_0|\right] \text{ if } \nu > \nu_0; \quad (6a)$$

$$\sigma(\nu) = \sigma_0 \exp\left[-r_-|\nu - \nu_0|\right] \text{ if } \nu < \nu_0, \quad (6b)$$

with ν_0=667.5 cm^{-1}, σ_0=3.71×10^{-23} m^2, $r_- = 0.092$ cm and $r_+ = 0.086$ cm. The absorption cross section for two different choices of the values of the set of parameters σ_0, r_- and r_+ is shown in **figure 1** in this box. The corresponding optical path as a function of W, computed with (4) and (5), is shown in **figure 2** in this box.

The parameter σ_0 is given in m^2 per molecule. To get the value of σ in m^2 kg^{-1}, we must multiply the value obtained from formula (6a,b) by Avogadro's number (i.e the number of molecules in one mole=6.022×10^{23}) and divide by the molar mass of carbon dioxide (0.044 kg).

Figure 2 (this box) shows δ for the interval 13 μm<λ< 17 μm as a function of W for the for two different choices of the values of the set of parameters σ_0, r_- and r_+. The optical path is not proportional to W, which would be the case if the absorption cross section were independent of the wavelength within the wavelength interval, 13 μm - 17 μm. This is due to the triangular shape of the graph. As W increases, a progressively smaller portion of the wavelength interval remains optically thin.

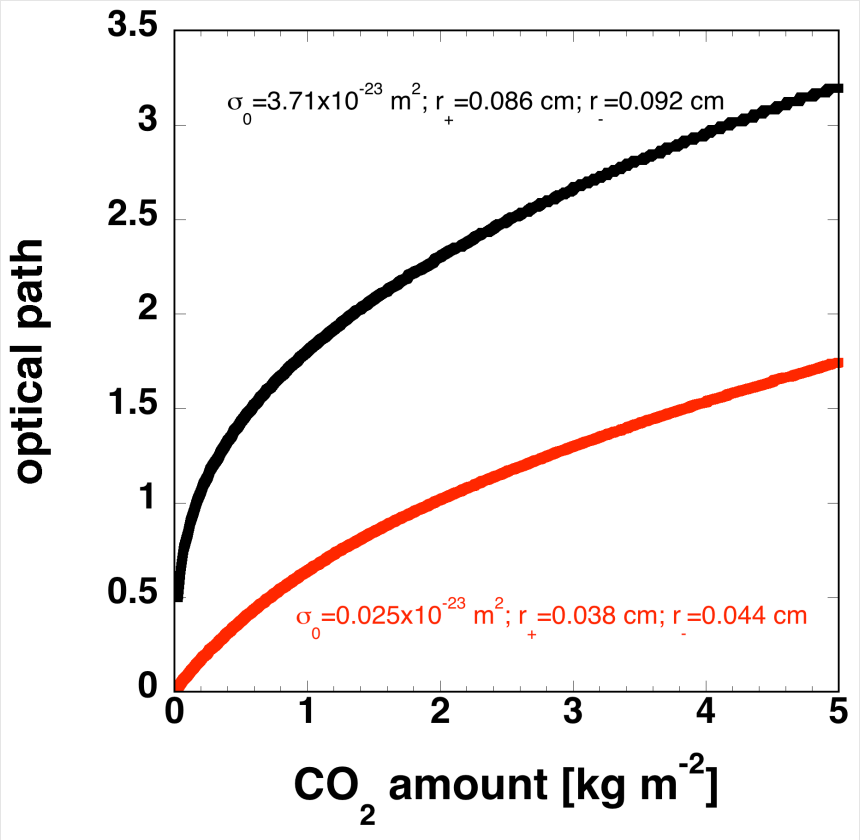

FIGURE 2, Box 2.6. Optical path of the absorber, carbon dioxide, as a function of absorber amount (W) in a column of air in the wavelength interval 13 μm - 17 μm (the CO_2 absorption band), assuming that the absorption crossection is given by eq. 6a,b, with ν_0=667.5 cm^{-1}, σ_0=3.71×10^{-23} m^2, $r_- = 0.092$ cm and $r_+ = 0.086$ cm (upper **black** curve) and with (probably more realistic values) ν_0=667.5 cm^{-1}, σ_0=0.025×10^{-23} m^2, $r_- = 0.044$ cm and $r_+ = 0.038$ cm (lower **red** curve), computed from eqs. 4 and 5.

The set of values of σ_0, r_- and r_+, corresponding to the lower (red) curve in the graph in **figure 2** of this box, seems more realistic, in the light of **figure 2.52,** which shows CO_2-absorption cross sections according to measurements analysed by Raymond Pierrehumbert.

In reality, the absorption cross-section varies by *several orders of magnitude over extremely small wavelength intervals*, as is illustrated by the dashed line in **figure 1 of Box 2.3**. This implies that the integration is not smooth. However, by rearranging the cross sections in order of their values, instead of the wavelengths to which they correspond, we can obtain a much smoother integrand, while not changing the value of the integration in (4). This so-called **"κ-distribution" method** (the symbol κ stands for absorption coefficient, **Box 2.2)** goes as follows. For the wavelength interval between λ_1 and λ_2 we define the probability, $f(\sigma)\mathrm{d}\sigma$, of occurrence of absoption cross sections in the interval $(\sigma, \sigma+\mathrm{d}\sigma)$, such that

$$\int_0^\infty f(\sigma)d\sigma = 1. \qquad (7)$$

The average transmissivity can now be evaluated from the following equation:

$$\tau(W) = \int_0^\infty f(\sigma)\exp(-\sigma W)d\sigma. \qquad (8)$$

The distribution function, $f(\sigma)$, may still be very erratic, implying that the integration in (8) is problematic. Instead we define the more smooth cumulative probability distribution function, $g(\sigma)$, as

$$g(\sigma) = \int_0^\sigma f(\sigma')d\sigma'. \qquad (9)$$

This function increases monotonically from 0 to 1. The absorption cross-section can be expresses as a function of the cumulative probability as $\sigma(g)$. The average transmissivity follows from

$$\tau(W) = \int_0^1 \exp(-\sigma(g)W)dg. \qquad (10)$$

The integral on the right hand side of (10) can be computed relatively accurately because of its "smoothness". This method of computing the transmissivity is called the **cumulative κ-distribution method**.

PROBLEM BOX 2.6. Optical path and band average absorption

What will the optical path be, as a function of CO_2-amount, if we used eq. (3) of **Box 2.3** to compute the band-average absorption cross section before using eqs. 4 and 5 of this Box to compute the optical depth?

2.17 Atmospheric infrared window and climate sensitivity

Neglecting the wavelength-dependence of absorption and emission of long wave radiation in the atmosphere simplifies calculations considerably, but it also leads to the omission of an essential aspect of the climate of Earth, namely that a **substantial portion of the radiation emitted by the Earth's surface can escape to space almost directly through the infrared window**. This important aspect of Earth's radiation balance was identified and analysed in detail first by G.C. Simpson (1928)[102].

In order to investigate the gross (first order accurate) effect of the atmospheric infrared window on the temperature we split the long wave spectrum into four bands. Band 1 (8-13 μm) represents the atmospheric infrared window (**figure 2.31**), band 2 (13-17 μm) represents the absorption band of the well-mixed greenhouse (our proxy for CO_2) [103], band 3 corresponds to the interval (17-21 μm), while band 4 represents the aggregate of the remaining wavelength intervals. We assume that radiation in bands 3 and 4 interacts only with water vapour and clouds, while radiation in band 1 interacts mainly with clouds. In band 2 radiation interacts with all these three constituents (**table 2.4**).

absorption crosssection [m^2 kg^{-1}]	in band 1 (~27%)	in band 2 (~19%)	in band 3 (~14%)	in band 4 (~54%)
water vapour	0.01	0.19	2.37	10.0
well-mixed gas (CO_2)	0	(box 2.6)	0	0
liquid water (clouds)	5	5	5	5

TABLE 2.4. Values of the long-wave absorption cross sections for the four long-wave absorption bands of the moist radiative convective model (see also **figures 2.51 and 2.52**). Band 1 represents the "atmospheric window" (~27% of the emitted radiative energy). Water vapour absorbs only weakly in this band. The absorption of radiation in band 2 due to CO_s is computed according to eqs. 4, 5 and 6a,b of Box 2.6. The absorption cross-sections in the hypothetical "grey" atmosphere are given in eqs. 2.53a,b,c. The dependence of the absorption cross-sections on pressure ("pressure broadening") and temperature is neglected. A reasonably realistic temperature profile is produced in both the "grey-case" and the "non-grey-case" (**figure 2.53**).

---

[102] Simpson, G.C., 1928: Further Studies in Terrestrial Radiation. **Mem.Roy.Meteorol.Soc.,** vol.**3**, no. 21, 1-26. Simpson concludes his paper with the following statement. "The lesson that can be learnt from this work is that totally misleading results follow from the assumption that water vapour absorbs like a grey body".

[103] Remember that this gas is similar to carbon dioxide, but due to the many simplifications we refrain from calling it carbon dioxide explicitly here. In his book entitled, *Principles of Planetary Climate*, R.T. Pierrehumbert makes the following similar remark. "The atmosphere (of a hypothetical planet, much like Earth), consists mostly of infrared-transparent N_2 and O_2 with a surface pressure of 10^5 Pa, like Earth. Unlike Earth, the only greenhouse gas is a mythical substance (call it *Oobleck*), which is a bit like CO_2 but much more simple to think about. It has the same molecular weight as CO_2, but it's absorption coefficient σ has an absorption band centered on wavenumber ν_0= 600cm^{-1}. Within 100cm^{-1} of ν_0, σ has the constant value σ_0. Outside of this limited range of wavenumbers, *Oobleck* is transparent to infrared, i.e. σ= 0. In order to make the life of an atmospheric physicist of this planet even more simple, σ is independent of both temperature and pressure. Like real CO_2, the specific concentration of *Oobleck* is constant throughout the depth of the atmosphere".
(http://geosci.uchicago.edu/~rtp1/PrinciplesPlanetaryClimate/index.html)

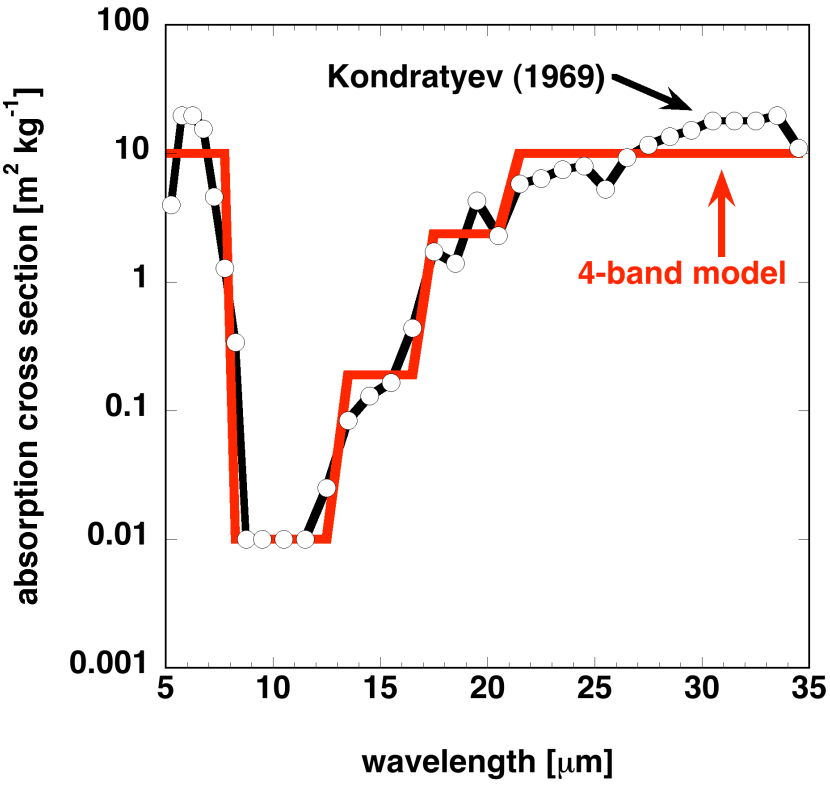

FIGURE 2.51. The **black** line indicates the absorption cross-section of water vapour for long-wave radiation as a function of wavelength, estimated from **observations**, taken from table 3.9 on page 119 of K.Y. Kondrayev (1969) (**Radiation in the atmosphere**. Academic Press, 912 pp.). The **red** line indicates the assumed value of the absorption cross-section of water vapour in the **four-band long wave radiation model**.

Ozone absorbs long wave radiation only in a narrow band within the window around 9.6 μm, while clouds (liquid water) absorb long wave radiation equally strong in all four bands. Therefore, ozone tends to block the radiation in the infrared window, but it does this significantly only at stratospheric levels that are "close" to the top of the atmosphere, so that radiation that is re-emitted upwards by ozone molecules within this wavelength interval can easily escape to space. We will neglect this effect. An overview of the long-wave radiation absorption cross sections of the well-mixed greenhouse gas (CO_2), water vapour and clouds (liquid water) in the "four-band" model is given in **table 2.4**.

About 27% of the energy that is emitted by the Earth or the atmosphere falls into band 1 (the infrared window) (**figure 2.31**). Similarly, bands 2 and 3 represent approximately 19 % and 14%, respectively, of the total irradiance in the long wave portion of the radiation spectrum. Of course, these proportions depend on the temperature of the emitting constituent, because Planck's curve shifts to larger wavelengths with decreasing temperature.

Figure 2.51 shows a graph of the absorption cross-section of water vapour as a function of wavelength, based on observations, compiled by Kondratyev (1969)[104], together with the values used in the 4-band long-wave radiation model.

Figure 2.52 shows the carbon dioxide absorption cross-sections as a function of wave number or frequency distilled from the high-resolution transmission molecular absorption database, "HITRAN" (http://www.cfa.harvard.edu/HITRAN/). In our radiative convective model we take account only of the absorption band in the frequency interval centred around 666 cm^{-1} (15 μm). This is illustrated in **figure 1** of **Box 2.6**.

[104] Kondratyev, K.Y., 1969: **Radiation in the atmosphere**. Academic Press, 912 pp.

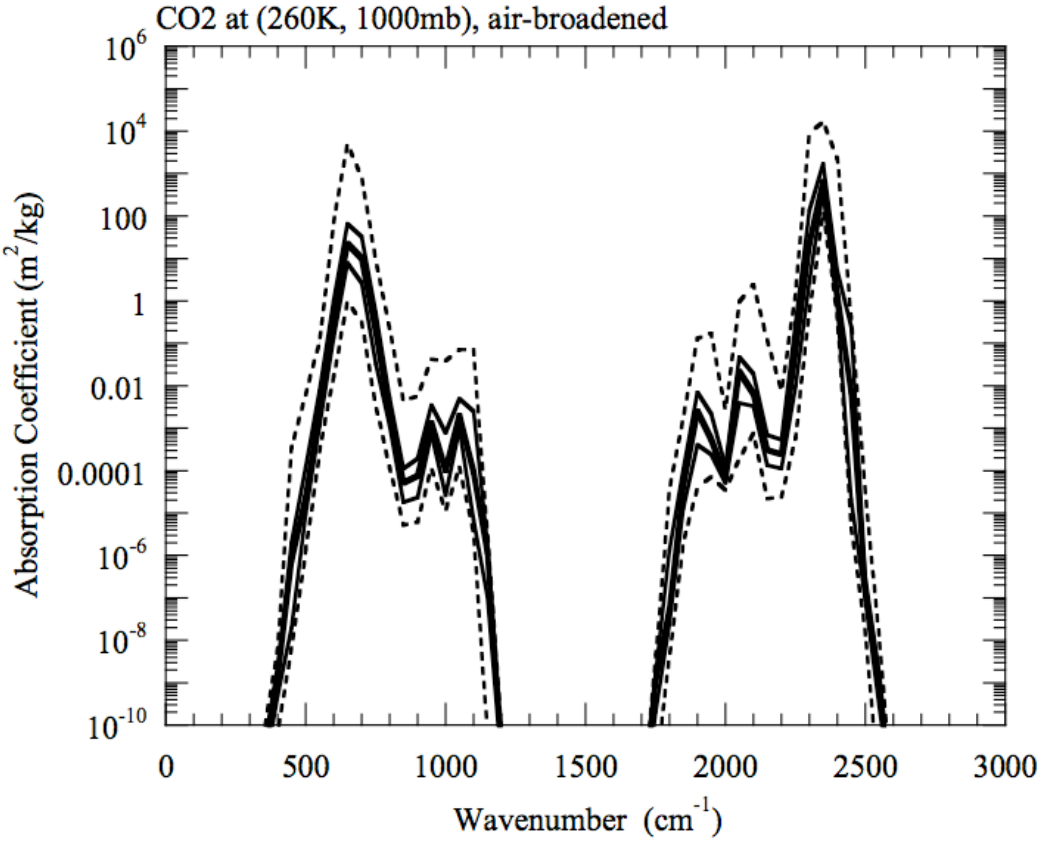

FIGURE 2.52. The minimum, 25th percentile, median, 75th percentile, and maximum absorption cross sections in bands of width 50 cm^{-1}, for CO_2 in air at T=260 K and p=1000 hPa, calculated from spectral data in the HITRAN database (http://www.cfa.harvard.edu/HITRAN/). The most important absorption band (for the Earth's atmosphere) is centred around 666 cm^{-1} (15 μm), while another absorption band is centred around 2400 cm^{-1} (4 μm). From Pierrehumbert, R.T., 2010: **Principles of Planetary Climate.** Cambridge University Press.

Figure 2.53 shows the equilibrium temperature as a function of pressure for the grey atmosphere and for the atmosphere with an infra-red window (non-grey). All parameter values are the same in the two cases, except the values of the long-wave absorption coefficients. In the grey case the absorption cross sections are given in eqs. 2.53a,b,c. In the non-grey case the absorption cross sections are shown in **table 2.4** and explained (for the CO_2) in **Box 2.6**. We see that the temperature profiles are very similar, and do not depart very much from the CIRA northern hemisphere average. The troposphere is too cold, probably because of too little absorption of Solar radiation by water vapour (and other constituents).

We are now ready to investigate the **influence of the "infrared window" on climate sensitivity**[105]. We'll investigate the sensitivity of the equilibrium temperature at the Earth's surface to changes in the concentration of the well-mixed greenhouse gas (CO_2) in the "clean case" where we neglect water and ozone. **Figure 2.54** shows the equilibrium temperature at the Earth's surface as a function of the concentration of the well-mixed greenhouse gas under a grey atmosphere and under a non-grey atmosphere with an infrared

[105] Traditionally "climate sensitivity", or more precisely, "**equilibrium climate sensitivity**" (ECS) is defined as the increase of the equilibrium temperature at the Earth's surface after a doubling of the CO_2-concentration (Box 211).

window. In the first case, the **net transmission coefficient** of the atmosphere (τ_p), defined as the fraction of the irradiance emitted by the Earth's surface that escapes directly to space, approaches zero as the greenhouse gas concentration is increased, while in the latter case the net transmission coefficient approaches an asymptotic finite value, since long wave radiation is absorbed only by carbon dioxide (there are no clouds). **It is said that the absorption bands are "saturated"** when the net tansmission coefficient approaches an asymptotic constant value. When the atmosphere is grey to long wave radiation this asymptotic value is zero. When long wave radiation is absorbed only in band 2, this asymptotic value is about 81 %. Band 2 is saturated first at about 400 ppmv. The surface temperature under a non-grey atmosphere increases at a much smaller rate with increasing greenhouse gas concentration than surface temperature under a grey atmosphere

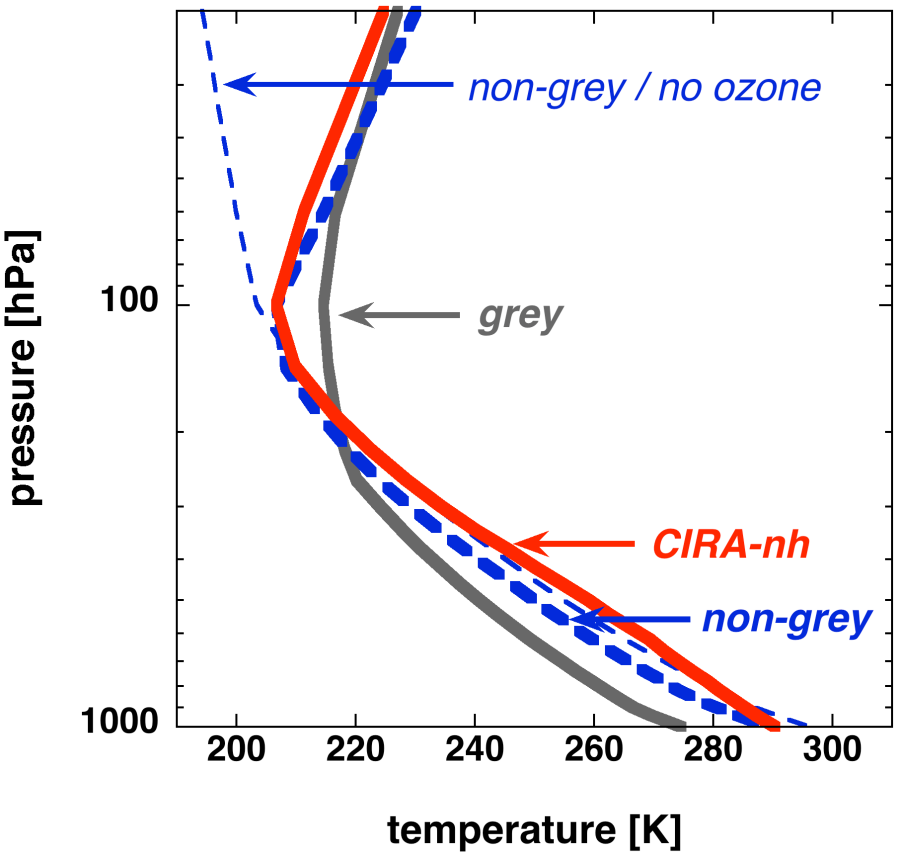

FIGURE 2.53. Radiative convective equilibrium temperature profile in the **case that the atmosphere is grey to long-wave radiation (grey curve)**, i.e. absorption coefficients are band-independent, and in the **case that long wave absorption coefficients depend on wavelength (table 2.4; Box 2.6) (blue dashed curves)**. The thin blue dashed curve corresponds to the equilibrium temperature in the non-grey case without ozone. For comparison, the **CIRA-northern hemisphere average temperature (red solid curve)** is shown. The atmospheric infrared window is defined as the interval between 8 μm and 13 μm, while the "well-mixed greenhouse gas-absorption band" is defined as the interval between 13 μm and 17 μm. Short wave absorption crosssections for ozone are as in the previous section. In the grey case short wave radiation **is not** absorbed by water vapour. In the non-grey case short wave radiation **is** absorbed by water vapour. Surface evaporative flux is 80 W m^{-2}. Other parameter values are H_v=2000 m, A_c=0.6, τ_c=1.5 hrs, and ε_g=1. The well-mixed greenhouse gas concentration (proxy for pCO_2) is 400 ppmv.

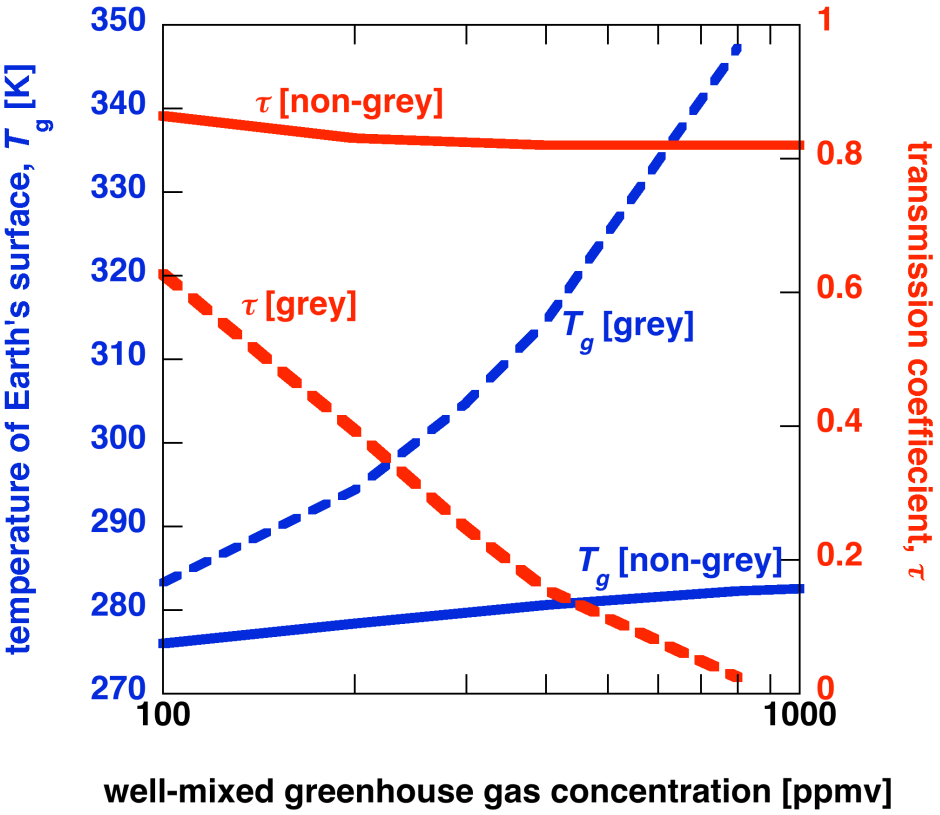

FIGURE 2.54. The **equilibrium temperature at the Earth's surface** and the **net atmospheric *long wave* transmission coefficient (τ)** as a function of concentration of the well-mixed greenhouse gas in a "grey" atmosphere (dashed curves) and in an atmosphere with infrared window (solid curves). The values of the absorption cross-sections are given in **table 2.4**. **There is no other greenhouse gas in the atmosphere in both cases, i.e. no water, nor ozone**. The planetary albedo is determined completely by the ground albedo (=0.1). With the infrared window the net transmission coefficient, τ, is nearly constant when the well-mixed greenhouse gas concentration exceeds about 400 ppmv, suggesting that atmospheric absorption by the greenhouse gas is *"saturated"*. Nevertheless, interestingly, ground temperature continues to increase with increasing greenhouse gas content (see the text for the interpretation)!

It is clear, therefore, that **the presence of the infrared window makes the climate at the Earth's surface very much less sensitive to changes in concentration of the well-mixed greenhouse gas**. Nevertheless, the increase of T_g with increasing greenhouse gas concentration is *not* arrested when the well-mixed greenhouse gas absorption band is "saturated". This is because radiation, which is emitted by the Earth's surface, is absorbed at lower levels in the atmosphere as the greenhouse gas concentration in the atmosphere increases. The "back radiation" of the atmosphere towards the Earth's surface increases also, because the warmer layers are closer to the Earth's surface. Note that the one-layer model of section 2.3 cannot reproduce this effect, because eq. 2.11 states that the atmospheric back-radiation at the Earth's surface depends only on the Solar constant, the planetary albedo and the net atmospheric absorption coefficient, ε (=1−τ). The analytical theory of **Box 2.4**, however, does give the correct indication that absorption band saturation *cannot* be used to argue that surface temperature will not increase further with increasing greenhouse gas

content (as is still done by so-called "climate skeptics") [106].

The climate of an atmosphere *without* an infrared window is extremely sensitive to changes in the concentration of the well-mixed greenhouse. It may very likely slide into a runaway greenhouse state, where, ultimately, temperatures rise above the boiling point of water and all liquid water is evaporated (section 2.6). Presumably, this has happened in the atmosphere of Venus, because this very thick atmosphere (surface pressure is 92 bar) consists mainly of CO_2 (96%, i.e. about 1 million kg of CO_2 per square metre!) and enough water vapour to make the atmosphere optically thick at all wavelengths.

Because of the presence of water in the atmosphere the infrared window represents only about 27% of the total irradiance that is emitted by an object with the typical temperature of 255 K. This implies that the asymptotic value of τ is not 0.81 (**figure 2.54**) but about 0.27 (remember that this is a very rough estimate!), assuming that the infrared window is perfectly transparent. This asymptotic value is, however, hardly ever reached, because of the blocking effect of clouds on radiation passing through the window. We'll investigate the important effect of clouds in the following section. The description of the radiative-convective model that is used for this investigation is scattered over the previous sections of this chapter. For the convenience of the reader a survey of the main characteristics and assumptions of this model is provided in **Box 2.8**.

PROBLEM 2.12 Interpreting measurements of the daily cycle of the surface energy balance

(a) Interprete measurements the surface energy balance made in Wageningen (Netherlands) on three consecutive winter days in January 2011 (28, 29 and 30 January).

(b) Interprete measurements the surface energy balance made in Wageningen (Netherlands) on the hot and sunny summer day of 2 July 2010.

The files can be downloaded from http://www.met.wau.nl/haarwegdata/dayfiles/.

Box 2.7. How well determined is the global average energy balance?

Earth's average energy balance has been the subject of serious research since the studies published by Abbot and Fowle in 1908[107], but, because it took advantage of the first reasonably accurate satellite measurements of the radiation fluxes at the top of the atmosphere, the study of Kiehl and Trenberth (1997) (Kiehl J.T., and K.E. Trenberth, K.E., 1997: Earth's annual global energy budget. **Bull.Am.Meteorol.Soc., 78,** 197-208), and with it **figure 2.10**, has acquired iconic dimensions in climate science. **Figure 2.10** is reproduced on the second page of chapter 1 in the fourth report of the Intergovernmental Panel on Climate Change (IPCC), which appeared in 2007 to illustrate the factors that determine Earth's climate. Kiehl and Trenberth employ a "narrow-band" radiation code (in section 2.17 we'll introduce a "broad" band version of such a code), which takes account of the fact that long wave radiation transfer depends on both the local temperature of the gaseous absorber

[106] See: http://www.aip.org/history/climate/Radmath.htm and http://www.realclimate.org/index.php/archives/2007/06/a-saturated-gassy-argument/

[107] Hunt, G.E., R. Kandel and A.T. Mecherikunnel, 1986: A history of presatellite investigations of the Earth's radiation budget. **Rev.Geoph., 24**, 351-356.

and the wavelength dependent efficiency of gases to absorb radiation, to compute the unknown energy fluxes for a *prescribed* temperature and water vapour distribution, for which they took the US-1976 Standard Atmosphere (**table 2.1** and **figure 2.50**). The consistency of the assumptions is checked, by comparing the computed value of *clear sky* OLR-TOA (262 W m^{-2}) with the observed value (265 W m^{-2}).

A point of criticism here is that the US-1976 Standard Atmosphere is of course not representative for the global conditions. In particular, the water vapour density is much lower than the global average. With H_v=2200 m and $\rho_{v,g}$=5.9 g m^{-3} (table 2.1) we find from eq. 1.27 that PW=13 kg m^{-3}. In fact, even worse, Kiehl and Trenberth were forced to reduce the specific humidity by 12% (p. 200 of their paper) to ensure agreement between computed and observed clear-sky flux. With such a low value of PW, it is actually very surprising that the computed downward long wave flux at the surface (324 W m^{-2}) is very similar to more recent estimates of actual global average (345 W m^{-2} according to ISCCP-FD[108]).

In a follow-up paper, Trenberth et al. (Trenberth, K.E., J.T. Fasullo and J. Kiehl, 2009: Earth's Global Energy Budget. **Bull.Amer.Meteorol.Soc., 90**, 311-324) state that the value of the downwelling long wave flux at the surface is one of the principal uncertainties in the global surface energy budget. The new estimates of the *net* upward long wave-flux at the surface are significantly lower (51 W m^{-2} according to ISCCP-FD, instead of 66 W m^{-2} in **figure 2.10** or 63 W m^{-2} in **figure 2.25**).

The surface latent heat flux is deduced from the global average preciptation rate, which, because of the lack of measurements over the oceans, is not very well known. Estimates of this quantity vary from 2.6 to 3.1 kg m^{-2} day^{-1} (see the main text). The uncertainty of about 0.5 kg m^{-2} day^{-1} represents about 14 W m^{-2}!

The surface sensible heat flux is determined from the closure of the surface energy budget, assuming equilibrium. This results in a value for H_s of 24 W m^{-2}. Later (**figure 2.25**) this estimate was reduced to H_s=17 W m^{-2}. However, there are serious indications that this value could be as low as 8 W m^{-2} [109].

Notable further follow up papers have appeared in **Journal of Climate** in 2011 (**vol. 24**, 4907-4924) and in **Nature Geoscience** in 2012 (**vol. 5**, 691-695), in which the global average energy budget is re-evaluated with the most recent satellite measurements and with reanalyses, showing, among other, that the climate system may be more strongly out of energy balance than is suggested by **figure 2.25**, which indicates that the climate system is absorbing 0.9 W m^{-2} (in particular the oceans). These studies indicate that this number may be a factor of 10 or more larger (**figure 1** of **Box 2.8**).

Finally, the radiation emitted by the Earth's surface, that manages to escape to space directly through the infra-red window, which was estimated to be 40 W m^{-2} in both **figure 2.10** and **figure 2.25**, has now (in 2012) been estimated to be only 20 W m^{-2} with an uncertainty of 4 W m^{-2}. [110]

---

[108] Zhang, Y. et al., 2004: Calculation of radiative fluxes from the surface to top of atmosphere based on ISCCP and other global data sets: Refinements of the radiative transfer model and the input data. **Journal of Geophysical Research**, 109, doi:10.1029/2003JD004457.

[109] Kanamitsu, M., et al., 2002: NCEP-DOE AMIP-II reanalysis (R2). **Bull.American Meteorol.Soc., 83**, 1631-1643.

[110] Costa, S.M.S., and K.P. Shine, 2012: Outgoing longwave radiation due to directly transmitted surface emission. **J.Atmos.Sci.,** 69, 1865-1870.

Box 2.8. Principal characteristics of the radiative-convective model

The following assumptions are made to calculate the global average, annual average temperature of the Earth's surface and of the atmosphere as a function of height.

1. The atmosphere is divided into 25 layers of equal mass.
2. The Earth's surface is a slab with a fixed heat capacity.
3. The radiation is split into 8 spectral bands (4 in the short wave and 4 long wave).
4. The sensible heat flux at the surface and in the atmosphere is parametrized according to eq. 2.36.
5. The latent heat flux at the surface is parametrized by prescribing the Bowen ratio (eq. 2.59) or by assuming that this flux depends linearly on the saturation vapour mixing ratio and the relative humidity near the surface (**Box 2.10**).
6. The ozone concentration is prescribed according to observations.
7. There is one well-mixed greenhouse gas that has the approximate absorption characteristics of CO_2 (**figure 1** of Box 2.6 and **figure 2.52**).
8. The distribution of water vapour is prescribed according to eq. 1.26.
9. Cloud cover fraction is related to relative humidity at the surface according to eq. 2.47.
10. Precipitation is parametrized as a relaxation process according to eq. 2.56.
11. Liquid water absorbs radiation equally in all four long wave spectral bands. Ice in clouds is neglected
12. Albedo of Earth's surface and of clouds is prescribed according to eq. 2.49.
13. Aerosols and scattering effects are neglected.
14. Solar radiation is absorbed by ozone, oxygen and water vapour.

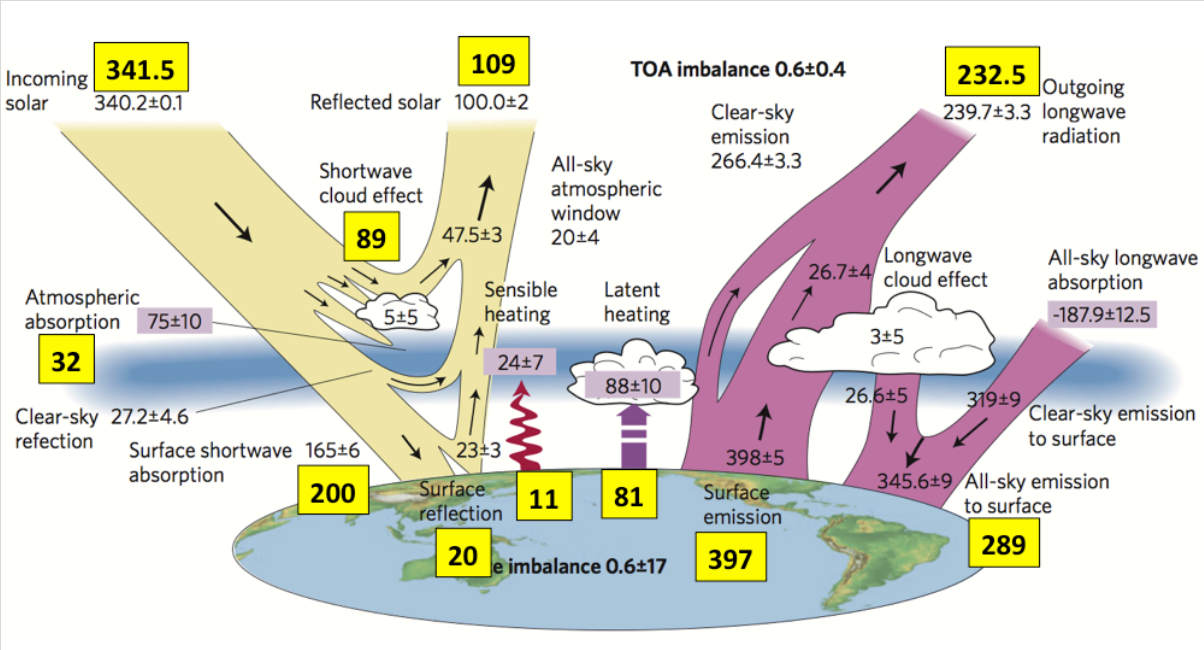

FIGURE 1, BOX 2.8. Observed global average energy fluxes (Stephens et al., 2012[111]) (see also **figure 2.10** and **figure 2.25**) and according to the radiative-convective model with the characteristics listed above. Surface evaporation is calculated according to eq. 1 in **Box 2.10** (http://www.staff.science.uu.nl/~delde102/RCM.htm).

[111] Stephens, G.L., J Li, M. Wild, C.A. Clayson, N. Loeb, S. Kato, T L'Ecuyer, P.W. Stackhouse Jr., M. Lebsock and T. Andrews, 2012: An update on Earth's energy balance in light of the latest global observations. **Nature Geoscience, 5**, 691-696.

Mathematically, the model consists of 27 "prognostic" coupled first order ordinary differential equations for the time-evolution of the temperature of 25 atmospheric layers, of the temperature of the surface and of the precipitable water, in addition to several diagnostic relations governing e.g. cloud cover and precipitation. The prognostic equations are integrated numerically until an equilibrium state is reached. The numerical time differencing scheme used is the Runge-Kutta scheme (http://en.wikipedia.org/wiki/Runge–Kutta_methods).

Figure 1 (this Box) shows the equilibrium energy fluxes calculated by the model, assuming a CO_2-concentrtaion of 400 ppmv, compared to the best estimate of these fluxes for present day conditions. Observe the "**compensating errors**", which are actually quite typical for energy balance models and radiation schemes.

2.18 Cloud cover and climate sensitivity

We now arrive at the question of how clouds interact with radiation. Because of the extremely complex structure of clouds and the many ways in which clouds interact with radiation, finding an answer to this question seems quite hopeless. Nevertheless, we may identify two basic mechanisms that govern this interaction. Stated simply, clouds interact with radiation due to two effects: **the "albedo-effect" and the "greenhouse effect"**. The most important manifestation of the "greenhouse effect of clouds" is the "closing" of the atmospheric window with increasing cloud cover fraction. However, the strength of this effect depends on the temperature of the cloud tops[112] compared to the temperature of the Earth's surface (**Box 2.12**) as well as on the liquid water path, i.e. "thickness" of the clouds. At the same time, an increase in cloud cover leads to an increase in planetary albedo and hence cooling. In other words, the greenhouse effect has a large effect on ground temperature only if cloud cover fraction (A_c) is high, and/or if cloud top temperatures are much lower than ground temperatures and/or if liquid water paths are large. At low values of A_c and/or cloud top temperatures that are similar to ground temperatures and/or small liquid water paths, the "greenhouse-effect" of clouds is less significant, and so the "albedo-effect" determines that temperature increases with decreasing cloud cover. In other words, low(high) A_c is associated with relatively high(low) temperatures, because the planetary albedo decreases with decreasing A_c.

Figure 2.55 illustrates the global effect of clouds on the equilibrium surface temperature, T_g, according to our moist radiative convective model (**Box 2.8**). The equilibrium temperature as a function of cloud cover is calculated for fixed surface evaporation. **Figure 2.55** indicates that the albedo effect dominates, i.e. **clouds have a cooling effect at the Earth's surface**. However, because of the so-called **water vapour feedback** (see also section 2.19), this relation is not as straightforward as it seems. The passage of long-wave radiation through the atmosphere is influenced by both clouds and water vapour. Precipitable water decreases with decreasing temperature approximately following the Clausius Clapeyron relation (section 1.9). Therefore, the decrease of the water vapour content explains a large part of the equilibrium temperature decrease with increasing cloud cover. Hence, **the albedo effect of clouds is enhanced by the water vapour feedback** (section 2.19).

[112] The cloud-top feedback was discussed in some detail first by Stephen Schneider in 1972 in a very readable article entitled "Cloudiness as a global climatic feedback mechanism" (**J.Atmos.Sci., 29**, 1413-1422).

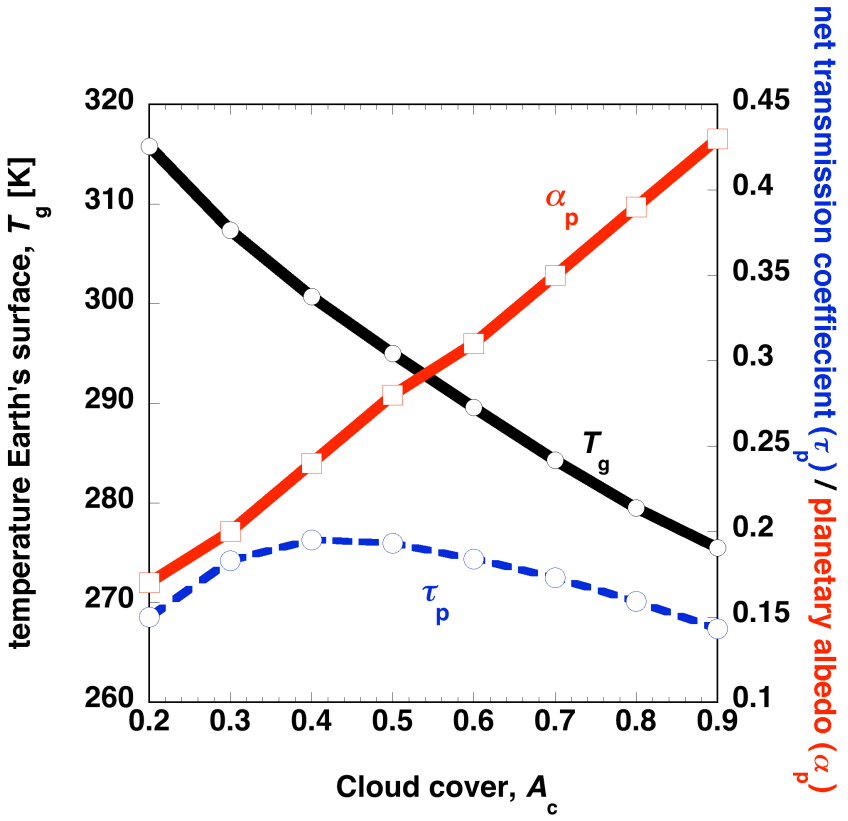

FIGURE 2.55. The influence of cloud cover on global average **surface equilibrium temperature**, according to the moist radiative convective model (**Box 2.8**). Also shown are the **net atmospheric (planetary) long wave transmission coefficient** (τ_p) the **planetary albedo** (α_p). The long wave transmission coefficient is defined as the fraction of the irradiance emitted by the Earth's surface that escapes to space. Surface evaporation is prescribed (80 W m^{-2}), H_v=2000 m and τ_v=2 hours. Absorption of Solar radiation by water vapour is neglected. Cloud albedo is 0.45; ground albedo is 0.1. The well-mixed greenhouse gas concentration (proxy for pCO_2) is 400 ppm.

The assumption of fixed cloud albedo is a strong simplification (**figure 2.40**). In reality both planetary albedo and long-wave atmospheric opacity depend also on the cloud type and cloud top height. A dense cloud that contains more liquid water has a higher albedo, but is also more opaque to long wave radiation. Furthermore, because Solar radiation reaching the Earth's surface decreases with increasing cloud cover, evaporation probably also decreases, which leads to thinner clouds (i.e. containing less condensed water), and therefore, a weaker greenhouse effect.

Obviously, a better representation is needed of the distribution of cloud properties, such as cloud top heights and condensed (and frozen) water contents and even cloud particle size distribution. Also, a more accurate knowledge of reflection, transmission and emission coefficients of clouds is needed before the effect of clouds on temperature can be studied with reasonable quantitative accuracy. Nevertheless, the qualitative global average effect of the interaction of clouds and radiation on the temperature at the ground is probably illustrated correctly in **figure 2.55**. This **figure** indicates that **a small change in cloud cover fraction may have a similar effect on ground temperature as a doubling of the concentration of the well-mixed greenhouse gas** (next section).

2.19 Water vapour feedback

A **feedback mechanism** is an interaction in which an initially imposed change in a variable causes some other variable to change, that then acts to modify the original change. If the original change is amplified, the feedback is said to be positive. Here we discuss the "**water vapour feedback**". The popular explanation of the water vapour feedback goes as follows. An increase in the concentration of the well-mixed greenhouse gas (principally carbon dioxide), leads to an increase in temperature at the Earth's surface, which increases the water holding capacity of the atmosphere (section 1.9). **Assuming that the relative humidity in the atmosphere remains approximately constant with increasing temperature**[113], this leads to a further intensification of the greenhouse effect, due to the increase of water vapour concentration with increasing temperature. In fact, with fixed relative humidity, the water vapour concentration increases nearly exponentially with increasing temperature (**figure 1.8**). According to this view, the water vapour feedback is a potentially very dangerous amplifier of human induced global warming.

The uncertainties in this theory are large, however, because it is not clear why relative humidity should remain approximately the same at all heights with changing temperatures. This question is important, moreover, because cloud cover fraction depends on relative humidity near the Earth's surface (**figure 2.39**). Because clouds interact strongly with both short wave and long wave radiation, it is important not to impose the constraint of fixed relative humidity (and therefore also fixed cloud cover fraction) in order to explore the role of clouds and the intensity of the hydrological cycle in the water vapour feedback mechanism.

Investigating one effect at a time, we first keep cloud cover fraction and surface evaporative flux fixed at 0.6 and 80 W m^{-2}, neglect absorption of Solar radiation by water vapour, and calculate the equilibrium surface temperature for different concentrations of the well-mixed greenhouse gas. The result is shown in **figure 2.56**. For comparison, the equilibrium surface temperature for the atmosphere *lacking water* is shown also (see also fig. 2.54). The divergence of the two curves with increasing concentration of the well-mixed greenhouse gas (**figure 2.56**) represents the **long wave water vapour feedback**. With water, the equilibrium temperature increases by about 3-5 K for every doubling of well-mixed greenhouse gas concentration, i.e. "**equilibrium climate sensitivity**" (ECS) is 3-5 K [114]. In the absence of water in the atmosphere, ECS is in the order of 1-2 K for values of the well-mixed greenhouse gas concentration below 3200 ppmv. In other words water makes Earth's climate about twice as sensitive to a change in well-mixed greenhouse gas concentration [115]. Equilibrium climate sensitivity seems to decrease with increasing well-mixed greenhouse gas concentration. We'll see that this effect becomes stronger when we introduce the possibility of a cloud feedback (**Box 2.12**).

---

[113] This hypothesis was put forward first by Arrhenius on page 263 of his famous paper (**Phil. Mag., 41** (1896) no. 25) and later also by F. Möller in 1963 (On the influence of changes in CO_2 concentration in air on the radiation balance of Earth's surface and on climate. **J.Geophys.Res., 68**, 3877-3886). It gained tremendous popularity due to S.Manabe and R.T.Wetherald in 1967. (Thermal equilibrium of the atmosphere with a fixed distribution of relative humidity. **J.Atmos.Sci., 24**, 241-259).

[114] The best estimate of ECS in 2006 was 2 - 5 K (Räisänen, J, 2006: How reliable are climate models?, **Tellus 59A**, 2-29).

[115] Manabe and Wetherald came to the same conclusion in 1967. (S.Manabe and R.T.Wetherald, 1967: Thermal equilibrium of the atmosphere with a fixed distribution of relative humidity. **J.Atmos.Sci., 24**, 241-259)

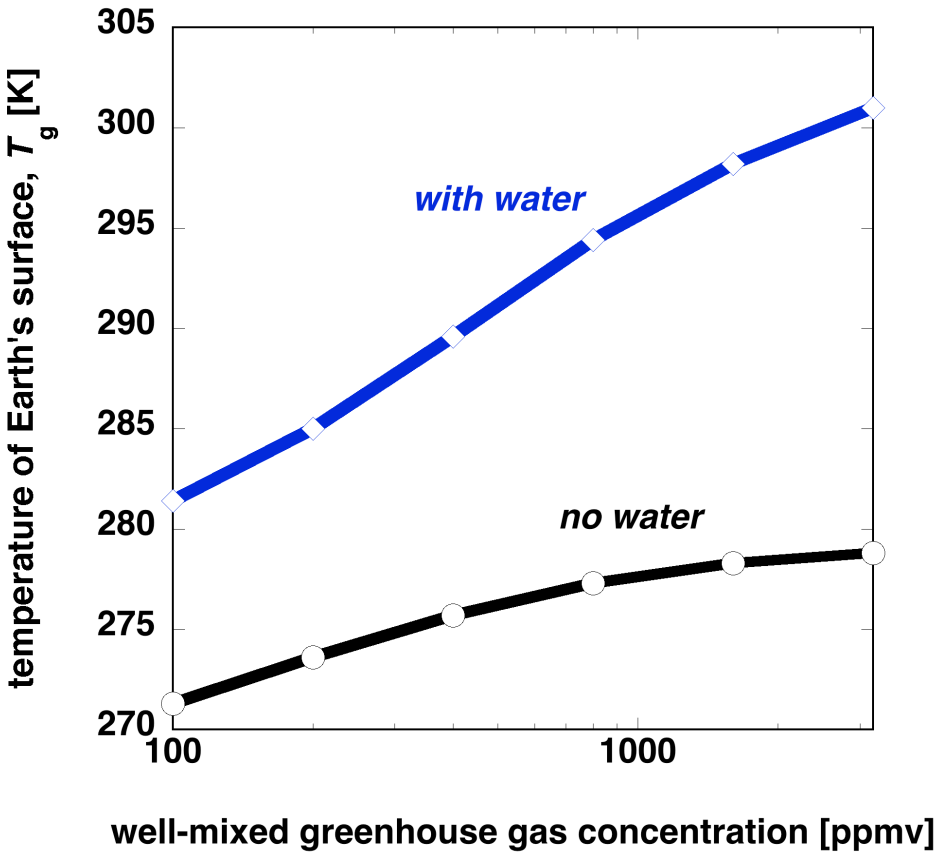

FIGURE 2.56. The water vapour feedback according to the moist radiative convective model. The equilibrium temperature at the Earth's surface is plotted as function of concentration of the well- mixed greenhouse gas (proxy for CO_2). The **solid blue line** is for an **atmosphere with water cycle**. Solar radiation is not absorbed by water vapour. The **solid black line** is the temperature for an **atmosphere lacking water**. Both evaporation at the Earth's surface (80 W m^{-2}) and cloud cover fraction (0.6) are held constant. Furthermore, H_v=2000 m and τ_c=1.5 hours.

Two feedback effects will probably mitigate the water vapour feedback. First, cloud cover fraction may change, which will have a strong influence on net radiation at the Earth's surface and surface temperature, as is seen in **figure 2.55**. We'll introduce the possibility of a **cloud feedback** by assuming that cloud cover fraction depends on relative humidity near the Earth's surface according to the empirical relation that is given in (2.47a,b), with C=1.28 and RH_0=0.34. If **Arrhenius's hypothesis of constant relative humidity** is true, no change of cloud cover fraction would occur under greenhouse warming. A change of relative humidity with greenhouse warming is, therefore, a critical matter. Second, in the real atmosphere more than 10 % of the **Solar irradiance is absorbed and scattered by water vapour and cloud particles**. Very likely, this will modify the long wave water vapour feedback by reducing the short wave radiative flux that reaches the Earth's surface when precipitable water increases, and thereby making less energy available for evaporation. A first estimate of the importance of this effect is obtained by repeating the calculations assuming a **fixed Bowen ratio** (eq. 2.59) instead of a fixed surface evaporative flux (**Box 2.9**). Evaporation will now, more realistically, depend on the net radiation flux at the surface.

Box 2.9. Bowen ratio

It is sometimes stated that each type of surface can be associated with a particular value of the Bowen ratio, H_s/LE_s. The table in this box gives an overview of the value of the annual average Bowen ratio, B, over various natural land surface types as well as over the tropical oceans and urban area. About 70 % of the globe is covered by ocean. Therefore, the global average value of B will be only slightly higher than the value (0.1) of B over the oceans. According to **figure 2.10**, B=0.31, while according to **figure 2.25**, B=0.21. Estimates of the global average value of B from the reanalysis (e.g. NCEP-2) yield a much lower value of B. For the moment we'll set B=0.15 in the radiative convective model (**Box 2.7**). But, the following cautionary note is in place.

The *annual average* surface sensible heat, H_s, is a strong function of latitude. In fact, at latitudes poleward of about 50° H_s<0, especially in the winter hemisphere (**figure 2.26**). At these latitudes, which represent about 25% of the global surface area, the Earth receives sensible heat from the atmosphere. Since the annual average value of the surface evaporation is positive everywhere, B<0(!) at these latitudes.

Land surface type	Bowen ratio	Evaporative Fraction
Tropical rain forest	0.1	0.91
Grassland	0.3	0.77
Deciduous forest	0.4	0.71
Coniferous forest	0.4	0.71
Savanna	0.6	0.62
Cropland	0.7	0.59
Bare sand	1.2	0.45
Semi desert	3.5	0.22
Urban area	2.0	0.33

TABLE Box 2.9. Estimate of the annual average value of the Bowen ratio and the associated evaporative fraction for different surfaces. Source: A. Baumgartner, 1984: Effects of deforestation and afforestation on climate. **GeoJournal, 8**, 283-288.

In classical hydrology a different measure of surface evaporation or evapo-transpiration is used in energy balance considerations: the "**evaporative fraction**", EF, which is defined as

$$EF \equiv \frac{LE_s}{R_{net}}, \qquad (1)$$

where R_{net} is the net radiation at the surface, that is available for evaporation. If there is energy balance at the surface we can write,

$$EF \equiv \frac{LE_s}{H_s + LE_s} = \frac{1}{1+B}\ . \qquad (2)$$

Over land areas three evapotranspiration regimes can be distinguished, depending on the presence of vegetation and the availability of water at the surface, i.e. depending on soil

moisture: a soil moisture-limited regime, a energy-limited regime and a transition regime (see the figure in this box). In the energy-limited regime, corresponding to soil moisture values larger than a critical value, *EF* is independent of the soil moisture content. This is the wet regime. Below this critical value of soil moisture content, *EF* is limited by soil moisture. This is the soil moisture limited evapotranspiration regime. For soil moisture content below a value corresponding to the "**wilting point**", this regime is referred to as the "dry regime" for which *E*=0. In the transition regime, interesting feedbacks between the atmosphere and the soil can occur.

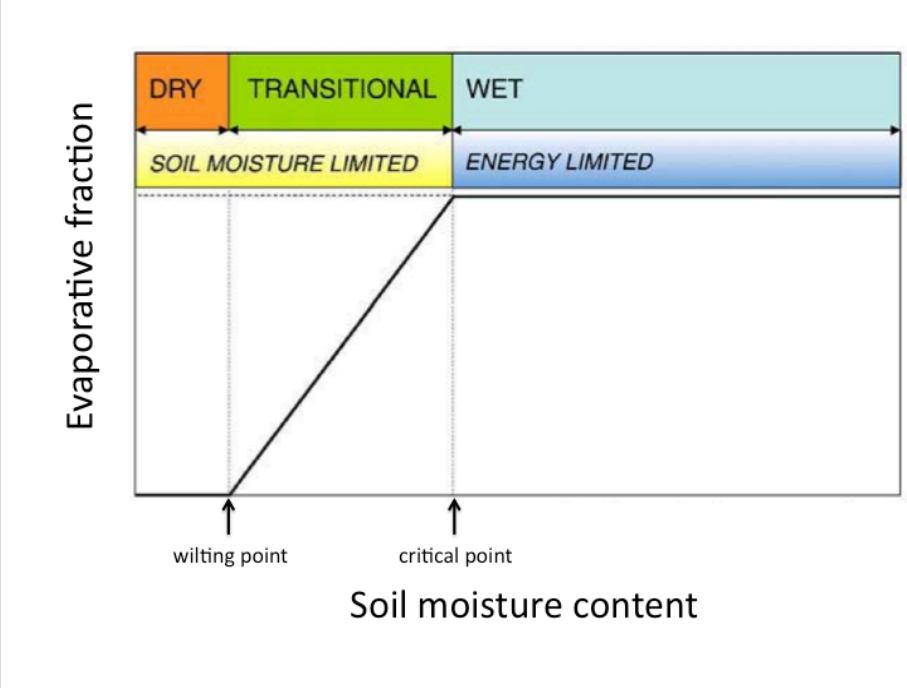

FIGURE 1 Box 2.9. Definition of the soil moisture regimes and corresponding evapotranspiration regimes (adapted from figure 5 in S.I. Seneviratne et al., 2010: Investigating soil moisture-climate interactions in a changing climate interactions in a changing climate: a review. **Earth-Science Reviews, 99**, 125-161).

The response of the water cycle to warming (due to increasing CO_2 concentrations) is shown in **figure 2.57**. Note that precipitable water appears to rise faster with increasing surface temperature than the saturation water vapour pressure corresponding to this surface temperature. This indicates that surface relative humidity increases with increasing surface temperature, which leads to increasing cloudiness. In fact, the cloudiness increases from 57% at a surface temperature of 284 K (at pCO_2=100 ppmv) to 71% at a surface temperature of 297.4 K (at pCO_2=6400 ppmv). Note that the model reproduces the observed global/annual average precipitation of 2.8 mm per day, as well as the observed global/annual average precipitable water (about 24 kg m^{-2}) under present day conditions (surface temperature of about 290 K) very well. We find that the precipitation decreaes with increasing temperature. This has to do with reduction of net radiation at the ground, which is the energy source for evaporation. The reduction of net radiation at the ground is larger when Solar near-infrared radiation (channel 4 in the model) is absorbed by water vapour, which leads to a stronger reduction of the pace of the water cycle, despite the exponential increase of precipitable water.

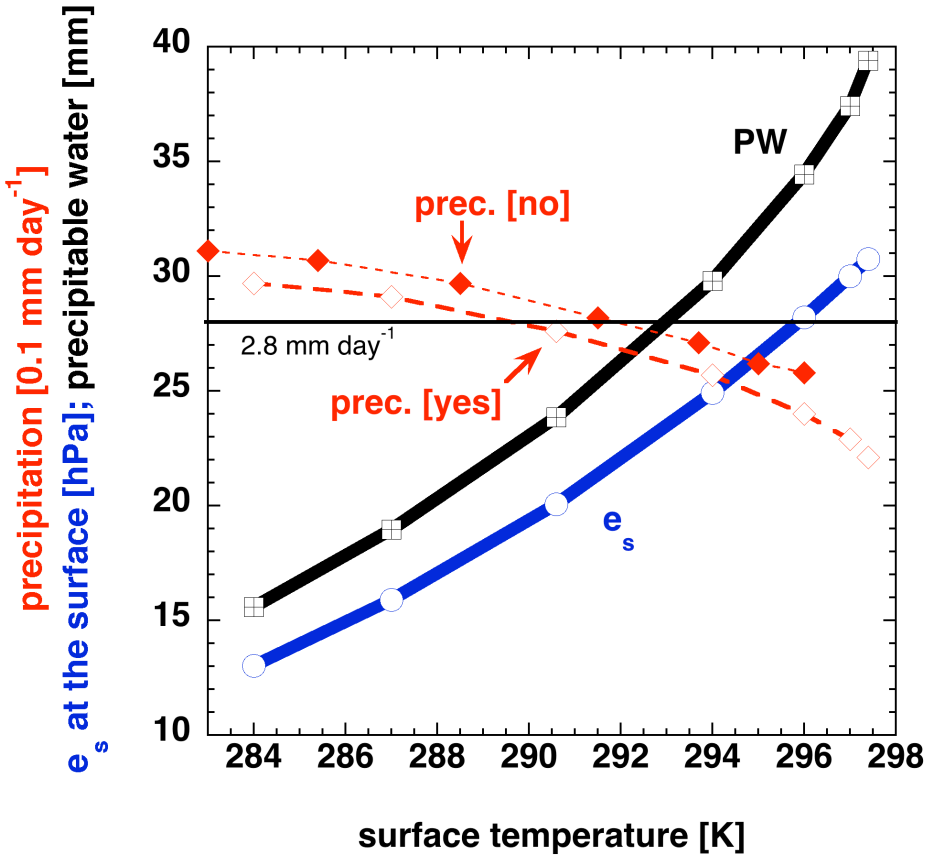

FIGURE 2.57. **Equilibrium precipitable water** and **equilibrium precipitation** as a function of equilibrium surface temperature according to the moist radiative convective model, assuming fixed Bowen ratio (=0.15). The model is integrated to equilibrium for values of the concentration of the well-mixed greenhouse gas varying from 100 ppmv to 6400 ppmv. Red closed squares (labeled "Prec.[no]") correspond to cases with **no** absorption of Solar radiation by water vapour. Red closed squares (labeled "Prec.[yes]") correspond to cases where absorption of Solar radiation by water vapour is taken into account. Water vapour absorbs near-infrared radiation, with wavelengths greater than 0.7 micron (σ_{vSW}[channel 4]=0.001 m^2kg^{-1}). The **saturation water vapour pressure at the Earth's surface** (according to the Clausius Clapeyron equation, 1.14) is shown in **blue**. H_v=2000 m and τ_c=1.5 hours.

Increasing cloud cover and increasing opacity of the atmosphere to short wave radiation with increasing temperature both act to significantly reduce the amplitude of the water vapour feedback. Equilibrium climate sensitivity for well-mixed greenhouse gas concentrations ranging from 200 ppmv to 800 ppmv is approximately 3.5 K, according to our one-dimensional moist radiative-convective model. Equilibrium climate sensitivity is further reduced when we do not prescribe the Bowen ratio and, instead, introduce a parametrization of evaporation (as explained in **Box 2.10**)

A more detailed analysis of the model results, which are illustrated in **figure 2.57**, reveals the extreme complexity of the system with its many interacting feedbacks. **Robust responses** to warming, involving the water cycle (**Box 2.10**), appear to be **(1)** that precipitable water increases at approximately the same rate with temperature as the saturation water vapour pressure at the Earth's surface, which makes the atmosphere more opaque to long-wave radiation, **(2)** that the atmosphere becomes more opaque to short wave radiation because of more absorption of Solar radiation by water vapour, and **(3)** that precipitation responds more weakly to warming than water vapour. On the other hand, the

response of cloud cover, which is also part of the water cycle, to warming is uncertain, because it depends on a relatively small change in relative humidity at the Earth's surface. In our radiative convective model cloud cover increases with temperature. This is a direct result of the increase of surface relative humidity with increasing surface temperature (i.e. precipitable water increases a little faster than saturation water vapour pressure at the Earth's surface) and our empirically based parametrization of cloud cover in terms of surface relative humidity (eq. 2.47). The response of cloud cover to warming, therefore, depends on a small deviation of the reponse of precipitable water (*PW*) from "Clausius Clapeyron". The sign of this deviation depends on the water vapour scale height, which is assumed constant here, but is likely *not* constant under global warming (eq. 1.25).

The response of clouds to global warming has been the subject of heated debates, especially since the publication of a controversial paper by Lindzen and co-workers in 2001[116] with the following soothing message. "The water vapour feedback is not as dangerous after all because of an **indirect negative feedback effect,** related to *reduced* cloud cover with increasing temperature, which more than cancels the positive water vapour feedback effect". This indirect negative feedback due to changing cloud cover was labeled the "**adaptive infrared iris**". Lindzen and co-workers tested the idea using observations made over the tropical Pacific. They found that clouds over the tropical Pacific Ocean recede when the surface temperature increases. Fewer clouds would open the infrared window through which heat could escape to space and thus cool the planet. Earth, they argued, has a natural response that counteracts rising temperatures, a bit like a human iris dilating to adapt to less light. However, others[117] have found no evidence of the existence of this infrared iris. Furthermore, **figure 2.55** indicates that fewer clouds will actually warm the planet! The controversy about the effect of clouds on surface temperature and about the feedback, i.e. the response of clouds to changing surface temperature, is still far from being resolved. Reasonably accurate modelling of the response of the water cycle to global warming, including the effect of clouds, depends crucially on the representation of surface evaporation and on soil moisture content. This issue is discussed further in **Box 2.10**.

A global average decrease in Solar radiation reaching the Earth's surface has been observed over the past 50 years or so. This has been attributed to an increase in the absorption of Solar radiation by **sulphate aerosols**, a phenomenon which has been known since the 1990's as **global dimming**[118]. This phenomenon appears to correlate very well with a decrease in observed evaporation[119]. However, in Europe, North America and Japan a "**brightening**" trend has set in since the middle of the 1980's, with the decline of aerosol loading of the atmosphere, which appears to correlate with an increase in both total precipitation and the number of intense precipitation events, but also with less cloudiness, less fog and more sunshine [120].

---

[116] R.S. Lindzen, M-D.Chou and A.Y.Hou, 2001: Does the Earth have an adaptive infrared iris? **Bull.American Meteorol.Soc., 82**, 417-432.

[117] D.L. Hartmann and M.L. Michelsen, 2002: No evidence for iris. **Bull.American Meteorol.Soc., 83**, 249-254. See also the response on page 1345 of the same volume.

[118] Wild, M., 2009: Global dimming and brightening: A review. **J.Geophys.Res., 114**, D00D16, doi:10.1029/2008JD011470, 2009.

[119] Roderick, M.L., and G.D. Farquhar, 2002: The cause of decreased pan evaporation over the past 50 years. **Science, 298**, 1410-1411.

[120] A.J. van Beelen and A.J. van Delden, 2012: Cleaner air brings better views, more sunshine and warmer summer days in The Netherlands. **Weather**, **67**, 21-25.

Box 2.10. Robust response of the water cycle to warming in models

Figure 2.57 demonstrates that preciptable water and precipitation respond very differently to "global warming". This is a robust response of state-of-the-art climate models (Allen and Ingram, 2002). According to the Clausius-Clapeyron equation, and assuming constant relative humidity, precipitable water increases with temperature by approximately 7% per K (**figure 1.8**), while precipitation very likely decreases with increasing temperature, depending upon the trend in cloud cover fraction and on how much Solar radiation is absorbed in the atmosphere by water vapour. This implies that the **residence time of water** in the atmosphere (obtained by dividing precipitable water by precipitation intensity) increases with "global warming". Some researchers claim that this will be accompanied by shorter and more intense precipitation events, while dry periods will be longer. In other words, both severe floods and severe droughts will increase in frequency. Finding an explanation for the "**muted response**" of the precipitation to global warming, as revealed by models, is a hot topic of present day climate research. The problem is linked to the problem of calculating evaporation of water from the surface. The subject is circumvented in the main text, by prescribing the Bowen ratio, but this clearly is not a very satisfactory solution. In state-of-the-art climate models evaporation (E_g) at the Earth's surface is calculated by assuming that it is proportional to the difference in water vapour pressure between the surface (subscript *g*) and the atmosphere (subscript *a*) near the surface:

$$E_g = K_E\left[e_s\left(T_g\right) - e\left(T_a\right)\right] \approx K_E\left[e_s\left(T_g\right) - e\left(T_g\right)\right] = K_E e_s\left(T_g\right)\left[1 - RH_g\right], \qquad (1)$$

where the subscript *s* is used here to indicate saturation (section 1.9). The constant K_E depends on the wind speed just above the surface. In the radiative convective model (Box 2.8) K_E is assumed constant (K_E=0.25 W m^{-2} Pa^{-1}). The exact value of K_E is found by calibrating it so that the model produces approximately the right precipitation and surface temperature for present-day conditions.

Eq. (1) reveals that, if the relative humidity at the Earth's surface, RH_g, remains constant, surface evaporation will also increase with temperature according to the Clausius Clapeyron relation. However, sensitivity experiments with state-of-the-art climate models reveal that the energy (net radiation), which is available for evaporation of water at the surface, does not "keep up" with the Clausius-Clapeyron relation. In fact, according to our radiative convective model, net radiation at the surface *decreases* with increasing surface temperature (**figure 1**, this Box). The reduction of the surface net radiation is due to increased absorption of Solar radiation by water vapour in the atmosphere as well as increased cloud cover, Increased cloud cover is due to increased relative humidity at the ground. Surface evaporation depends on the relative humidity also as is demonstrated by eq. 1. An increase of relative humidity at the surface will directly reduce evaporation.

The above arguments indicate that E_g does not increase with temperature at the pace dictated by the Clausius Clapeyron relation. In fact, for fixed Bowen ratio, the moist radiative convective model indicates a decrease of surface evaporation and precipitation with increasing surface temperature (**figure 2.57**)! The Bowen ratio, however, is not constant with global warming. Many models[121] show a decrease of the Bowen ratio with increasing temperature, most likely implying a reduction of surface sensible heat flux. In our

[121] J. Lu and M. Cai, 2009: Stabilization of the atmospheric boundary layer and the muted global hydrological cycle response to global warming. **J.Hydrometeorology, 10**, 347-352.

moist radiative convective model a decrease of the Bowen ratio with increasing surface temperature is observed only for CO_2 concentrations lower than about 1000 ppmv. Whether this effect compensates for the reduction in surface net radiation is in general still a matter of debate. In other words, the consequences of the reduction of net radiation at surface for surface evaporation, and with it the response of the water cycle, are highly uncertain.

The long wave water vapour feedback, illustrated in **figure 2.56**, seems to be a robust response to the increase of the CO_2 concentration and so is the muted response of evaporation (at a pace significantly less than "Clausius-Clapeyron), but quantifying the response of many parts of the water cyle, especially the response of clouds, is at present quite rudimentary.

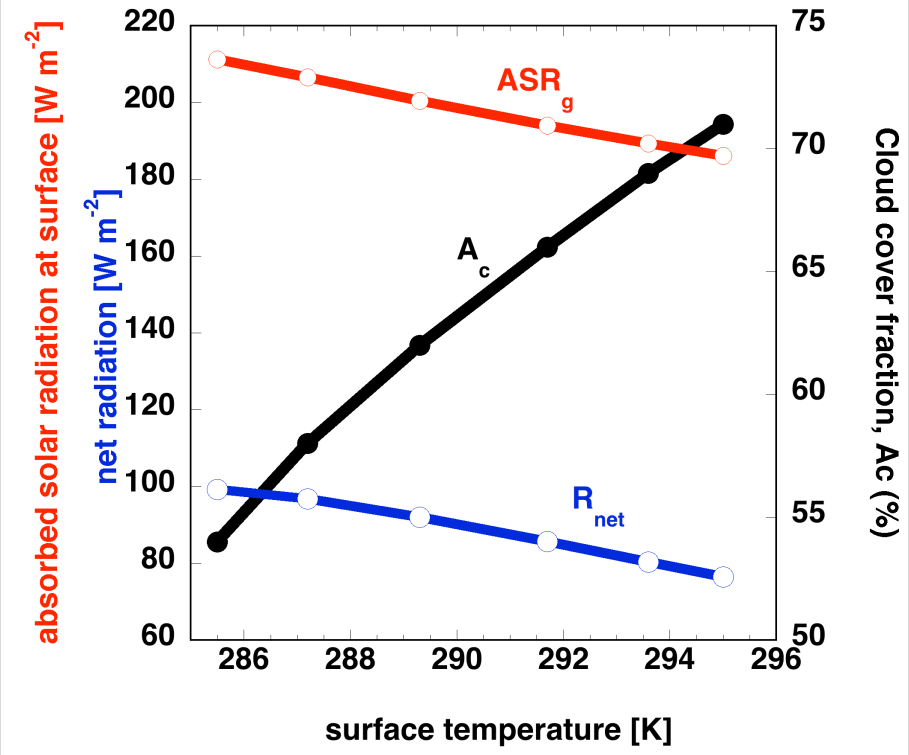

FIGURE 1, BOX 2.10. Equilibrium **net radiation at the surface (R_{net})** (positive downwards), equilibrium **absorbed Solar radiation (ASR) at the surface**, and equilibrium **cloud cover fraction** (**Ac**) as a function of equilibrium surface temperature according the radiative-convective model with the characteristics listed in Box 2.8. The model is run to equlibrium for different CO_2-concentrations, ranging from 100 ppmv to 3200 ppmv.

Figure 2 (this Box) demonstrates that the short wave water vapour feedback, together with the cloud cover feedback may significantly reduce the long wave water vapour feedback (**figure 2.56**). Equilibrium climate sensitivity in the most realistic version of the radiative convective model, with the parametrization of evaporation given in (1), is no more than 2.4 K.

Finally, it must be stated that eq. 1 assumes that water is always available for evaporation at the surface. Over the oceans (70% of the Earth's surface) this is true, but over large parts of the subtropical continents this is not true (**figure 1.18**). It is, therefore, necessary to add an equation that tracks the **evolution of soil water** under influence of accumulated precipitation, run-off by rivers and leakage to the deeper soil layers (Seneviratne et al., 2010). State-of-the-art climate models are, indeed, "equipped" with such an equation.

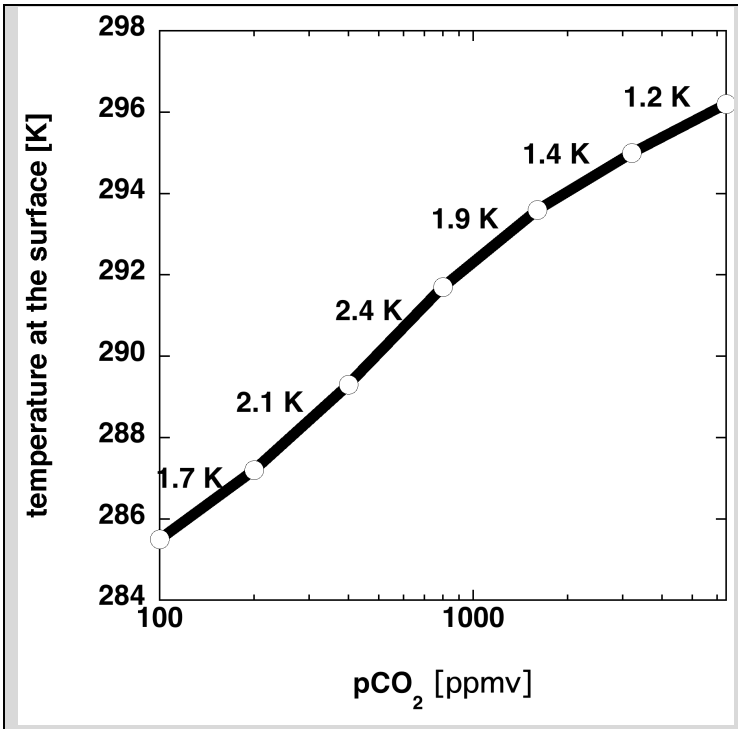

FIGURE 2, BOX 2.10. Equilibrium temperature as a function of CO_2 concentration, showing the temperature increase for each doubling of the concentration. Due to the cloud cover feedback and other feedbacks in the system the equilibrium sensitivity is much smaller than is suggested by figure 2.56, which assumes only a water vapour feedback. Moreover, equilibrium sensitivity is not constant with increasing CO_2 concentration.

References to Box 2.10

Allen, M.R., and W.J. Ingram, 2002: Constraints on future changes in climate and the hydrological cycle. **Nature., 419**, 224-232.

Seneviratne, S.I., et al., 2010: Investigating soil moisture-climate interactions in a changing climate: A review. **Earth Science Reviews, 99,** 125-161.

Box 2.11. Climate sensitivity in "the world of big models"

Since the time of Arrhenius (1896), climate scientists have tried to estimate equilibrium climate sensitivity, i.e. the long-term equilibrium near-surface temperature response to a doubling of atmospheric carbon dioxide. In 2007 the Intergovernmental Panel on Climate Change (IPCC) (http://www.ipcc.ch/publications_and_data/ar4/wg1/en/ch10s10-5.html#box-10-2) concluded that this quantity is likely to be in the range 2 K to 4.5 K, with a 30% chance that it is outside this range. The lower bound is very probably no lower than 1.6 K. However, the upper bound is not known. Based on a 2017-member grand ensemble of unique simulations using one particular climate model including a simple "slab-ocean", Stainforth et al. (2005) have proposed a range from 1.9 K to 11.5 K. The idea behind this study is that the values of the model parameters, that are associated with parametrization schemes, are not exactly known. For instance, the global average Bowen ratio is equal to 0.3 if we use the data from **figure 2.10**, but it is 0.21 if we use the data from **figure 2.25**. Moreover, the value of parameters, such as the Bowen ratio, or the cloud albedo, or ground albedo may change due to changes in vegetation, or due to changes in liquid water path, or due to changes in the area covered by snow or ice (section 2.21) when climate changes. Repeating the double-CO_2 climate model simulations with slightly perturbed parameter values will yield different estimates of equilibrium climate sensitivity. Grouping of the

estimates into "bins" of, for example 1 K, yields a probability distribution as is shown in **figure 1** (this Box).

Estimates of equilibrium climate sensitivity that have appeared in the literature over the past century have been based on very diverse assumptions and models, from simplified one-dimensional radiative convective models, such as our model (Box 2.8) to complex three-dimensional climate models. The latter type of model obviously accounts for much more physics than the former type of model. For example, it describes the transport of latent heat from the sub-tropics to both the tropics and extratropics (section 1.38). In other words, in a three-dimensional climate model energy can be transferred from regions where the atmosphere is optically thick for long wave radiative transfer (the tropics) to regions where the atmosphere is optically thin for long wave radiative transfer (the extra-tropics), where the energy more easily escapes to space by long wave emission. In this sense, the extra-tropics function in the same way as the infra-red atmospheric window (section 2.17). Climate sensitivity of three-dimensional climate models is, therefore, expected to be lower than the climate sensitivity of one-dimensional radiative-convective models. This topic will be discussed further in chapter 12.

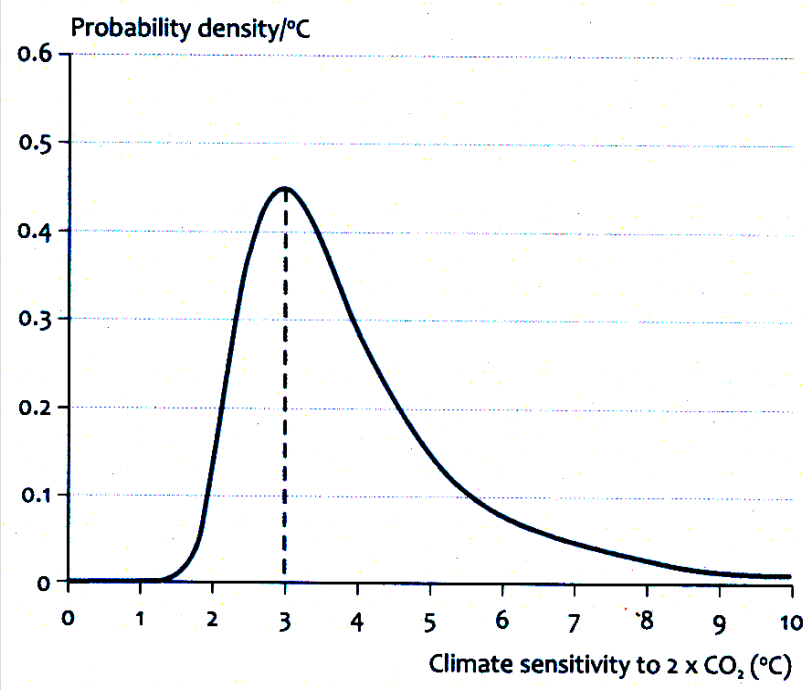

FIGURE 1, BOX 2.11. Probability distribution of climate sensitivity (smoothed curve), deduced from model simulations.

If one is concerned with climate forecasting for the coming century, equilibrium climate sensitivity is, in fact, not a very useful concept. "Non-equilibrium" climate sensitivity **depends crucially on our knowledge of how the ocean and the cryosphere respond to greenhouse forcing**. We know that the ocean and the large ice caps react extremely slowly to forcing (in the order of hundreds of years or more). Due to this, the climate system is, and will not be, in equilibrium as long as greenhouse gas concentrations keep increasing at the present relatively very rapid rate.

Reference to Box 2.11.

Stainforth, D.A., et al., 2005: Uncertainty in predicitions of the climate response to rising levels of greenhouse gases. **Nature**, **433**, 403-406.

PROBLEM 2.13. **Probability density function of equilibrium climate sensitivity**
Investigate the probability density function of equilibrium climate sensitivity (Box 2.11) for the moist radiative convective model by perturbing the values of parameters such as the albedo of clouds, α_c, the albedo of the ground, α_g, the precipitation relaxation time, τ_c, and the water vapour scale height, H_v. (See http://www.staff.science.uu.nl/~delde102/RCM.htm).

PROBLEM 2.14. **Faint young Sun paradox**
There is geological evidence that *liquid water was present on Earth as early as 3.8 billion years ago, when Solar radiation was 25% less than today* (the "faint young Sun"). Assume that the mixing ratio of the principal well-mixed greenhouse gas (CO_2) was the same 3.8 billion years ago as today. What would be the surface temperature of the Earth at that time? Would liquid water be present? It is thought that a stronger greenhouse effect offsets the effect of a weaker Sun. What well-mixed greenhouse gas concentration is required to offset the effect of the faint young Sun? Use the moist radiative convective model (see problem 2.13) to find an answer. How could clouds offset the effect of the faint young Sun instead of carbon dioxide?

2.20 Radiative forcing

The effect on climate of an increase in the concentration of a greenhouse gas is usually expressed in terms of the associated *instantaneous* radiative perturbation at some level above the troposphere. This quantity can be computed rather quickly even for the most complex three-dimensional climate models (called "general circulation models", or "GCM's").

The "**radiative forcing**" caused by a change Δm in the mass of a greenhouse gas X is defined as the resulting flux imbalance in the radiative budget for the Earth-atmosphere system keeping everything else constant, *including temperature*. **Figure 2.58** shows the outgoing long-wave radiation flux at 70 km above sea level, with a temperature profile that follows the 1976 US standard atmosphere, plotted as a function of atmospheric carbon dioxide concentration, calculated with a radiation model that is able to resolve the spectral details of longwave radiation absorption (**figure 2.48**) depending on the concentration of gases such as ozone, methane, water vapour and carbon dioxide[122]. If the atmosphere contains no ozone, no methane, no water vapour and no carbon dioxide 347 W m^{-2} escapes to space as long wave radiation. If we subsequently add the annual average stratospheric ozone concentration, we find that 340 W m^{-2} escapes to space, i.e. the "greenhouse effect" or "**radiative forcing**" of stratospheric ozone is 7 W m^{-2}. If we now add the mid-latitude average amount of water vapour and neglect clouds, we find that the outgoing long wave radiation flux is further reduced by 51 W m^{-2}. If we now add 380 ppmv of homogeneously distributed carbon dioxide, the outgoing long wave radiation flux is further reduced, by 27.5 W m^{-2}, to 261 W m^{-2}.

However, if we now further increase the CO_2 concentration to say 1000 ppmv (still neglecting clouds!), we find that the long wave radiation flux is further reduced by only 3.9 W m^{-2}! This implies that the radiative forcing of carbon dioxide per unit ppmv decreases with increasing CO_2 concentrations, in accord with what we have seen in previous sections.

[122] You can run this model yourself from David Archer's website: http://forecast.uchicago.edu/models.html

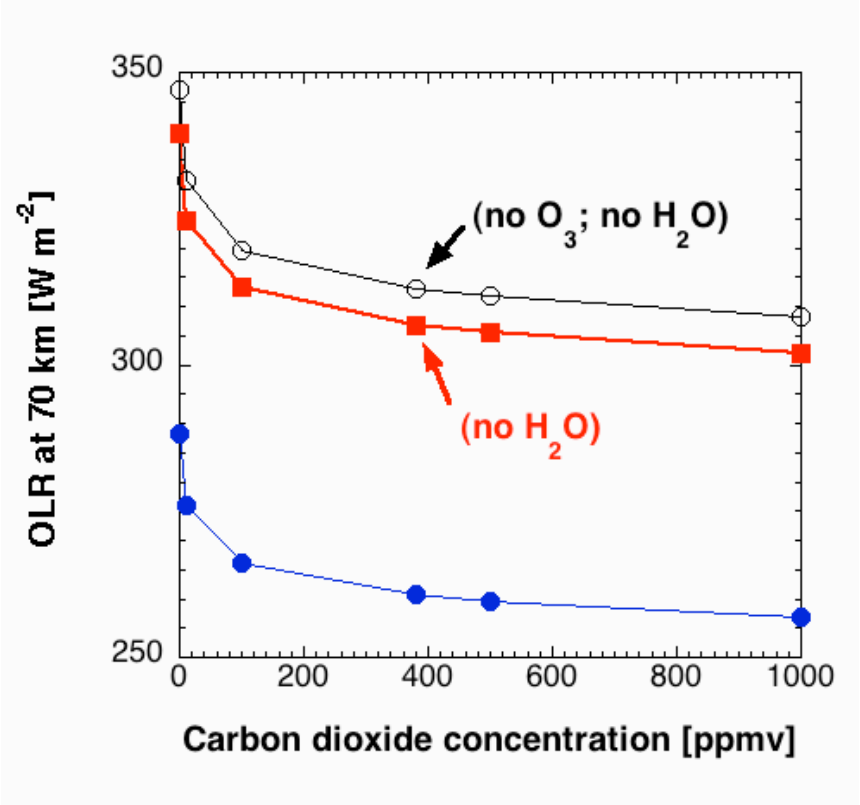

FIGURE 2.58. Outgoing long-wave radiation at 70 km as a function of carbon dioxide concentration for an atmosphere without clouds containing no methane and prescribing the temperature according to the 1976 US standard atmosphere (where for instance the temperature of the Earth's surface is 288.2 K, see **table 2.1**). The upper curve is for an atmosphere containing no ozone and no water vapour. The middle curve is for an atmosphere with average stratospheric ozone concentration, but no water vapour, while the lower curve is for an atmosphere with average stratospheric ozone concentration as well as average mid-latitude water vapour (H_2O-partial pressure at the Earth's surface is approximately 7 hPa). Source: http://climatemodels.uchicago.edu/modtran/modtran.doc.html.

The effect of the human induced doubling of CO_2 concentrations from a pre-industrial value of about 280 ppm to 560 ppm, somewhere in the twenty first century, will have less *effect on the outgoing long wave radiation*[123] than the concentration fluctuations with an amplitude of about 100 ppm that were associated with the glacial-interglacial cycles of the past 1 million years (figure 2.6).

Spectra of the radiation "observed" at 70 km above the Earth's surface for the US 1976 standard atmosphere for three cases differing only in assumed CO_2 concentration are plotted in **figure 2.59**. CO_2 absorbs radiation in a broad spectral band centred at 700 cycles cm^{-1} (wavelength: 14.3 μm). Radiation in this wave number interval, which is emitted by the ground and the lower parts of the atmosphere, is quickly depleted at upper levels in the atmosphere. Carbon dioxide at upper levels emits radiation within the same wave number interval, but at a lower temperature, and thus with a lower intensity. This appears as a "bight" in the spectrum. Since the total radiation leaving the system is proportional to the area beneath the sprectral curve in **figure 2.59**, less energy will leave the system as the "bight' becomes "deeper", but also broader. The "deepening" will be arrested when the spectral intensity of radiation within the absorption band approaches the black-body curve corresponding to the lowest temperature in the atmosphere (about 215 K) (**table 2.1**).

[123] But not necessarily less effect on the surface temperature!

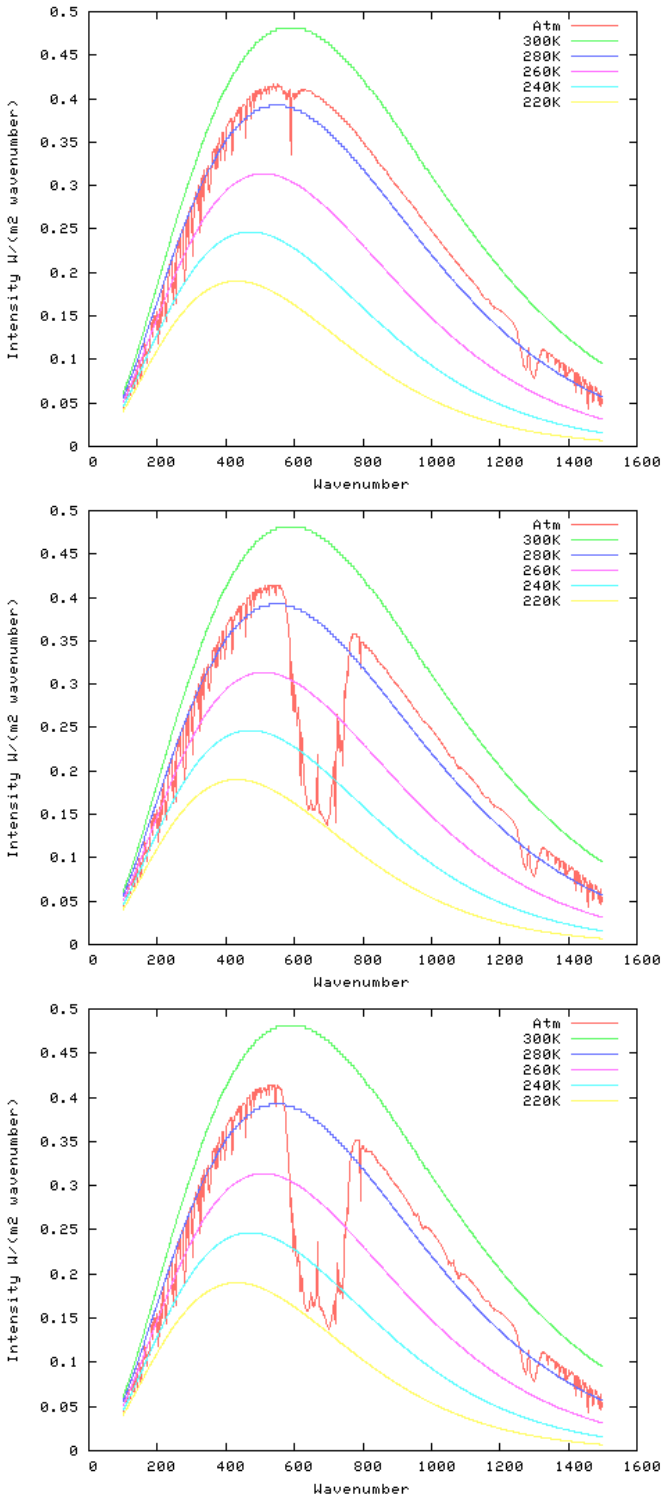

FIGURE 2.59. Demonstration of band saturation, using David Archer's model (see problem 2.15). Outgoing long-wave radiation at 70 km above the Earth's surface, given the temperature distribution and assuming that the atmosphere contains no water vapour, no methane and no ozone. Temperature follows the 1976 US standard atmosphere (**table 2.1**). The carbon dioxide concentration is varied. The upper panel is the spectrum for an atmosphere without CO_2. If the CO_2 content is increased to 380 ppmv (present value) the "bight" in the spectrum appears. This bight hardly changes when the CO_2 content is increased to 1000 ppmv (lower panel). The smooth curves represent the black body emission as function of wave number, in cycles per second, for different temperatures computed with eq. 1 of Box 1.3. See David Archer's lectures 7 and 8, entitled "Greenhouse Gases in the Atmosphere" (http://forecast.uchicago.edu/lectures.html).

However, at the flanks of the absorption band, absorption is less effective (absorption cross-sections are lower), and therefore further increasing the carbon dioxide content will continue to deepen the "bight" at the flanks, which will appear in the graph as a slight broadening of the absorption band and further slight increase in the intensity of the radiative forcing. The importance of this "**band saturation effect**" for "anthropogenic global warming" has been the subject of intense discussion in the climate research community [124].

Box 2.12. Radiative forcing of clouds

The problem of understanding and predicting the influence of clouds on Earth's temperature under influence of changing atmospheric composition is the most intractable of all climate problems. The role of clouds in climate has been interpreted mostly in terms of the radiative forcing of clouds. The long wave forcing of clouds and the short wave forcing of clouds is frequently discussed separately. The long wave forcing of clouds is illustrated in a classic figure, due to Manabe and Wetherald (1967) (see the list of references at the end of this Box), shown below (**figure 1**). Due to the greenhouse effect, OLR-TOA increases with surface temperature more slowly than is predicted by Stefan-Boltzmann's law (Box 1.3).

.

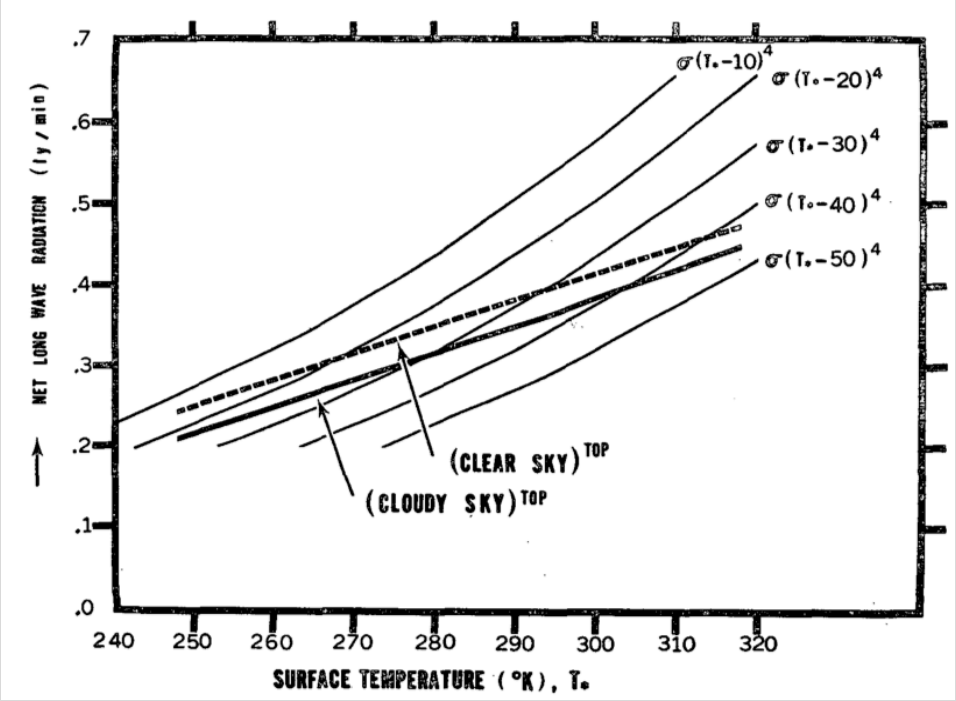

FIGURE 1, BOX 2.12. Instantaneous outgoing long wave radiation at the top of the atmosphere (OLR-TOA) as a function of surface temperature for the set of temperature profiles, shown in **figure 2** in this Box (note that these temperature-profiles are not equilibrium profiles), calculated with a radiative-convective model with relative humidity and cloud distribution kept fixed, The cloud distribution is prescribed according to a simplified representation of the observed cloud distribution, as explained in the text of this Box. The unit of energy flux is Langley per minute (ly/min), which is equivalent to 697.3 W m^{-2}.

[124] http://www.realclimate.org/index.php/archives/2007/06/a-saturated-gassy-argument/. See also figure 2.54. See David Archer's lectures 7 and 8, entitled "Greenhouse Gases in the Atmosphere" (http://forecast.uchicago.edu/lectures.html).

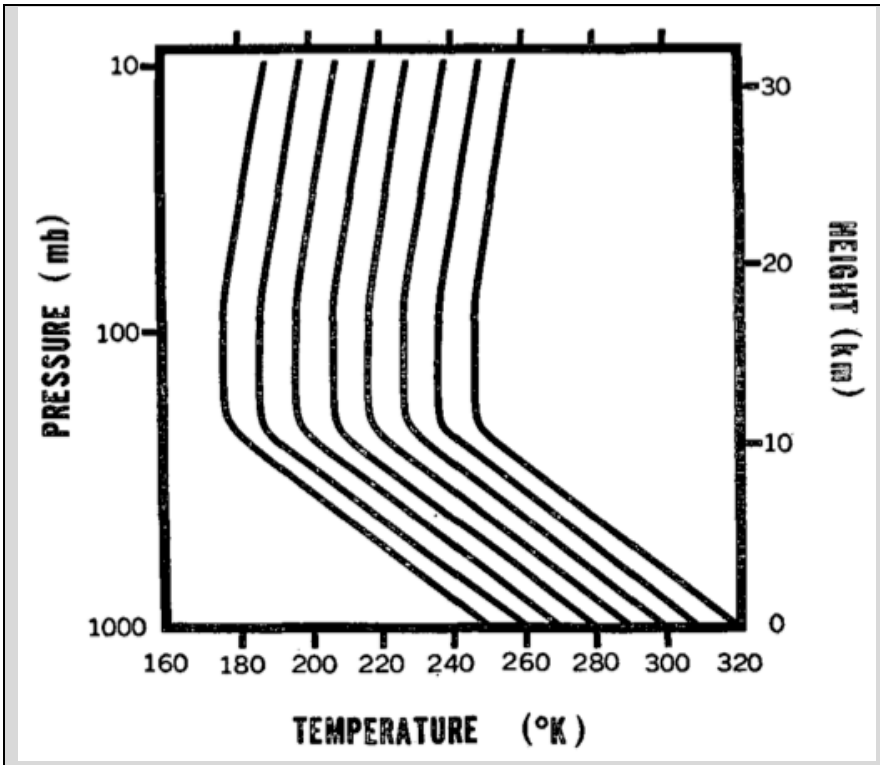

FIGURE, BOX 2.12. Vertical temperature profiles adopted for the computations of the radiative fluxes shown in **figure 1.**

The graphs in **figure 1** suggest an approximation of OLR-TOA by the formula,

$$\boxed{\text{OLR - TOA} \equiv I = I_0 + bT_s + cA_c}, \qquad (1)$$

where T_s is the temperature at the Earth's surface in °C(!!), and I_0, b and c are empirical constants. Budyko (1974) gave the following estimates of the values of these constants

$$I_0 = 226 \text{ W m}^{-2};\ b = 2.26 \text{ W m}^{-2}\text{°C}^{-1};\ c = -25.83 \text{ W m}^{-2}. \qquad (2)$$

The negative value of c implies that clouds reduce OLR-TOA. Later theoretical and observational studies (using radiation models and satellite data) have revealed that the parameter, c, is (approximately) proportional to the temperature difference between cloud-top and the Earth's surface, i.e.

$$c \approx -1.7\left(T_s - T_c\right), \qquad (3)$$

where T_c, is the temperature at the height of the top of the cloud (Ramanathan, 1977; Thompson and Warren, 1982). Low cloud tops emit radiation at approximately the same temperature as the Earth's surface and, therefore, hardly reduce OLR-TOA compared to clear conditions. High clouds, on the other hand, emit long wave radiation at much lower temperatures and thus strongly reduce OLR-TOA relative to the clear sky case, provided that they emit radiation as a black body.

The short wave radiative forcing of clouds is relatively easy to understand. It has to do with the high albedo of clouds relative to the average albedo of the Earth's surface (eq. 2.49). Quantifying this effect is, however, not so easy because cloud albedo depends on the

water content of the cloud and, to a lesser extent, on the Solar zenith angle (Stephens, 1978). The equation that expresses the dependence of absorbed Solar radiation (ASR) on the two well-known cloud parameters, i.e. the albedo (α_c) of clouds and cloud cover cover fraction (A_c), is

$$\mathrm{ASR} \equiv Q = \frac{S_0}{4}\left(1 - \alpha_c A_c - \alpha_g\left(1 - A_c\right)\right), \qquad (4)$$

where α_g is the albedo of the Earth's surface. Because $\alpha_c > \alpha_g$ (except if the globe is covered by ice and snow), ASR decreases with increasing cloud cover fraction, i.e. the **Solar sensitivity coefficient** is less than zero:

$$\frac{\partial Q}{\partial A_c} < 0. \qquad (5)$$

The value of the Solar sensitivity coefficient according to different authors lies in the range -85 to -130 W m^{-2}.

The **long wave sensitivity coefficient** is defined as (eq. 1)

$$\frac{\partial I}{\partial A_c} = c. \qquad (6)$$

The **net sensitivity coefficient**, δ, to cloud cover fraction is equal to the difference between the Solar sensitivity coefficient and the long wave sensitivity coefficient:

$$\delta \equiv \frac{\partial Q}{\partial A_c} - \frac{\partial I}{\partial A_c}. \qquad (7)$$

With Budyko's estimate of c (-25.83 W m^{-2}) the net sensitivity is negative, i.e. clouds have a cooling effect, due to the increase of albedo with increasing cloud cover. According to (3) Budyko's estimate of c implies (T_s-T_c)=15 K. With an average lapse rate of 6.5 K km^{-1} this would imply that the average cloud top height is about 2.3 km. Obviously, this estimate is too low. Satellite-based estimates of global average cloud top height yield a value of about 6 km (Rossow and Schiffer, 1991, 1999). Indeed, later estimates of the value of the long wave sensitivity coefficient have yielded much higher values in the range of -35 to -110 W m^{-2} (Arking, 1991), which are more consistent with (T_s-T_c) in the range 20 to 65 K. The latter value would imply a cloud top height of about 10 km.

Manabe and Wetherald (1967) did not identify the cloud-top feedback effect, because they used a fixed distribution of cloud characteristics (**table 2.3**) with clouds divided into three types: low clouds, middle clouds and high clouds. Each cloud type has a characteristic fixed albedo, cloud top height and frequency. This classification is adopted in most versions of the radiative convective model. A difficulty with this classification is that high clouds in reality have widely differing albedo's, depending on whether they are cirrus clouds or cumulo-nimbus clouds. Therefore, the specific albedo that is assigned to high clouds is a weighted average of the albedo of cumulo-nimbus clouds (about 0.75) and the albedo of cirrus clouds (about 0.1) (**figure 2.40**). Since cirrus clouds are much more frequent than deep convective clouds (Rossow and Schiffer, 1999, page 2282), this weighted albedo of "high-level" cloud tops is relatively low (about 0.2). Obviously, this value is very uncertain. Therefore, even though a trustworthy evaluation of the sign of the cloud feedback on

climate, which encompasses the effects of the albedo-feedback and the cloud-top feedback, is very problematic, it should have high priority in the climate-research program.

References to Box 2.12.

Arking, A., 1991: The radiative effects of clouds and their impact on climate. **Bull.Amer.Meteorol.Soc., 71**, 795-813.

Budyko, M.I., 1974: **Climate and Life.** Academic Press, 508 pp.

S.Manabe and R.T.Wetherald, 1967. Thermal equilibrium of the atmosphere with a fixed distribution of relative humidity. **J.Atmos.Sci., 24**, 241-259).

Ramanathan, V., 1977: Interaction between ice-albedo, lapse-rate, and cloud-top feedback: an analysis of the nonlinear response of a GCM-climate model. **J. Atmos. Sci., 34**, 1885-1897.

Rossow, W.B., and R.A. Schiffer, 1991: ISCCP cloud data products. **Bull.Amer.Meteorol.Soc., 72**, 2-20.

Rossow, W.B., and R.A. Schiffer, 1999: Advances in understanding clouds from ISCCP. **Bull.Amer.Meteorol.Soc., 80**, 2261-2287.

Stephens, G.L., 1978: Radiation profiles in extended water clouds. II Parameterization schemes. **J. Atmos. Sci., 35**, 2123-2132..

Thompson, S.L. and Warren, S.G., 1982: Parameterization of outgoing infrared radiation derived from detailed radiative calculations. **J. Atmos. Sci., 39**, 2667–2680.

PROBLEM 2.15. Radiative forcing

(a) Use modtran* to investigate the radiative forcing of methane (CH_4) compared to carbon dioxide. Compare the radiative forcing of CH_4 and CO_2 over the past 200 years. Recommended reading: Zhong, W., and J.D. Haigh, 2013: The greenhouse effect and carbon dioxide. **Weather, 68**, 100-105.

*(see http://climatemodels.uchicago.edu/modtran/modtran.doc.html)

(b) Investigate the effect of clouds on long wave radiative forcing with the same model. Write a short essay (500-1000 words) on the radiative effect of different cloud types (cirrus, stratus, cumulus, etc.). Discuss the importance of this effect compared to the radiative effect of CH_4 and CO_2.

Box 2.13. The oceanic solubility pump for carbon dioxide

During the past 50 years the atmospheric carbon dioxide content increased by about 3 billion tons per year. This corresponds to about half the amount emitted by fossil fuel burning. Where did the other half go? Probably into the ocean. The atmosphere exchanges carbon dioxide with two larger reservoirs of inorganic carbon: the land biosphere and the ocean. The ocean reservoir is by far the largest: it contains about 50-60 times more carbon than the atmosphere. Only 0.5% of this carbon in the ocean is in the form of dissolved CO_2 gas.

The carbon dioxide uptake by the ocean is governed by the CO_2 solubility, α, in sea-water. The partial pressure of carbon dioxide (pCO_2) in water depends on its solubility and its concentration in water as

$$pCO_2 = \frac{[CO_2]}{\alpha}, \qquad (1)$$

where $[CO_2]$ is the concentration in units of moles of solute per kg of solution (a mixing ratio). The **solubility of carbon dioxide is higher at lower temperatures**. The surface

water of the ocean is nearly always approximately in equilibrium with the atmosphere, meaning that the CO_2 partial pressure difference between the ocean and the atmosphere tends to zero. For water at equilibrium with the atmosphere of a fixed pCO_2, the concentration of CO_2 in the water decrease as the temperature increases. Conversely, the atmospheric pCO_2 will decrease if the solubility decreases, i.e. when the temperature decreases. Could this explain the low atmospheric pCO_2 during glacial cycles (**figure 1, this Box**)? If so, this effect may act as a positive feedback which acts to re-enforce the climatic effect of weak orbital Solar irradiance fluctuations that are thought to be the pacemakers of the glacial cycles.

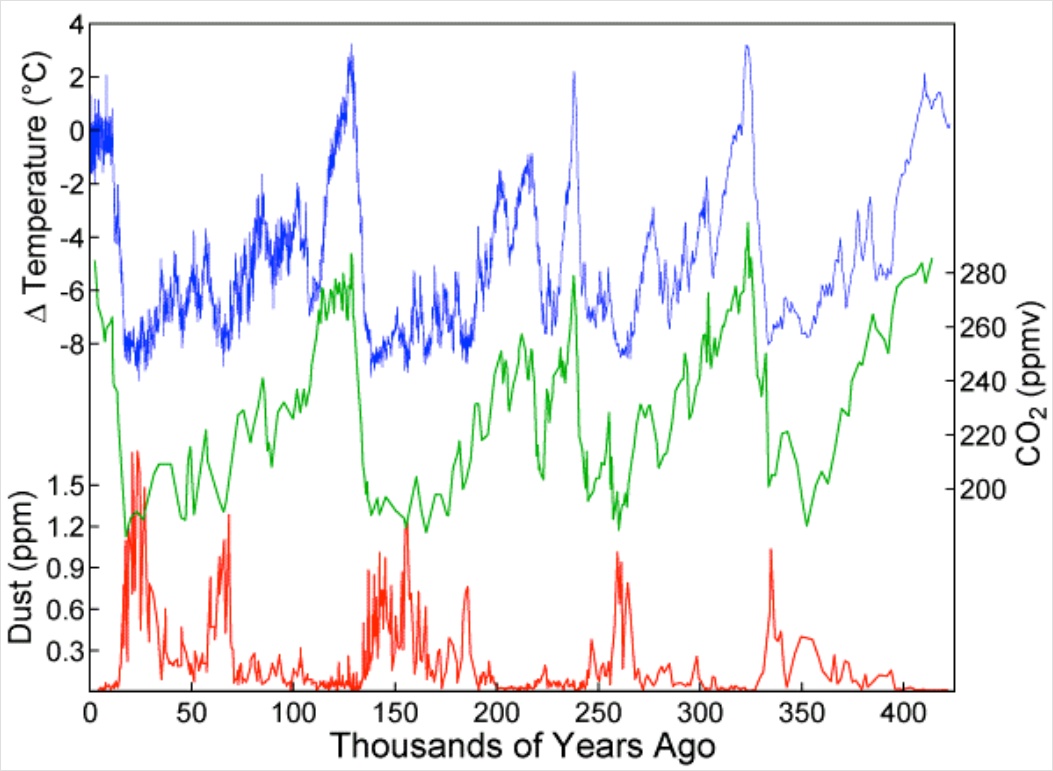

FIGURE 1 (BOX 2.13). Graph of CO_2, temperature and dust concentration measured from the Vostok (Antarctica) ice core as reported by Petit et al. (**Nature**, 399 (1999), 429-436). The low temperatures during the glacial periods are caused by the decrease of insolation at the summer poles due to changes in the Earth's orbit around the Sun. More snow and ice can then survive the summer. The world is drier during glacial periods. Therefore the temperaure decrease is reinforced by a reduction of the strength of the greenhouse-effect due to a reduction of both atmospheric water vapour- and CO_2-concentrations and by the blocking of Solar radiation by dust in the atmosphere. The reduction of the CO_2 concentration during glacials is probably caused by increased uptake of CO_2 by oceans during cold periods. However, this increased ocean uptake is counteracted by reduced uptake by the less active biosphere. The CO_2-signal lags the temperature-signal by approximately 800 years.

The uptake of carbon dioxide by the ocean does not only depend on the sea surface temperature, T, but also on the total **dissolved inorganic carbon** in the sea water, DIC, on the total alkalinity in sea water, ALK, and on salinity, S. This dependence can be expressed in the following equation for the change in equilibrium partial pressure of sea water:

$$dpCO_2 = \frac{\partial pCO_2}{\partial T} dT + \frac{\partial pCO_2}{\partial DIC} dDIC + \frac{\partial pCO_2}{\partial ALK} dALK + \frac{\partial pCO_2}{\partial S} dS, \qquad (2)$$

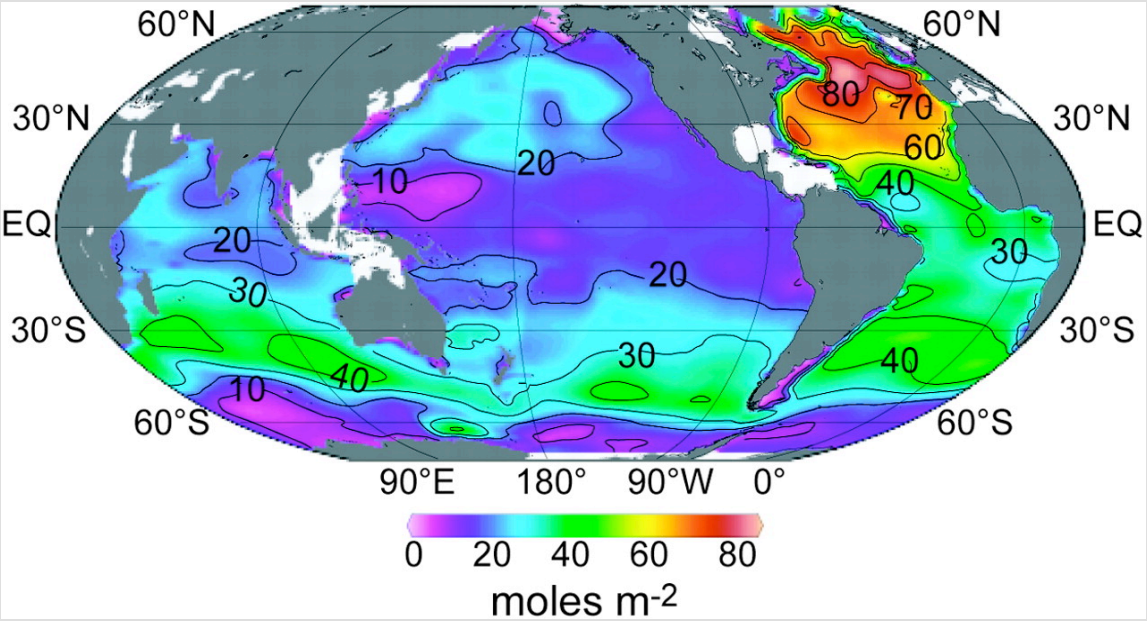

FIGURE 2 (BOX 2.13). Column inventory of anthropogenic CO_2 in the ocean (mol m^{-2}). High inventories are associated with deep water formation in the North Atlantic and intermediate and mode water formation between 30° and 50°S. Total inventory of shaded regions is 106 ± 17 Pg C (Sabine, C.L. et al., 2004).

where, empirically:

$$\frac{\partial \ln pCO_2}{\partial T} = 0.042\ \mathrm{K}^{-1};\ \frac{\partial \ln pCO_2}{\partial \ln DIC} = 10;\ \frac{\partial \ln pCO_2}{\partial \ln ALK} = -9.4;\ \frac{\partial \ln pCO_2}{\partial \ln S} = 0.94 \quad (3)$$

The consequence of the value of the first thermodynamic quantity (governing the temperature dependence of the carbon dioxide content of the ocean) can be translated as follows (Archer, 2010, p. 68):

"If you take a bucket of sea water and warm it up 1°C, its pCO_2 value, which is the equilibrium partial pressure of carbon dioxide that the air above would reach, increases by 4%. CO_2-molecules, that are excited by thermal energy, would prefer to move around nearly unhampered in the gas phase rather than to be bogged down in the liquid".

The second thermodynamic quantity in (3) is commonly referred to as the **Revelle factor** or **buffer capacity**. The value of 10, given to this quantity in (3), is a global average and, in fact, not constant. It depends weakly on ALK. Lower values are generally found in warm waters and higher values are found in cold waters. The capacity of the ocean to take up anthropogenic CO_2 is proportional to the inverse of the buffer capacity or Revelle factor. High concentrations of anthropogenic CO_2 are found in the subtropical North Atlantic surface waters because of the low Revelle factor in that region.

Most of the anthropogenic CO_2 is in the upper 500 m of the ocean. If the water stays at the surface and warms up as it moves around the globe, CO_2 will relatively quickly escape back to the atmosphere. However, if water sinks to the deep ocean, the carbon can be stored for hundreds to thousands of years before the ocean circulation returns it to the surface. Cold waters sink to the deep ocean principally in the North Atlantic Ocean. This region is therefore a major CO_2- removal area of the ocean (**figure 2, this Box**). This process is referred to as the solubility pump.

Can the solubility pump explain the variations of CO_2 of about 80 ppmv (**figure 1**) across glacial cycles? If yes, then this would imply an approximate 10°C variation of the ocean temperature during glacial cycles. The deep ocean cannot have exhibited these large variations in temperature. At present, the average deep ocean temperature is about 2°C. The freezing point of sea water is about-2°C. Therefore, the solubility pump can only account for about 24 ppmv variation of pCO_2 between glacial and interglacial periods

References to Box 2.13

Archer, D., 2010: **The Global Carbon Cycle**. Princeton University Press.
Revelle, R., and H.S. Suess, 1957: Carbon dioxide exchange between atmosphere and ocean and the question of an increase of atmospheric CO2 during the past decades. **Tellus, 9**, 19-27.
Sabine, C.L. et al., 2004: The oceanic sink for anthropogenic CO_2. **Science, 305**, 367-371.
Takahashi, T, J. Olafsson, J.G. Goddard, 1993: Seasonal variation of CO_2 and nutrients in the high-latitude surface oceans: a comparative study. **Global Biochemical Cycles**, 7, 843-878.

2.21 The ice albedo feedback

Climate in this chapter is defined as the time average physical state of the atmosphere, ocean and cryosphere, including the regular diurnal and seasonal cycle of weather elements. The averaging time is always finite, for instance 30 years. Climate is principally determined by the orbit and position of the Earth relative to the Sun. These factors determine how much energy is received by the climate system and how this energy is distributed over the globe. We know that the position of the Earth relative to the Sun varies on the seasonal timescale as well as on longer timescales (Box 2.1 and section 2.2). Although this induces only small variations in global average incoming Solar radiation, we'll learn in this section that, due to the **non-linear** character of interactions between different parts of the "climate system" (for instance between the cryosphere and the atmosphere), this may have large consequences. The saying goes that **"**weather is what you get and climate is what you expect". In reality, like the weather, climate holds surprises.

The discovery, in the nineteenth century, of the existence in Earth's history of long periods of time during which huge volumes of ice covered areas that are now densely populated, was a great surprise and therefore hard to swallow for many[125]. At present it is thought that the Earth has experienced five "**ice ages**". An ice age is a period of long term (millions of years) reduction in the average temperature near the Earth's surface, resulting in the inception or expansion of ice-sheets and glaciers. At present we are still in the fifth ice age, because large ice sheets exist at the South Pole and over Greenland. The fifth ice age, however, seems to be coming to its end, aided by the human induced greenhouse effect. The present ice age consists of "**glacial cycles**" (**figure 1, Box 2.13**), where warm "**interglacial**" periods (such as the present "Holocene" period) alternate with "**glacial**" periods, each lasting several tens of thousands of years. The timing of these glacial cycles has been related to small periodic changes in Solar irradiance. How such small changes in irradiance can induce such large changes in the climate system is a question that still keeps researchers

[125] The book by John Imbrie and Katherine Palmer Imbrie (**Ice Ages: Solving the mystery**. The MacMillan Press (1979)) tells the fascinating story of this discovery.

occupied. In any case, it is certain that the "**ice-albedo feedback effect**" plays an important role in the answer to this question.

For the Earth as a whole and averaged over at least one year the absorbed Solar radiation and the outgoing long wave radiation at the top of the atmosphere are approximately in balance, i.e.

$$\boxed{Q(1-\alpha)=I} \qquad (2.70)$$

In this equation $Q=S_0/4$ is the Solar radiation reaching the top of the atmosphere (TOA), $\alpha(T)$ is the albedo and $I(T)$ is the outgoing long wave radiation at TOA. T is the temperature at the Earth's surface. Note that the variables in eq. (2.70) do not depend on pressure or latitude. In section 2.22 the latitude-dependence will be introduced. We assume that I can be expressed as a function of T. This is referred to as "**parametrization**". Budyko[126] suggested the following parametrization for I (Box 2.12).

$$\boxed{I=I_0+bT}\,. \qquad (2.71)$$

In this formula T is expressed in °C! The constants I_0 and b are empirical. The linear relation (2.71) can also be obtained theoretically by linearization of the black body emission as follows. Using the binomial theorem we can write:

$$\sigma(273.15+T)^4 \approx \sigma(273.15)^4 + 4\sigma(273.15)^3 T\,.$$

Now, comparing the above formulae we obtain (with σ=5.67×10^{-8}) :

$$I_0 = \sigma(273.15)^4 = 315.64 \text{ W m}^{-2}$$

and

$$b = 4\sigma(273.15)^3 = 4.62 \text{ W m}^{-2} \text{ °C}^{-1}\,.$$

Empirically, Budyko (1969) obtained

$$I_0 = 205 \text{ W m}^{-2},$$

although he also cites a value of 223 W m^{-2} in his book "*Climate and life*", which is cited in Box 2.12. For the parameter b, which is a measure of climate sensitivity (see below) Budyko obtains

$$b = 2.23 \text{ W m}^{-2} {}^{\circ}C^{-1}.$$

PROBLEM 2.16. **Physical meaning of model parameters**
Explain the difference between the empirical values and the theoretical values of the coefficients I_0 and b. Estimate the values of I_0 and b from figure 2.15. Estimate the emission coefficient of the Earth-atmosphere system from Budyko's estimate of I_0 and b.

---

[126] Budyko, M.I., 1969, **Tellus**, **21**, 610-619

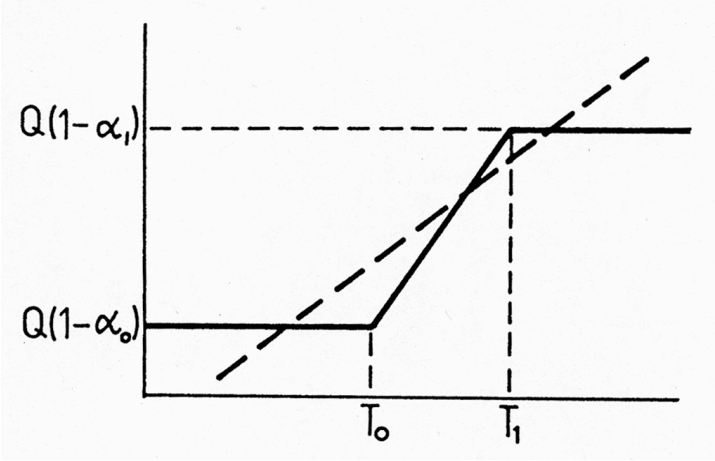

FIGURE 2.60. Absorbed Solar radiation (solid line) and energy loss by outgoing terrestrial radiation and dynamical energy fluxes (broken line) (figure due to J. Oerlemans).

Let us analyze the **climate sensitivity** of the planet using the Budyko parametrization of outgoing radiation at TOA. The equilibrium state can be expressed as follows.

$$Q(1-\alpha) = I_0 + bT$$

Differentiating this equation with respect to Q we obtain

$$\frac{dT}{dQ} = \frac{(1-\alpha)}{b}. \tag{2.72}$$

We have assumed that albedo and the other empirical parameters are independent of Q. **Climate sensitivity is defined here as the global temperature change for a 1% change in the Solar irradiance**, i.e using the parameter

$$\mu = \frac{Q}{100}\frac{dT}{dQ} = Q\frac{(1-\alpha)}{100b}. \tag{2.73}$$

This implies that the **sensitivity of the climate to changes in the incoming Solar radiation depends on albedo and the parameter *b*** (compare (2.72) with (2.24)).

Earth's albedo depends on degree of snow- or ice cover. This, in turn, depends on the temperature. In order to investigate the influence of this effect we introduce a temperature-dependent albedo as follows.

$$\begin{aligned}
&\alpha = \alpha_0 \text{ if } T \le T_0;\\
&\alpha = \alpha_0 + \frac{T - T_0}{T_1 - T_0}(\alpha_1 - \alpha_0) \text{ if } T_1 \ge T > T_0;\\
&\alpha = \alpha_1 \text{ if } T > T_1.
\end{aligned} \tag{2.74}$$

Here α_0 corresponds to the albedo of a snow-covered surface, while α_1 corresponds to the average albedo of a vegetation-covered surface. T_0 and T_1 are temperatures below and above which the surface is, respectively, completely snow-covered or completely free of snow and ice.

Absorbed Solar radiation depends on temperature in a rather non-linear fashion, as is shown by the solid line in **figure 2.60**. The broken line in **figure 2.60** represents the outgoing long-wave radiation. Equilibrium states are represented by intersections of solid and broken lines. Apparently, the model possesses "**multiple equlibria**". Depending on the value of I_0, three equilibrium states are possible for the same parameter values when

$$\eta \equiv \frac{Q(\alpha_0 - \alpha_1)}{(T_1 - T_0)} > b, \tag{2.75}$$

whereas only one equilibrium state is possible when

$$\eta < b \tag{2.76}$$

The relevant **control parameters** are b/η and I_0. The equilibrium surface in control parameter space is displayed in **figure 2.61**. Factors favouring the ocurrence of multiple equilibria are strong albedo feedback (large η) and weak "damping" due to outgoing long-wave radiation (small b).

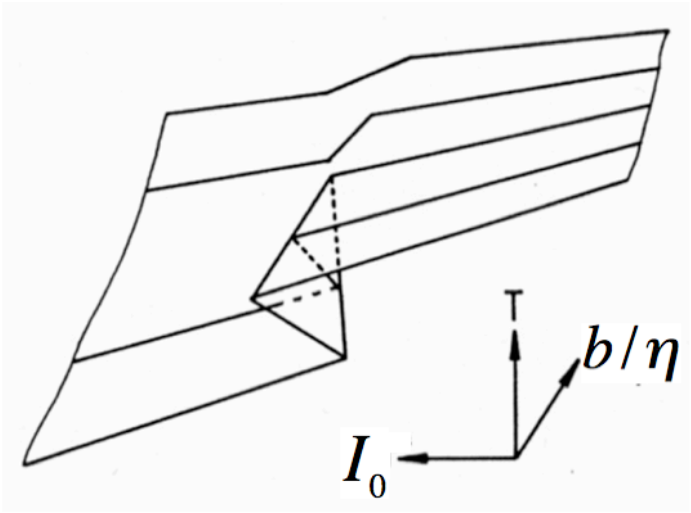

FIGURE 2.61. Equilibrium surface of the simple energy balance model with piecewise linear albedo feedback (figure due to J. Oerlemans).

The stability characteristics of these equilibria can be investigated with the temperature-evolution equation:

$$C\frac{dT}{dt} = Q(1-\alpha) - I_0 - bT. \tag{2.77}$$

C is the heat capacity of the system per unit surface area. The standard method of investigating the stability of the equilibrium solution, T_{eq}, of (2.77) is to add a perturbation, T', such that

$$T(t) = T_{eq} + T'(t). \tag{2.78}$$

Albedo may be expressed as:

$$\alpha(T) = \alpha\left(T_{eq}\right) + \frac{d\alpha}{dT}T'. \tag{2.79}$$

Inserting (2.78) and (2.79) into (2.77) we obtain

$$\frac{dT'}{dt} = -\lambda T' \tag{2.80}$$

with

$$\lambda = \frac{b + Q\dfrac{d\alpha}{dT}}{C}. \tag{2.81}$$

The solution of (2.80) is

$$T' = T'(0)\exp(-\lambda t). \tag{2.82}$$

Therefore, the perturbation decays to zero if $\lambda>0$, while there is exponential growth of the amplitude of the perturbation, i.e. instability, if $\lambda<0$.

The sign of λ is determined by the sign of $d\alpha/dT$. For $T>T_1$ or $T<T_0$ $d\alpha/dT=0$. Therefore, the equilibria corresponding to $T>T_1$ or $T<T_0$ are stable to small perturbations (because $b>0$). For $T_0<T<T_1$, $d\alpha/dT<0$. Therefore, the solution for this intermediate equilibrium state is unstable if

$$\frac{d\alpha}{dT} < -\frac{b}{Q}. \tag{2.83}$$

PROBLEM 2.17. **Ice-albedo feedback**

The equation governing the global average, yearly average temperature, T, of the Earth's surface is eq. 2.77

(a) What physical processes are captured by this equation?

(b) Assume that within a certain range of temperatures $T_0<T<T_1$ the global average albedo, α, is temperature-dependent as given (2.74) (T is expressed in°C). The empirical parameters have the following values: $\alpha_0=0.6$; $T_0=-10$°C; $\alpha_1=0.25$; $T_1=0$°C. In other words, three temperature intervals can be distinguished with different behaviour of the albedo. How many equilibrium states does the system have given that $S_0=1366$ W m^{-2}?

(c) Calculate the radiative equilibrium temperature in the middle temperature range ($T_1>T>T_0$)

(d) Can the equilibrium temperature calculated in (c) be sustained? In other words, is it a stable equilibrium?

2.22 The pole-equator temperature contrast

For the Earth as a whole and averaged over at least one year the absorbed Solar radiation and the outgoing long wave radiation at the top of the atmosphere are approximately in balance. However, at a specific latitude this is obviously not the case. This is illustrated in **figure 1.94**. At the equator more radiation is absorbed than is lost to space. At the poles the reverse is the case. Obviously, the poles are warmer than would be expected on the grounds of radiation balance, while the equator is colder than would be expected on the grounds of radiation balance. The physical process that is responsible for the deviation from radiative balance at almost all latitudes is **transport of energy due to the meridional circulation in both the ocean and the atmosphere**.

Budyko and Sellers[127] were the first to construct a model of the latitudinal dependence of Earth's energy balance, incorporating the energy transport by the circulation. For **mean annual conditions**, the equation for the vertically, zonally averaged energy balance of the Earth-atmosphere system is

$$\boxed{Q(1-\alpha) = I + A} \tag{2.84}$$

In this equation $Q(\phi)$ is the Solar radiation coming at the top of the atmosphere (TOA), $\alpha(\phi, T)$ is the albedo, $I(\phi, T)$ is the outgoing long wave radiation at TOA and $A(\phi, T)$ is the loss of energy from a particular latitude belt as a result of the circulation in the atmosphere and the ocean. ***T* is the temperature at sea level**. Note that the variables in eq. 2.84 do not depend on pressure or height. If A is expressed as a function of sea-level temperature, eq. 2.84 can be solved.

So, the question now is: how do we parametrize the meridional energy flux divergence in terms of sea-level temperature? Rather adhoc, Budyko suggested the following simple relation.

$$\boxed{A = \beta(T - T_p)} \tag{2.85}$$

with

$$T_p = \frac{1}{2}\int_{-1}^{1} T dx \tag{2.86}$$

and

$$x = \sin\phi. \tag{2.87}$$

T_P represents the planetary mean sea-level temperature; β in this context is a relaxation coefficient. Sellers, on the other hand suggested the following parametrization:

$$A = \frac{\partial}{\partial x}\left(1 - x^2\right) K_H \frac{\partial T}{\partial x}. \tag{2.88}$$

[127] Budyko, M.I., 1969, Tellus, 21, 610-619; Sellers, W.D., 1969, J.Appl.Meteor., 8, 392-400.

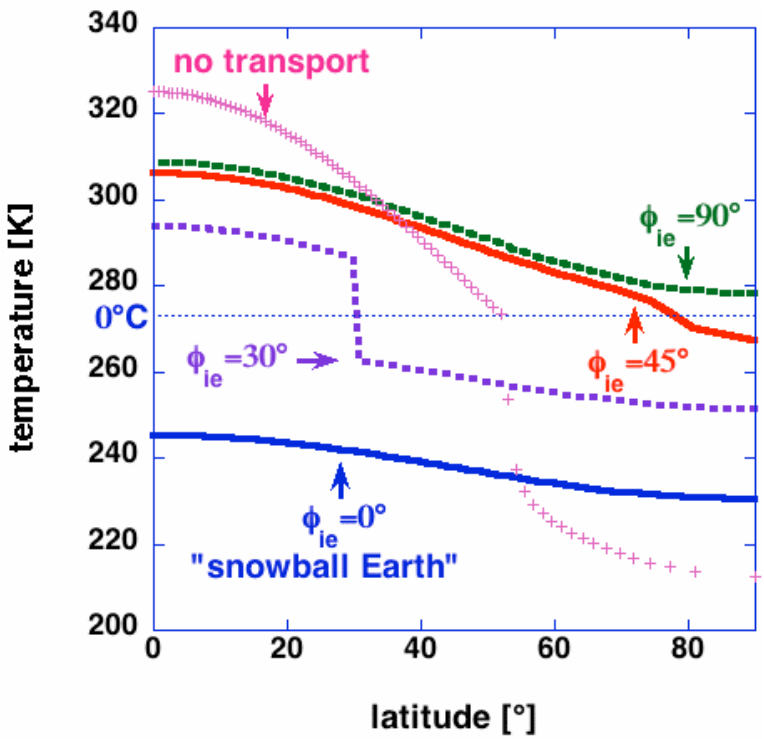

FIGURE 2.63. Equilibrium solutions of (2.84) with S_0=1366 W m^{-2}, I_0=204 W m^{-2}, b=2.17 W m^{-2}K^{-1}, T_0=263 K, T_1=273 K, α_0=0.62, α_1=0.25, β=3.8 W m^{-2}K^{-1} (in one case β=0, implying no meridional transport of energy) for different initial positions of the ice edge, ϕ_{IE}, indicated in degrees latitude. The temperature at t=0 is specified such that it is -30°C poleward of the ice-edge and +37°C equatorward of the ice-edge. The source code can be found at http://www.staff.science.uu.nl/~delde102/EBM.htm.

Here, K_H is the diffusivity (W m^{-2} K^{-1}). This parametrization is analogous to the parametrization of the momentum flux due to eddies in the boundary layer (see section 1.4). The value of the parameter β or of K_H is adjusted to fit the model to the observations. This is referred to as "**model-tuning**". Obviously, a model with many "tunable" parameters is not a good model.

Budyko's parametrization of outgoing long wave radiation (2.71) is modified slightly by incorporating the height, h, above sea level of the Earth's surface as follows.

$$I = I_0 + b(T - h\Gamma) \tag{2.89}$$

Here, Γ is the temperature lapse rate.

With Budyko's parametrization (2.85) of A, (2.84) becomes (using 2.89)

$$Q(1-\alpha) = I_0 + b(T - h\Gamma) + \beta(T - T_p) \equiv a^* + b^* T \tag{2.90}$$

with

$$a^* \equiv I_0 - bh\Gamma - \beta T_p \text{ and } b^* \equiv b + \beta . \tag{2.91}$$

The annual mean insolation, Q, can be expressed as a function of latitude as follows.

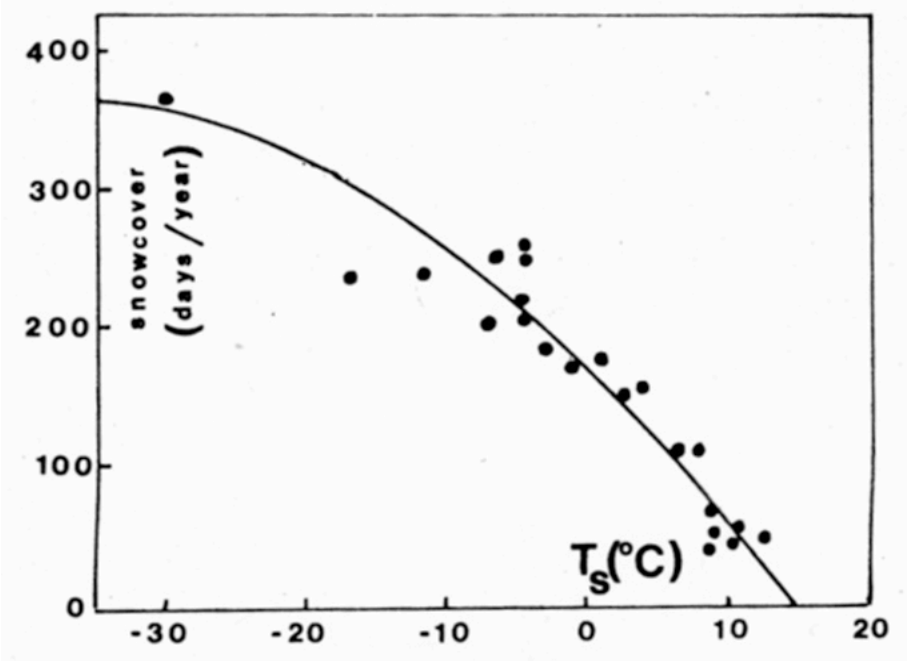

FIGURE 2.64. The number of days with snow cover as a function of the annual mean temperature. The curve represents the parametrization used by Oerlemans and van den Dool (1978) (**J.Atmos.Sci., 35**, 371-381).

$$Q = \frac{S_0}{4} s(x), \tag{2.92}$$

where

$$s(x) = 1.0 - 0.477 P_2(x) \tag{2.93}$$

with

$$P_2(x) = \frac{1}{2}\left(3x^2 - 1\right) \tag{2.94}$$

The distribution function $s(x)$ is defined as the annual mean insolation at a particular latitude divided by the global average insolation. The global average of $s(x)$ is 1.

Albedo, α, is specified as a function of x following the recipe in (2.74). The most straightforward way to solve (2.90) is to make it time-dependent as follows.

$$C\frac{dT}{dt} = Q(1-\alpha) - a^* - b^* T. \tag{2.95}$$

Here, C is a hypothetical heat capacity. The value of C is not important as long as the interest is focussed exclusively on the equilibrium solution of (2.95), whereby

$$\frac{dT}{dt} = 0.$$

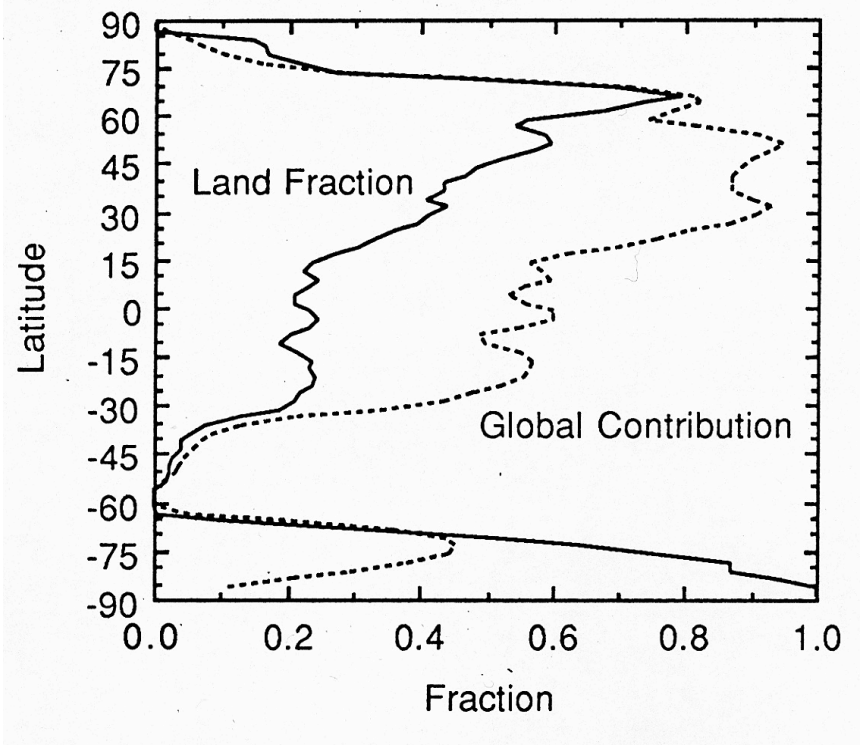

FIGURE 2.65. Fraction of surface area covered by land as a function of latitude (solid line) and contribution of each latitude belt to the global land surface area (dashed line) (from D.L. Hartmann, 1994: **Global Physical Climatology**. Academic Press, figure 1.12).

The equilibrium solution is found by integrating eq. 2.95 numerically in time until a steady state is attained according to a specified convergence criterium. The initial state is specified by the latitude, ϕ_{IE}, of the ice-edge. Poleward of this latitude the temperature is 243 K and equatorward of this latitude the temperature is 310 K initially.

Figure 2.63 demonstrates that the equilibrium solution depends strongly on the initial conditions. **If we set ϕ_{IE}=70° initially, the ice over the poles does not survive, i.e the Earth becomes completely ice-free. However, if we set ϕ_{IE}=30° initially, everything else being the same, the ice survives.** It is even possible to obtain a solution whereby the Earth is completely ice-covered for the same insolation as in the ice-free solution. The completely ice-covered Earth has been termed "**snowball Earth**" by geologists[128] who have found indications that this state has actually existed about 580 to 750 million years before present. Gabrielle Walker has described Snowball Earth as follows.

> Picture a world entirely sheathed in ice, its oceans smothered by a freezing white blanket nearly a mile thick. Vast glaciers creep across the continents. Nothing else moves. There are no clouds, save perhaps a handful of high wispy streaks made from frozen crystals of carbon dioxide. With the temperature a chilling 40 degrees below zero, only a few living things survive. Algae cling to the meager warmth of volcanic springs, and bacteria eke out a living around hot-water vents deep in the ocean. For millions of years, nothing changes. This is no far-off planet or alien moon. It's a view of Earth just a few hundred million years ago.

The ice cap-free state has also existed in the past. In fact, it is thought that the Earth was ice-free throughout most of its history. During these periods snow cover existed over the

[128] see http://www.snowballearth.org/index.html and http://en.wikipedia.org/wiki/Snowball_Earth

continents, and the polar seas were covered with ice only in winter[129].

Without meridional transport of energy (i.e. A=0), the temperature difference between pole and equator is about 113 K! The temperature at the equator is a blistering 52°C while the temperature at the poles is a shivering -61°C. The ice-edge is found at a latitude of 53°. The sub-Solar point is at the equator permanently. Therefore, seasons do not exist. In these circumstances Life is really only possible between the latitude of 22°, where the temperature is close to 40°C, and the permanent ice-edge at 53°.

When $A \neq 0$ the temperature difference between pole and equator is reduced to about 30 K in the case of the ice free-solution, and about 39 K in the solution with ice cover poleward of 80°, which is a situation quite similar to present day conditions (**figure 2.3**).

Many articles on the one-dimensional "Budyko-Sellers" energy balance model were written and published in the 1970's. Some authors[130] have suggested a more sophisticated albedo parametrization, whereby account is taken of the potential snow cover and the surface area covered by land within a latitude belt (**figure 2.65**). For instance, by letting the albedo, α, depend on the fraction of ice- or snow-cover within a particular latidude belt on Earth (α=0.6 if the Earth is covered by ice/snow), vegetation without ice or snow (α=0.3), or ocean (α=0.1, although this is actually a complex function of zenit angle, wind speed and cloud cover). Potential snow cover, i.e. the snow cover that would exist if open water did not melt the falling snow, is dependence of snow cover. Based on these observational data, the snow cover in the model is given as a function of surface temperature by

$$\text{snow cover} = 1 \text{ if } T \leq -40°\text{C};$$
$$\text{snow cover} = 1 - 0.00033(T + 40)^2 \text{ if } -40°\text{C} < T \leq +15°\text{C};$$
$$\text{snow cover} = 0 \text{ if } T > 15°\text{C}.$$

If one goes this far with the albedo parametrization, one must also take account of the fraction of surface area covered by land. This fraction is shown in **figure 2.65** as a function of latitude, along with the contribution of each latitude belt to the global land surface area. The ocean is ice-covered (in which case α=0.6), if the temperature is lower than a certain threshold value.

Including the more sophisticated albedo parametrization does actually not alter the qualitative aspects of the solution. **Figure 2.66** shows the steady state **global average temperature** as a function of Solar irradiance as a fraction of the present irradiance (1366 W m^{-2})[131]. For a relatively wide range of values of the Solar irradiance around the present value, the model possesses two **stable** steady state solutions: a partially ice-covered Earth and a completely ice-covered Earth. A negative perturbation of 10% of the present Solar irradiance is required to bring the climate into the glaciated state. A larger positive perturbation of the Solar irradiance is required to bring the climate *back* into the warm state. This implies that **climate sensitivity depends on its history**.

There is strong evidence that Earth's climate has switched quite rapidly from a warm "**interglacial**" state to a cold "**glacial**" state and vice versa over the past 0.8 million years (**figure 2.67**). The transition from glacial to interglacial seems to take place relatively very rapidly (within a century or so). Over the past 420,000 years the time period between interglacials is approximately 100 thousand years. This period has been linked to the

---

[129] L.C. Sloan and E.J. Barron, 1990: "Equable" climate during Earth history? **Geology**, 18, 489-492.

[130] For instance: Oerlemans, J, and H.M. van den Dool, 1978: **J.Atmos.Sci., 35**, 371-381.

[131] According to Oerlemans, J, and H.M. van den Dool (1978), who parametrized the tranport term according to (2.88).

variations of Solar irradiance caused by changes in the orbit of the Earth around the Sun. However, the theory presented in this section requires larger variations in global- and yearly average insolation than those that have taken place in reality. Probably, the Budyko-Sellers model is too strongly simplified to capture the transition between glacial periods and interglacial periods under influence of varying insolation. At present experts[132] think that the summer insolation in the polar regions (especially in the northern hemisphere) is a crucial factor in producing polar ice sheets that grow over many years. Summer insolation at high latitudes is weak if the obliquity is small and at the same time both the eccentricity of the orbit of the Earth around the Sun is large *and* aphelion falls in the summer of the northern hemisphere (section 2.2). The ocean CO_2-solubility pump (Box 2.13) may intensify the response to these variations in the geographical distribution of insolation.

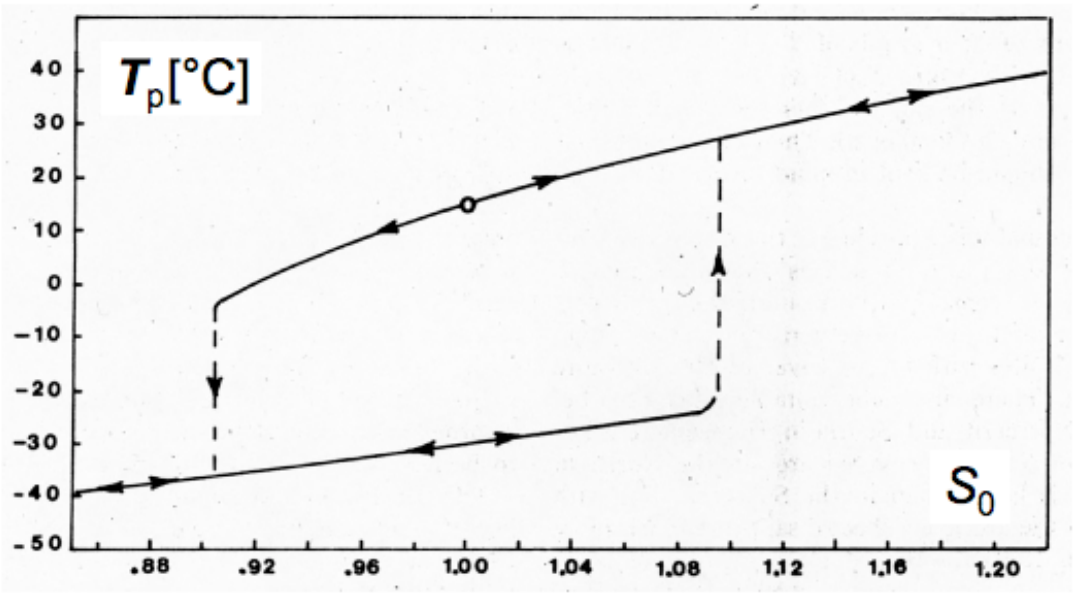

FIGURE 2.66. Solutions of the one-dimensional energy balance model with Seller's parametrization of the transport term obtained by Oerlemans and van den Dool (1978) (**J.Atmos.Sci., 35**, 371-381), in terms of the global mean surface temperature as a function of Solar irradiance.

PROBLEM 2.18. Budyko_Sellers model with seasonally varying heating

Program the Budyko Sellers energy balance model, including a parametrization of latitude- and season dependent insolation, following the theory described in box 2.1. Investigate the dependence of the solutions on obliquity and eccentricity.

PROBLEM 2.19. Sensitivity of solutions to parameter values.

Investigate the sensitivity of the solutions of the Budyko Sellers energy balance model to changes in the parameters I_0 and b.

---

132 See http://earthobservatory.nasa.gov/Study/Paleoclimatology_Evidence/

Roe, G, 2006: In defense of Milankovitch. **Geoph.Res.Lett., 33**, L24703, doi10.1029/2006GL027817.

PROBLEM 2.20. Hysteresis and CO_2-concentration.

Huntingford et al. (2003)[133] have investigated the solutions of the Budyko-Sellers energy balance model with a slightly different parametrization of outgoing long-wave radiation. Instead of (2.71) they used

$$I = I_0 + bT - 5.397 \ln\left(\frac{pCO_2}{280}\right),$$

where pCO_2 is the CO_2-concentration in ppmv, I_0=203.34 W m^{-2} and b=2.09 W m^{-2}K^{-1}. Investigate the hysteresis (illustrated in figure 2.66) using the EBM with this parametrization. What do you think of the concept of equailibrium climate sensitivity in the light of the existence of the ice-albedo feedback?

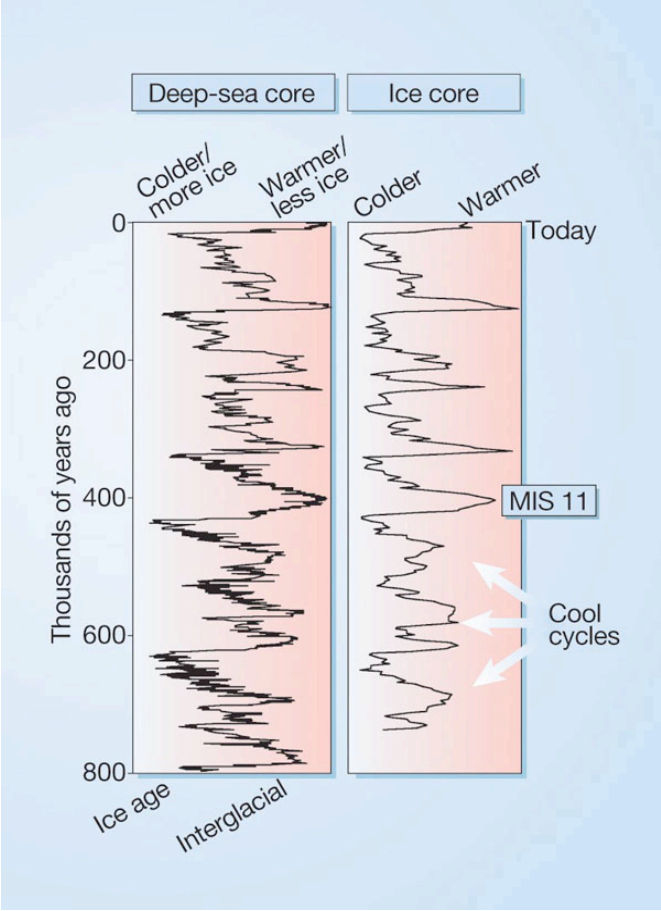

FIGURE 2.67. The history of deep-ocean temperatures and global ice volume is inferred from a high-resolution record of oxygen-isotope ratios measured in bottom-dwelling foraminifera shells preserved as microfossils in Atlantic Ocean sediments. Air temperatures over Antarctica are inferred from the ratio of deuterium and hydrogen in the ice at Dome C (Antarctica). Marine Isotope Stage 11 (MIS 11) is an interglacial that bears some similarity to the most recent warm period, yet lasted many thousands of years longer. Note the smaller magnitude and less-pronounced interglacial warmth of the glacial cycles that preceded MIS 11. (Jerry F. McManus, A great grand-daddy of ice cores. **Nature 429**, 611-612 (10 June 2004)).

---

[133] Huntingford, C., J.C. Hargreaves, T.M. Lenton and J.D. Annan, 2003: Extent of partial ice cover due to carbon cycle feedback in a zonal energy balance model. **Hydrology and Earth Sytem Science, 7(2),** 213-219.

ABSTRACT OF CHAPTER 2

The central questions of chapter 2 are the following. What processes determine the temperature in the atmosphere? What exactly is the greenhouse effect? Is the atmosphere of the Earth in radiative balance? Can we also explain the division of the atmosphere into a troposphere and a stratosphere? What physical processes characterize the troposphere as opposed to the stratosphere? What is the role of clouds in determining the temperature distribution? What determines the pole-equator temperature difference? Can we explain the existence in the distant past of "ice ages" on the basis of energy balance considerations?

We have given some definitive and some more tentative answers to these questions on the basis of the energy balance of the Earth-atmosphere system. The first important message is the following. The atmosphere of any planet containing well-mixed greenhouse gases can be subdivided into two layers. The upper layer is called the **stratosphere**. *Globally averaged and annually averaged* the stratosphere is in radiative balance. The lower layer is called the **troposphere**. This layer responds thermally to the Solar heating of the Earth's surface through mixing by convection, aided mainly by release of latent heat due to condensation of water vapour that enters the atmosphere through evaporation at the Earth's surface. Due to latent heat release the **tropopause** (the boundary separating the two layers) is located at about 200 hPa (10-15 km above sea level) instead of at about 600 hPa (4-5 km above sea level).

A second important message is that, because of the existence of an "**infrared window**" in the emission spectrum of the atmosphere, Earth's equilibrium climate is relatively insensitive to changes in greenhouse gas concentrations or variations in Solar irradiance. **The influence of the water cycle on climate sensitivity is extremely complex** due to the myriad feedbacks that come into play with clouds, evaporation and precipitation, but most probably reduces climate sensitivity also, despite the presence of a positive **water vapour feedback**, which, *in the absence* of cloud feedbacks and other feedbacks related to the water cycle, appears to double the otherwise relatively weak equilibrium climate sensitivity to CO_2-concentration changes.

A third important message is the following. The temperature is determined by **non-linear** feedbacks between radiation, convection, water vapour, surface evaporation, clouds and snow/ice cover. Non-linearity usually implies that climate has more that one steady state for identical values of the externally imposed forcing parameters, such as insolation and the greenhouse gas content. This fact puts the discussion about climate sensitivity (i.e. in sections 2.17-2.19 and in Boxes 2.10-2.12), which is frequently defined as the response of global average surface equilibrium temperature to doubling of CO_2-concentration, in a completely different perspective. **Theoretically, the Earth can be nearly completely ice-covered, even with present day insolation intensity and greenhouse gas concentrations**.

A fourth and final important message is that the thermal structure of the atmosphere cannot be explained exclusively with reference to only radiation. **Energy transport by air motions or by motions in the ocean is a crucial part of the energy balance, determining the pole-equator temperature difference**. This is the subject of the remaining chapters of these lecture notes, culminating in chapter 12, with the topic of the radiative dynamical adjustment of the atmosphere.

Further reading

Books

Archer, D., 2007: **Global warming: understanding the forecast**. Blackwell Publishing Ltd., 194 pp. (A very readable but also authorative book on all aspects of climate change, supplemented by Archer's website, including the online radiation model, "Modtran": http://forecast.uchicago.edu/index.html).

Bohren, C.F., and E.E. Clothiaux, 2006: **Fundamentals of Atmospheric radiation**. Wiley-VCH, 472 pp. (A didactic jewel: discusses the fundamental concepts, laws and equations of the emission and transmission of radiation through the atmosphere, focusing on physical interpretation and avoiding the use of complex mathematics).

Finnlayson-Pitts, B.J., and J.N.Pitts Jr., 2000: **Chemistry of the upper and lower atmophere. Acaddemic Press**. 969 pp. (This very complete treatment of atmospheric chemistry, including fundamental aspects of radiation, merits the following qualification. "What is written with effort, is in general read with pleasure").

Hartmann, D.L., 1994: **Global Physical Climatology**. Academic Press, 408 pp. (A good and broad introduction to the physics of the climate system of the Earth).

IPCC, 2007: **Fourth assesment report of the Intergovernmental Panel on Climate Change** (IPCC). Cambridge University Press (http://ipcc-wg1.ucar.edu/wg1/wg1_home.html). (The authoritative review of climate science).

Jacobs, D.A., 1999: **Introduction to Atmospheric Chemistry**. Princeton University Press (chapter 7). (Chapter 7 on the greenhouse effect is very well written).

Liou, K.N., 1992: **Radiation and Cloud Processes in the Atmosphere**. Oxford University Press. 487 pp. (A clear and rather complete treatment of cloud processs, atmospheric radiation and their complicated interaction)

Pierrehumbert, R.T., 2010: **Principles of Planetary Climate.** Cambridge University Press. (This book has the potential of becoming a standard in the field of climate science, although it is restricted to role of radiation in climate).
(http://geosci.uchicago.edu/~rtp1/PrinciplesPlanetaryClimate/index.html)

Ruddiman, W., 2001: **Earth's Climate: Past and Future**. W.H. Freeman and company. 465 pp. (A beautifully illustrated geologist's view of Earth's climate. A second updated edition of this book has been published in 2007).

Stensrud, D.J., 2007: **Parameterization Schemes: Keys to understanding numerical weather prediction models**. Cambridge University Press. 459 pp. (Gives a good and broad overview of the parametrization problem in climate and weather modelling, including parametrizations of surface energy fluxes, cloud cover and radiation)

Ingersoll, A.P. 2013: **Planetary Climates**. Princeton University Press, 278 pp. (A clear treatment of the diverse climates of planetary atmospheres within the Solar system)

Zdunkowski, W., T. Trautmann and A. Bott, 2007: **Radiation in the Atmosphere**. Cambridge University Press. 482 pp. (well-written treatment of the many technical details of radiative transfer)

Articles

Broecker, W.S., 1975: Climatic change: are we on the brink of a pronounced global warming? **Science**, 189, 406-463. (Example of a very accurate prediction of climate change over a period of 30 years.)

Held, I.M., and B.J. Soden, 2000: Water vapor feedback and global warming. **Annu.Rev. Energy Environ., 25**, 441-475. (An authorative review of the water vapour feedback (section 2.19).)

Kiehl J.T., and K.E. Trenberth, K.E., 1997: Earth's annual global energy budget. **Bull.Am.Meteorol.Soc., 78,** 197-208. (Analysis of the global mean annual mean energy budget leading to the well-known diagram in **figure 2.10**).

Lovelock, J.E. and A.J. Watson, 1982: The regulation of carbon dioxide and climate: Gaia or geochemistry. **Planet.Space Sci.,** 30, 795-802. (How the biosphere determines the composition of the atmosphere.)

Pierrehumbert, R.T., 2011: Infrared radiation and planetary temperature. **Physics Today**, 64, 33-38. (This paper gives a first impression of the recent book on the subject of radiation and climate, listed on the previous page).

Roe, G., 2009: Feedbacks, timscales and seeing red. **Annu.Rev.Earth Planet.Sci.,37**, 93-115. (A clear and fascinating review of how feedbacks are quantified in climate models)

Stephens, G.L., 2005: Cloud Feedbacks in the Climate System: A Critical Review. **J.Climate, 18**, 237-273. (Review paper about the important and still little understood role of clouds in climate)

Stevens, B., and S. Bony, 2013: Water in the Atmosphere. **Physics Today**, June 2013, 29-34. (Good basic description of the many ways in which water affects Earth's climate)

Trenberth, K.E., and D.P. Stepaniak, 2004: The flow of energy through Earth's climate system. **Quart.J. R.Meteorol.Soc**., 130, 2677-2701. (Overview written by specialists in the analysis of observations and re-analyses.)

Webster, P.J., 1994: The role of hydrological processes in Ocean-atmosphere interactions. **Rev.Geophysics, 32**, 427-476. (Interesting review paper about the water cycle and its interaction with radiation and dynamics.)

Wielicki, B.A., T. Wong, N. Loeb, P. Minnis, K. Priestley and R. Kandel, 2005: Changes in Earth's albedo measured by satellite. **Science**, 308, 825. (About Earth's albedo and its still inaccurate determination.)

Zhong, W., and J.D. Haigh, 2013: The greenhouse effect and carbon dioxide. **Weather, 68**, 100-105.

Internet sites

http://forecast.uchicago.edu/lectures.html (David Archers lecture series on Climate are warmly recommended)
http://www.aip.org/history/climate/ (a very good account of the history of the discovery of the greenhouse effect)
http://www.cpc.ncep.noaa.gov/ (climate information from the American National Weather Service)
http://www.realclimate.org/ (discussions on issues related to climate research)
http://www.staff.science.uu.nl/~delde102/AtmosphericDynamics.htm (information about these lecture notes)

List of problems (chapter 2)

The atmosphere at night, according to Vincent van Gogh: a starry night at Arles, seen from the bank of the Rhone river. Musée d'Orsay, Paris, 14 October 2012.

This is the Appril 2015 edition of chapter 2 of the lecture notes on Atmospheric Dynamics., written by Aarnout van Delden (IMAU, Utrecht University, Netherlands, a.j.vandelden@uu.nl).
http://www.staff.science.uu.nl/~delde102/AtmosphericDynamics.htm